THEORETICAL ASPECTS OF CHANNEL ELECTRODES; APPLICATION TO THE DEVELOPMENT OF VOLTAMMETRIC IMMUNOASSAY

by

Stephen G. Weber

A Thesis Submitted to the Faculty of Graduate Studies and Research in Partial Fulfillment of the Requirements for the Degree of Doctor of Philosophy

Department of Chemistry
McGill University
Montreal, Quebec, Canada

March 1979

To Carol and Jessica

Theoretical Aspects of Channel Electrodes;
Application to the Development of Voltammetric Immunoassay

Abstract

The concept of the diffusion layer, generally used in a steady-state context, is used as a time-dependent or space-dependent unknown in the differential equations of diffusion. The electrochemical current which is predicted with this approximation is compared to exact mathematical treatments for a potentiostatic transient in a thin-layer cell and for a potentiostatic transient with a CE mechanism. Channel electrodes are studied using this approximation. The validity of the expressions for ordinary three-electrode cells and for four-electrode cells is proven experimentally. The mathematical description of the channel electrode is used to determine optimum operating conditions under a variety of circumstances. Conditions under which a channel electrode will not detect the product of a preceding homogeneous reaction are calculated. Employing a channel electrode under these conditions allows the performance of a homogeneous voltammetric immunoassay.

Etude théorique de l'électrode du type "canal" et son application comme méthode de détermination immunologique voltamétrique

Résumé

Le concept de zone de diffusion, généralement utilisé dans un contexte d'état stationnaire, est employé comme paramètre temporalement et spacialement dépendant dans l'équation différentielle de diffusion. Le courant électrochimique prédit, par cette approximation, est comparé au traitement mathématique rigoureux d'un potentiel fixe dans une cellule à couche mince et d'un potentiel fixe avec un mécanisme chimique électrochimique (CE). Les électrodes de type "canal" sont étudiées selon cette approximation.

La validité de ce traitement pour une cellule à trois ou quatre électrodes est prouvée expérimentalement. Le traitement mathématique de l'électrode du type "canal" est employé pour la détermination des conditions optimum d'opération au cours d'une variété de conditions expérimentales. Les conditions, pour lesquelles une électrode du type "canal" ne détectera pas le produit d'une réaction homogène précédente, sont calculées. Dans ces conditions, une électrode du type "canal" permet la réalisation d'une détermination immunologique voltamétrique homogène.

ACKNOWLEDGEMENTS

I would like to express my gratitude to Professor William C. Purdy for his guidance, encouragement and wisdom given during the course of this work. By his example, I have learned to consider my work with a balanced perspective.

I would as well like to thank:

Bradford R. Hepler for many helpful discussions and criticisms.

Assunta Cerrone for the careful typing of the manuscript.

My wife, Carol, for her support in so many spheres during the course of this work.

McGill University for Summer Research Fellowships and Assistant Demonstratorships.

Table of Contents

Page

Page

List of Figures

Page

Page

Page

List of Tables

Page

Preface

Immunoassay is a frequently performed class of biochemical analysis. The discontinuous nature of immunoassays currently performed contrasts greatly with the continuous, automated nature of most other tests in the clinical laboratory. An improvement in the immunoassay technique which would allow the possibility of automation is required.

One detection technique which permits, indeed depends upon a flowing stream for its excellent sensitivity, is electrochemical detection (1). This technique has been often used but has been scrutinized very little. It was decided to theoretically explore the electrochemical detector called a channel electrode to learn more about its behavior. It was hoped that a theoretical procedure could be developed to explore the possibilities of performing immunoassay with electrochemical detection. Once the theory was in hand, and conditions were met for performing voltammetric immunoassay, the feasibility of the voltammetric immunoassay could be ascertained. This thesis develops the theory required to understand the channel electrode. The theory is used to predict, among other things, conditions under which voltammetric immunoassay may be performed. The thesis also discusses potential usefulness and drawbacks of voltammetric immunoassay.

---

(1) P.T. Kissinger, Anal. Chem., 49 (1977) 447A.

CHAPTER I

Electrochemistry in Flowing Streams

A) Basic Electrochemical Principles

Two major divisions of electrochemistry may be discerned, ionics and electrodics. The former is the study of equilibrium and steady state distributions of charge, potential and dipole orientation in physicochemical systems. The latter is the study of interfacial electron transfer and the physical and chemical parameters which affect this transfer. In electroanalytical techniques in which a current passes across an electrode-electrolyte interface the fundamentals of electrodics play a very important part and thus it is this aspect of electrochemistry which is pertinent to the present problem.

1) The Butler-Volmer Equation, Charge Transfer Overpotential

Early attacks on the fundamentals of electrodics were in error because the properties of reversible thermodynamics were applied to systems which were controlled by kinetics. It was not until the 1930's that the fundamental rate laws of electrodics were enunciated (1-3). The equation that describes the current which is caused to flow across the

electrolyte-solution interface as a function of the potential difference applied between the bulk electrode and the bulk solution is called the Butler-Volmer equation:

$$i = i_o[e^{(1-\beta)F\eta/RT} - e^{-\beta F\eta/RT}]$$

The definition of the terms appearing in this equation will serve to elucidate the behaviour of the system described by this equation. The term i is the current density, in units of Ampères per square centimeter caused by the one electron oxidation or reduction of the chemical species under study. This current density is being measured at an overpotential η, the difference between the potential difference measured between the electrode and the solution when there is no current flowing and the potential difference measured between the electrode and the solution when there is a current density i flowing.

A digression to discuss two semantic points is appropriate. It is common in electrochemistry to speak of a "potential" when in fact the "potential difference" between two phases is meant. Furthermore the potential difference which is taken to mean difference between two phases is actually measured between two electrodes. One of the electrodes is called a reference electrode and has a potential which is constant over the course of an experiment. It is also in equilibrium

with the solution phase, therefore the solution will adopt a potential which is equal to the reference electrode potential plus an unknown constant. The absolute potential difference between two phases can therefore not be measured. The reference electrode has the property that, for small enough currents, its potential will be constant. Therefore changes in potential to an electrode-solution-reference electrode system all occur across the electrode-solution interface. Practically, this means that a plot of current density as a function of potential (called an i-E curve) will retain its shape but be shifted along the E axis if the same electrode-solution interface is studied with various reference electrodes. In order to assign numerical values to this E axis one particularly well-behaved reference electrode may be arbitrarily assigned a value of 0 volts. The hydrogen electrode, calomel electrode and silver-silver chloride electrode are all currently in use as 0 volt references. To avoid confusion, the reference electrode to which potential is referred is always stated. To recapitulate the "difference between the potential difference of an electrode-solution interface and the potential difference of a reference electrode-solution interface" will be called the "potential of the electrode solution interface" or even "the electrode potential".

To return to overpotential η, it may be seen that η represents a perturbation on a system at equilibrium, and i

represents the dynamics of the system as it returns to equilibrium. For small η, the exponential terms in the Butler-Volmer equation may be expanded to yield

$$i = \frac{i_o F}{RT} \eta$$

The term RT/i_oF is called the Faradaic impedance in obvious analogy to Ohm's law. In fact it is pointed out by Bockris and Reddy (4) and by Adams (5) that the overpotential-current-Faradaic impedance relationship is just another example of a flux which is proportional to a driving force, as diffusive flux is to gradient of concentration, reaction flux is to gradient of chemical potential, bulk flux is to gradient of pressure, etc.

F, R, and T have their usual meaning of Faraday's constant, the gas constant and temperature. β is called the symmetry factor, and i_o the exchange current density. It can be seen from the Butler-Volmer equation that when $\eta = 0$, $i = 0$. But notice that the equation also reads $i = i_o - i_o$, i.e., equal current densities are occurring in opposite directions. The exchange current density may be given by (4)

$$i_o = F\vec{k}_c C_o e^{-\beta F \Delta\phi_E/RT}$$

$$= F\overleftarrow{k}_c C_r e^{(1-\beta) F \Delta\phi_E/RT}$$

for the reaction

$$O^{n+} + e^- \rightarrow R^{(n-1)+}$$

The rate constants $\vec{k}_c$ and $\overleftarrow{k}_c$ are chemical rate constants of the form $(kT/h)\exp(-\Delta G_c^{0\neq}/RT)$. By analogy, it can be seen that the terms $-\beta F\Delta\phi_E/RT$ and $(1-\beta)F\Delta\phi_E/RT$ represent the contribution of the applied potential (here, the equilibrium potential ϕ_E) to the free energy of activation. It is presumed that the potential difference between the electrode and the solution occurs linearly across the Helmholtz layer extending roughly 2-4 Å into the solution. Since the charge transfer will occur across this layer, the transition state will occur in the layer. Hence only a fraction of the potential, β, will be contributed to the free energy of activation for the reduction, and the remainder, $(1-\beta)$, will be contributed to the oxidation. This is diagrammed in Figure 1.

Another form of the Butler-Volmer equation makes the analogy with homogeneous chemical reactions clear:

$$i = FC_o\vec{k}(\eta) - FC_r\overleftarrow{k}(\eta)$$

where $\overleftarrow{k}(\eta)$ and $\vec{k}(\eta)$ are the potential dependent rate constants,

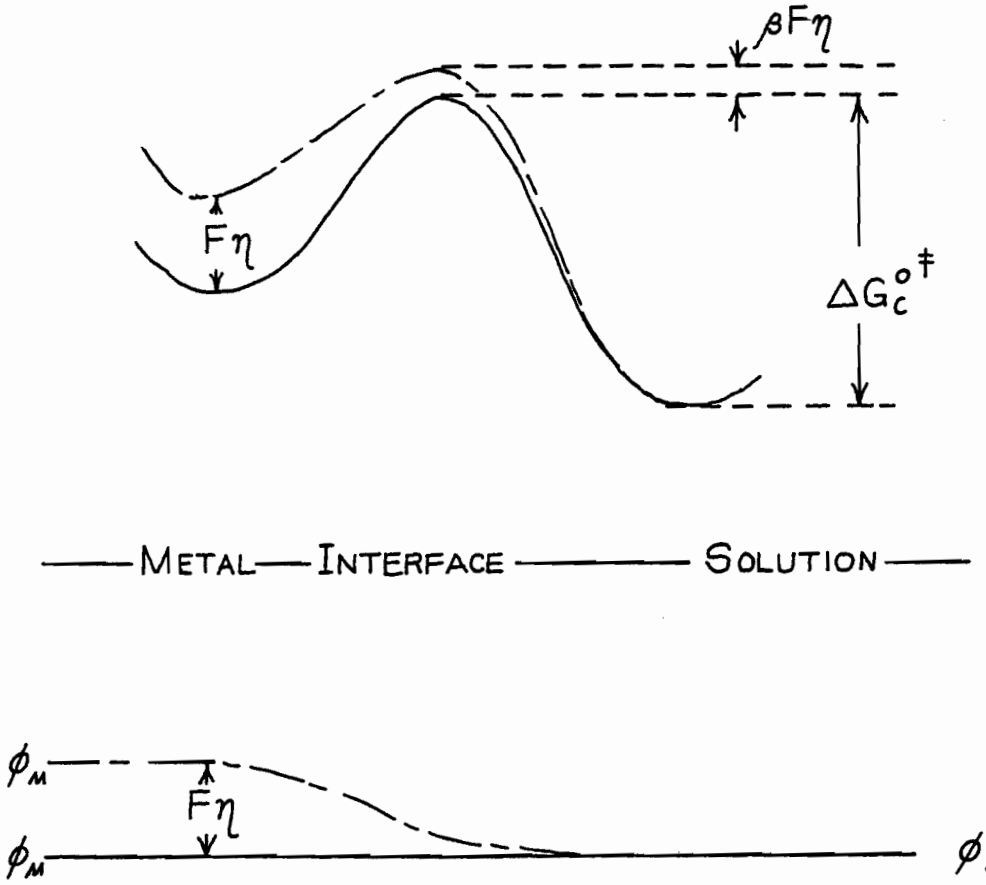

Figure 1: The potential energy vs distance diagram for an electron being transferred from the solution phase on the right, across the interface, into the metal phase on the left. The energy is given in the absence (———) and in the presence (— - —) of applied overpotential, η. Note that at zero overpotential, ϕ_s is not necessarily equal to ϕ_m. These have been diagrammed as equal for clarity in presentation of the effect of η.

C_o and C_r represent surface concentrations of oxidized and reduced species, respectively.

2) Other Contributions to Overpotential

Overpotential is not only caused by the finite rate of charge-transfer at the electrode surface as exemplified by the Butler-Volmer equation. In fact, any impedance in the overall rate will cause an overpotential to arise. Vetter (6) in his monograph on electrochemical principles enunciated several types of overpotential besides the charge transfer overpotential discussed above. If a chemical species in solution must undergo a slow homogeneous reaction to form a species which may then react at the electrode (in a heterogeneous reaction) and if this rate is the limiting rate in the reaction, the overpotential may be called reaction overpotential. If the transport of the electrochemically active species from the bulk of solution to the electrode surface is rate limiting, then the overpotential is termed mass-transport overpotential. Since a finite amount of voltage is required to cause a current to flow in any non-superconducting system, there is necessarily an ohmic overpotential.

In order to achieve reproducible results and to enhance sensitivity, most electroanalytical systems are designed to be mass transport controlled. The difficulty of reproducing physical conditions at the solution-electrode interface,

thus affecting i_o, makes it unwise to operate an analytical system in which the bulk of the overpotential is charge transfer overpotential, i.e., in which the charge transfer reaction is the rate determining step. In general, since mass transport is easily reproduced, most analytical systems operate in this region. Practically, this means that enough potential is applied to the system so that the heterogeneous rate constant for either the forward or backward reactions is effectively infinite, and as soon as a molecule of the electroactive species contacts the electrode, it reacts. Necessarily, for identical conditions of temperature, concentrations, and electrodes, mass transport controlled current will be higher than charge-transfer controlled current; another analytical advantage.

3) Current-Voltage Measurement, the Potentiostat

The means of measuring d.c. current-voltage curves is quite uniform throughout the field. Older (pre 1950's) measurements of current were by measurement of the voltage drop across a standard resistor. Potential was applied from a battery or power supply, controlled by a variable resistor. This arrangement was deficient in several ways. Current which was measured passed through the reference electrode. Reference electrodes were chosen, in part, because of a large i_o, i.e., a small current could be drawn with virtually no

overpotential. However some overpotential at the reference electrode was necessary. This overpotential was presumed to be at the working electrode-solution interface, thus an error resulted. One could operate with sufficiently low error, but then the current densities attainable were restricted. Large reference electrodes were desired to minimize i for a given analytical current making it difficult to place the reference electrode close to the working electrode. This resulted in sometimes significant iR drop in the solution.

The potentiostat is a three electrode device which became popular in the 1960's. The potentiostat only gained wide usage with the general availability of solid state operational amplifiers in the 1960's, although it was first reported in 1942 (8) and [as pointed out in a review (9)] brought to its current design by the biophysicists Hodgkin, Huxley and Katz (10,11) in studies on the nerve membrane potential. Britz (7) differentiates between two types of potentiostats, additive and differential. The additive sort is currently popular because several voltage sources may be added and then be applied to the electrochemical system. The potentiostat, by virtue of a third " auxiliary " electrode, relieves the reference electrode of the burden of carrying current. In so doing it allows one to construct a small diameter solution bridge (Luggin probe) between the reference electrode and the solution very near the working electrode

which then makes the solution at that point adopt the reference potential. Since the resistance of the solution is proportional to the distance that the current travels through it, and since the distance between the working electrode and the tip of a Luggin probe is much less than the distance between a working electrode and a large reference electrode in the older two electrode system, the iR drop is minimized by the potentiostat. There is still a resistance between the Luggin probe tip and the working electrode which may be overcome by clever cell design (12 and references therein) [but note that the current distribution must not be significantly upset (13)]. Alternatively, electronic methods (7) may be preferred.

B) Cell Geometry

The best analytical results are obtained when mass transport controls the current. Any device which can bring solution containing electroactive species to the electrode will increase the current. In a non-moving system diffusion is the only means of mass transport, while in a moving system both diffusion and bulk solution transport play a role (5,14), thus currents are higher and analytical sensitivity is greater in a moving system. Since the ultimate goal of this research was to at least show feasibility of a clinical chemistry technique, which virtually demands continuous analysis, it

was obvious that a technique in which the solution moved with respect to the electrode was preferred over one in which the electrode moved with respect to the solution. This ruled out the rotating disk (14-16). Systems in which turbulent flow is achieved (17-21), although yielding higher currents than laminar flow systems, are noisier due to the random nature of eddy current formation and decay. Hiroaki Matsuda and his group in Japan have studied several electrode geometries in laminar flowing streams (22-24) which would be suitable for analytical use and several (25-28) which would probably not be suitable. The former include the tube, wall-jet and channel electrodes (Figure 2).

The tubular electrode was described by Levich (14), demonstrated analytically by Blaedel and co-workers (29-31) and later combined with pulse polarization for increased sensitivity (32). It was felt that this system, although adequate for some investigations may not be adequate for an investigation where the physical dimensions of the cell would need to be altered since the electrode defines the cell, therefore a different cell dimension demands a different electrode.

The wall-jet electrode (23) offers the possibility of large signal currents since fluid transport is vertical (jet) to the electrode (wall). The only potential drawbacks are that the good sensitivity of the detector depends strongly on the diameter of the jet, and that the relative position

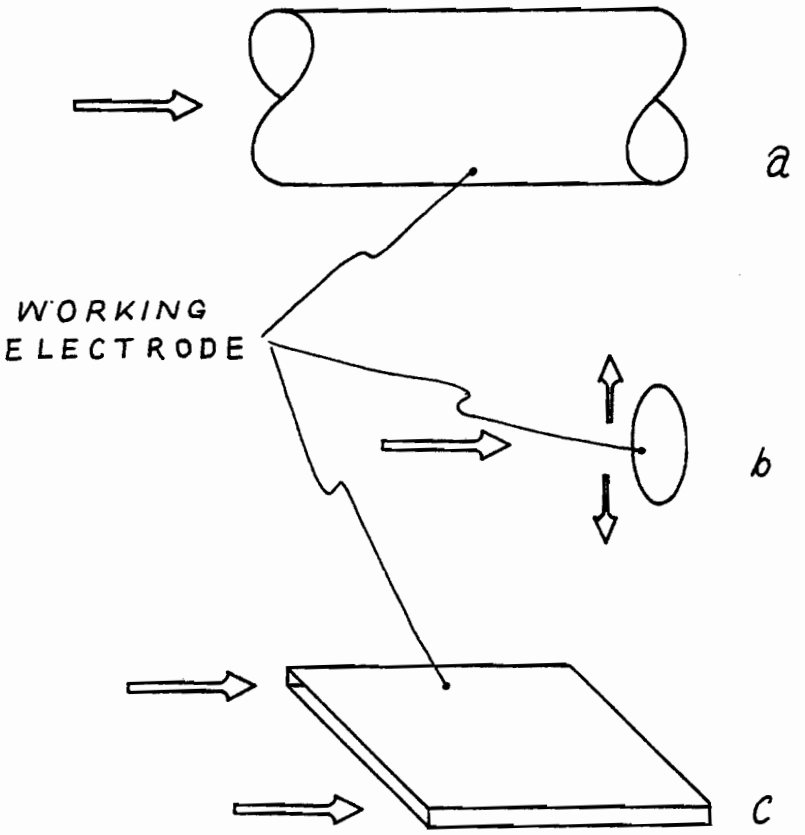

Figure 2: Three electrodes which are analytically useful; a, the tubular electrode, b, the wall-jet electrode and c, the channel electrode. The direction of solution flow is given by the arrows.

of the electrode and the jet are not conducive to optimum electrode geometry. In the former case, a jet less than .025 cm diameter is required for competitive sensitivity. This orifice may be partially blocked during routine analysis leading to irreproducibility. Concerning the second drawback, it is optimum to have the auxiliary electrode opposite and parallel to the working electrode. Since the jet is directly opposed to the working electrode the auxiliary electrode cannot occupy that position. It may, however, take the shape of a ring around the jet.

The channel electrode was described by Matsuda (22) and used for electrochemical detection by Kissinger and co-workers (33). This latter publication initiated an explosion in the use of all types of electrochemical detectors, particularly in high performance liquid chromatography, but especially the tubular, wall-jet and channel configurations. A recent review (34) and a commercial bibliography (35) with 94 references on the application of electrochemical detection to liquid chromatography attest to the popularity of this device. The advantages of the channel electrode are that the cell size is not intimately related to the electrode, the geometry can be brought to a near optimum configuration for a three-electrode potentiostat, the mass transfer rate is easily controlled by changing the thickness or height of the channel, and finally it is simple to build and maintain. The

success is in large part due to the fact that the original design (33) was almost optimal from the start. The only major change made was the placement of the auxiliary electrode opposite to the working electrode (36,37) to improve linearity, but even this alteration was not found necessary in work on differential detection (38,39) where the problems caused by iR drop would be most severe.

C) Theoretical Aspects of Mass Transfer in Flowing Streams

1) The Basic Equation

The differential equations defining heat transfer and mass transfer are, under most circumstances, the same. In each case the flux of heat or mass is equal to a constant times the gradient of the concentration of heat or mass. This gradient, and thus the flux (in an electrochemical context, the current), may be determined by solving a differential equation which is derived from mass balance considerations, i.e., for some species, the number of particles entering any small volume element plus the number created in that volume element minus the number which leave, must equal the change in the number of particles in that volume element in a given time. These similarities allow quantities calculated for heat transfer to be used directly in mass transfer problems. Furthermore, techniques of solution and approximations to ease

solution may be shared by both fields.

With the approximations that the diffusion coefficient and kinematic viscosity are constants, that diffusion in the direction of motion is negligible, that the bulk fluid is incompressible, and that frictional dissipation of heat is negligible the relevant differential equation in three dimensions is (40):

$$\frac{\partial C_i}{\partial t} = D_i \nabla^2 C_i - \vec{v}.\text{grad}C_i + r(C_i, C_j \ldots)$$

where C_i is the concentration of the i^{th} chemical species, t is time, D_i is the diffusion coefficient of the i^{th} species $\vec{v}$ is the velocity vector of the solution and $r(C_i, C_j \ldots)$ represents sources or sinks of species i, i.e., chemical reactions. The early work was concerned with steady state solutions with no source or sink terms, considerably simplifying the equation:

$$D\nabla^2 C = \vec{v}.\text{grad}C$$

The solution of this equation was carried out usually in one of two ways; either by separation of variables or by polynomial approximation of the solutions (specific references will be cited below). If the variables can be separated one

of the resulting differential equations is of the Sturm-Liouville type (41). This type of equation has a solution which is an infinite series of eigen functions multiplied by constants. This set of eigen functions is orthogonal with respect to a weighting function, and so any function may be described by a suitable combination of these functions (42). The solution of this eigenvalue problem is usually done numerically. The polynomial approximation for concentration, introduced by Pohlhausen (43) and von Karman (44), may be used to simplify these problems. Here the coefficients of a polynomial describing C are determined to satisfy the boundary conditions of concentration. The coefficients are dependent upon at least one independent variable. This dependence is determined from the differential equation above.

2) Solutions

The first solution to a problem of this nature was the determination by Graetz (45,46) of the heat flux from a solution initially at a temperature T_1 which flows (in fully developed laminar flow) through a tube held at temperature T_2. The analogous problem in a channel was first solved by Norris and Stried (47) and Prins et al. (48). Fully developed laminar flow is flow in which the functional dependence of velocity on distance from a solid surface is not a function

of distance in the direction of flow. This, of course, is only possible in an enclosed system such as a tube or channel. This does not mean that all flow in enclosed spaces is fully developed; on the contrary when fluid with a uniform velocity enters an enclosed space the retardation effect of the wall affects first only the solution closest to the wall (see Figure 3). Gradually, as the fluid moves farther into the

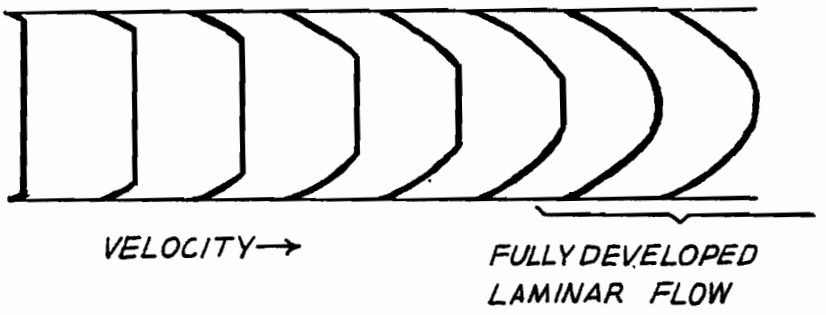

Figure 3

Developing Laminar Flow

enclosed space the effect of the wall on one side of the space meets the effect of the wall on the other side of the space, then the flow is fully developed. The distance that the fluid must flow into the space before the flow is fully developed is given differently according to author and geometry, but for a channel it is roughly .01 $D_h Re$ (49-51)

and for tubes .06 D_hRe (40). D_h is the hydraulic diameter, 4x cross sectional area ÷ perimeter, Re is Reynold's number, VD_h/ν, V = velocity, ν = kinematic viscosity.

Schenk (52) appears to be the first to have studied the problem of a channel in which there is heat flux at one wall and no heat flux at the other wall, (adiabatic wall), analogous to the case in mass transport in which only one wall of a channel is an electrode. By numerically determining the eigenfunctions and eigenvalues of the relevant equation he determined heat fluxes which were calculated easily for long channels but with difficulty for short channels. Sparrow (50) considered the same problem in the case of developing flow and fully developed flow. Using the method of von Karman and Pohlhausen he obtained approximate results valid for short channels. Others (53,54) studied the heat or mass transfer with developing laminar flow and obtained similar results to those previously obtained. Wranglen and Nillson (54) appear to be the first to derive and test a channel device in an electrochemical context. Their results are valid for short channels with developing laminar flow. In a fairly complex analysis Lundberg et al. (55) solved the general problem of heat flux out of a space formed by coaxial cylinders with fully developed laminar flow between the cylinders. The tube is the limiting case when $r_1/r_2 = 0$, (r_1 is the radius of the inside tube and r_2 is the radius of the outside tube), and a pair of flat plates

is the limiting case for $r_1/r_2 = 1$. The solutions are once again in numerical form, due to the expression of final results in series form.

Unlike previous investigators, Matsuda (22) used the Laplace transformation technique to determine current to an electrode in one wall of a short channel with fully developed laminar flow. The use of Laplace transformation allows the determination of current as a function of voltage applied to the electrode. Furthermore, Matsuda determined the current to the electrode when a chemical reaction precedes the electrochemical reaction ($Y \longrightarrow A$; $A \xrightarrow{ne^-} B$), provided that the rate of the chemical reaction meets certain requirements. An Argentinian group (56) tested the theoretical predictions of three investigators [Levich (14) (for the plane plate, not an enclosed channel) Norris and Streid (47) and Matsuda (22)] and found results in qualitative agreement with all three predictions but quantitatively currents were about 10% lower than predicted.

Levich's group (57-59) determined the "complete absorption length", that length of electrode required to electroreact 99% of the material which entered the channel. For electrodes (channels) this long , series solutions previously mentioned can be truncated at one term, and therefore calculations are easy. They compared the complete absorption length for a channel with an electrode in each face to a channel

with an electrode in one face and found the latter to be longer by about a factor of three. Essentially the same result was found by Schenk (52). This same group studied the transient current when changes in the flow rate of solution were made. This has possible analytical implications.

A cell designed for electro-organic synthesis, cylindrical capillary gap cell, was studied by Dworak and Wendt (60). This cell consists of plane disks. Solution emanates from the center of a stack of disks and flows radially. They determined a rigorous solution for not too thinly spaced disks. This solution is a series of polynomial series, each polynomial multiplied by an exponential factor. Using the method of von Karman and Pohlhausen they found that the approximate results were in excellent agreement with the rigorous results.

Recently Matsuda's group (61) has extended its earlier efforts (22) to include catalytic reactions in a short channel with an electrode in one face and with fully developed laminar flow. A catalytic reaction is one in which the product of the electrochemical reaction at the electrode reacts with a species in solution to form the initial electrochemically active species. They have also generalized the preceding chemical reaction mechanism (22) to include slower reactions (62). To solve this case the general principles of Koutecky and Koryta (63) are used to separate the coupled

differential equations. An approximation which had to be made to achieve the result was that the diffusion coefficients of the two species involved were identical.

REFERENCES

1. J.A.V. Butler, Trans. Faraday Soc., 19 (1924) 729.
2. T. Erdey-Gruz and M. Volmer, Z. Physik. Chem. (Leipzig) 150 (1930) 203.
3. H. Eyring, S. Glasstone and K.J. Laidler, J. Chem. Phys., 7 (1939) 1053.
4. J. O'M. Bockris and A.K.N. Reddy, "Modern Electrochemistry" Plenum Press, New York, 1970.
5. R.N. Adams, "Electrochemistry at Solid Electrodes" Marcel Dekker, New York, 1969.
6. K. Vetter, "Electrochemical Kinetics", Academic Press, New York, 1967.
7. D. Britz, J. Electroanal. Chem., 88 (1978) 309.
8. A. Hickling, Trans. Faraday Soc., 38 (1942) 27.
9. D.K. Roe and P. Eggiman, Anal. Chem., 48 (1974) 9R.
10. A. Hodgkin, A. Huxley and B. Katz, J. Physiol., 116 (1952) 424.
11. A. Hodgkin, A. Huxley and B. Katz, Arch. Sci. Physiol., 3 (1949) 129.
12. R. Piontelli, J. Electrochem. Soc., 115 (1968) 1259.
13. B.R. Sundheim, J. Electrochem. Soc., 115 (1968) 158.
14. V.G. Levich, "Physicochemical Hydrodynamics", Prentice Hall, Englewood Cliffs, N.J., 1962.
15. V.G. Levich, Acta Physicochim URSS, 17 (1942) 257.

16. S. Bruckenstein and B. Miller, Acc. Chem. Res., 10 (1977) 54.

17. W.J. Blaedel and G.W. Schieffer, Anal. Chem., 46 (1974) 1564.

18. W.J. Blaedel and G.W. Schieffer, J. Electroanal. Chem., 80 (1977) 259.

19. M. Varadi and E. Pungor, Anal. Chim. Acta, 80 (1975) 31.

20. M. Varadi, M. Gratzl and E. Pungor, Anal. Chim. Acta, 83 (1976) 1.

21. M. Varadi and E. Pungor, Anal. Chim. Acta, 94 (1977) 349.

22. H. Matsuda, J. Electroanal. Chem., 15 (1967) 325.

23. J. Yamada and H. Matsuda, J. Electroanal. Chem., 94 (1973) 189.

24. K. Tokuda and H. Matsuda, J. Electroanal. Chem., 79 (1977) 237.

25. H. Matsuda, J. Electroanal. Chem., 15 (1967) 109.

26. H. Matsuda, J. Electroanal. Chem., 21 (1969) 433.

27. H. Matsuda, J. Electroanal. Chem., 22 (1969) 413.

28. H. Matsuda, J. Electroanal. Chem., 25 (1970) 461.

29. W.J. Blaedel, C.L. Olson and L.R. Sharma, Anal. Chem., 35 (1963) 2100.

30. W.J. Blaedel and L.N. Klatt, Anal. Chem., 38 (1966) 879.

31. W.J. Blaedel and S. Boyer, Anal. Chem., 43 (1971) 1533.

32. K. Stulik and V. Hora, J. Electroanal. Chem., 70 (1976) 253.

33. P.T. Kissinger, C. Refshauge, R. Dreiling and R.N. Adams,

Anal. Letters, 6 (1973) 465.

34. P.T. Kissinger, Anal. Chem., 49 (1977) 447A.

35. Brinkman Instruments, HPLC Bibliography Number 256 (1978).

36. J. Lankelma and H. Poppe, J. Chromatogr., 125 (1976) 375.

37. C. Bollet, P. Oliva and M. Caude, J. Chromatogr., 149 (1977) 625.

38. C.L. Blank, J. Chromatogr., 117 (1976) 35.

39. D.G. Swartzfager, Anal. Chem., 48 (1976) 2189.

40. F.J. Bayley, J.M. Owen and A.B. Turner, "Heat Transfer" Thomas Nelson and Sons Ltd., London, 1972.

41. S.N. Singh, Appl. Sci. Res., Section A, 7 (1958) 237.

42. L.A. Pipes and L.R. Harvill, "Applied Mathematics for Engineers and Physicists" 3rd Ed., McGraw-Hill, New York, 1970.

43. K. Pohlhausen, Z. Angew. Math. Mech., 1 (1921) 252.

44. T. von Karman, Z. Angew. Math. Mech., 1 (1921) 233.

45. L. Graetz, Ann. Physik., 18 (1883) 79.

46. L. Graetz, Ann. Physik., 25 (1885) 337.

47. R.H. Norris and D.D. Streid, Trans. Am. Soc. Mech. Eng., 62 (1940) 525.

48. J.A. Prins, J. Mulder and J. Schenk, Appl. Sci. Res., A2 (1951) 431.

49. H. Schlichting, "Boundary Layer Theory" McGraw-Hill, New York, 1955.

50. E.M. Sparrow, NACA Tech. Note, 3331 (1955).

51. L.S. Han, J. Appl. Mech., 82 (1960) 403.

52. J. Schenk, Appl. Sci. Res., Section A, 5 (1955) 241.

53. K. Stephan, Chemie-Ing.-Techn., 32 (1960) 401.

54. G. Wranglen and O. Nilsson, Electrochimica Acta, 7 (1962) 121.

55. R.E. Lundberg, W.C. Reynolds and W.M. Kays, NASA Tech. Note, D-1972 (1963).

56. A.P. de Iribarne, S.L. Marchiano and A.J. Arvia, Electrochimica Acta, 15 (1970) 1827.

57. E. Ya. Klimenkov, B.M. Grafov, V.G. Levich and I.V. Strizhevskii, Elektrokhimiya, 5 (1969) 202.

58. E. Ya. Klimenkov, B.M. Grafov, V.G. Levich and I.V. Strizhevskii, Elektrokhimiya, 6 (1970) 1024.

59. E. Ya. Klimenkov, B.M. Grafov, V.G. Levich and I.V. Strizhevskii, Elektrokhimiya, 6 (1970) 1028.

60. R. Dworak and H. Wendt, Ber. Bunsenges. Phys. Chem., 80 (1976) 77.

61. K. Aoki, K. Tokuda and H. Matsuda, J. Electroanal. Chem., 76 (1977) 217.

62. K. Tokuda, K. Aoki and H. Matsuda, J. Electroanal. Chem., 80 (1977) 211.

63. J. Koutecky and J. Koryta, Electrochim. Acta, 3 (1961) 318.

CHAPTER II

Immunoassay

A) General Principles

Immunoassay, and more generally, saturation analysis or competitive binding analysis, involves three components; a ligand, a "tagged" ligand and a binder. The two types of ligands each bind to the binder with an affinity K,

$$L + B \rightleftarrows LB$$

and

$$L^* + B \rightleftarrows L^*B$$

yielding

$$\frac{[LB]}{[L][B]} = K_1$$

$$\frac{[LB]}{[L^*][B]} = K_2$$

where L stands for ligand, L* for "tagged" ligand and B for binder. The ligand is generally the analyte and the "tagged" ligand is an analog to the ligand which has been chemically modified in some way so that L* may be measured in the presence

of L. The binder may be an antibody, biological binding protein, biological receptor, or enzyme. For example, in the first reports of such a technique by Yalow and Berson (1,2), the ligand was insulin, the tagged ligand was radioiodinated (^{131}I) insulin and the binder was antibody to human insulin obtained from guinea pigs. Clearly, here the tag is radioactive iodine.

The principle of the technique rests on the fact that both L and L* bind to B. In an equilibrium system containing only L* and B there will be a certain amount of L* bound to B (L^*_b) and a certain amount not bound to B ("free", L^*_f). If to this system an amount of L were added, then, by mass action, L^*_f would increase and L^*_b would decrease. By measuring L^*_f or L^*_b one can determine the amount of L added from a suitable calibration curve. In speaking of the measurement of L^*_f or L^*_b a separation of bound ligand from free ligand is tacitly assumed. A separation step is utilized for most immunoassays, although some do not require it (vide infra). The latter are called homogeneous assays.

For the sake of completeness it should be stated that in certain cases the antibody rather than the ligand is the analyte. In another class of assays [immunoradiometric assay (3)] the antibody is labeled while the analyte (ligand) is not.

Ultimately the sensitivity of an immunoassay depends upon the binding constant for the antibody antigen complex. A higher binding constant will yield a more sensitive assay. Sensitivity is taken to mean the slope of the analytical curve. If one creates an analytical curve by plotting the ratio of bound ligand to free ligand versus the total ligand concentration, the resulting curve is hyperbolic, with a large slope initially and a small slope at large concentration of ligand. Now the concentration of ligand is the sum of the labeled and unlabeled (analyte) ligand. The portion of the curve at which the slope is measured to determine sensitivity is where the concentration of analyte goes to zero. At this point the only ligand in the system is labeled, and therefore, the sensitivity of the assay may be increased by lowering the concentration of labeled ligand.

To achieve maximum sensitivity for a given antibody, and at a given antibody concentration, the concentration of labeled ligand should be a minimum. This definition of sensitivity does not include precision, and thus the conditions for minimizing the lowest detectable quantity of ligand may not be met from a consideration of sensitivity alone. Ekins (4) recognizing the lack of agreement within the field, published a comprehensive paper considering, among other things, the conditions which would minimize the lowest detectable limit. For his analysis he defines sensitivity as the quantity

of analyte ligand which will change the measured quantity (ratio of bound labeled ligand to unbound labeled ligand) by an amount equal to the standard deviation of the measured quantity (measured when analyte concentration is zero). This quantity contains information from the sensitivity (concentration of analyte ligand ↔ measured quantity) and the signal to noise ratio (measured quantity/standard deviation of the measured quantity). It is closely related to the currently accepted figure of merit, the detection limit. As such the derivations based on this quantity are meaningful for practical analytical problems.

Ekins (4) considered the problem in the presence of two noise contributions, counting error and "experimental error". The former error is, of course, valid for spectrophotometric assays which are shot noise limited and photon counting assays. The "experimental" error represents the laboratory preparation error such as pipetting, sample inhomogeneity and other errors. It was shown that, where only counting error is significant, the optimum concentration of labeled ligand is 4/K and that of antibody is 3/K, K is the binding constant of the antibody-antigen complex. One can think of the rather large concentration of labeled ligand as being a compromise between sensitivity (low concentration) and low relative counting error (high concentration). In the case where the experimental error is non-zero, the above concentrations

are no longer optimal. The ratio of the relative standard deviation of the experimental error to the relative standard deviation of the counting error (taken for a concentration of label equal to 1/K) is the criterion on which optimum concentrations of antibody and labeled ligand are based. When this figure is greater than 100, the optimum concentration for antibody is 1/K and that for labeled ligand approaches zero. These conditions strongly resemble the conditions for maximum sensitivity, which is reasonable, since under these conditions a relatively large change in signal (experimental error) will elicit a relatively small change in calculated concentration.

In all cases the concentrations used in the assay are related to K, thus in all cases a more sensitive assay will result from an increase in the binding constant. The analysis of the labeled ligand does not limit the sensitivity, however the precision involved in carrying out the assay does affect the limit of detection. In the previously mentioned report Ekins (4) demonstrated that detection limit lost due to experimental error may be regained by an increase in K.

Zettner (5) pointed out that besides the conditions stated above for zero experimental error, and Berson and Yalow's (6) criterion for maximal sensitivity (concentration of antibody = 0.5/K, concentration of labeled ligand → 0) there is a third often used set of conditions. When the

concentration of antibody is increased, the sensitivity of the assay decreases, however the range of the assay increases. Thus for concentrations of analyte much larger than 1/K, the optimum concentration of antibody is larger than, say, 10/K, the actual value depending on the range desired. The optimum concentration of labeled antigen is 4/3 times the concentration of antibody.

These considerations are important for the creation of new labels. The measurement precision should be such that the label can be measured to a satisfactory degree of precision at a level near the lower limit of the range of values expected for the unknown concentration. It is for this reason that radioactive labels and fluorescent labels have been very popular; they are among the most sensitively detected molecules in analysis. Another criterion for a suitable label is that a similar measurement signal not be present in the native specimen. It is acceptable if there are similar signals in the specimen which may be deliberately not measured, in favor of the intentionally measured label. Radioactivity satisfies both criteria excellently, and as such has been the most widely used label.

B) Non-Radioactive Labels

At the present time, radioactive labels are popular since

the sensitivity of the assay is quite high due to this method of detection. However the cost of counting equipment, the dangers of radiation and the practical problems associated with a radiation laboratory have led to the development of non-isotopic labels which may be used for immunoassay. The requirements of a label are that it lead to sensitive analysis and that it be fairly unique so that the background problem is controllable.

An interesting, if little used, label is bacteriophage (7,8). That antibodies inactivate viruses is well known. If an antigenic group (hapten) is chemically bound to the surface of the phage, then antibody to this hapten will inactivate the phage. When the phage is mixed with a bacterial colony and the colony allowed to grow, the growth may be used as a measure of virus activity and therefore, indirectly as a measure of free hapten (L) in the sample.

A label which is attractive for its simplicity is sheep red blood cells (9). In this analysis a bovine serum albumin (BSA) conjugate of the ligand is coated onto sheep erythrocytes by adsorption. If a certain concentration of these treated erythrocytes is suspended in a suitable buffer and the cells are allowed to settle, they will settle to the bottom of a conical vessel in a clump. In the presence of antibody the cells agglutinate and settle in a diffuse pattern. If free ligand is introduced into the latter system before the

settling period begins, then the antibody will bind to the free ligand, allowing the cells to settle in a pattern visually like the case in wich there is no antibody. This test allows only semiquantitation (by titre). It is also time consuming because of the settling period. The test is called hemagglutination inhibition (HAI).

Fluorescence, being a sensitive analytical tool, has been used as a label (10). In this technique, similar to the techniques of fluorescent microscopy, the assay is for the antibodies. Antigen (ligand) is bound to a paper support. Antibodies to the antigen from a sample will bind to the paper. A fluorescent labeled anti-human IgG is introduced to the paper. After washing, the fluorescent anti-human IgG is eluted from the paper and the fluorescence measured. This gives a measure of the IgG present on the paper and thus in the sample.

In a more elegant fluorescent assay (11-14), the ligand is labeled with a fluorescent molecule. The fluorescence analysis is carried out in synchrony with a rotating polarizer at the source. When a photon is absorbed by a molecule in solution, the molecule remains in an excited state for a short period of time. A molecule in solution also undergoes random rotational motion, characterized by a rotational rate constant or a characteristic rotational time. If the characteristic rotational time is short with respect to the excited state

lifetime, then a population of these molecules absorbing polarized radiation will emit unpolarized radiation. If, on the other hand, the characteristic rotational time is long with respect to the excited state lifetime, then a population of these molecules absorbing polarized radiation will emit only slightly less polarized radiation. Fortuitously, the lifetime of an excited state in fluorescence lies between the characteristic rotational times for low molecular weight ligands ($\sim$ 1000) and high molecular weight [150,000 (15)] ligand-antibody complexes (12). By the previous arguments, it is easily seen that only that ligand which is bound (and has therefore an effective molecular weight of 150,000) will give rise to a polarized fluorescence signal. This method of immunoassay is homogeneous, that is, it does not require separation of bound and free ligand to detect only one or the other. This is a technical advantage of some significance.

Two other fluorescent techniques are being developed by Ullman (16,17). They both may be classed as fluorescence quenching assays but depend on different mechanisms for the quenching. A well known technique for investigating protein structure, radiation transfer, is used in one assay. The ligand is labeled with fluorescine, and the antibody is labeled with rhodamine. Photons emitted from a fluorescing fluorescine molecule may be absorbed by rhodamine with a high efficiency when the rhodamine molecule is close to the fluorescine

molecule. Hence, when the antibody has bound the ligand, and the fluorescine is excited by light, there is a good chance that the analytical signal from the fluorescine fluorescence will be quenched by the rhodamine. Light emitted from free ligand will only be quenched to an insignificant degree. The amount of free ligand may be determined by measuring fluorescine fluorescence, and the amount of bound ligand may be determined by measuring rhodamine fluorescence. In the other quenching technique there are two antibodies present in the system. One is an antibody to the ligand as in other assays. This ligand is labeled with a fluorescent molecule. This fluorescent molecule is the hapten for the second antibody in the system. When the ligand is not bound to the antibody which recognizes it, it may be bound <u>via</u> the fluorescent tag to the antibody recognizing the tag. This causes quenching of the fluorescence. If, however, the labeled ligand is bound to the antibody recognizing the ligand, the antibody to the fluorescent label cannot bind to the label and therefore cannot "quench" the fluorescence. By determining the amount of fluorescence quenching the proportion of ligand bound to antibody may be determined.

Another label which allows homogeneous assay is the nitrosyl free radical (18,19). When the nitrosyl containing molecule is bound to protein it is subjected to local magnetic fields. Since, in the time frame of the experiment, the

protein is relatively motionless, these local magnetic fields cause the absorbance to be very broad. The envelope of energies in the absorbance represents the different magnetic environments of the variously oriented protein bound nitrosyl labels. In contradistinction, the unbound nitrosyl-tagged antigen is free to move on a shorter time scale, causing the local magnetic contributions to the total field to be averaged. Thus each molecule experiences roughly the same field, and the absorbance is sharp. The broad absorbance caused by the protein bound label is, analytically, virtually indistinguishable from background, hence a measurement of the magnitude of microwave absorbance of a sample containing both bound and free ligand, will reflect the concentration of free ligand only. Note the similarity in mechanism between the free-radical detection technique and the polarization fluorescence technique.

Currently, the most popular alternative to radioimmunoassay is enzyme immunoassay (20,21). Three reviews on the same subject (22-24) have appeared in the last three years attesting to its wide acceptance. The label is an enzyme. When the ligand is bound to antibody the enzyme (attached to the ligand) becomes inactivated. When the ligand is free, the enzyme functions, and converts substrate to product. Analytically it is the enzyme reaction which is measured. Two substrate or product measurements are made at different

times, and the difference between them may be related to enzyme activity, hence to free ligand. The initial enzyme reaction used was lysozyme, and the analytical measurement was nephelometric (20,21). As bacterial cell wall fragments were lysed, they dissolved, decreasing light scattering. Many other enzymes have been utilized (22) primarily to obtain higher sensitivity, for instance using NADH fluorescence in a NADH requiring enzyme label. An advantage of the enzyme label is that one can increase sensitivity (and also lower the detection limit) by increasing the time that the enzyme is allowed to manufacture product. Once again this is a homogeneous assay.

A French patent has been awarded to Compagnia d'Ingegneria per la Realizzazione di Opere Techniche S.p.A. (25) for a device which detects the change in enthalpy caused by the binding of ligand to antibody. The antibody is bound to an aluminum substrate which contains a thermal detector. A German patent (26) has been issued for an antigen containing membrane across which a potential difference develops when antibody is on one side of the membrane and not the other.

C) Automated Immunoassay

Immunoassay is only beginning to be automated. The major problem has been the separation of bound and free fractions

for radioimmunoassay. This and the discrete nature of the counting process have impeded the development of labor saving mechanization and automation. Early mechanical aids certainly made the process faster and more reproducible. Devices which aspirate a sample from one test tube and eject the same with an appropriate volume of a buffer (pipettor-dilutor) have been used. Centrifuges for separating precipitated proteins have been made to accept large test tube racks. Counters which automatically place a specimen into the counting area and remove it after a specified time are now common.

The most easily mechanized assays are the homogeneous assays since the troublesome physical separation is avoided. Most of the work, however, has been towards mechanizing the radioimmunoassay, since they are sensitive and have been well tested by various investigators. In a recent review (27) Pollard described a total of 13 "automatic" radioimmunoassay systems, five of which are commercially available. The problem of the separation of bound and free antigen has been solved in several ingenious ways. Johnson (28) used antibody coated test tubes, enabling bound and free to be separated by simply pouring out the contents of the tube after incubation, leaving the bound fraction on the walls of the tube. Landon (29) has championed the use of antibody supported on magnetic particles. They are utilized in a continuous flow system as any soluble reagent. At an appropriate time and place in

the system the particles are held motionless by an electromagnet where they may be washed by the continually flowing stream. After washing away the free fraction, the particles are allowed to flow to a counter where the bound fraction is counted. Union Carbide's contribution is called Centria. Using the centrifugal analysis technique (30) reagents are mixed and incubated. The separation of bound and free fractions is by molecular exclusion chromatography, aided by centrifugal force, making the process sufficiently rapid for routine work. Other systems are immobilized antibody (27), and several separate free ligand after adsorbing it on dextran coated charcoal by filtering out the charcoal.

A more recent contribution (31) not covered in Pollard's review, uses commonly available segmented continuous flow apparatus (as does Landon's magnetic particle instrument). The separation is accomplished by forced filtration of fluid out of the reagent stream which contains antibody bound to Sepharose particles (average diameter 40 μM). This leaves only the bound fraction in the flow stream to continue to the measurement device. This group has suggested that their instrument is useful, not only for radioactively labeled tags, but for enzyme and fluorescent tags as well.

This summary is not comprehensive, there are other less elegant methods of separation of bound from free label. These methods include separation by filtration onto paper

REFERENCES

1. R.S. Yalow and S.A. Berson, Nature, 184 (1959) 1648.
2. R.S. Yalow and S.A. Berson, J. Clin. Invest., 39 (1960) 1157.
3. D. Rodbard and G.H. Weiss, Anal. Biochem., 52 (1973) 10.
4. R.P. Ekins, G.B. Newman and J.L.H. O'Riordan in "Radio Isotopes in Medicine: In Vitro Studies", R.L. Hayes, E.A. Goswitz, B.E.P. Murphy (eds.), U.S. Atomic Energy Commission, Oak Ridge, Tenn. 1968, p. 59.
5. A. Zettner, Clin. Chem., 19 (1973) 699.
6. S.A. Berson and R.S. Yalow, Clin. Chim. Acta, 22 (1968) 51.
7. J. Haimovich, E. Hurwitz, N. Novik and M. Sela, Biochim. Biophys. Acta, 207 (1970) 115.
8. J. Haimovich, E. Hurwitz, N. Novik and M. Sela, Biochim. Biophys. Acta, 207 (1970) 125.
9. F.L. Adler and C.-T. Liu, J. Immunol., 106 (1971) 1684.
10. R.C. Aalberse, Clin. Chim. Acta, 48 (1973) 109.
11. R.D. Spencer, F.B. Toledo, B.T. Williams and N.L. Yoss, Clin. Chem., 19 (1973) 838.
12. W.B. Dandliker, R.J. Kelley, J. Dandliker, J. Farguhar and J. Levin, Immunochemistry, 10 (1973) 219.
13. R.A.A. Watson, J. Landon, E.J. Shaw and D.S. Smith, Clin. Chim. Acta, 73 (1976) 51.

14. A.R. McGregor, J.O. Crookall-Greening, J. Landon and D.S. Smith, Clin. Chim. Acta, 83 (1978) 161.

15. A. White, P. Handler and E.L. Smith, "Principles of Biochemistry", 4th Ed., McGraw-Hill Book Company, New York, 1968, p. 711.

16. E.F. Ullman, A. Schwarzberg and K.E. Rubenstein, J. Biol. Chem., 251 (1976) 4172.

17. E.F. Ullman, Clin. Chem., 24 (1978) 973.

18. R.K. Leute, E.F. Ullman, A. Goldstein and L. Herzenberg, Nature, 236 (1971) 253.

19. R.K. Leute, E.F. Ullman and A. Goldstein, J. Amer. Med. Assoc., 221 (1972) 1231.

20. R.S. Schneider, P. Lindquist, E.T. Wong, K. Rubenstein and E.F. Ullman, Clin. Chem., 19 (1973) 821.

21. K.E. Rubenstein, R.S. Schneider and E.F. Ullman, Biochem. Biophys. Res. Commun., 47 (1972) 846.

22. S.L. Scharpe, W.M. Cooreman, W.J. Blomme and G.M. Laekman, Clin. Chem., 22 (1976) 733.

23. G.B. Wisdom, Clin. Chem., 22 (1976) 1243.

24. A.H.W.M. Schuurs and B.K. van Neeman, Clin. Chim. Acta, 81 (1977) 1.

25. S. Suzuki, M. Aizawa, I. Ishiguro, R. Shinohara and Y. Nagamura, Patent (German) 2,711,288 (Japanese Application) 76/29,632; Chemical Abstracts, Vol. 87, P148332 (1977).

26. C.I.R.O.T. (Compagnia d'Ingegneria per la Realizzazione di Opere Techniche), French demande 2,319,903; Chemical Abstracts, Vol. 87, P196857 (1977).

27. A. Pollard in "Automated Immunoanalysis, Part 2", R.F. Ritchie, ed., Marcel Dekker Inc., New York, 1978, p. 507.

28. E.G. Johnson, B.E. Sturgis and T.E. Stonecypher, Clin. Chem., 22 (1976) 1164.

29. G.C. Forrest and J. Landon in "Automated Immunoanalysis, Part 2", R.F. Ritchie, ed., Marcel Dekker Inc., New York, 1978, p. 567.

30. G. Ertingshausen, S.I. Shapiro, G. Green and G. Zborowski, Clin. Chem., 21 (1975) 1305.

31. A.A.A. Ismail, P.M. West and D.J. Goldie, Clin. Chem., 24 (1978) 571.

32. D. Bagshawe in "Automated Immunoanalysis, Part 2", R.F. Ritchie, ed., Marcel Dekker Inc., New York, 1978, p. 541.

33. H.H. Johnston and B.B. Barbarow in "Automated Immunoanalysis, Part 2", R.F. Ritchie, ed., Marcel Dekker Inc., New York, 1978, p. 549.

CHAPTER III

Preparation and Properties of the Ester of Ferrocene Carboxylic Acid and Morphine

A) Preparation of 3-O-Morphinyl Ferrocene Carboxylate

1) Preparation of Ferrocene Carbonyl Chloride

Ferrocene carboxylic acid (I) was purchased 95% pure from Aldrich Chemical Company, Milwaukee, Wisconsin. In order to purify the compound, the steps involved in the workup

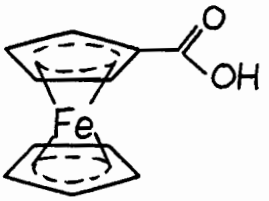

(I)

of a patented process (1) were followed. The final recrystallization was from gasoline, for which petroleum ether was substituted. This did not dissolve sufficient I to be of value. Another recrystallization was attempted after dissolving I in ethanol, adding sufficient water to begin precipitation of solid, warming to redissolve the precipitate and refrigerating the solution for one hour (4°C). The crystals

were collected, washed and subjected to thin-layer chromatography (Methanol:Benzene 10:90 on silica gel G). By comparison to the original material no significant purification was achieved. From similarity in R_f value to a standard, it was thought that one of the impurities was ferrocene. For this reason a recrystallization was attempted from benzene: ethanol (100:50) since the more hydrophobic ferrocene would tend to remain in solution. Sufficient material was not recovered from this step for it to be of value. Although realizing that it would lower the total yield and make the final separation more difficult, it was decided to use the 95% pure material supplied by Aldrich without further purification.

The acid chloride (II) was prepared following Lorkowski et al. (2). Preparations were made for the following reaction:

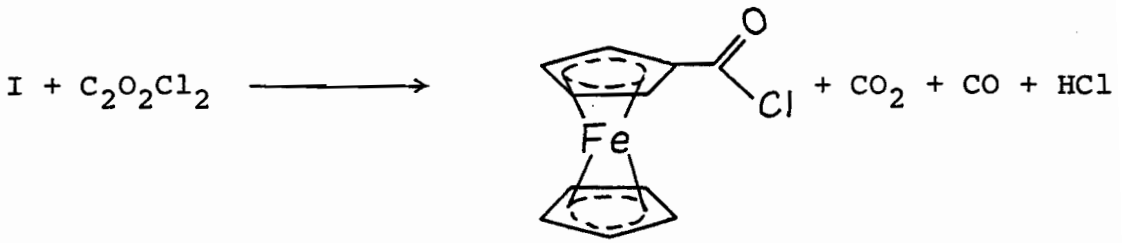

(II)

i) 3.45 g (15 mmole) of I were dried overnight under vacuum at 56°C (boiling acetone) in the presence of P_2O_5;

ii) CH_2Cl_2 was obtained fresh from the storeroom the day

before the reaction. CaH_2 was added to the bottle to remove water;

iii) Glassware and a polytetrafluoroethylene covered magnetic stirring bar were oven dried at 150°C overnight up to the time of the reaction. The vessels were removed from the oven and capped immediately and carried to a fume hood where dry CH_2Cl_2 was poured into the flasks until they were cool.

Into a dry 50 mL round bottom flask 5.7 g of oxalyl chloride were weighed. 20 mL of dry CH_2Cl_2 were added to this flask. The weighed I and 50 mL of CH_2Cl_2 were put in a 100 mL round bottom flask and stirred on ice for 15 minutes, after which time dissolution of the material was not complete. The CH_2Cl_2 had become sufficiently colored (yellow) that the reaction was initiated. One mL aliquots of the oxalyl chloride solution were added under dry N_2 with a flame-dried disposable glass delivery pipette at roughly one minute intervals. The addition took place over the course of 30 minutes. The suspension turned reddish orange. The mixture was kept in an ice-water bath the entire time. When the addition of oxalyl chloride was complete the ice bath was removed. As the mixture warmed to ambient temperature, vigorous evolution of gas commenced. The glass stopper on the flask was replaced with a septum-needle-drying tube (Drierite, $CaSO_4$) to allow free passage of the gases. After 1 hr at ambient temperature

the suspension was placed on a 50°C oil bath causing the suspended solids to dissolve. After 45 minutes on the oil bath, the solvent and excess volatile reagents were removed by applying a vacuum while the flask was on a rotary evaporator. The flask was maintained at 50°C. The vacuum was applied with a water aspirator. This necessitated placing a drying tube (Drierite, $CaSO_4$) in series with the trap and aspirator to guard against hydrolysis of the product. The evaporated solvent was collected at liquid N_2 temperature. The product was a red oil with the characteristic odour of an acid chloride. In the original reference (2) the material stood 15 hr before solidifying, thus the oil was kept, capped, at ambient temperature overnight.

The oil had not solidified overnight, nevertheless, the literature procedure was followed. The oil was extracted thrice with boiling pentane. A green sticky oil remained in the reaction vessel after the extraction. The pentane extract was evaporated to about 10 mL and put in a dessicator to stand. A red oil came out of the pentane. The pentane was removed by applying a vacuum to the dessicator. The red oil was placed in the freezer (-15°C) for 10 minutes. Upon warming to ambient temperature, red crystals were seen in the oil. After crystallization had proceeded for 2 hr, the mixture (about half oil half solid) was dissolved in CH_2Cl_2 (2 mL) and placed in a hood to allow crystallization from

solution to occur. After 16 hr the product had turned to a brown oil.

The previous synthesis was considered successful except for the final step. With respect to the lability of II, the synthesis was repeated exactly the same way except that one fifth of the starting material was used. No effort was made to crystallize the red oil obtained from the resynthesis. The presence of a green residue in the reaction mixture and the alteration of the material on exposure to air were sufficient warning that II was suceptible to oxidation. For this reason extensive purification and crystallization steps were not undertaken. The oil was kept on ice and capped and the reaction with morphine was commenced without delay.

2) Preparation of Morphine

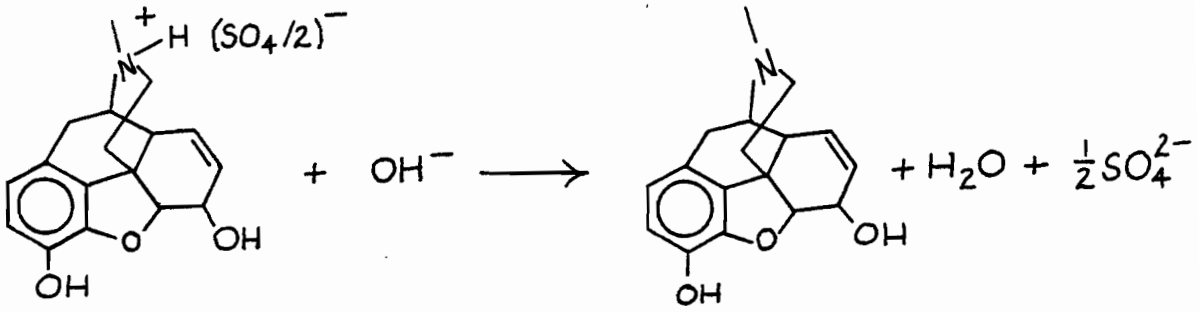

Before the synthesis of II was initiated, morphine was

prepared from morphine sulfate, supplied by Allan and Hanburys, Toronto. About one millimole (365 mg, 1.05 mmole) of morphine sulfate was dissolved in roughly 10 mL of distilled water. One and a tenth mL of 1 M KOH were added. The precipitate was filtered with a fine fritted glass Büchner funnel and washed with water. After overnight drying under vacuum at 56°C (boiling acetone) in the presence of P_2O_5, 230 mg of morphine were obtained (.81 mmole, 77%). This material was stored in a dessicator (silica gel dessicant) in the dark. This precipitation was repeated as necessary to obtain free base.

3) Preparation of the 3-O-Morphinyl Ester of Ferrocene Carboxylic Acid

II + 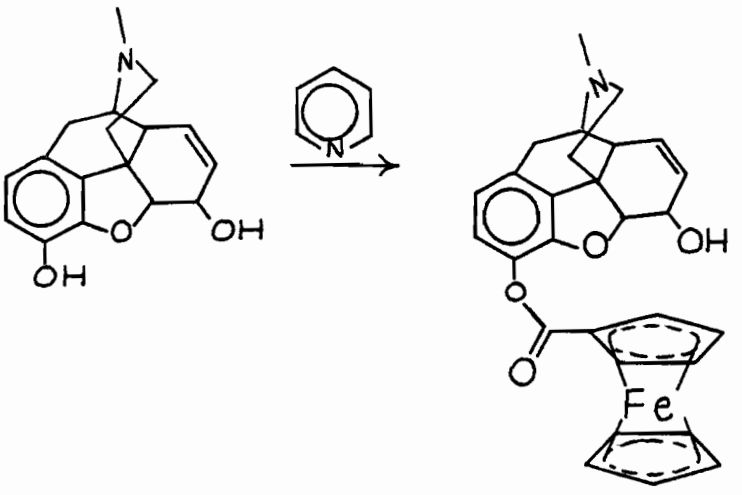 + salts

About one millimole (294 mg, 1.03 mmole) of morphine was dissolved in a few mL of dry pyridine. The pyridine had been distilled from KOH and stored over activated molecular sieves (Linde 3A). To minimize the exposure of II to air, the oil was added dropwise with a dried disposable glass delivery pipette to the morphine solution, without weighing. To determine when the appropriate amount of II had been added, the reaction was monitored by thin-layer chromatography. Since the product was not on hand before the reaction, the thin-layer chromatographic properties of the product (III) had to be anticipated. The phenol group is sufficiently acidic that a relatively strong solvent is required to lend morphine a significant R_f on silica gel. Substitution at the phenol group, as in codeine (3-O-methyl morphine) makes the compound more mobile resulting in a larger R_f. Thus any product of the reaction would be expected to have a larger R_f than morphine. Besides the R_f information, chemical information can be garnered from interpretation of the reactions of spray reagents with the components of a mixture. The ferrocene derivatives are yellow and thus spots with a yellow color can reasonably be expected to have a ferrocene moiety. Confirmation of this fact could come from reaction of the yellow spot in I_2 vapour to yield a light blue to blue-green spot, indication of the oxidation of the ferrocene moiety to ferricinium (iodide). Morphine and other opium

alkaloids have been analyzed for many years by thin-layer chromatography, resulting in some very sensitive and relatively specific spray reagents. The most popular reagent is probably a mixture of chloroplatinic acid and potassium iodide called iodoplatinate (3, p. 883). Morphine yields a midnight-blue spot and codeine yields a mottled-purple spot upon application of iodoplatinate, if the basic components of the solvent system have been sufficiently removed by oven drying. This reagent reacts with most tertiary amines, and with other amines to varying degrees. The solvent system chosen was methanol:aqueous ammonia (30%) (95:5). As will be pointed out later it is not a particularly good system, but it gave sufficient resolution to show spots in the reaction mixture chromatogram which were not present in a chromatogram of a mixture of morphine and I.

The reaction was initiated by adding ten drops of the red oil II to the pyridine solution of morphine. Ten minutes later a sample was taken for thin-layer chromatography [Methanol:aqueous ammonia (30%), (95:5)]. The results are shown in Table 1. The spot at R_f 0.59 fulfilled the expectations of the reaction product. The blue nature of the region near R_f 0.8, which may be associated with the yellow spot at R_f 0.83 and thus be interpreted as a product of morphine, is probably due to pyridine. The qualitative appearance of this blue region was a large and diffuse spot,

Table 1

Thin-layer chromatography of starting materials and reaction products on silica gel G (Merck), solvent system, methanol:aqueous ammonia (30%) (95:5).

Sample	Component	R_f	Color	Reaction with iodoplatinate
standard	morphine	0.56	-	blue
standard	I	0.87	yellow	-
reaction		0.56	-	blue
		0.59	yellow	purple
		0.83	yellow	blue around edge
		0.87	yellow	-
standard	pyridine	∿0.8	-	blue

as was the standard spot of pyridine due to its relatively large diffusion coefficient. Thus the spot at 0.59 was assumed to reflect the course of the reaction, although its nature was not, at that point, known. After additions of 7 drops of II at 20 minutes, 7 drops at 50 minutes, 5 drops at 80 minutes and thin-layer chromatography at 10 minutes, 30 minutes, 60 minutes, 100 minutes, it was decided that the reaction was not proceeding any further and that more reaction time would increase the risk of product hydrolysis or oxidation. The reaction mixture was diluted with 20 mL of dry (CaH_2) CH_2Cl_2 and filtered through a medium glass fritted Büchner funnel to remove pyridinium hydrochloride. The filtrate, a clear red-brown solution, was capped and stored in the freezer (-15°C) overnight.

The solution did not change overnight. Initial attempts to obtain crystals from concentrating the solution or keeping the resulting oil in the freezer were fruitless. A thin-layer chromatography check showed that there was virtually no change in the mixture due to the manipulations. Before attempting chromatographic separation of the mixture a more suitable solvent system was needed. Reference to Stahl (3, p. 440) provided two potentially useful systems based on the separation of morphine and codeine; $CHCl_2$:acetone:diethylamine (50:40:10) on silica gel G was purported to yield R_f's: morphine .10, codeine .38, and $CHCl_3$:diethylamine

(90:10) was purported to yield, morphine 0.08, codeine 0.53. The latter system was tried with the favorable results shown in Table 2. There are two components which may be ferrocene

Table 2

Thin-layer chromatography showing adequate separation of starting materials from reaction products. Silica gel G adsorbent, solvent; $CHCl_3$:diethylamine (90:10).

Sample	Component	R_f	Color	Reaction with iodoplatinate
standard	morphine	0.10	-	blue
standard	I	0.05	yellow	-
reaction		0.05	yellow	-
		0.10	-	blue
		0.65	yellow	blue (major spot)
		0.70	yellow	blue
		0.88	yellow	-

carboxylic acid esters of morphine, one represented by a spot at R_f 0.65, the major reaction product, and a minor spot at R_f 0.70. The component corresponding to the major spot was isolated by preparative thin-layer chromatography. The plates, prepared by Dr. Ogilvie's research group, were 1 mm thick

silica gel G (Merck) with calcium sulfate binder. The oil resulting from the synthesis was diluted 50:50 with CH_2Cl_2 and half of the solution was streaked on two plates which had been dried 24 hr at 110°C. The other half was stored in the freezer. The mixture was separated using $CHCl_3$:diethylamine (90:10), the appropriate region of silica gel was collected and the orange material was eluted from the silica gel with $CHCl_3$ and diethylamine. The solvents were evaporated, the oil taken up in one half mL benzene. While shaking this solution, 20-30 mL of petroleum ether were rapidly added to the solution. The precipitated solid was collected on a fine fritted glass Büchner funnel. At this point nuclear magnetic resonance spectra were taken to aid in the identification of the material. Although it is improbable that major absorption shifts or splitting pattern shifts due to the esterification would have occurred, it was thought advisable to compare the spectrum to un-esterified morphine to determine if there were absorption or splitting changes indicative of another product. Infra-red spectra were recorded of a pellet (KBr) made from the product, and a pellet with a mixture of morphine and ferrocene carboxylic acid. This particular batch of III will be called IIIa to differentiate it from the other batch of III to be discussed.

After several interesting but low yield attempts at other derivatives, IIIa (which had been kept at room temperature

for four months) was repurified by preparative thin-layer chromatography. Before repurification, the impurity seen in the chromatogram was only a few percent (estimated by spot area) of the total material. This material was chromatographed with a solvent of $CHCl_3$:acetone:diethylamine (50:40:10). The material was eluted from the silica gel with acetone. Overnight orange crystals appeared. A sample of these crystals was subjected to 90 MHz FT-NMR (^1H).

The remaining crude material from the reaction, after having been in the freezer (-15°C) for four months, was subjected to preparative thin-layer chromatography using $CHCl_3$:acetone:diethylamine (50:40:10) which was kept in the chromatography chamber 24 hr before the separation. This saturation (usual saturation times were on the order of one hour) increased the resolution and a clean separation of the major product was obtained. The material was eluted from the silica gel with acetone, a little $CHCl_3$ and a few drops of methanol. The resulting material, when checked by thin-layer chromatography, was found to have a small amount of material which did not correspond to the major product. Clearly another separation step was in order but, since the remarkably good resolution of the previous separation was not adequate, another solvent system was sought. Mixtures of other solvents with solubility parameters similar to $CHCl_3$ (toluene, diethyl ether), and diethylamine could not separate

the two similar reaction products (corresponding to R_f 0.65 and 0.70 in Table 2). Thus various mixtures of $CHCl_3$ and diethylamine were attempted with the results shown in Figure 1. The separation is adequate between 60 and 85 volume percent $CHCl_3$ in a $CHCl_3$:diethylamine solvent system. Qualitatively the separation appeared best in the 85 volume percent $CHCl_3$ system, and it was this that was used for the second preparative thin-layer chromatography separation of III. Using procedures already stated the appropriate band was separated cleanly and eluted from the silica gel. Slow evaporation of solvent yielded orange crystals. This fraction is labeled IIIb.

B) The Examination of the Product by Physical and Chemical Methods

The examination of a compound by physical methods reveals two indistinctly separated classes of information. On the one hand there is information which is expected to result from a given examination, and this information is generally used as proof of a structure. On the other hand there is information which is new information which cannot prove a structure but which can give a clearer picture of a molecule's properties, and may be used to support a hypothesized structure. The difference between the two classes is in the quantity of existing experimental and theoretical information

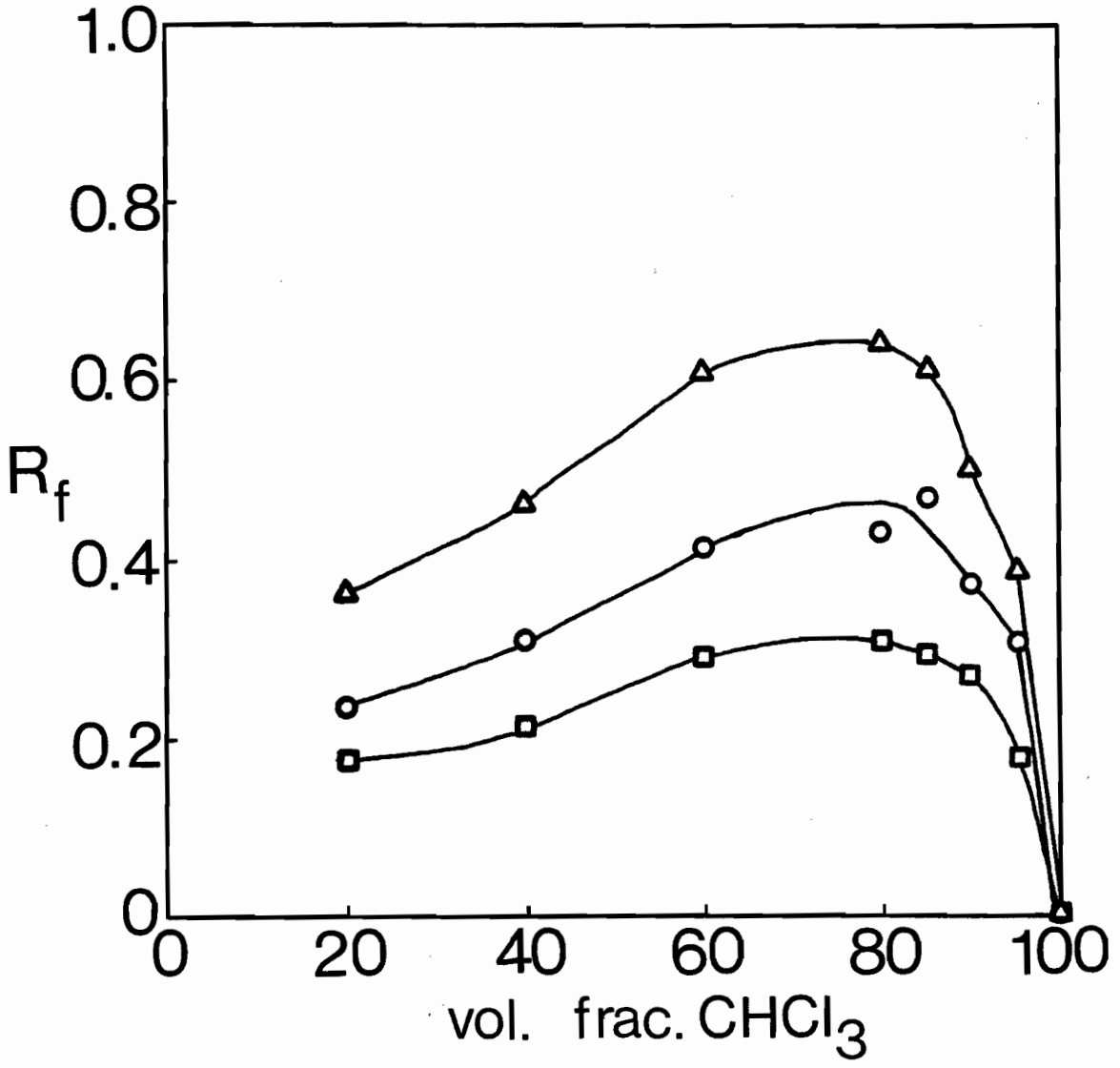

Figure 1: R_f plotted as a function of volume fraction of $CHCl_3$ in a binary solvent mixture of $CHCl_3$ and diethylamine. △ undesired impurity, O major reaction product, □ minor reaction product in IIIb.

pertaining to the physical measurement under consideration. Most of the information generated was of the former category. No one piece of information conclusively proves the structure of III, but all the evidence taken together strongly indicates that the structure of III is the 3-O-morphinyl ester of ferrocene carboxylic acid.

1) Evidence which indicates the Ferrocene Moiety is Present

a) Color: The compound has the characteristic color of ferrocene compounds, an orange-yellow. This color is not separable from the morphine-like properties in any chromatographic system tried.

b) ^{1}H-NMR: The spectra of ferrocene carboxylic acid, morphine, and III are shown in Figues 2-5. Ferrocene carboxylic acid displays a singlet at 4.28 ppm (δ) vs TMS (all absorbances will be referred to TMS, although in some cases they were measured against residual acetone in d_6-acetone or $CHCl_3$ in $CDCl_3$), a multiplet at 4.48 ppm and another multiplet coupled to the first at 4.85 ppm. The pair of multiplets integrate to 25 and the singlet integrates to 30. This is in accord with assignments like those for acetylferrocene (4, p. 88) the singlet corresponds to the unsubstituted ring and the multiplets to the substituted ring, the downfield multiplet represents the protons ortho to the substitution. Except for an absorbance near 4.8 ppm (partially occluded

Figure 2: 60 MHz ^{1}H-NMR of ferrocene carboxylic acid in deuterated acetone.

Figure 3: 100 MHz ^{1}H-NMR of morphine (free base) in deuterated methanol.

Figure 4: 100 MHz ^{1}H-NMR of IIIa in deuterated methanol.

Figure 5: 90 MHz ^{1}H-FTNMR of IIIb in deuterated acetone plus deuterated chloroform.

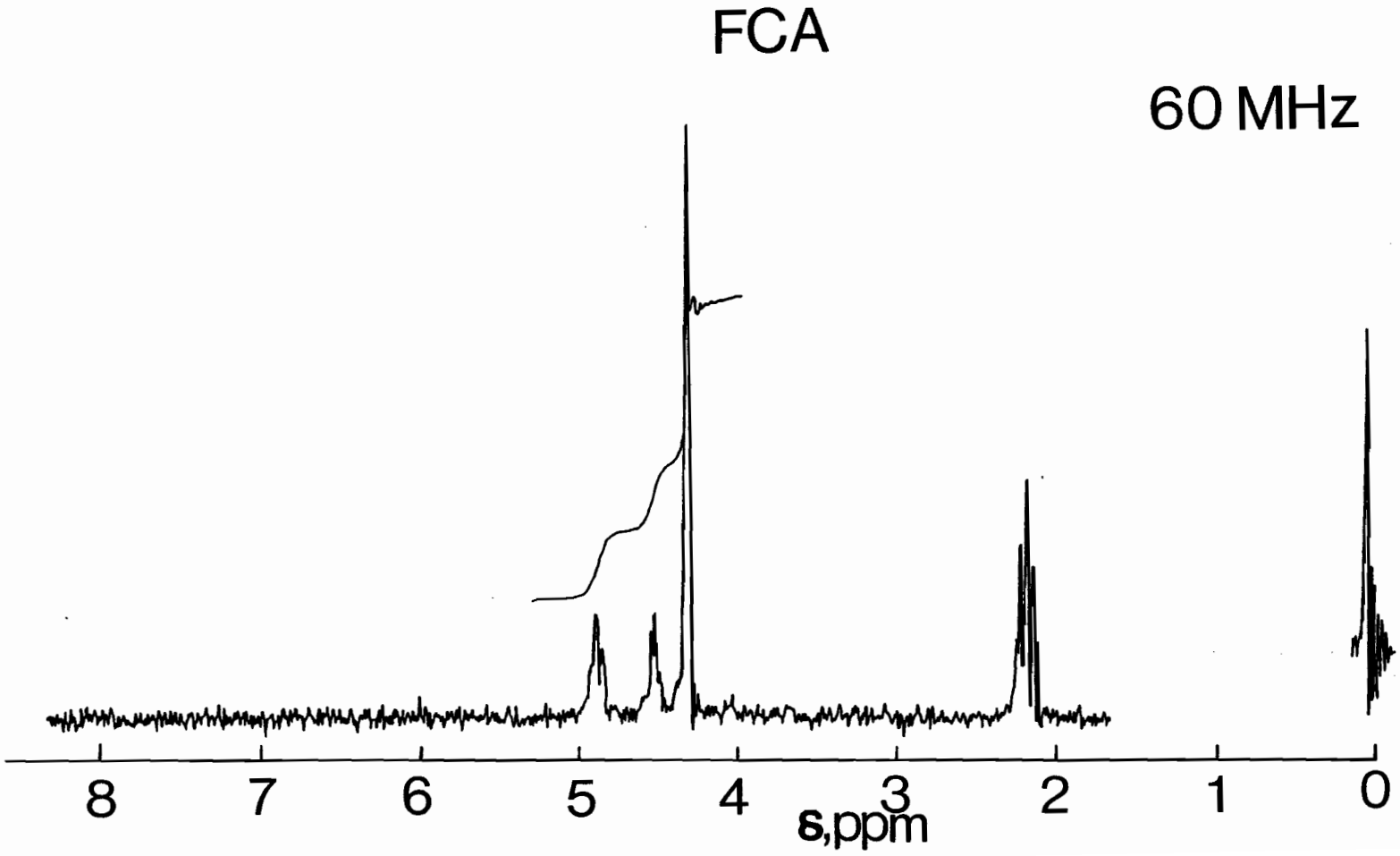
FCA
60 MHz
8
7
6
5
4
3
2
1
0
δ,ppm

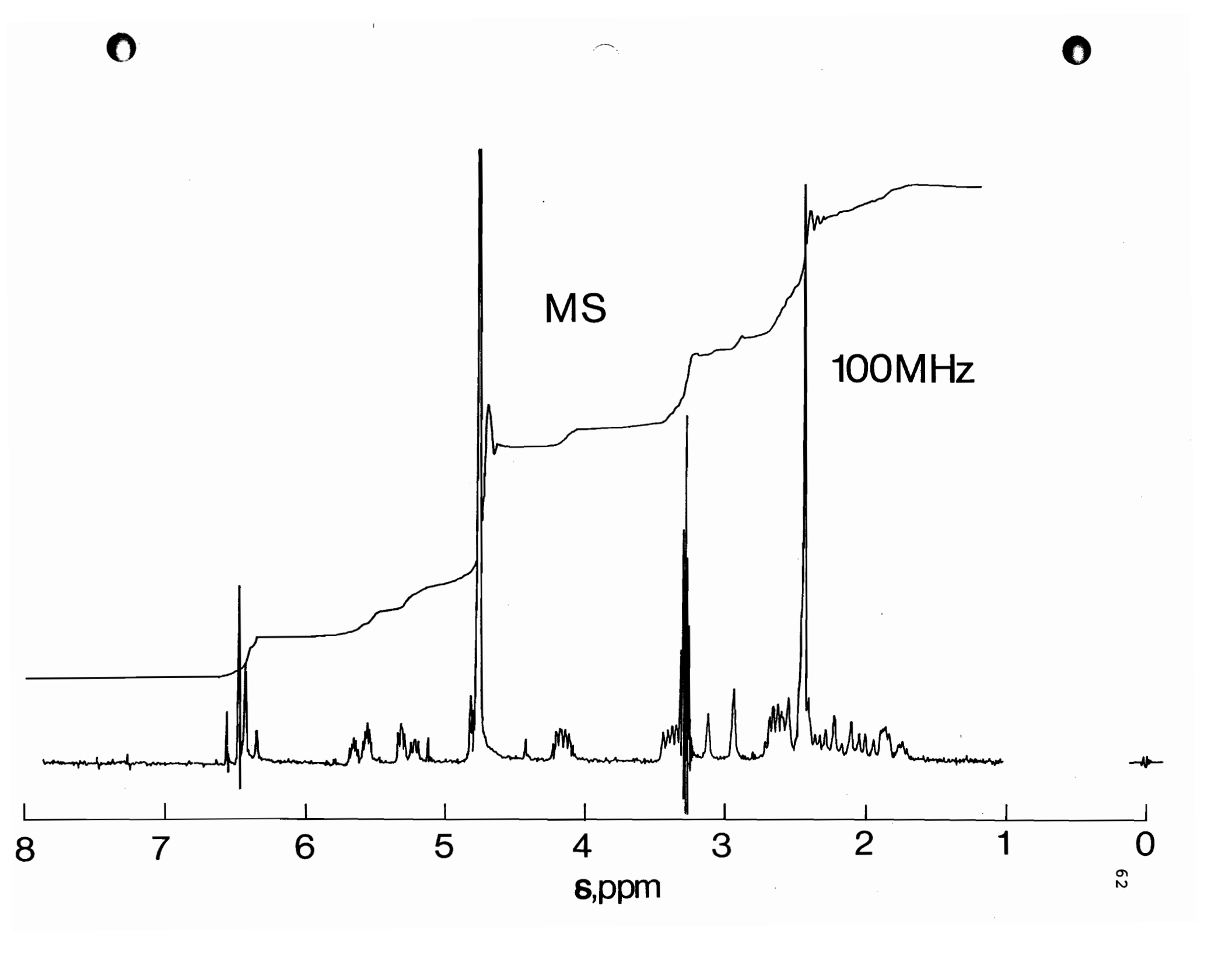
MS
100MHz
8
7
6
5
4
3
2
1
0
δ,ppm

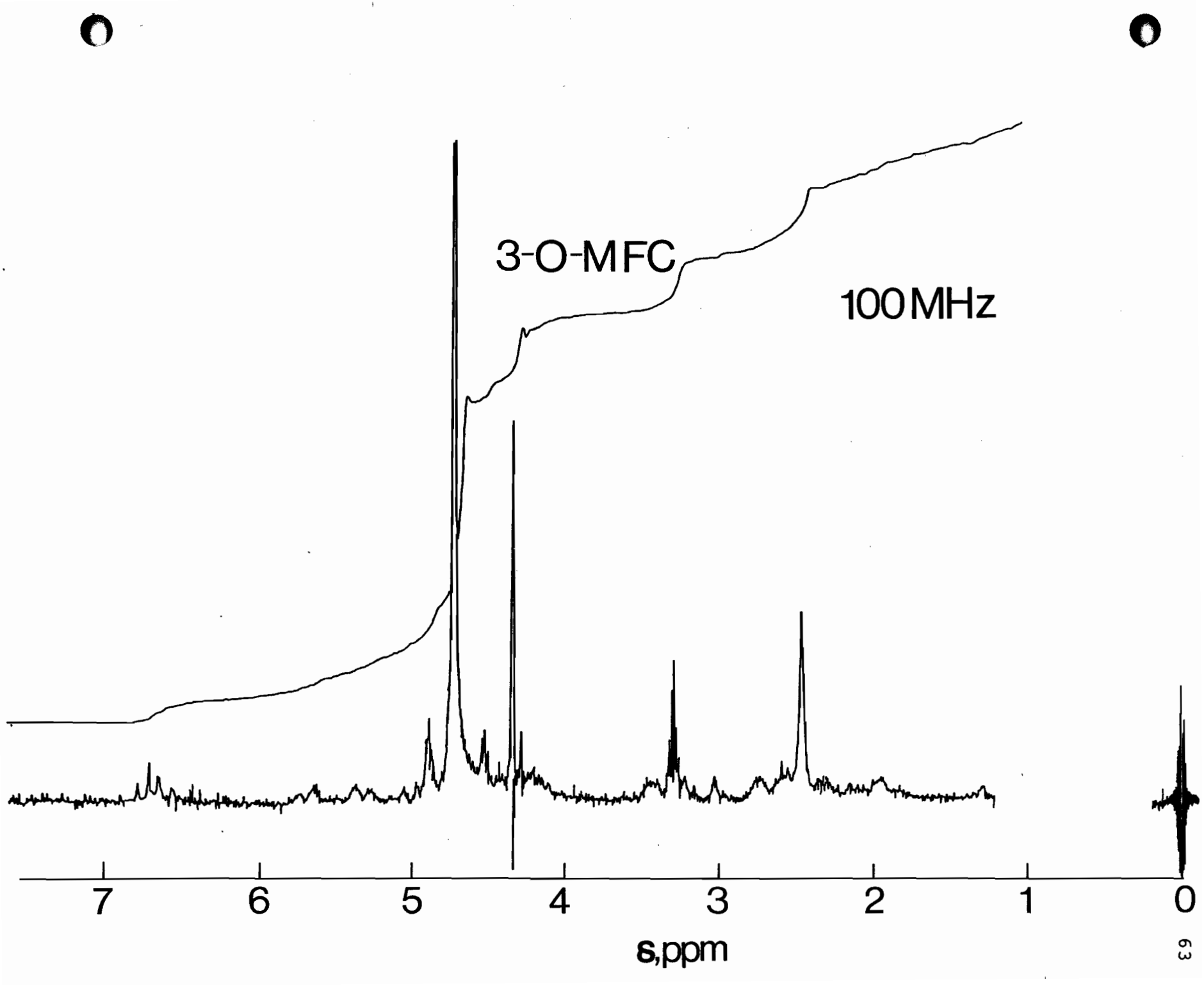
3-O-MFC
100MHz
7
6
5
4
3
2
1
0
δ,ppm

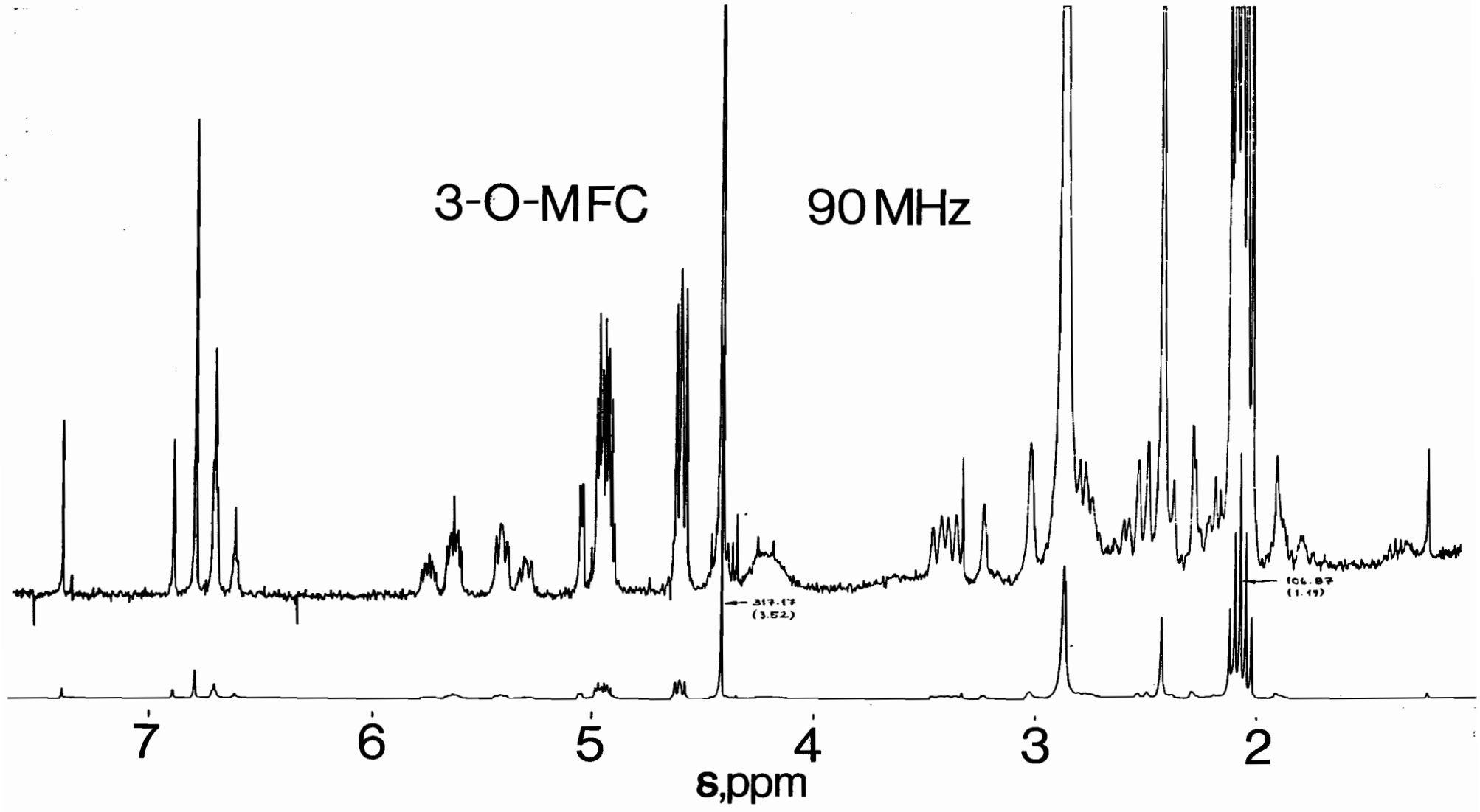
3-O-MFC
90 MHz
317.17
(3.52)
104.87
(1.19)
7
6
5
4
3
2
δ,ppm

by the OH absorption from methanol in the CD_3OD) morphine is free of features in this region from δ=4.2 to 5.0 (Figure 3). In Figures 4 (IIIa after only one thin-layer chromatographic purification) and 5 (IIIb) these features of the carboxy-substituted ferrocene are clearly in evidence. IIIa demonstrates a singlet at δ=4.34 ppm and a triplet at 4.52 ppm with a multiplet at 4.90 ppm and IIIb demonstrates a singlet at 4.41 a triplet at 4.60 and a multiplet at 4.94 ppm. In Figure 5 (IIIb) it can be seen that the multiplet appears to be a pair of triplets indicating a difference in chemical shift between the two protons ortho to the carboxyl substitution.

c) U.V.-visible spectrophotometry: Transmission spectra were recorded with a Beckman DB spectrophotometer using Beckman 1 cm pathlength silica cells. The reference cell contained the solvent 0.1 M pH 6.0 phosphate buffer. The visible portion of the spectrum shown in Figure 6 demonstrates similar absorbances for ferrocene carboxylic acid (I) and III; a broad absorbance at 440 nm for I and a broad absorbance at 450 nm for III. Morphine is featureless in this region. Concentrations were I, 4.13×10^{-4}M, morphine sulfate 4.82×10^{-4}M, III, 217×10^{-4}M.

2) Evidence which indicates the Morphine Moiety is Present

a) Reaction with iodoplatinate: As previously mentioned

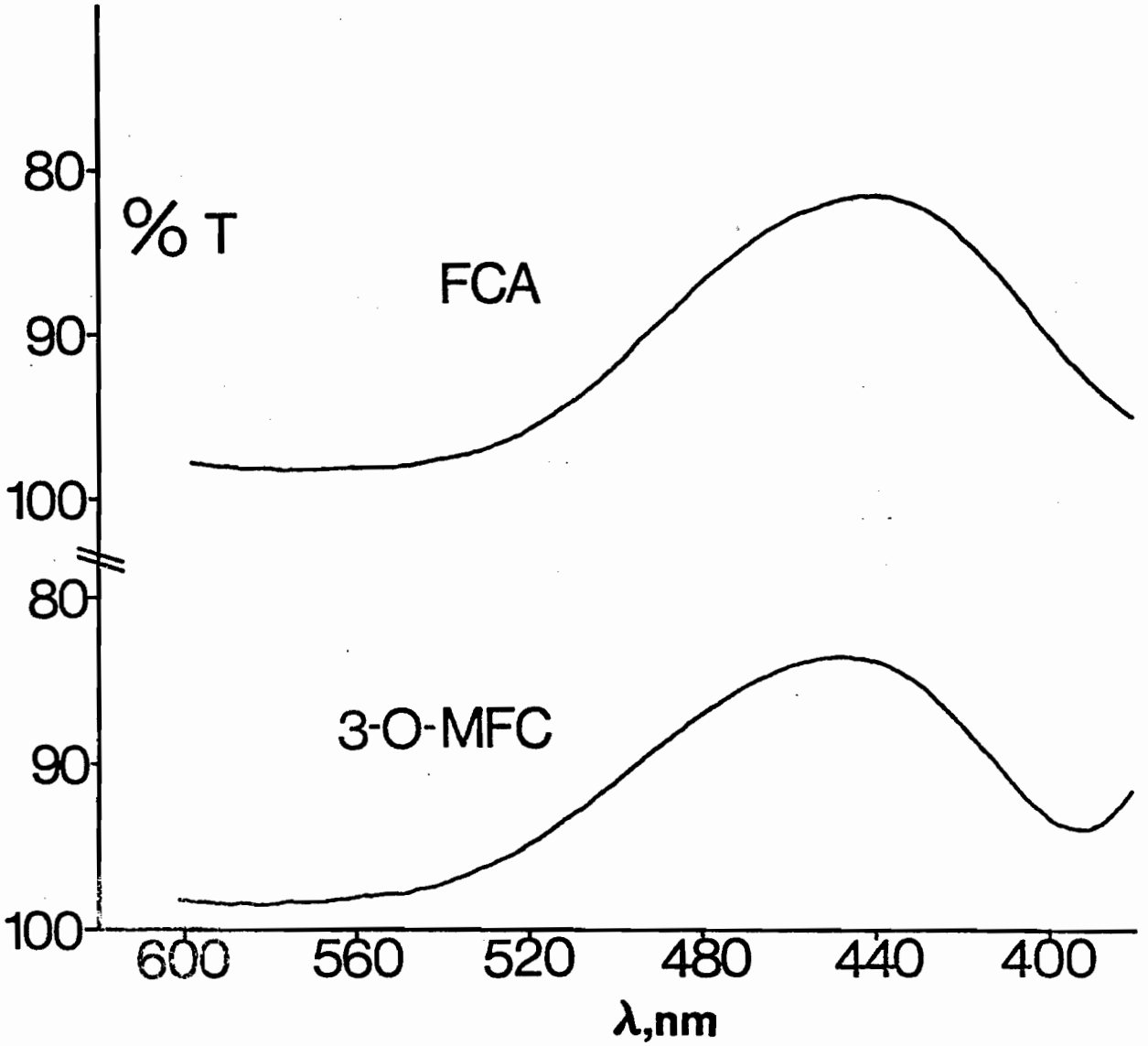

Figure 6: Visible transmittance spectra of I (labeled FCA) and IIIb (labeled 3-O-MFC). The solvent was aqueous 0.1 M pH 6.0 phosphate buffer. The scan rate was 40 nm min^{-1}, the slit program was "medium", on the Beckman DB. The reference path contained the buffer alone. One cm path length silica cuvettes were used.

the reaction of III with iodoplatinate was very similar to the reaction of codeine with iodoplatinate.

b) ^{1}H-NMR: Reference to Figures 2-5 demonstrates the similar nature of proton absorbance for III and for morphine. In particular a few clear cut features are produced in each spectrum. Between δ=6 and 7 the absorbances due to the two aromatic protons on the morphine are visible. The splitting pattern is unchanged indicating no alterations in the position of the substitutions in the ring. Between δ=5.2 and 5.8 the allylic absorption is virtually identical in each spectrum. At δ=2.42 in each spectrum the N-CH_3 singlet is seen. Other general features of the aliphatic portion of the spectrum are noticeable.

c) U.V.-visible spectrophotometry: Figures 7a-c show the U.V. transmittance spectra of I, morphine, and III in 0.1 M pH 6.0 phosphate buffer recorded vs the phosphate buffer. The phenol absorbance in morphine can be seen at 283 nm (ε=1,300). I is featureless at $\sim$ 280 nm and III demonstrates a distinct shoulder at $\sim$ 280 nm. The concentrations of the analytes were I; 4.13×10^{-4} M, morphine; 4.82×10^{-4} M, III; 2.17×10^{-4} M.

3) Evidence which indicates that III is the 3-O-Morphinyl Ester of Ferrocene Carboxylic Acid

a) When the morphine phenol undergoes a one electron

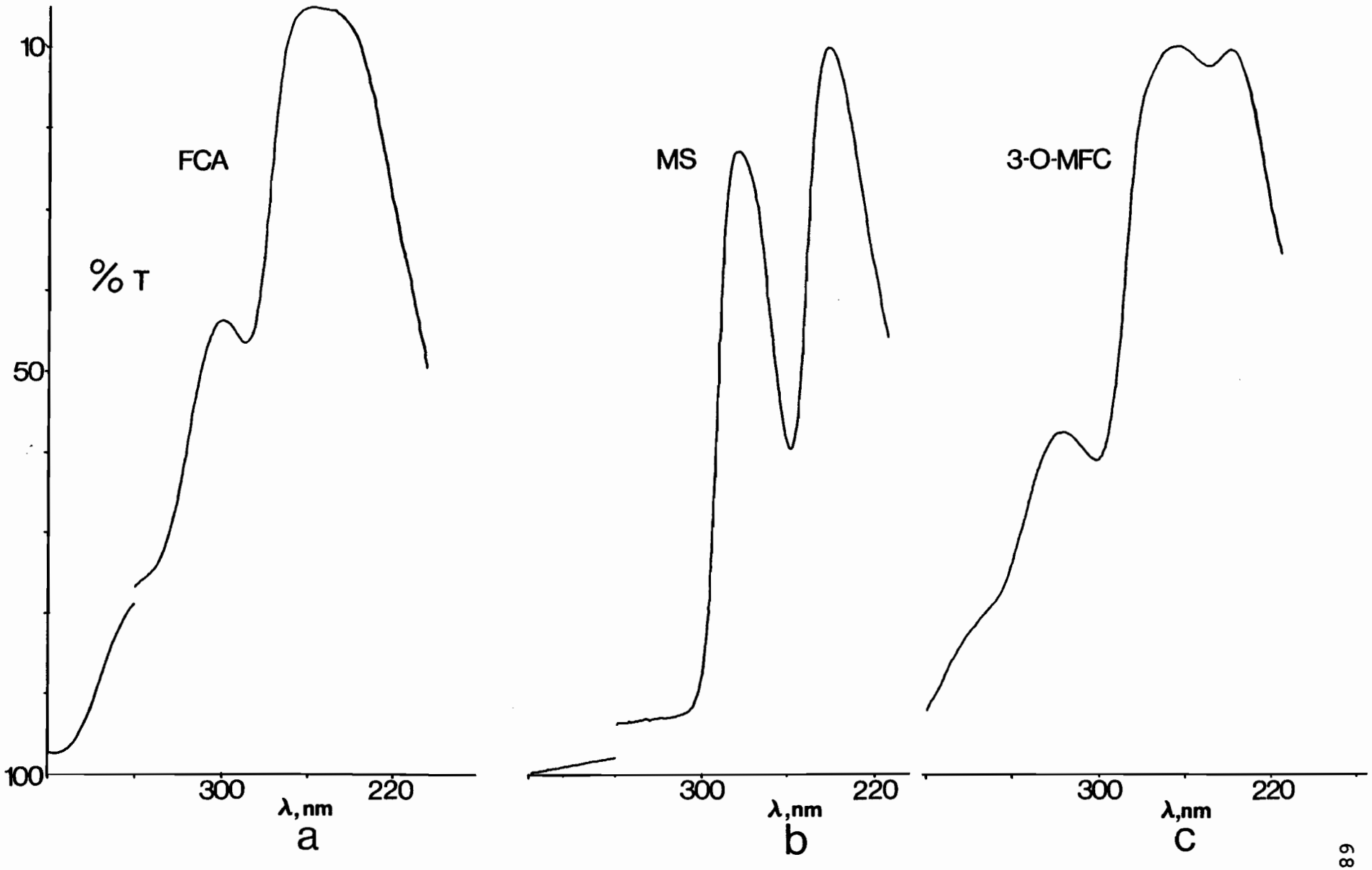

Figure 7: Ultraviolet transmittance spectra of a) I, b) morphine sulfate and c) IIIb. The D_2 lamp was used for wavelengths less than 340 nm. Other conditions were as in Figure 6.

oxidation a dimerization occurs at the 2 position to yield the fluorescent pseudomorphine (5). According to Stahl (3, p. 438), the use of the Kupferberg reagent, which is a mild one electron oxidant (a mixture of potassium hexacyanoferrate (II) and potassium hexacyanoferrate (III)) is specific for phenanthrene derivatives containing free phenol. Morphine falls in this category, while codeine and the presumed structure for III do not. Accordingly, after chromatography, the Kupferberg reagent, prepared by dissolving 7.8 mg of $K_4Fe(CN)_6$ and 57 mg of $K_3Fe(CN)_6$ in 100 mL of distilled water, was sprayed on the plate with the results shown in Table 3. It would seem that III is not a phenanthrene

Table 3

Thin-layer chromatography of morphine, codeine and III on silica gel G, solvent $CHCl_3$:acetone:diethylamine (50:40:10). F_1 indicates fluorescence elicited by a "long wavelength" (∿340 nm) lamp before spraying with Kupferberg reagent. F_2 indicates fluorescence elicited by the same lamp after spraying with the Kupferberg reagent.

Sample	Component	R_f	F_1	F_2	Color
standard	morphine	.07	no	yes	none
standard	codeine	?	no	no	none
III		.47	no	no	yellow

derivative containing a free phenol. That much of the phenanthrene structure is preserved in III is borne out by the ^{1}H-NMR evidence, thus in all probability III is not a free phenol.

b) Infra-red: The infra-red absorption spectrum of IIIa was taken as a KBr pellet. The instrument used was a Perkin Elmer 297. The scan time was 8 minutes. The spectra are shown in Figure 8, 1.1 mg morphine + 1.1 mg ferrocene carboxylic acid + 100 mg KBr, and Figure 9 2.0 mg III + 100 mg KBr. Table 4 reveals the salient features of the spectra

Table 4

Infrared Spectra-Features

Component	Figure	Absorbance	Feature
I	8	∿3000 broad	carboxylic acid OH---O stretch
morphine	8	∿3200-3250 broad	phenolic OH---O stretch
?	9	3500 sharp	?
	8	3360	(?) overtone of C=O
?	9	3510 sharp	?
III	9	3500 broad	aliphatic OH---O stretch
I	8	1660	C=O
III	9	1720	C=O

MS + FCA

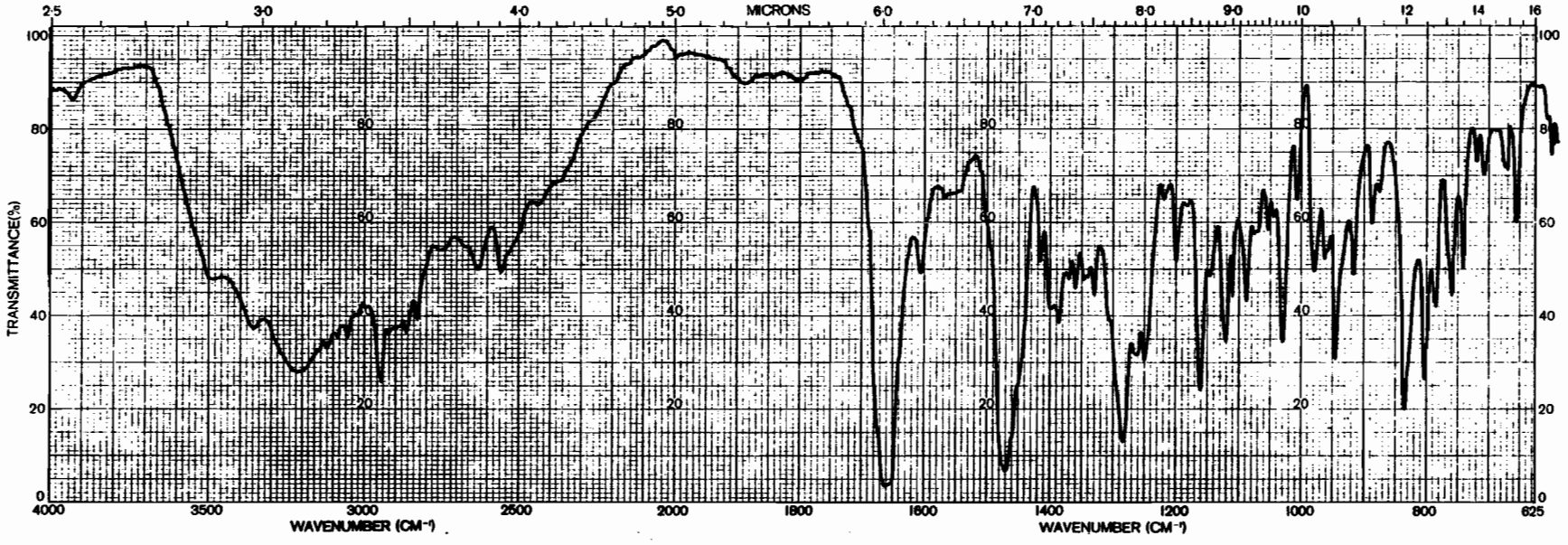

Figure 8: I.R. transmittance spectrum of morphine (free base) plus I. The KBr pellet (100 mg) contained 1.1 mg of I and 1.1 mg of morphine. Scan time was 8 minutes.

3-O-MFC

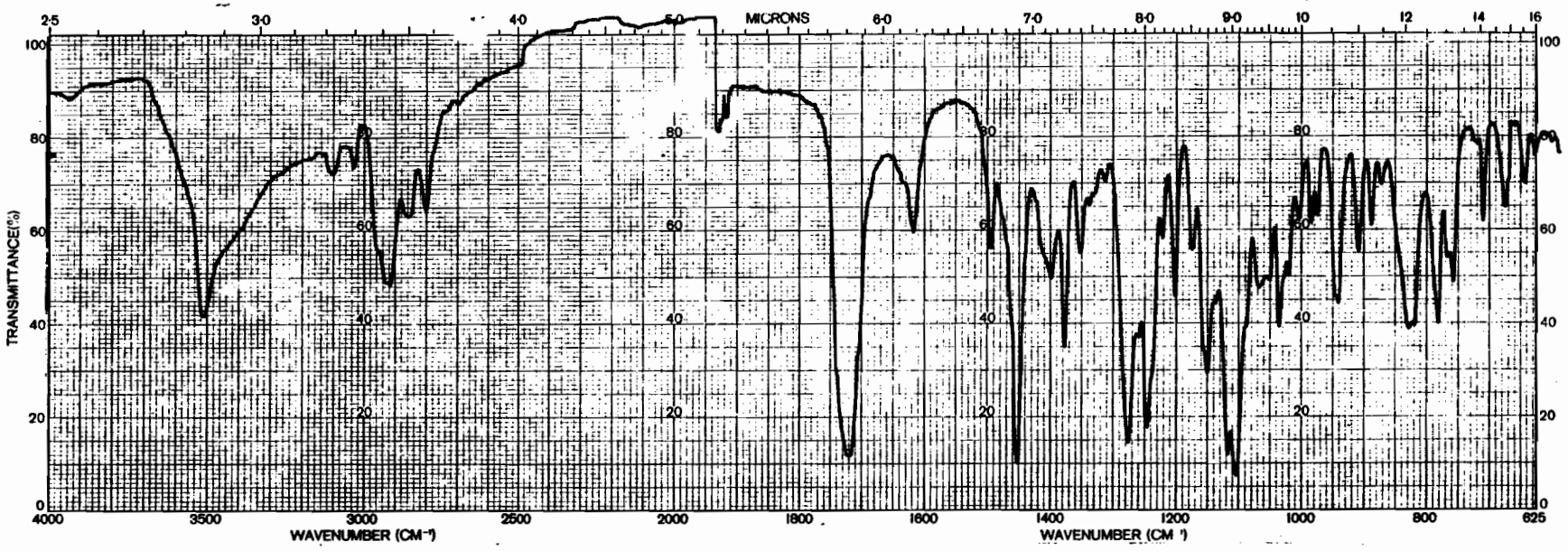

Figure 9: I.R. transmittance spectrum of IIIa, 2.0 mg in 100 mg of KBr. Instrument conditions were the same as for Figure 8.

which tend to corroborate the structure assumed for III. The spectral features and their assignments were made with the aid of Colthup et al. (6) and Silverstein et al. (7). The 3000-3600 region contains absorption due to, in this case, hydrogen bonded OH stretching. The broad absorbance near 3000 cm^{-1} and extending to lower energies is due to the acid (probably dimer) OH stretch, while the broad band at 3200-3250 cm^{-1} is typical of phenols. Both of these features are absent from the spectrum of III, strongly suggesting the ester formation. Further evidence is found in the carbonyl absorption shift typical of ester.

c) Hydrolysis: Compound III, if it is the ester, would be expected to yield morphine (actually the phenoxide anion) and ferrocene carboxylate upon exposure to base. As a preliminary check a small quantity of III in methanol was mixed with 1 M KOH and the turbid mixture spotted on a silica gel G thin-layer chromatography plate. Material which was not exposed to base was also spotted. The plate was developed in $CHCl_3$:acetone:diethylamine (50:40:10) and sprayed with iodoplatinate after noting any yellow spots. The sample exposed to base indeed demonstrated a spot representing morphine and a fast running (R_f 0.68) yellow spot with no reaction to iodoplatinate, besides a spot representing some unhydrolyzed III.

To 2.0 mL of 2.17×10^{-5} M III in pH 6.0 0.01 M PO_4 buffer

was added 0.5 ml of 1 M KOH. The transmittance at 300 nm (phenoxide) was monitored with time. After five minutes the transmittance had reached a constant value and the spectrum was scanned. Figures 10a-c show the spectra of I, morphine and III in aqueous base (pH > 13). The spectrum which would be expected if the spectrum of III was the sum of the spectra of I and morphine is also shown in Figure 10. This spectrum was calculated using the Texas Instrument TI-59 programmable calculator. It can be seen that the qualitative features of the spectra are identical. The quantitative discrepancy near 250 nm is not understood.

d) Elemental analysis:

i) CHN analysis. A specimen of III was sent to Spang Microanalytical Laboratory, Eagle Harbor Michigan. Duplicate C H and N analyses were requested. Calculated (found) are C; 67.62 (68.15, 68.29) H; 5.47 (6.02, 6.12) N; 2.82 (2.56, 2.70) percent. The agreement is not impressive, but the weight of evidence points towards the structure proposed, indicating that III may not be pure.

ii) Iron analysis. An analysis for iron was carried out by graphite furnace atomic absorption spectrophotometry. Although this flameless technique is less precise (typical stated figure 5%) than the flame technique (typical stated figure 1%) it was felt that the savings in material was more important. The total yield of III was not more than 40 mg,

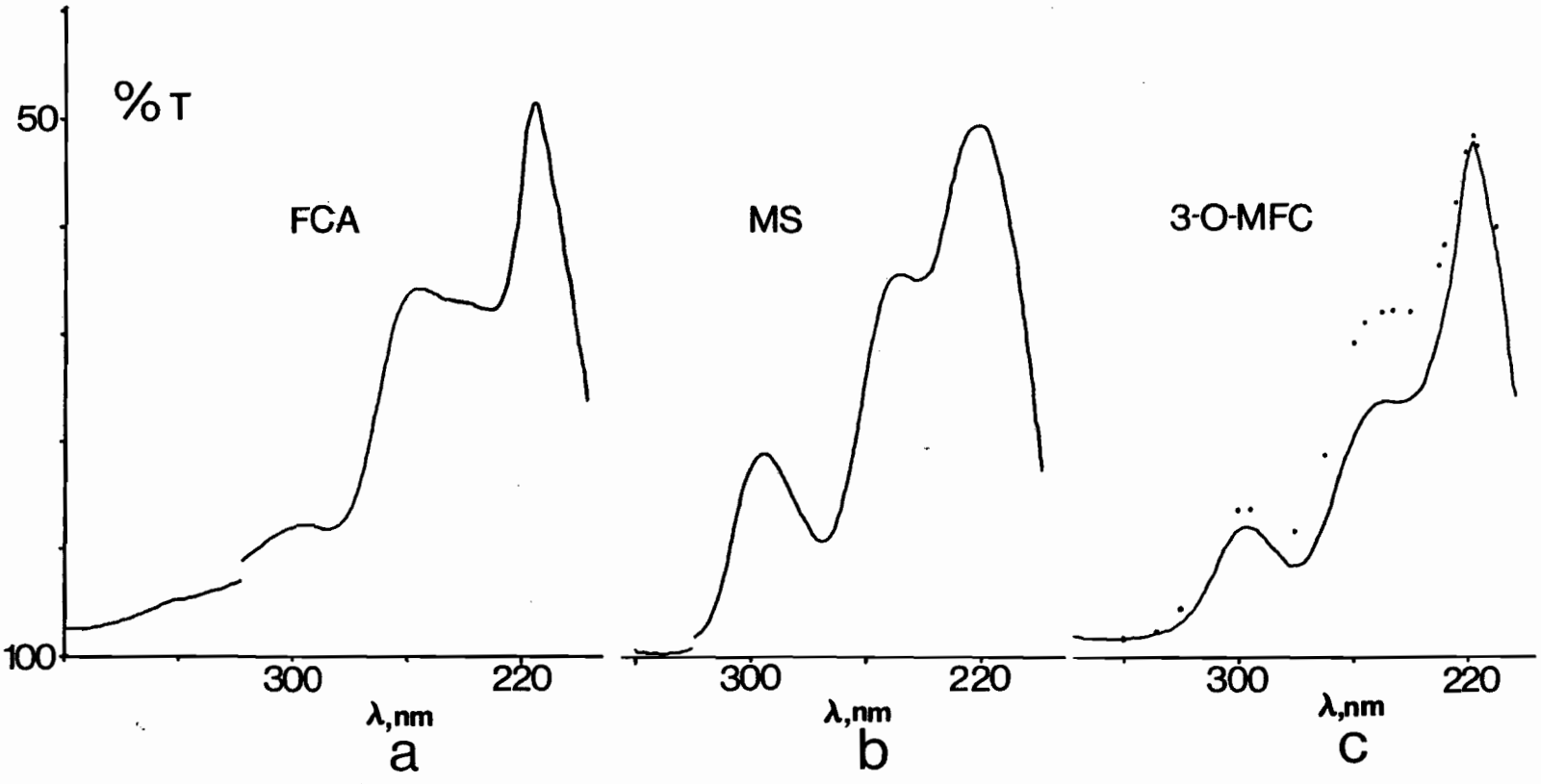

Figure 10: Ultraviolet spectra in aqueous base. Conditions were the same as in Figure 7 with the exception of the solvent. The solvents were 2.0 mL of 0.01 M phosphate buffer, pH 6.0, plus 0.5 mL 1.0 M KOH. The dots on Figure 10c show the spectrum calculated for the hydrolysis of 3-O-MFC. The calculations used the spectra in Figures 10a and 10b.

and this had to suffice for analysis and utilization in the analytical procedure.

Polyethylene bottles for storage of standards and unknowns and volumetric flasks were cleaned prior to use to minimize the chance of trace element contamination. The cleaning protocol was determined by Dr. Shalom Levi. Glassware was first washed in soap (Sparkleen, Fisher Chemical Co.) and water to remove oil and grease. Then both polyethylene bottles and glassware were soaked overnight in a mixture of hydrochloric and nitric acid of roughly one molar concentration. A three-fold rinse in house distilled water was followed by a rinse in deionized water. The water was house distilled which had been deionized by passage through two columns of Barnstead mixed bed resin. Following the rinse, the vessels were filled with deionized water and were soaked for three days. At the end of three days the vessels were emptied and rinsed once with deionized, doubly glass distilled water (supplied by Professor Belleau). The vessels were allowed to dry overnight and were then capped and stored until use.

An iron standard was prepared from Baker Analyzed (100.0%) 0.009" iron wire which was dissolved in about five mL of 6 M Ultrex (J.T. Baker) HNO_3. Once dissolved this solution was diluted to 100.0 mL with deionized, doubly glass distilled water (supplied by Professor Belleau). A series of standards was prepared covering the range of

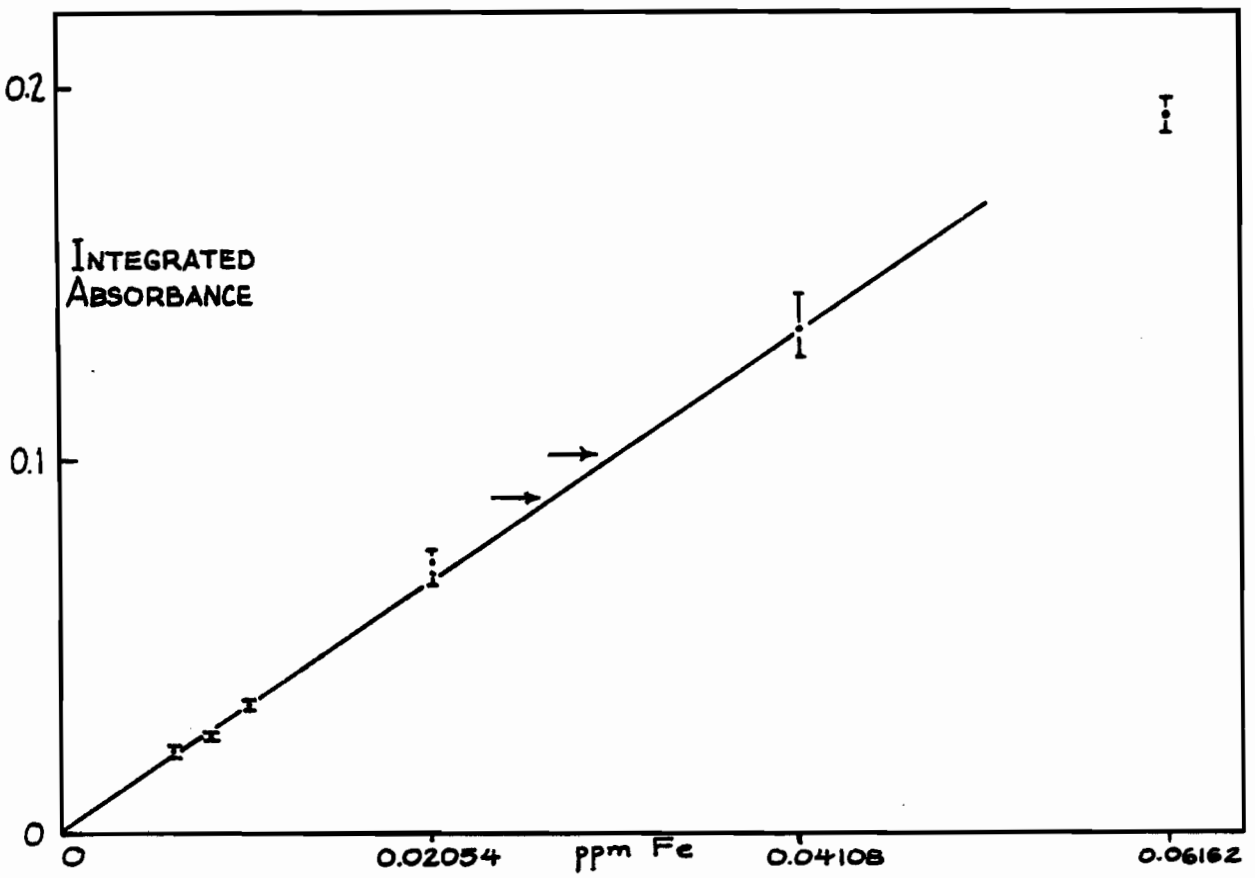

Figure 11: Calibration curve for graphite furnace atomic absorption spectrometry of iron. The error bars indicate the range of values obtained, the dot indicates the average. The point near .02 ppm was analyzed before and after the unknowns showing good agreement. Each specimen was 50 µL. The arrows show the absorbance of the two unknowns. Conditions for the analysis are in Table 5.

0 → 0.1 ppm Fe. Samples of IIIb were weighed out after having been under vacuum at room temperature overnight. On a Cahn Ratio Electrobalance (Ventron Inc.) the following weights were measured 0.3032 mg, 0.6057 mg, 0.3682 mg. To avoid contamination, glass spatula was used but the static charge on the glass made it very difficult to work with, thus a chrome-plated metal spatula was used. These three samples were dissolved in 1:1 HNO_3 used to dissolve the iron wire. In the process of dissolution the compound was oxidized to the corresponding ferricinium ion, as indicated by the blue color of the solutions. The process of dissolution (or oxidation followed by dissolution) was slow, requiring at least one hour. The sample from the second weighing never completely dissolved and as a consequence was not analyzed.

The graphite furnace (Perkin Elmer HGA 2000) in conjunction with the Perkin Elmer 603 atomic absorption unit, was set up with the parameters indicated in Table 5. Samples were introduced into the graphite tube with the aid of a piston-type micropipette (Eppendorff). Every attempt was made to place the aliquot of sample in the same place in the furnace and in the same way each time. At least four, and usually more, injections were made for each standard and sample in the linear range of the calibration curve (Figure 11). The line was drawn by eye. For the standard near .04 ppm the relative standard error was .032 (n=11) and

Table 5

Atomic Absorption Instrument Conditions

Wavelength	248.3	(496.6 second order)
Slit	0.2 nm	
Flow time	3 sec	
Drying temperature	150°C	time 30 s
Char	500°C	10 s
Atomize	2000	10 s
Peaks integrated		

for the standard near .02 ppm the relative standard error was .034 (n=8). These two standards bracketed the sample concentrations so the minimum error in the answer was around 0.033. By suitable dilution (1.00:50.0) the two samples of IIIb were calculated to contain .2426 and .2922 ppm IIIb. From the calibration curve the respective concentrations of Fe are .0275 and .0310 ppm. This yields weight fractions Fe/IIIb of 0.113 ± .004, 0.106 ± .003 (standard error). The theoretical value (55.847/497.380) is 0.112. The agreement is close enough to show that III is not the diester (i.e., 3-O, 6-O morphinyl-diferrocenecarboxylic acid ester).

e) Electrochemistry: Cyclic voltammetry and pulse

experiments were performed with a P.A.R.C. Model 173/179 potentiostat with a P.A.R.C. Model 175 programmer. The data were recorded on a Houston Instruments Omnigraphic X-Y recorder (Model 2000), a DM-63 Telequipment oscilloscope, or a Heath-Schlumberger Model SR 204 strip chart recorder. A three-electrode arrangement was used for all studies. The reference electrode was an S.C.E. and the auxiliary electrode was Pt foil. The reference potential was measured near the working electrode by employing a solution bridge and a Luggin probe. The working electrode was shielded to insure that the net diffusion of electroactive species only occurred perpendicular to the electrode.

Buffers herein called phosphate buffers were prepared by adjusting the pH of a solution of sodium monobasic phosphate (Anachemia) of the indicated molarity to the indicated pH value.

Cyclic voltammograms representative of morphine, ferrocene carboxylic acid and III are shown in Figure 12. The morphine demonstrates an ill-defined anodic wave and no cathodic wave. Follow-up reactions, which may occur once the morphine is oxidized, may include the formation of pseudomorphine (9). The ferrocene carboxylic acid appears to be almost reversible, as does III. These solutions were run at pH 6.0 in 0.1 M phosphate buffer. To dissolve III trituration in a small quantity of 1 M H_2SO_4 was required. The resultant solution pH was 2.69. The similarity of the

Figure 12: Cyclic voltammetry at a 0.69 cm^2 glassy carbon electrode. Sweep rate 100 mV s^{-1} 3-O-MFC (IIIa) pH 2.69 in a phosphate-sulfate medium, FCA pH 6.0 0.1 M phosphate buffer, MS in the same solvent. Potential is vs SCE in mV.

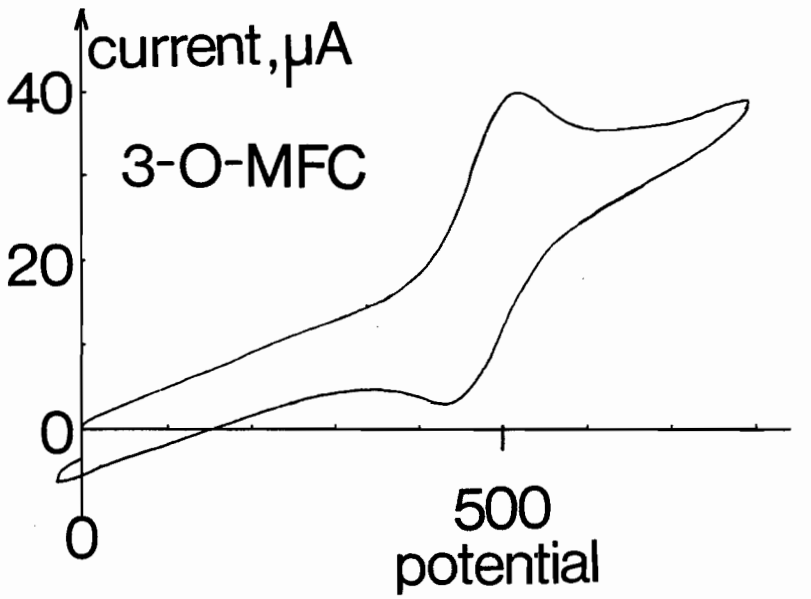
current, μA
40
3-O-MFC
20
0
0
500
potential

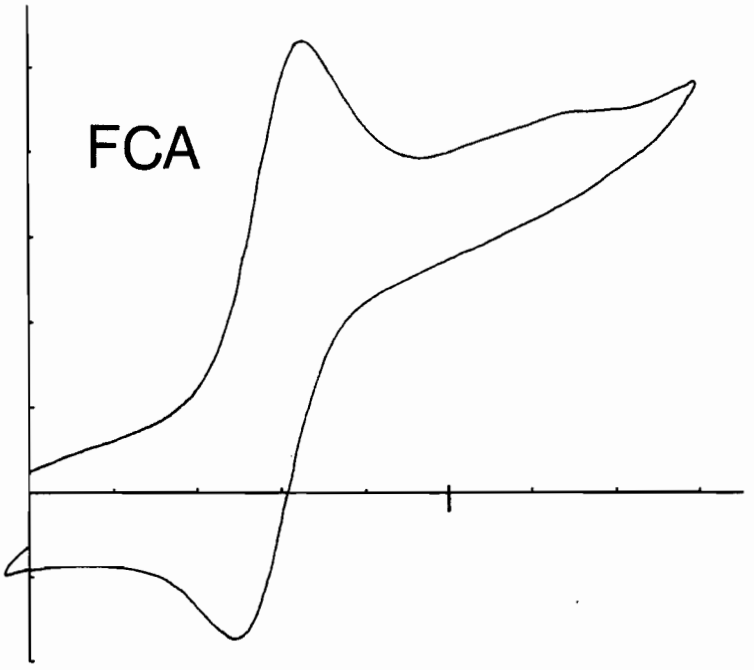
FCA

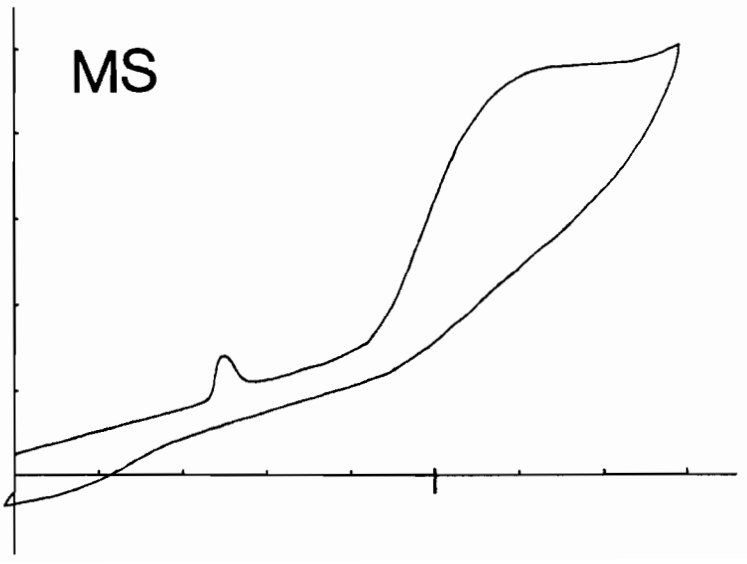
MS

cyclic voltammograms of I and III support the hypothesis that ferrocene is present in the compound and the absence of a morphine-like wave indicates the absence of the free phenol. The average of the anodic and cathodic peak potentials of I is 287 mV and that of III is 476 mV.

When the diagnostic criteria for cyclic voltammograms of III, as presented by Nicholson and Shain (8), were applied to cyclic voltammograms run in a 10^{-3} M H_3PO_4, 0.01 M KNO_3 solution, they seemed to indicate that a following reaction was occurring. In other words, upon oxidation to the ferricinium derivative of morphine, the compound participated in a homogeneous chemical reaction. The three criteria used are i) current function, a number proportional to the measured anodic peak current, i_{pa}, divided by the square root of the sweep rate ii) ratio of cathodic to anodic peak currents iii) rate of shift of peak potential; all are studied as a function of sweep rate.

In cases of reversible charge transfer the current function is not a function of sweep rate, and in cases of quasi-reversible (10) behavior, the current function tends to fall slowly as a function of sweep rate. The current function in this case increased with sweep rate and rather sharply. This, and the qualitative nature of the voltammograms, suggested the possibility of adsorption occurring. Since this effect was not taken into account in the paper of Nicholson and Shain

(8) these inferences are at most tentative. It was decided to carry out further tests in more concentrated electrolyte.

Since there is evidence (11-13) that ferricinium is unstable under certain conditions, pulse experiments were undertaken to attempt to find a following reaction after oxidation of III. The double pulse potentiostatic method of Schwarz and Shain (14) was decided upon since it is simple and has the advantage that the diffusion coefficient and concentration of electroactive species need not be known. Solutions of III were prepared by trituration of III in 1 M H_2SO_4 and dissolving in 0.1 M pH 6.0 phosphate buffer. Solutions of I were prepared by dissolving in a few drops of 1 M KOH and diluting with the same buffer. Currents were measured at various times along a pulse. Pulses of 10, 100, 1000 milliseconds and 100 seconds were applied. Appropriate blank values were subtracted. The data were plotted on the curves of Figure 2 in reference 14. For a pulse length of 100 msec the data fit the curve fairly well, but the data for a pulse length of 1000 msec did not fit the curves in Figure 2 of reference 14. Even if the 1000 msec data were assumed not to fit because of random experimental error, the value for the homogeneous rate constant thus tenuously calculated differs from that calculated from the 100 msec pulse by a factor of 20. Thus the data do not fit the model.

At the same time cyclic voltammetry was repeated. The

Figure 13a: $i/v^{1/2}$ vs v for FCA and 3-O-MFC (IIIa). Current axis is in μA.

Figure 13b: Ratio of cathodic to anodic peak current for; Δ, ICA and 0 3-O-MFC (IIIa).

Figure 13c: Rate of change of peak potential with sweep rate, Δ, FCA, 0, 3-O-MFC (IIIa)

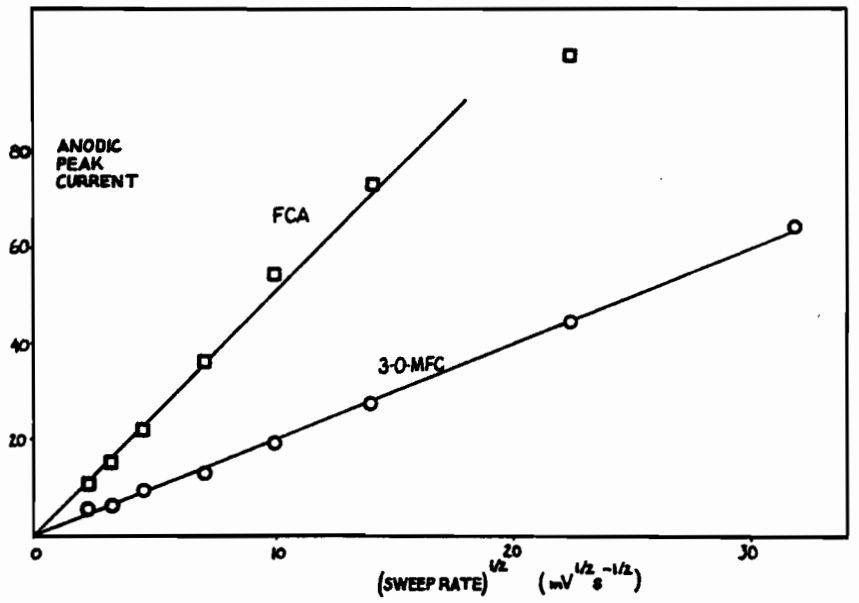
ANODIC
PEAK
CURRENT
FCA
3-O-MFC
80
60
40
20
0
10
20
30
(SWEEP RATE)^1/2 (mV^1/2 s^-1/2)

a

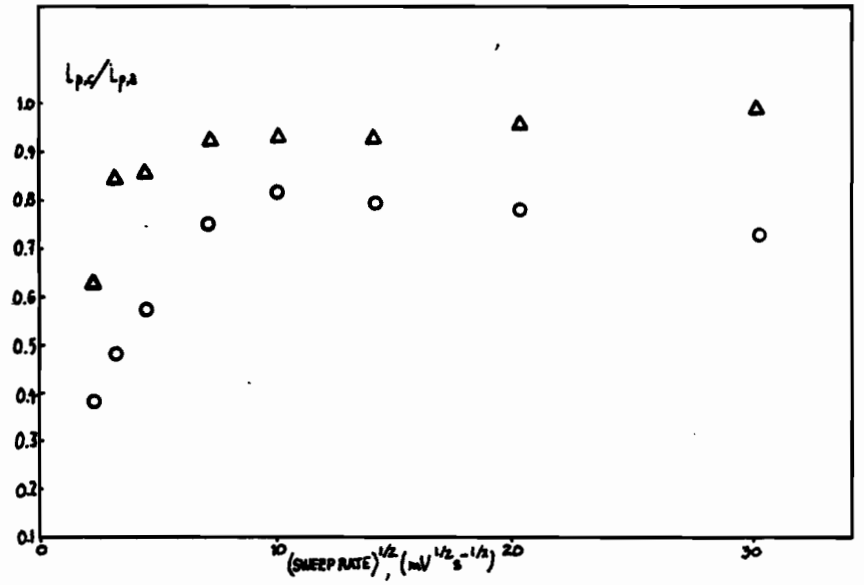
$i_{p,c}/i_{p,a}$
1.0
0.9
0.8
0.7
0.6
0.5
0.4
0.3
0.2
0.1
0
10
20
30
(SWEEP RATE)^1/2, (mV^1/2 s^-1/2)

b

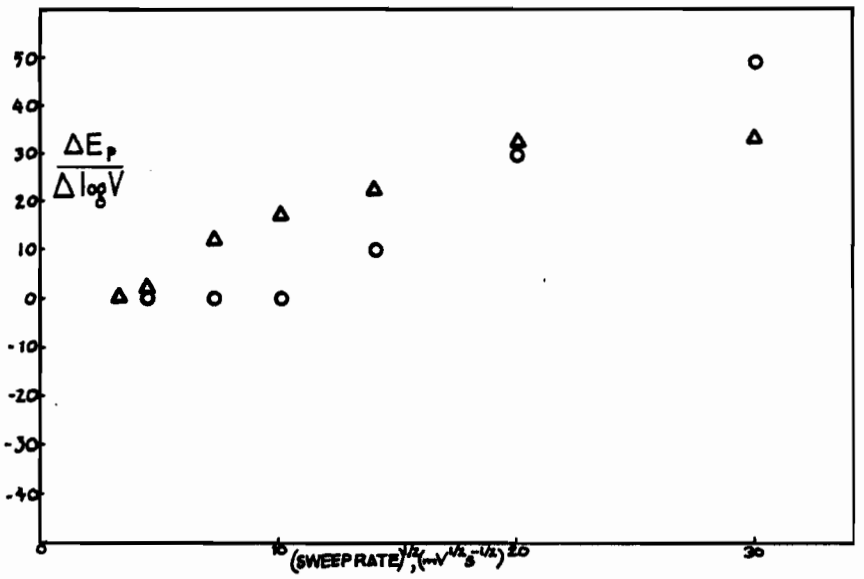
$\frac{\Delta E_p}{\Delta \log V}$
50
40
30
20
10
0
-10
-20
-30
-40
0
10
20
30
(SWEEP RATE)^1/2, (mV^1/2 s^-1/2)

c

current function, a relatively insensitive parameter, was constant for III and almost constant for I. This is demonstrated by the linear relationship between i_{pa} and the square root of sweep rate (Figure 13a). The other two diagnostic criteria are shown in Figures 13b and c. The data for I are consistent with a transition from reversible to irreversible behavior (quasi-reversible) a case not covered in Reference 8, but taken up later (10). The data for III are more interesting, especially i_{pc}/i_{pa}. This curve seems to indicate the presence of an irreversible following reaction at slow sweep rates and a reversible following reaction for fast sweep rates.

The double-pulse potentiostatic calculations used (14) considered only the case of the irreversible following reaction, i.e.,

$$A \rightleftarrows B+e^-$$

$$B \xrightarrow{k} C$$

Only recently was the case of the reversible following reaction treated (15). This treatment required slightly different data than that of Reference 14 so the pulse experiments were repeated to determine whether the data supported the same conclusion as that drawn from cyclic voltammetry.

The buffer used in these experiments was 0.05 M tris (hydroxymethyl)aminomethane maleate (Sigma Chemical Co.) pH 6.0. The buffer system was changed because this was the buffer being used in the flow-through electrode experiments. Dissolving III in aqueous solution is difficult, so it was decided to dissolve the compound in methanol and further dilute it in an aqueous buffer. For these experiments, the final solution composition was 5% methanol in tris buffer. It was determined that, under these conditions, there is definitely an irreversible following reaction since the cathodic peak is zero at low sweep rates. In the region where the ratio of cathodic to anodic peak heights is changing (100 mVs^{-1} to 500 mVs^{-1}) this ratio was measured. The peaks were measured by the method of Nicholson (16). The data are compared to the theoretical expectation for reversible charge transfer followed by an irreversible chemical reaction (8) in Figure 14a. The agreement is not quantitative, but the same trend is observed. The point at 2.2 sec for the experimental data is equivalent to log $k\tau = 1$ (8). This yields a k of about .45 s^{-1}.

Double pulse potentiostatic experiments were carried out with the same solutions. Previous pulse studies had shown anomalous behavior (rising currents) up to a few tens of milliseconds. For these experiments particular care was taken to place an auxiliary electrode opposite and parallel

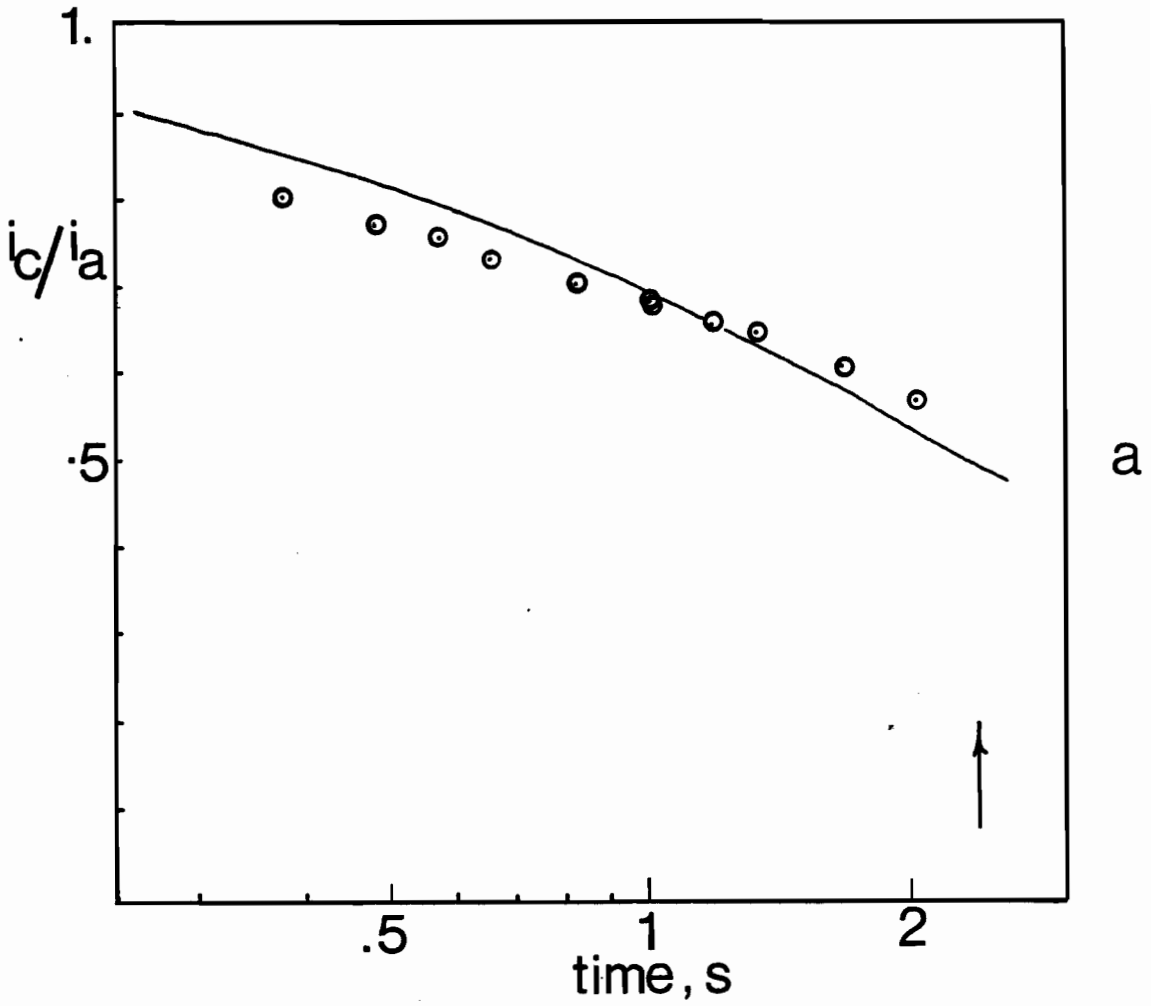

Figure 14a: Ratio of cathodic to anodic peak currents for IIIb in 5% methanol, tris(hydroxymethyl) aminomethane 0.05 M pH 6.0. The current ratio is plotted against the time required to sweep the voltage from E° to the switching potential. The solid line is the theoretical response for an irreversible following reaction (8) and the circled points are data.

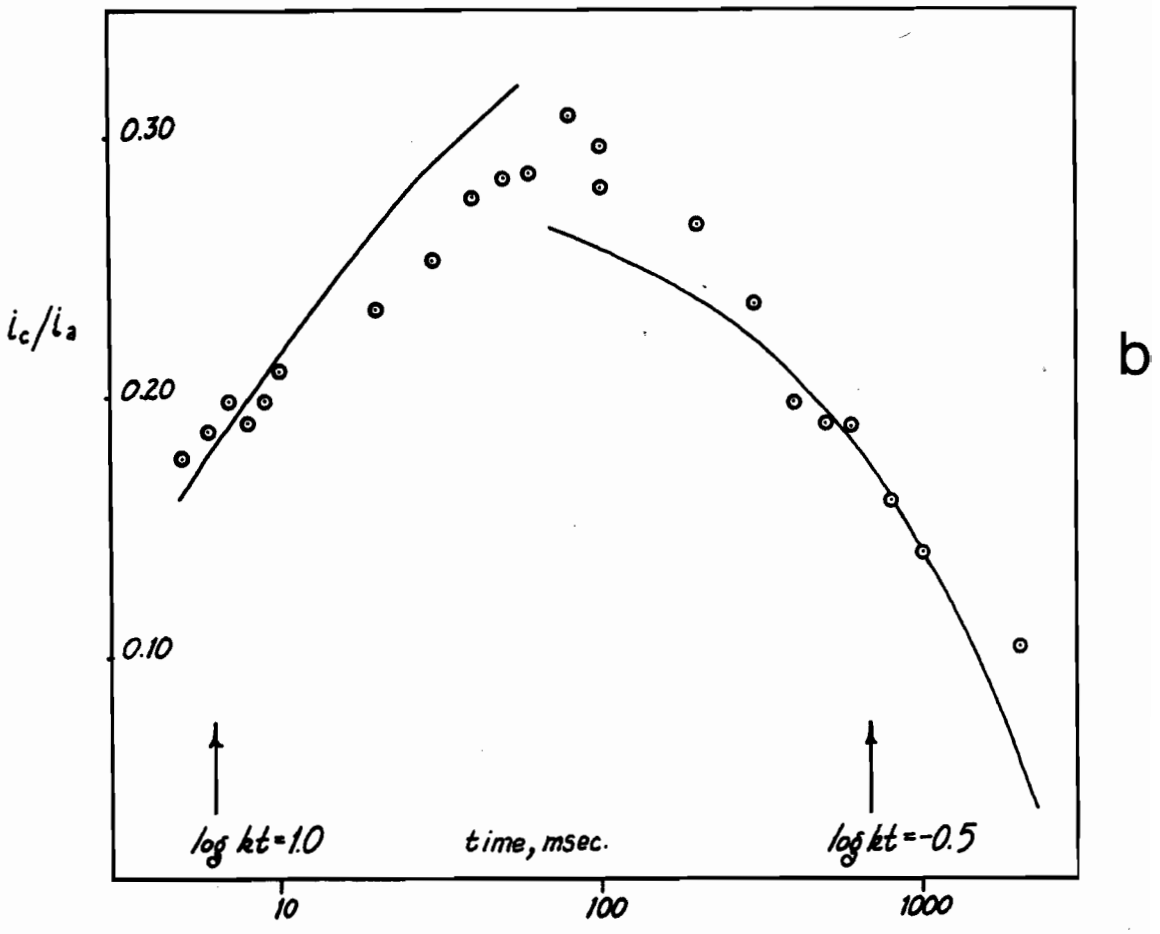

Figure 14b: Ratio of cathodic to anodic currents for double pulse chronoamperometry. Same solutions as in Figure 14a. The left hand curve is the fast time reversible part of the curve. This is from curve 4, set 1, Figure 5 (15). The point on their curve at log kt = 1.0 is marked. The right hand curve (curve 1, set 1, Figure 5 (15)) is the long time irreversible part of the curve. The point on the curve of reference (15) corresponding to log kt = 0.5 is marked. The data are circled.

to the shielded glassy carbon working electrode. The potential at the interface was measured (controlled) at the end of a Luggin probe maintained a distance of two O.D. away from the electrode surface. O.D. is the probe tip's outside diameter. The probe tip was between the auxiliary and working electrodes. The reference electrode was connected to the Luggin probe via a solution bridge. With this arrangement the same anomalous behavior was seen, but it only lasted a few milliseconds.

The results of the experiments are shown in Figure 14b. It can be seen that for times on the cyclic voltammetry scale (>300 msec) the reaction appears as an irreversible following reaction (curve 1, set 1, Figure 5 (15)). The point on the time axis of the experimental data at 680 msec corresponds to log kt = -.5 on the curve mentioned from Hanafey et al. (15). This yields a k of about .46 s^{-1}, in agreement with the cyclic voltammetry data. For shorter times the experimental data take on the appearance of a reversible following reaction (curve 4, set 1, Figure 5 (15)). The data correspond to $k_b/k_f = 0.1$ and $k_f = 1.6 \times 10^3$ s^{-1} for the scheme

$$A \longrightarrow B + e^-$$

$$B \underset{k_b}{\overset{k_f}{\rightleftharpoons}} C$$

Perusal of Hanafey et al. (15) demonstrates no mechanism with the shape of the data found in Figure 14b. Although one cannot be too specific about the actual course of the mechanism it is entirely possible that the following general scheme is occurring.

$$III_r \rightleftarrows III_o + e^-$$

$$III_o \underset{k_b}{\overset{k_f}{\rightleftharpoons}} A \qquad \text{fast}$$

$$A \longrightarrow B \qquad \text{slow}$$

III_r is the reduced form of III, and III_o its oxidized form. Since the irreversible reaction is slow, fast measurements can be made which will not discern it. For slower investigations the fast reaction is in complete equilibrium and kinetic investigations would appear as if III_o were directly involved in an irreversible reaction. The only effect of the fast intermediate reaction is that the actual measured rate would differ from the rate predicted by neglecting the fast reaction by a constant, k_f/k_b.

It cannot be stressed enough that this scheme is general, no specific mechanism can be hypothesized with these data alone. One other piece of evidence infers an irreversible

reaction and shows that the direction of the reaction is towards breaking the ferricinium apart. Exhaustive electrolysis leads to a clear colorless solution with no apparent voltammetric characteristics. This would be expected for the breakdown of III_o to iron (III) which would be precipitated as the hydroxide.

According to Schwarz and Shain (14) the current from the first pulse of a double pulse experiment is not affected very much from the following homogeneous kinetics, and according to Nicholson (16) neither is the first peak in the cyclic voltammetry affected much. Using the pulse and cyclic voltammetry data, determinations of the number of electrons transferred and diffusion coefficients could be made.

1) n. According to Nicholson and Shain (8)

$$i_p/v^{1/2} = 602\ n^{3/2}\ A\sqrt{D}\ C \quad (446.3)$$

n = number of electrons transferred

A = electrode area cm^2

D = diffusion coefficient $cm^2 s^{-1}$

C = concentration mM

i_p = peak current μA

v = sweep rate Vs^{-1}

The well-known Cottrell equation states that for an infinite potential pulse

$$it^{1/2} = nFA\sqrt{D}\ C\ /\sqrt{\pi}$$

F = Faraday 96,486 coulombs/equiv.

t = time s

i = current μA

The ratio of the two equations yields

$$\frac{i_p/v^{1/2}}{it^{1/2}} = 4.935\ \frac{C_{cv}}{C_p}\ n^{1/2}$$

where C_{cv} is the concentration used in the cyclic voltammetry experiments and C_p is the concentration used in the pulse experiments. Ideally the experiments are performed in the same solution and these two concentrations are equal. The cyclic voltammetry was performed in 0.1 M pH 6.0 phosphate buffer and the pulse experiments were performed in 0.0075 M H_3PO_4/0.01 M KNO_3. I have assumed a negligible change in diffusion coefficient due to change in salt concentration of this magnitude. This is not a good assumption, but since D enters as the square root, changes of several tens of percent will not be sufficient to obscure the value of n. The electrode was the same in each case. Table 6 shows these calculations.

The value for I corresponds closely to n=1, the value for III is not accurate but implies n=1. Using these values, diffusion coefficients in 0.0075 M H_3PO_4/0.01 M KNO_3

Table 6

Calculation of n

Compound	$i_p/v^{1/2}$ ($\mu AV^{-1/2}s^{1/2}$)	$it^{1/2}$ ($\mu As^{1/2}$)	C_{cv}	C_r	n
I	158.1	161	.409	1.91	.86
III	63.2	59.3	.217	.805	.64

$i_p v^{1/2}$ is the slope of Figure 13a. $it^{1/2}$ was calculated from 10 points on a pulse of 1 sec duration. The standard error for $it^{1/2}$ of I is 3.7% and for III 4.6%. Concentrations are millimolar.

may be calculated from the value of n and the Cottrell equation. A equals 0.69 cm^2 (17). For I, D = $5.05 \times 10^{-6} cm^2 s^{-1}$ and for III, D = $3.85 \times 10^{-6} cm^2 s^{-1}$. If some rather ideal assumptions hold (spherical molecules, equal densities of compounds) the diffusion coefficients of two like species can be related through the cube root of their molecular weights (18). For the pair I and III this

$$D_I \times \left(\frac{MW_I}{MW_{III}}\right)^{1/3} = D_{III}$$

$$5.05 \times 10^{-6} (cm^2 s^{-1}) \times .7735 = 3.91 \times 10^{-6} (cm^2 s^{-1})$$

calculation is in good agreement with the experimental value.

f) Melting points: Both IIIa and IIIb begin to decompose at 217°C to a black substance.

REFERENCES

1. V. Weinmayr in Chem. Abstracts, 49 (1955) 10364a, U.S. Patent 2,683,157 (1954).
2. H.-J. Lorkowski, R. Pannier and A. Wende, J. Prakt. Chemie, 35 (1967) 149.
3. E. Stahl,"Thin-Layer Chromatography," Springer-Verlag, New York (1969).
4. M. Rosenblum, "Chemistry of the Iron Group Metallocenes: Ferrocene Ruthenocene, Osmocene, Part One", Wiley Interscience, New York, 1965.
5. H.J. Kupferberg, A. Berkhalter and E.L. Way, J. Pharmacol. Exp. Ther., 145 (1964) 247.
6. N.B. Colthup , L.H. Daly and S.E. Wiberley, "Introduction to Infrared and Raman Spectroscopy", Academic Press, New York, 1964.
7. R.M. Silverstein, G.C. Bassler and T.C. Morrill, "Spectrometric Identification of Organic Compounds", John Wiley & Sons, Inc., New York, 1974.
8. R.S. Nicholson and I. Shain, Anal. Chem., 36 (1964) 706.
9. B. Proska and L. Molnar, Anal. Chim. Acta, 97 (1978) 149.
10. R.S. Nicholson, Anal. Chem., 37 (1965) 1351.
11. G. Wilkinson, J. Am. Chem. Soc., 74 (1952) 6146.
12. J.A. Page and G. Wilkinson, J. Am. Chem. Soc., 74 (1952) 6149.

13. J.C.D. Brand and W. Snedden, Trans. Far. Soc., 53 (1957) 894.

14. W.M. Schwarz and I. Shain, J. Phys. Chem., 69 (1965) 30.

15. M.K. Hanafey, R.L. Scott, T.H. Ridgeway and C.N. Reilley, Anal. Chem., 50 (1978) 116.

16. R.S. Nicholson, Anal. Chem., 38 (1966) 1406.

17. B.R. Hepler, S.G. Weber and W.C. Purdy, Anal. Chim. Acta, 102 (1979) 41.

18. W.C. Purdy, Electroanalytical Methods in Biochemistry, McGraw Hill, New York, 1965, p. 98.

CHAPTER IV

Theory

A) Introduction

The objective of this work is to fully explore the behavior of the channel electrode as used in continuous flow voltammetry or high performance liquid chromatography. The results of these labors can then be applied to the development of various analytical techniques. The differential equations and boundary conditions describing this system under many different circumstances are easily written down. Solving them is quite another matter. Several approximations have been made in order to solve a particular problem, but none seem general enough to be utilized under all the conditions which are felt to be worth exploring. Of course, an exact solution is to be desired whenever possible. However, the most active researcher in this field, Hiroaki Matsuda, has not been able to find an exact solution to the problem in which I am most interested. For this reason approximations have to be considered.

The diffusion layer is an old concept. Its thickness is the distance from the surface of an electrode to the point where the bulk solution is not perturbed by the occurrences

at the electrode. The diffusion layer is generally used in a steady state context, thus the concentration of depolarizer varies linearly with distance within the diffusion layer. It seems not entirely unreasonable to expect that if one allowed the diffusion layer thickness to vary with time, then one might extend the usefulness of the concept from the steady state in one dimension to transient phenomena. Some quick calculations confirmed that the current to a planar electrode for a simple reversible reaction was predicted correctly to within a constant ($\approx$1) for chronoamperometry and chronopotentiometry. A perusal of the literature determined that Oldham (1) had the same idea ten years ago. He has been referenced once since then, by Posey and Meyer (2), who applied the approximation to the determination of chronopotentiometric transients in flowing streams. The concept was established, but the application of it to several new sets of conditions is desired before it can be applied to the situation which will be present in voltammetric immunoassay.

In a voltammetric immunoassay there are three possible occurrences which may lead to the production of current. First unbound electrochemically tagged ligand L* may react at the electrode. Second, bound electrochemically tagged ligand Ab·L* may react at the electrode. Third, Ab·L* may dissociate yielding L* which may then react at the electrode. If the first example occurs in the absence of the second and third,

then, effectively bound L* has been "separated" from free L*. The essential question which must be answered by the theoretical analysis is, "Under what conditions can an electrochemical measurement of free ligand be made in the presence of bound ligand?". There are good reasons to assume that antibody bound ligand will yield small currents. The diffusion coefficient of the bound ligand is very small so that its arrival at the electrode surface is slow. Once a molecule does reach the electrode surface, it must diffuse rotationally until the electrochemically active portion (the bound ligand) is at the interface. Once this position is reached there must be no steric hindrance by the immunoglobulin which would keep the electrochemical label away from the electrode surface. These considerations make it unlikely that the antibody ligand complex will react directly at the electrode. What is postulated is that in order for bound ligand to contribute to current it must first dissociate yielding free ligand which can then react. Thus the situation is just that of a CE mechanism (chemical step followed by electrochemical step):

$$A \underset{kK}{\overset{k}{\rightleftharpoons}} B$$

$$B \rightarrow C + e^-$$

In terms of the voltammetric immunoassay this becomes

$$Ab \cdot L^* \underset{kK[Ab]}{\overset{k}{\rightleftharpoons}} L^*$$

$$L_r^* \longrightarrow L_o^* + e^-$$

where L_r^* is reduced L* and L_o^* is oxidized L*. Note that [Ab] has been taken as a constant. This is a good assumption. As far as any molecule of Ab is concerned, the difference between L_r^* and L_o^* is likely to be very small. Recall that the antibody recognizes the "L" part of L*, not the "star" or tagged part. This means that near the electrode surface where L_r^* is low and L_o^* is high the perturbation experienced by Ab is small since it feels the presence of (L_o^* and L_r^*).

The use of the diffusion layer approximation must therefore be able to correctly predict currents in thin channels, currents in flowing streams and currents in the presence of chemical reactions. These cases have been investigated (3,4), and these investigations are the subject of this chapter.

In order to make the reading of this chapter more fluent the main assumptions, questions, and conclusions have been stated in the body of each section. Detailed derivations and computer calculations have been relegated to appendices.

B) The Diffusion Layer Approximation-Transients

1) Derivation of the Basic Equations

For the assumed concentration profile in the reduction shown in Figure 1 the concentration gradient at the electrode surface for the oxidized species is

$$[C^\circ - C(o,t)]/\delta(t) \tag{1}$$

where C° is the bulk concentration, $C(o,t)$ is the concentration at $x=0$, the electrode surface, at any time t, and $\delta(t)$ is the time dependent diffusion layer thickness. Analogously for the reduced species indicated by a prime, one has

$$[C^{\circ\prime} - C'(o,t)]/\delta'(t) \tag{2}$$

for the concentration gradient. From Fick's first law one can write

$$J = D[C^\circ - C(o,t)]/\delta(t) = -D'(C^{\circ\prime} - C'(o,t)/\delta'(t) \tag{3}$$

where J is the flux of reduced species. The Butler-Volmer equation states that

$$J = k_1 C(o,t) - k_{-1} C'(o,t) \tag{4}$$

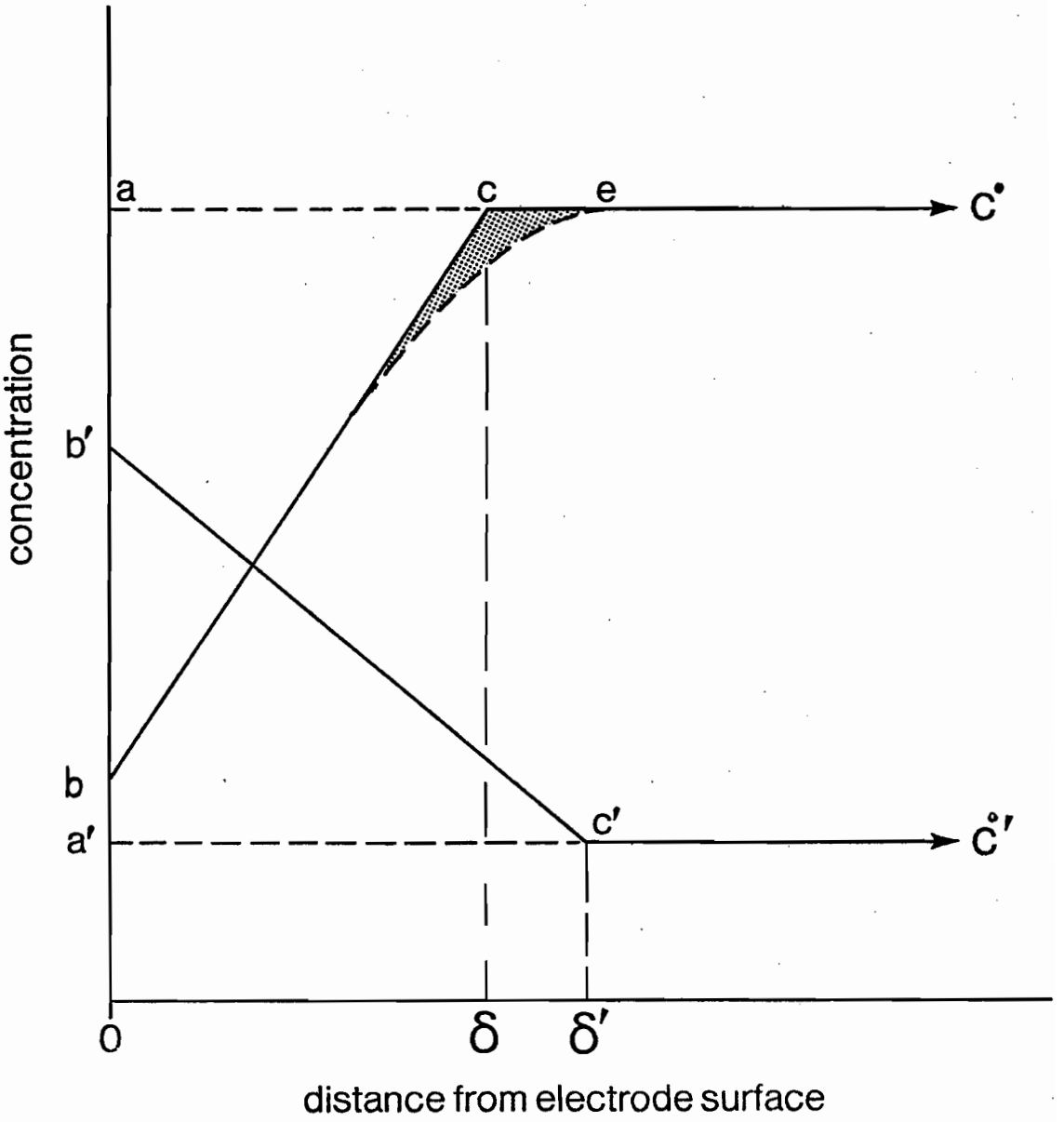

Figure 1: The diffusion layer approximation for semi-infinite diffusion. The diffusion layer thickness for species C is δ and the diffusion layer thickness for species C' is δ'.

where the k's are the potential dependent rate constants. By Faraday's Law, the amount of oxidized species destroyed is equivalent to the amount of reduced species produced, thus area abc must equal area a'b'c' (Figure 1). If these areas are denoted by R, then

$$R = [C^\circ - C(o,t)]\delta(t)/2 = [C^{\circ\prime} - C'(o,t)]\delta'(t)/2 \qquad (5)$$

From the conservation of mass the change in area of R with time must equal the flux. When homogenous reactions are considered, there may be a source or sink term, r, which may be a function of any concentrations, δ's and constants. This yields

$$dR/dt = \pm J \pm r \qquad (6)$$

where the +J is used for the reduced species and -J for the oxidized species.

Both J (equation 3) and R (equation 5) are equations of C(o,t) and $\delta(t)$ (or C'(o,t) and $\delta'(t)$). J and R may be eliminated from equations 1-5 to yield expressions for C(o,t) and C'(o,t) as a function of diffusion layer thicknesses, diffusion coefficients and heterogeneous rate constants,

$$C(o,t) = \left[\left(\frac{D}{k_1 \delta(t)} + \frac{k_{-1}}{k_1}\gamma \right) C^\circ + \frac{k_{-1}}{k_1} C^{\circ\prime} \right] \Bigg/ \left[1 + \frac{k_{-1}}{k_1}\gamma + \frac{D}{k_1 \delta(t)} \right] \qquad (7)$$

$$C'(o,t) = \left[\left(\frac{D'}{k_{-1}\delta'(t)} + \frac{k_1}{k_{-1}}\gamma^{-1} \right) C^{o\prime} + \frac{k_1}{k_{-1}} C^{o} \right] \Bigg/ \left[1 + \frac{k_1}{k_{-1}}\gamma^{-1} + \frac{D'}{k_{-1}\delta'(t)} \right] \quad (7)$$

where $\gamma = (D/D')^{1/2}$.

Equation 7 can be used in equations 3 and 5, and when r=0, substitution of the resulting equations into equation 6 will yield a first order, but not necessarily linear, differential equation for $\delta(t)$ or $\delta'(t)$. The boundary conditions generally applied in electrochemical diffusion problems are contained in equation 7. This equation also demonstrates an approximate definition for reversibility. When the reaction velocity k_1 (or k_{-1}) is much larger than the diffusional velocity D/δ (or d'/δ'), then equation 7 reduces to a form derivable from conservation of mass and the Nernst equation, i.e., a reversible reaction.

If the above-mentioned differential equation is solved for $\delta(t)$, and the current $i(t)$ then determined from equations 2 and 7 with $i = nFAJ$, the finding will necessarily be in error because the physical system does not display a linear concentration vs distance relationship. A solution to this dilemma has been proposed by Oldham (1). He argues that the area that should be considered is not R, but the slightly larger area aceb (Figure 1). It can be seen that R is a fraction, f, of this area. Equation 6 must then be rewritten to state

$$d(R/f)/dt = \pm J \pm r \qquad (6a)$$

An analogous expression holds for the primed species. Unfortunately, the fraction f is an unknown quantity. It should most generally be considered a function of time, and is strongly dependent on the shape of the actual concentration profile. Hence, to determine f one must know the exact solution of $C(x,t)$, a task one is explicitly trying to avoid. For reversible potentiostatic cases f may be taken as constant and equal to $\pi/4$ (1). This value will be used here, but the limitations on its use will become apparent.

The derivation of equation 7 tacitly assumed semi-infinite diffusion. If the current in a thin layer cell is being measured these equations will only be valid while the diffusion layer thickness is smaller than the cell thickness, ℓ. At this point and thereafter the flux will be given by

$$J = D[C(\ell,t)-C(o,t)]/\ell \qquad (8)$$

The triangular area pqrs (Figure 2) will be given by

$$S = C(\ell,t)/2 - C(o,t)\ell/2 \qquad (9)$$

and the rectangular area pstu will be given by

$$T = C(o,t)\ell \qquad (10)$$

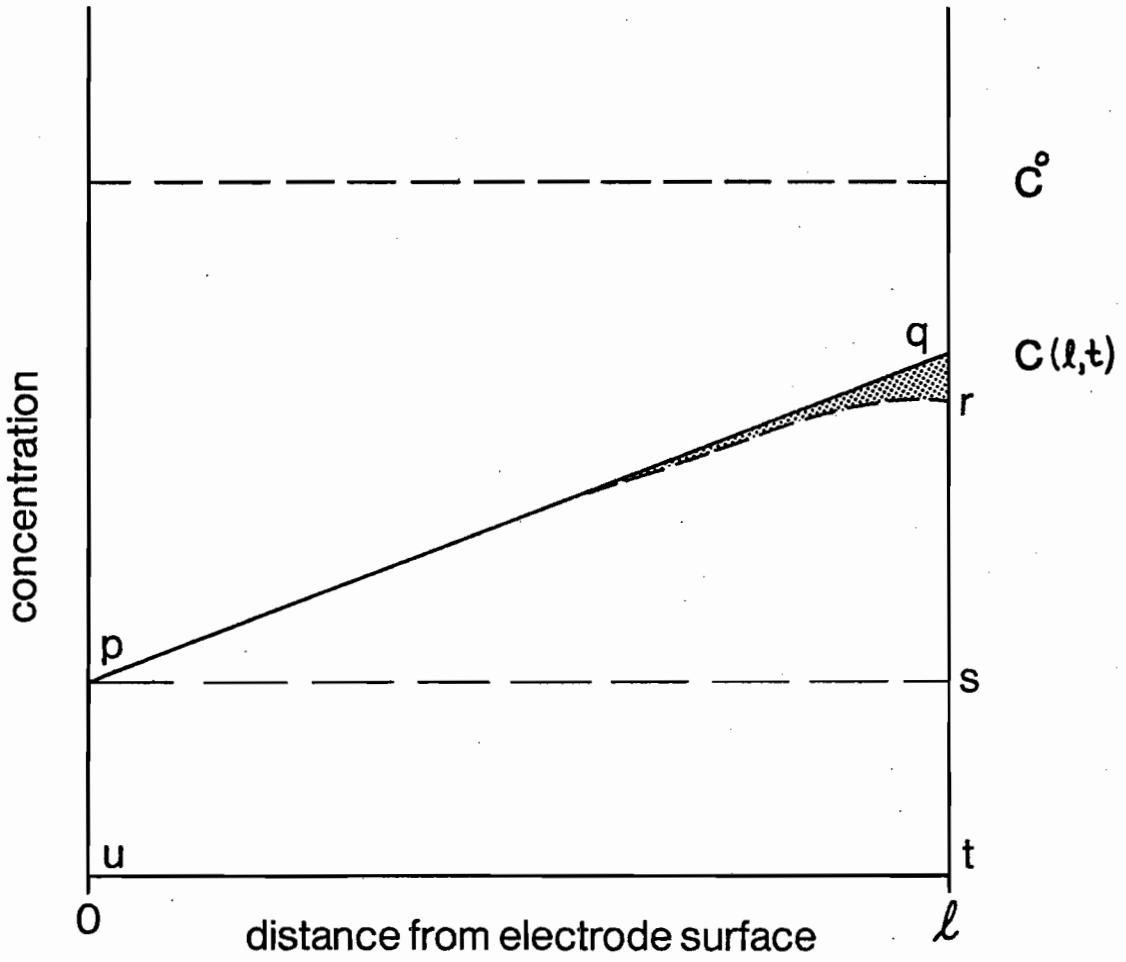

Figure 2: The diffusion layer approximation in thin layer cells

In fact the area which is of interest is the smaller area prs. Thus, analogous to 6a, one may write

$$d(gS+T)/dt = \pm J \pm r \tag{11}$$

where a similar expression holds for the primed species. Analogous to equation 7 one has

$$C(o,t) = \left[C(\ell,t)\left(\frac{D}{\ell k_1} + \frac{k_{-1}}{k}(\gamma^{-1}) \right) + \frac{k_{-1}}{k_1}(C^\circ + C^{\circ\prime}) \right] \Bigg/ \left[1 + \frac{D}{\ell k_1} + \frac{k_{-1}}{k_1}\gamma \right]$$

$$C'(o,t) = \left[C'(\ell,t)\left(\frac{D'}{\ell k_{-1}} + \frac{k_1}{k_{-1}}(\gamma^{-1}-1) \right) + \frac{k_1}{k_{-1}}(C^\circ + C^{\circ 1}) \right] \Bigg/ \left[1 + \frac{D'}{\ell k_{-1}} + \frac{k_1}{k_{-1}}\gamma^{-1} \right] \tag{12}$$

In deriving equation 12 the binary expansion to two terms has been used to find

$$(D+D')/2D \simeq (D'/D)^{1/2} \quad \text{and} \quad (D'-D)/2D \simeq (D'/D)^{1/2} - 1$$

When equations 8-10 with equation 12 substituted for $C(o,t)$ are used in equation 11, a differential equation for $C(\ell,t)$ will result. This can be used with the solution up to $\delta(t) = \ell$ from equation 6a to yield a complete solution ($t=0$ to ∞) for thin layer cells.

2) Specific Examples

a) Thin-layer chronoamperometry, infinite potential pulse: For this case, the Cottrell equation (which may be deduced from the equations given here and in reference 1) is used at small times, and an equation for long times is derived from equation 11.

For an "infinite" potential pulse $C(o,t) = 0$, with no homogeneous reaction $r \rightarrow 0$, thus equation 1 becomes

$$dg\ell\left(-\frac{C(\ell,t)}{2}\right)\Big/dt = DC(\ell,t)/\ell \qquad (13)$$

If g is taken as a constant, equation 13 may be integrated from an initial time $\bar{t}$ to t to give

$$\ln[C(\ell,t)/C(\ell,\bar{t})] = 2D(\bar{t}-t)/g\ell^2 \qquad (14)$$

where $\bar{t}$ represents the time at which the Cottrell equation is no longer valid. $C(\ell,\bar{t})$, g, and $\bar{t}$ may be deduced from the matching conditions: (i) when $t=\bar{t}$, the current calculated from the Cottrell equation must equal the current calculated from equation (14); (ii) at $t=\bar{t}$, the derivatives of current with respect to time calculated from the Cottrell equation and equation 14 must also be equal; and (iii) the integral of current from t=0 to $t=\infty$ must equal the number of coulombs

in the system (nFVC°, V = volume of solution in front of the planar electrode). The situation at $t=\bar{t}$ is represented in Figure 3.

The Cottrell equation as derived by Oldham (1) is

$$i = nFADC°/(4fDt)^{1/2}$$

If f is taken as $\pi/4$ this reduces to the familiar form of this equation. Requirement (i) from above becomes

$C°/\bar{\delta} = (1+\alpha)C°/\ell$ where $(1+\alpha)C° = C(\ell,\bar{t})$ (see Figure 3).

Requirement (ii) becomes

$$f/\bar{\delta}^3 = (1+\alpha)/g\ell^3 \text{ where } \bar{\delta} = (4fD\bar{t})^{1/2}$$

Requirement (iii) becomes

$$\bar{\delta}/2f\ell + (1+\alpha)g/2 = 1$$

These equations may be solved simultaneously to yield

$$(1+\alpha) = 1/f;\ \bar{\delta} = f\ell;\ g = f$$

Because the reaction is diffusion-controlled and potentiostatic,

let $f = \pi/4$. Then the final form of the equation for current is:

$$i = nFAD^{1/2}C^{\circ}/(\pi t)^{1/2} \quad \text{for } 0<t<\pi\ell^2/16D$$

$$i = (4nFADC^{\circ}/\pi\ell)\exp\tfrac{1}{2}(\exp\{-8Dt/\pi\ell^2\}) \quad \text{for } \pi\ell^2/16D<t \tag{15}$$

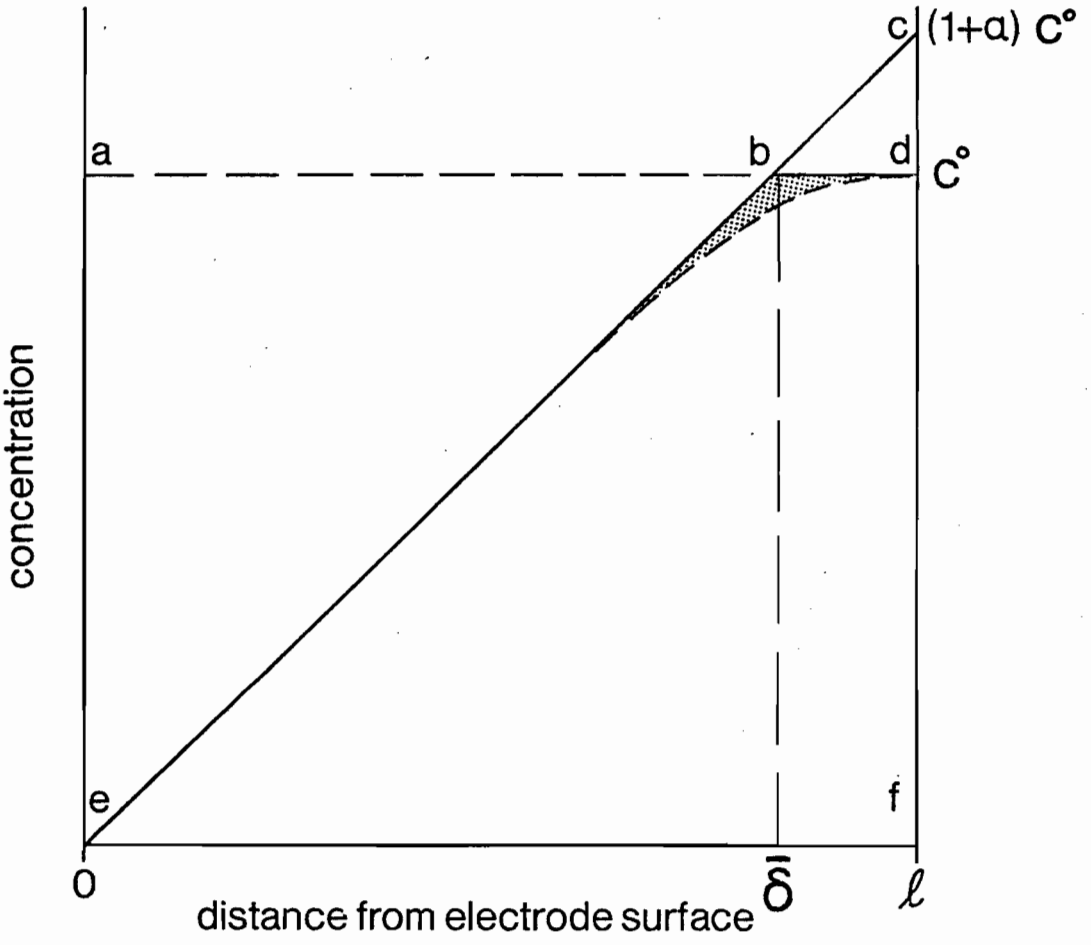

Figure 3: The diffusion layer approximation at the transition from semi-infinite treatment to thin cell treatment.

This may be compared with the expression given by Oglesby et al. (5) obtained by solution of the Laplace transformation of Fick's second law for C(x,t) and inverse transformation of the result.

$$i = (2nFADC°/\ell) \sum_{m=1}^{\infty} \exp\{-(2m-1)^2\pi^2 Dt/4\ell^2\} \qquad (16)$$

The agreement between the two results is more readily appreciated by inspection of Figure 4.

b) Chronoamperometry, homogeneous preceding reaction: The system being studied may be represented by

$$A \underset{k_b}{\overset{k_f}{\rightleftharpoons}} B$$

$$B + ne^- \rightarrow C$$

Assume that it is experimentally feasible to make the concentration of A large enough so that it does not significantly deviate from its equilibrium value, A°, during the course of the reaction. In terms of the present work one can state that the total change in area of triangle abc (Figure 1) is equal to the separate changes caused by electroreaction and homogenous reaction. The change in area

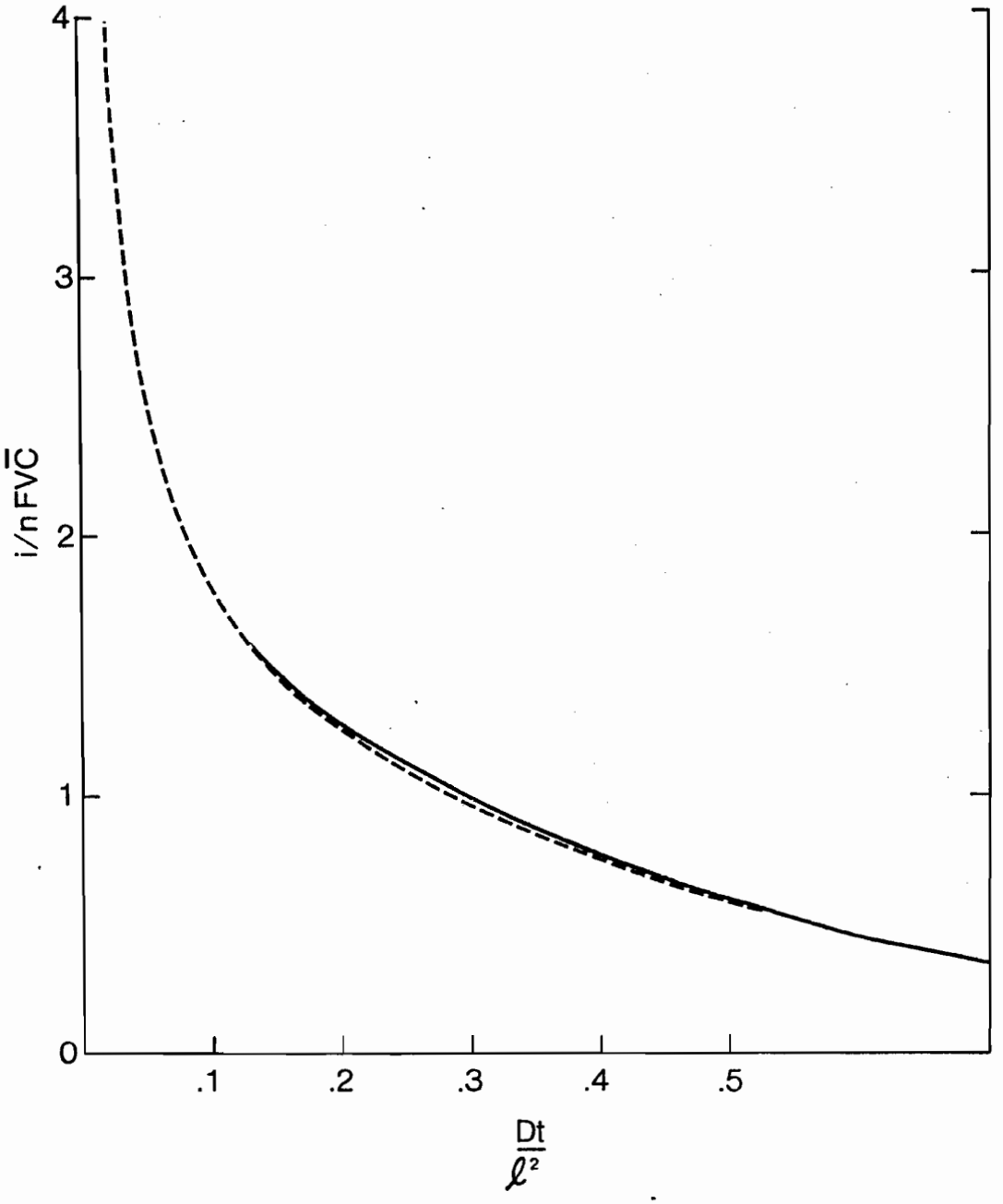

Figure 4: A comparison of equations 15 (solid line) and 16 (dotted line) for a chronoamperometric experiment in a thin cell.

(R) per unit time caused by the homogenous reaction will be the sum of the reaction products formed per unit time at each x (distance from electrode) from x=0 to x=∞,

$$(d(R/h)/dt)_{reaction} = \int_{o}^{\infty} (\partial[B(x)]/\partial t)dx \qquad (17)$$

where [B(x)] is the concentration of B as a function of x, and h is a shape correction factor analogous to f and g. Since,

$$\partial[B(x)]/\partial t = k_f[A(x)]-k_b[B(x)],$$

[A(x)] = A° by assumption, and $k_fA° = k_bB°$, one has

$$\partial[B(x)]/\partial t = k_b(B°-[B(x)]) \qquad (18)$$

Combining equations 17 and 18 yields

$$(dR/dt)_{reaction} = h\int_{o}^{\infty} k_b(B°-[B(x)])dx=hk_bR$$

Under the potentiostatic conditions with an infinite potential applied (B(o,t)=0) one can write from equation 6a,

$$d(B^\circ\delta)/dt = \pi D(B^\circ/2\delta) - hk_b B^\circ\delta \qquad (19)$$

where f has been taken as $\pi/4$. Solution of the exact equation at the steady state reveals that

$$B(x) = B^\circ(1-\exp\{-(k_b/D)^{1/2}x\})$$

and therefore that the steady state current is equal to $nFAB^\circ\sqrt{k_b D}$. This information may be used to evaluate h. At steady state, equation 19 predicts a current $i = nFAB^\circ\sqrt{k_b D}(2h/\pi)$, therefore $h = \pi/2$. Equation 19 is now easily solved (in terms of δ^2) to yield

$$\delta = (D/k_b)^{1/2}(1-\exp\{-\pi k_b t\})^{1/2} \qquad (20)$$

The current may be given by

$$i = nFAB^\circ(k_b D)^{1/2}(1-\exp\{-\pi k_b t\})^{-1/2} \qquad (21)$$

This can be compared with the exact solution (6)

$$i = nFAB^\circ(k_b D)^{1/2}\{\mathrm{erf}(k_b t)^{1/2} + [1/(\pi k_b t)^{1/2}]\exp(-k_b t)\} \qquad (22)$$

A comparison of the two results is made in Figure 5.

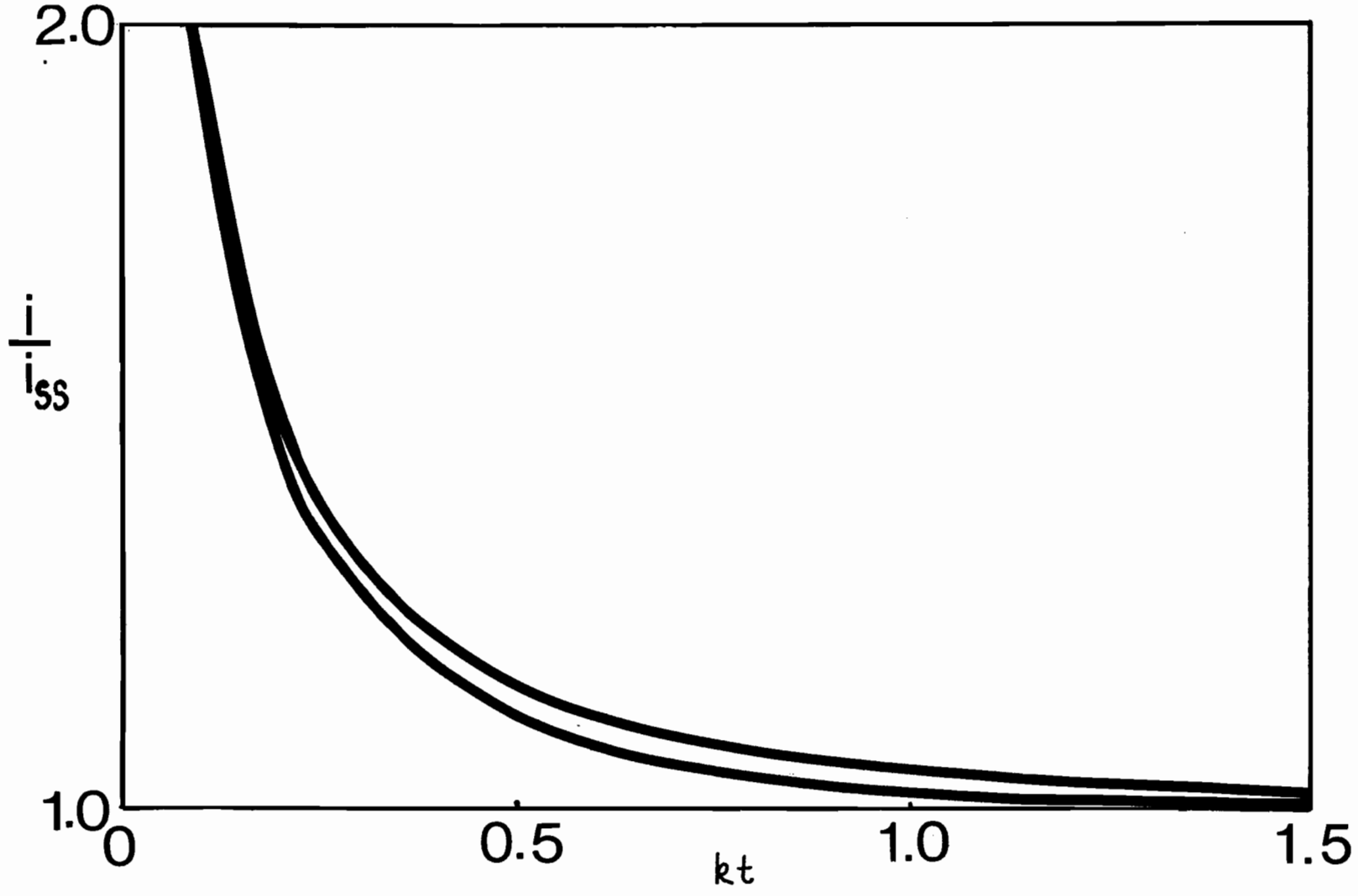

Figure 5: A comparison of equations 21 (lower line) and 22 (upper line) for a chronoamperometric experiment with a preceding homogeneous reaction.

3) Conclusions: The diffusion layer approximation has been successfully extended to cover thin-layer cells and homogenous reaction. The agreement with the exact solution in the thin-layer cell case was excellent, while the agreement for the simple reaction considered was fair. It must not be supposed that the diffusion layer approximation is such a good approximation that it yields these results on its own merits. It is very probable that the matching conditions and Faraday's Law forced a "good" solution to come from the approximate analysis of the thin-layer cell. It is equally likely that forcing the solution to agree with the exact solution at t=0 and t=∞ caused the homogenous reaction case to yield a "good" solution. Further analysis will help to justify these suppositions.

Consider equation 6a

$$d(R/f)dt = \pm J \pm r \qquad (6a)$$

Now, Fick's second law states that

$$\frac{\partial C}{\partial t} = D \frac{\partial^2 C}{\partial x^2}$$

and if one makes provisions for other sources or sinks of C one can write

$$\frac{\partial C}{\partial t} = D \frac{\partial^2 C}{\partial x^2} \pm \rho$$

Let us integrate over x, from x=0 to x=∞ (semi-infinite diffusion) or x=ℓ (thin cells)

$$\int_0^{\infty,\ell} \frac{\partial C}{\partial t}\, dx = D\int_0^{\infty,\ell} \frac{\partial^2 C}{\partial x^2}\, dx \pm \int_0^{\infty,\ell} \rho dx$$

$$\frac{\partial}{\partial t} \int_0^{\infty,\ell} C dx = -D\left(\frac{\partial C}{\partial x}\right)_{x=0} \pm \int_0^{\infty,\ell} \rho dx \qquad (23)$$

It is easily seen that $\int_0^{\infty,\ell} C dx$ is equivalent to R/f, $-D\left(\frac{\partial C}{\partial x}\right)_{x=0}$ is just J and $\pm\int_0^{\infty,\ell} \rho dx$ is equivalent to r. Equation 6a is just the integrated form of Fick's second law.

Depending upon how the diffusion layer thickness is defined, it may enter equation 6a differently. Here it has been defined so that $C^\circ/\delta = (\partial C/\partial x)_{x=0}$. For this reason the flux, J, in terms of δ will be exactly correct. This causes problems in that now $R \neq \int_0^{\infty,\ell} C dx$ and $r \neq \int_0^{\infty,\ell} \rho dx$. More specifically, one should write

$$R(t) = f(t)\int_0^{\infty,\ell} C(x,t) dx$$

$$r(t) = h(t)\int_{0}^{\infty,\ell} \rho(x,t)\,dx.$$

It can now be seen why the incorporation of numerical factors is both valid and necessary. It is intuitively obvious that the more knowledge about the system which can be incorporated into the solution, the better will be the solution. This knowledge is incorporated in the form of f(t) and h(t).

It has been shown that equation 6a can be exact if f(t) and h(t) are known. This analysis demonstrates the validity of the factors f, g and h which the analysis presented earlier did not foster. The value of the earlier analysis is that it reveals the mechanics of the procedure to find a solution under given initial and boundary conditions.

C) The Diffusion Layer Approximation - Two Dimensional Steady State in Channel Electrodes

1. Assumptions and Definitions

The current to a planar electrode located in one wall of a channel through which solution flows in a laminar fashion will be determined. Initially the electrode will be taken to be at infinite potential. Later potential dependence will be considered. Finally, the case of a homogeneous

preceding reaction (CE mechanism) will be considered.

The coordinate system and characteristic dimensions of the channel electrode are shown in Figure 6. Fluid flows in the x direction with a mean velocity $\bar{V}$. The electrode is placed at least a distance L_e away from the entrance to insure that the flow is completely developed laminar flow. L_e is given by $L_e \simeq 0.05\ ReD_h$ (7) where Re is the Reynolds number for the system ($Re = \bar{V}b/\nu$, ν = kinematic viscosity) and D_h is the hydraulic diameter given by four times the cross-sectional area divided by the perimeter (in this case $2W_cb/(W_c+b)$). The flow is considered to be uniform across the width of the channel, a fair assumption for thin channels. Longitudinal diffusion is neglected, and the steady state is presumed to prevail.

2. The Governing Equation

With the above restrictions, except the steady state (and not considering homogenous reactions), the analog to Fick's second law is

$$\frac{\partial C}{\partial t} = D\ \frac{\partial^2 C}{\partial z^2} - V(z)\ \frac{\partial C}{\partial x} \qquad (24)$$

The second term on the right hand side (RHS) represents the

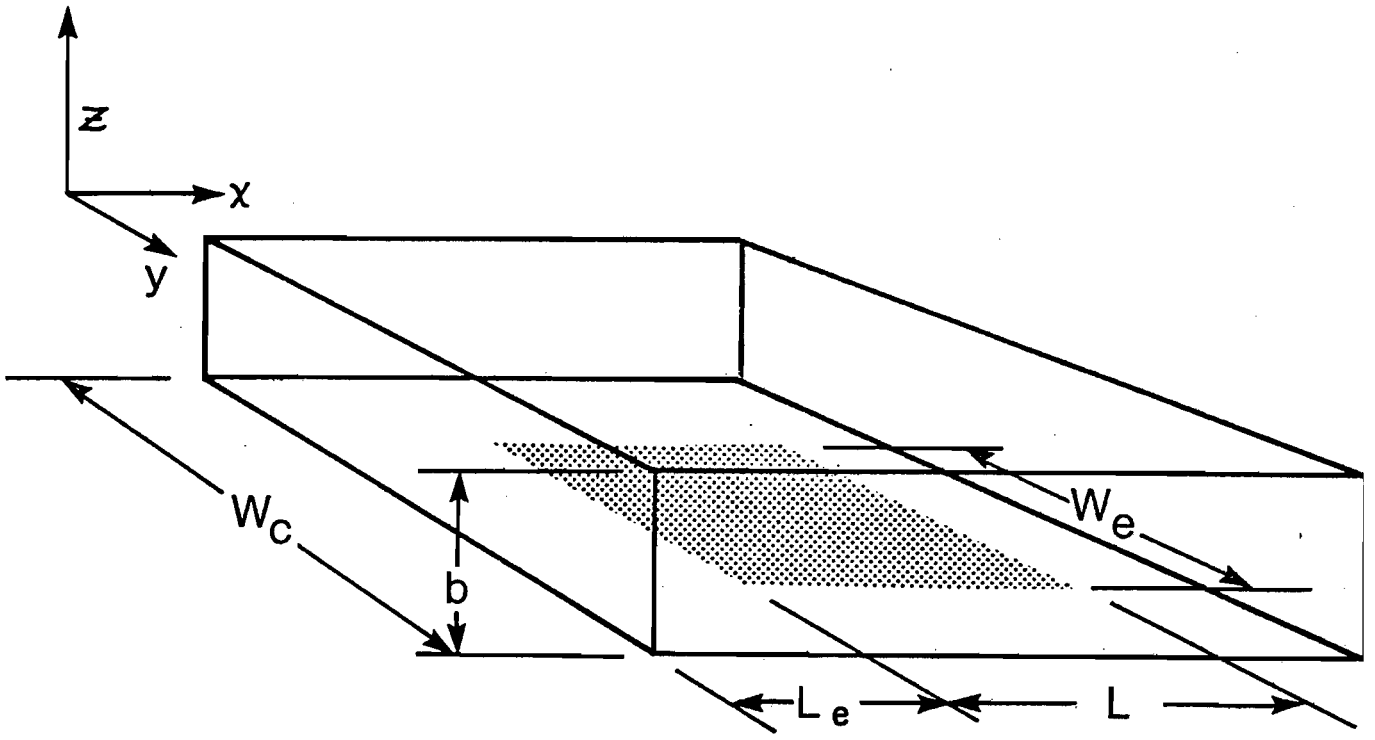

Figure 6: The channel electrode. Solution flows in the x direction over the electrode of length L and width W_e. The channel dimensions are, thickness,b, and width W_c.

contribution to the change in concentration with time in any volume element due to bulk motion. Consider a volume element $\Delta x\Delta y\Delta z$. At one face of this cell, say at point (x,y,z), the bulk motion of the fluid will cause a flux $V(z)C(x,y,z)$, or a net change in moles per time of $V(z)C(x,y,z)\Delta y\Delta z$ since the area of the face of the cell through which the solution is passing is $\Delta y\Delta z$. At the other end of the cell the flux will be $-V(z)C(x+\Delta x,y,z)$, and in moles per time, $-V(z)C(x+\Delta x,y,z)$ $\Delta y\Delta z$. Per unit volume, then, the total change (moles $cm^{-3}s^{-1}$) due to bulk motion will be

$$[V(z)C(x,y,z) - V(z)C(x+\Delta x,y,z)]/\Delta x.$$

As $\Delta x \rightarrow 0$, this becomes

$$-V(z)\ \frac{\partial C}{\partial x}$$

3) Integration of the Governing Equation

For laminar flow between parallel plates (neglecting the walls beside the electrode) $V(z) = 6\bar{V}\bar{z}(1-\bar{z})$ where $\bar{z} = \bar{z}/b$. Let $\bar{x} = xD/6\bar{V}b^2$. Now equation 24 at the steady state becomes,

$$\partial^2 C/\partial \bar{z}^2 - \bar{z}(1-\bar{z})\ \partial C/\partial \bar{x} = 0 \qquad (25)$$

Integrating equation 25 from $\bar{z}=0$ to $\bar{z}=1$ and incorporating the boundary condition $(\partial C/\partial \bar{z})_{\bar{z}=1} = 0$, one obtains

$$-(\partial C/\partial \bar{z})_{\bar{z}=0} = (\partial/\partial \bar{x})\int_0^1 \bar{z}(1-\bar{z})C d\bar{z} \qquad (26)$$

4) Derivation of the Equation for Current

The expression for current will ensue from equation 26. The final expression will in fact be a pair of expressions reflecting the fact that the approximate equation for C is different, depending upon whether the concentration at $\bar{z}=1$ is equal to the bulk concentration or not. For brevity the former case may be called Case I and the latter Case II. The approximations made are as follows.

a) Incorporation of an approximate expression for C by using the linear concentration. In Case I for an infinite potential pulse

$$C = C^\circ \bar{z}/\bar{\delta}(\bar{x}) \qquad 0<\bar{z}\leq\bar{\delta}$$

$$C = C^\circ \qquad \bar{\delta}<\bar{z}\leq 1 \qquad (27)$$

where $\bar{\delta}(\bar{x})$ is the ratio of the diffusion layer thickness to the height of the channel, b, and C° is the bulk concentration.

In Case II

$$C = C(1,\bar{x})\bar{z} \tag{28}$$

where $C(1,\bar{x})$ is the concentration at $\bar{z}=1$. In Case I, the gradient of concentration at the electrode surface will be given by $C°/\bar{\delta}(\bar{x})$, and in Case II, one will have $C(1,\bar{x})$. Current as a function of $\bar{x}$ may be found from these functions. The total measured current will be

$$I(L) = \int_{0}^{\bar{x}_L} i(\bar{x})d\bar{x} \tag{29}$$

where $\bar{x}_L = LD/6\bar{V}b^2$.

b) Incorporation of shape correction factors: As in the case of transients, it is expected that the best solution will be obtained by incorporating as much information as possible about the system into the equations. Four conditions must be met.

i) At $\bar{z} \to 0$, agreement with the equation of Meyer et al. (8) must be obtained, i.e., $I = 1.467\ nFC°W_e(DL/b)^{2/3}(\bar{U}/W_c)^{1/3}$ where $\bar{U}$ is the average volume flow rate, $\bar{U} = \bar{V}bW_c$.

ii) At some distance along the electrode, say $\bar{x}_c$, $\bar{\delta}$ will equal some critical value $\bar{\delta}_c$ at which point the transition

from Case I to Case II will occur. At this point,

$$i(\bar{x})_I = i(\bar{x})_{II}$$

iii) $(\partial i(\bar{x})/\partial \bar{x})_{\bar{x}_c,I} = (\partial i(\bar{x})/\partial \bar{x})_{\bar{x}_c,II}$

iv) At $\bar{z} \to \infty$, 100% coulometric conversion will be obtained, i.e., $I = nF\bar{U}C^{\circ}W_e/W_c$.

The solution (Appendix A) thus obtained is

$$I = nF\bar{U}C^{\circ}(W_e/W_c)\phi(r)$$

where

$$\phi(r) = 1.4032\ \bar{\delta}_L^{\,2} - 0.8024\ \bar{\delta}_L^{\,2} \qquad 0<r<0.3337 \tag{A12}$$

$$= 1.000 - 0.3992\ \exp\{2.505(0.3337) - r_L)\} \qquad r \geq 0.3337$$

$$r_L = 0.9355\ \bar{\delta}_L^{\,3} - 0.6018\ \bar{\delta}_L^{\,4} \quad \text{yields } \bar{\delta}_L \tag{A13}$$

from a knowledge of r_L ($r_L = 6\bar{x}_L$) (Appendix B).

5) Discussion of the Validity and Utility of the Equation

The equation for current to a channel electrode under conditions of laminar flow agrees with the exact equation at

small r by design. To determine its validity for larger r, one can compare it to the equation given by Klimenkov et al. (10). By the use of a series, this group could determine the current to a long electrode (r large) by using only one term in the series. They thus determined the "complete absorption length", i.e., that length which would be required to electro-react 99% of the depolarizer in the flowing stream. They found that a value of r=1.86 will accomplish this. Equation A12 predicts that at r=1.82, 99% conversion will be obtained. The equation is likely to be valid for values of r between very low and very high values. Nonetheless, an experimental verification (to be discussed later) was undertaken.

A convenient representation of equation A12 may be seen in Figure 7. Here, the logarithm of the coulometric yield of the electrochemical reaction is plotted as a function of the logarithm of $r_L^{2/3}$. The curve yields two linear regions, one for $r < 0.016$ and one for $r > 2$. The former region may be called the simple amperometric region, where the current varies as $r_L^{2/3}$ and the latter may be called the coulometric region where $i = nF\bar{U}C^\circ(W_e/W_c)$. For practical purposes, the error is not too large (<10%) if the simple amperometric region is taken to be up to $r \simeq 0.3$.

The value of the simple model is that it allows one to have a semiquantitative description of a complex process.

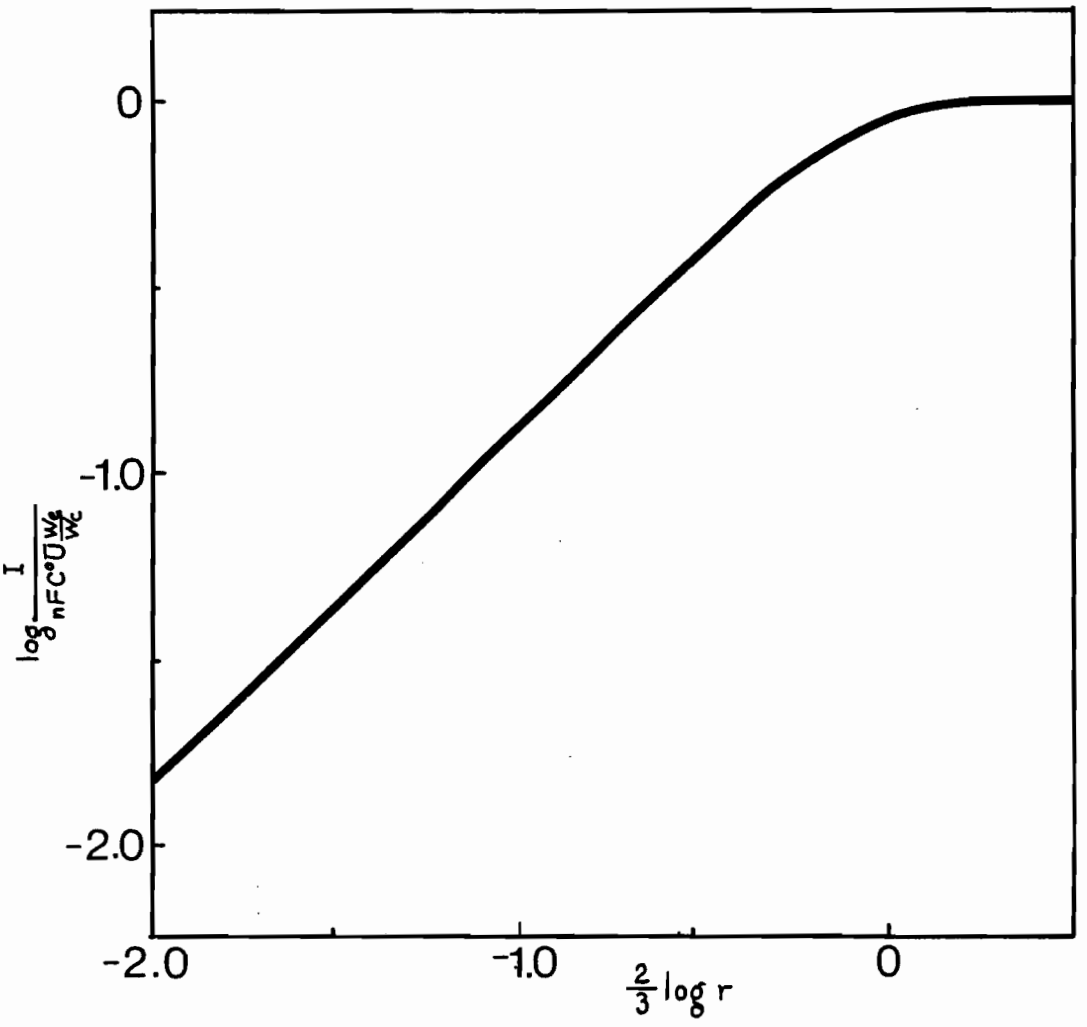

Figure 7: Equation A 12 plotted as the logarithm of the coulometric yield versus the logarithm of $r_L^{2/3}$.

The value of a closed form expression is in the ability to manipulate it easily to determine more information about the system which it describes. More complex processes will be discussed later. Here the differentiation of A12 to find maxima is presented.

In any analytical endeavor, sensitivity, detection limits and selectivity are of concern.

a) Sensitivity: The sensitivity of an analytical procedure may be taken as the slope of the analytical curve. From equation A12 it can be seen that sensitivity is proportional to $\phi(r)$. This obvious results means that coulometric detectors are always more sensitive than amperometric detectors operated at the same flow rate.

b) Detection limit: The detection limit of an analytical procedure may be taken as that quantity of substance required to produce a signal which is equal to twice the rms noise of the system. To be able to use any theoretical expression for signal intensity in the calculation of detection limits or optimum conditions, some knowledge of the noise in the system is needed. To calculate detection limits, quantitative information about the noise is necessary. To determine optimum conditions, qualitative information will suffice. Noise in highly sensitive electroanalytical systems is not nearly as well characterized as noise in optical systems, so that some hypothesizing must be done. It is a natural

tendency to think of residual current as the unwanted element in analysis. In fact, if the residual current for a given system is large but more reproducible and noise-free than another system with a low residual current, then the detection limit will necessarily be lower in the former case. Lankelma and Poppe (11) studied the noise in a channel electrode flow-through system. Interestingly, the two plausible sources which they gave for noise would both demonstrate a linear dependence of noise intensity on electrode area. The signal to noise ratio (SNR) will be taken to have the form current divided by electrode area, not necessarily because residual current is proportional to area, but because of the hypotheses of Lankelma and Poppe (11). It is hoped that future studies will bring to light all the sources of noise in an electrochemical measurement of this sort so that more valid optimization can be accomplished.

The increase of W_e from some value less than W_c to $W_e=W_c$ will increase current and area proportionally, thus W_e does not affect SNR. For this reason $W_e=W_c$ should be used, for it provides amplification of signal with concomitant addition of noise, whereas electronic amplification inevitably adds more noise. All the following calculations are based on $W_e=W_c$. The SNR will equal equation A12 divided by $W_eL=W_cL=A$.

$$SNR = \frac{nFC^{\circ}\bar{U}}{A}\,\phi(r) = \frac{nFC^{\circ}\bar{U}}{A}\,\phi\left(\frac{AD}{\bar{U}b}\right) \qquad (30)$$

Note that SNR depends on A, not W_e and L independently. Thus there is no optimum electrode shape. Furthermore, it can be seen that SNR increases as A decreases and also as b decreases. This means that the cell which has the highest SNR is vanishingly small and vanishingly thin. In this case the noise in the amplification system will become limiting as $A \rightarrow 0$, and the cell should be made only as small as this noise source will allow.

It may be necessary to utilize a constant cell volume, e.g. to insure a specific residence time in the cell for any given flow rate. In this case, the cell volume V=bA. If b is replaced by V/A in equation 30 and the resulting expression is differentiated with respect to A, the derivative has a zero, a maximum at r=0.42. The same result is obtained if A is replaced by V/b and the expression differentiated with respect to b. The maximum SNR will be obtained when $b = (VD/0.42\ \bar{U})^{1/2}$ and A=V/b.

Rotation rate modulation of rotating disk electrodes has proven useful (12-14). The effect of altering the flow rate to obtain a difference signal has been studied by Blaedel and Iverson (15), who used times of 18 sec between changes in flow. Faster changes in flow rate would elicit a signal detectable with a lock-in amplifier. To find the maximum SNR under these circumstances, an expression proportional to the a.c. signal must be found. Since $\Delta I/\Delta\bar{U}$

is being measured, a reasonable approximation to the signal would be $\partial I/\partial \bar{U}$. This expression must then be differentiated with respect to A or b to find the zeros. There is a zero of $\partial^2 I/\partial \bar{U} \partial A$ at r=0.52, a maximum. A cell should be constructed with b as small as possible and then A found from r=0.52.

c) Selectivity: In an electrochemical context, selectivity is best obtained by control of the potential. The relationship between current and voltage is explored later, so a discussion of selectivity will be delayed until then.

It has been shown that the simple approximation used may lead to valid results in the hydrodynamic case. The utility of having a closed form solution to the problem has been demonstrated.

D) The Diffusion Layer Approximation - Special Cases of Channel Electrode Behavior

1) Regenerative Systems

The auxiliary electrode in an electrochemical cell carries the current produced at the working electrode. The auxiliary electrode current is opposite in sign to the working electrode current, i.e., for an anodic working electrode current the auxiliary electrode current will be cathodic. In the context of a thin-layer cell, if the auxiliary

electrode is placed opposite and parallel to the working electrode, the possibility of the regeneration of starting material by the auxiliary electrode may be seen to occur in the following fashion. A molecule of depolarizer is first oxidized at the working electrode surface. By diffusion it travels away from the electrode surface until it reaches the auxilliary electrode where it may be reduced to yield starting material. The same molecule will diffuse back to the working electrode. The process may continue ad infinitum. Non-moving systems such as this have been studied (16). These studies were carried out with a dual working electrode potentiostat. The two working electrodes were aligned parallel and opposed to each other. The potentiostat allowed independent control of the two working electrode potentials. These are called four-electrode systems.

In flowing streams this effect has been alluded to once (11) where the researchers were trying to avoid it, and once (16) where the effect seemed not to work. Using the diffusion layer treatment an approximate description of the current to be expected from such a system may be obtained.

For a cathodic auxiliary electrode, if the potential required to regenerate starting material is less reducing than the potential required to reduce supporting electrolyte or solvent, then virtually all of the oxidized starting material which reaches the auxiliary electrode will be reduced.

This is equivalent to the four-electrode system in which the second working electrode is at a large enough potential to insure complete reduction of oxidized starting material. The two systems can be considered identical under these conditions. Let the working electrode be at a large enough potential to insure complete oxidation of starting material at its surface. This situation is shown in Figure 8.

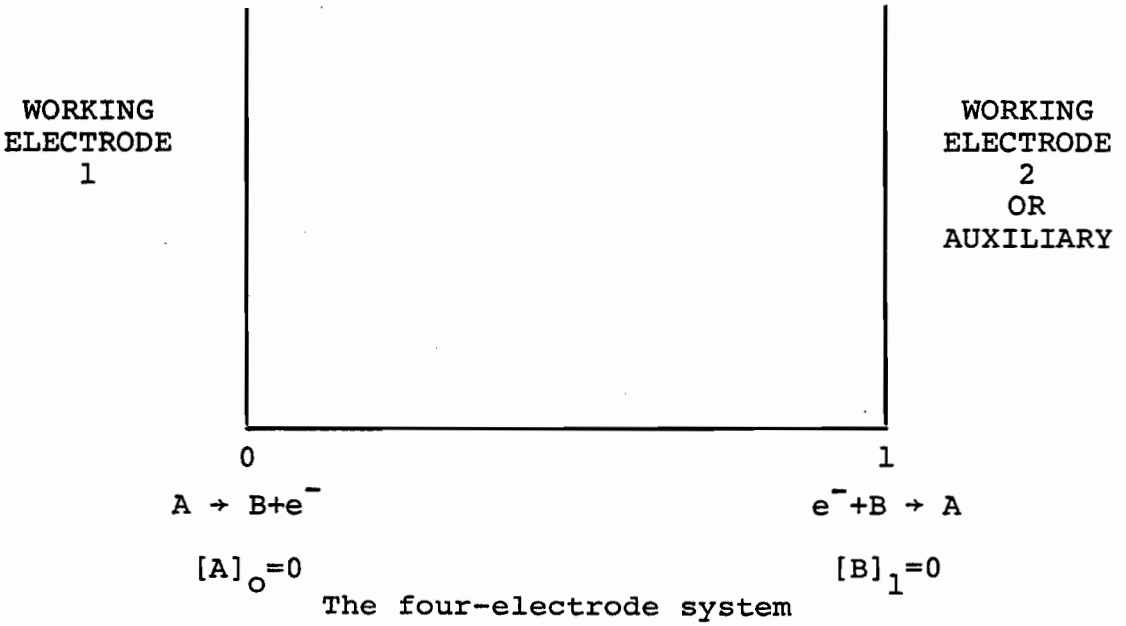

The four-electrode system

Figure 8

This system is no different from the system considered in part C up to the point when the diffusion layer thickness of B equals 1. From equation A12 at $\bar{\delta}_L=1$, the current to this point is $0.6008\ nFC°\bar{U}(W_e/W_c)$. Hereafter the concentration distance relationship will not change, since as B is produced at z=0, it is utilized at z=1. Then $(\partial C/\partial z)_{z=0} = C°/1 = C°$

(for $D_A=D_B$), and $\bar{\delta}=1$. Utilizing equation A5 with a lower limit of integration equal to r=0.3337 (corresponding to $\bar{\delta}=1$) one finds that the current produced after r=.3337 is just

$$I_{r>0.3337} = nF\bar{U}C^{\circ}(W_e/W_c)\ (r_L-0.3337).$$

Adding this to the value obtained previously for current up to r=0.3337 one obtains

$$I = nF\bar{U}C^{\circ}(W_e/W_c)\ (0.2671+r) \qquad (31)$$

or

$$\phi(r) = 0.2671+r \qquad (32)$$

A considerable improvement in sensitivity can thus be obtained for large r.

Suppose that instead of introducing the reduced species, A, one introduces the oxidized species, B, into the flow stream. The measurements will still be taken at the anode. In this case, no current will be observed up to r=0.3337, but then, thereafter, the same situation as above will prevail.

$$\phi(r) = r-0.3337 \qquad (33)$$

Suppose that equal concentrations of both the oxidized and reduced forms of the material, A and B, are introduced

into the flow stream. Consider first species A from which one obtains an anodic current at r=0. From $\bar{z}$=0 (anode) the diffusion layer will begin to grow into the solution. At $\bar{z}$=1 A is being created from B and on top of the bulk concentration of A already present, there is an additional amount from reduction of B. This is shown in Figure 9. Again for equal diffusion coefficients, these two layers will meet at $\bar{z}$=0.5,

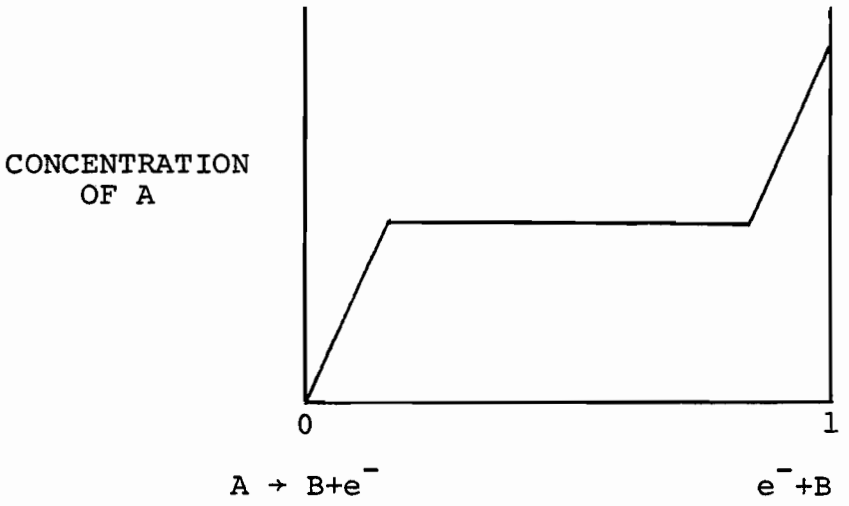

The four-electrode system with both oxidant and reductant

Figure 9

$\bar{\delta}$ will be 1 and for equal bulk concentrations, C°, the gradient of concentration will be 2C°. At $\bar{\delta}$=0.5, r=.1087, and at this point $\phi(r)$=0.2505. Thereafter, $\phi(r) = 2(r-0.1087)$. The sum of the $\phi(r)$'s from the two regions yield

$$\phi(r) = (2r+0.0331) \qquad (34)$$

Equations 32-34 may be written

$$I/nFC_A = LDW_c/b + 0.2671\ \bar{U} \qquad (32a)$$

$$I/nFC_B = LDW_c/b - 0.3337\ \bar{U} \qquad (33a)$$

$$I/nFC_A = 2LDW_c/b + 0.0331\ \bar{U} \qquad (34a)$$

affording a method to experimentally verify this effect. This has been done and the results will be described later.

2) Potential Dependent Behavior

In the case of potential dependent behavior, the basic equations are the same as in part C, except that $C(0)\neq 0$. This surface concentration will be a function of potential. Equations similar to 7 and 12 are anticipated. The results, derived in Appendix C, follow.

$$I/nF\bar{U}(W_e/W_c) = (\bar{k}_f C^\circ - \bar{k}_b C^{\circ\prime})\phi(r,p) \qquad (\bar{\delta}_L<1)$$

$$\phi(r,p) = \frac{\bar{\delta}_L}{1+\bar{\delta}_L p}\left(\bar{\delta}_L^{\,2} - \frac{1}{2}\bar{\delta}_L^{\,3}\right) \qquad (C17)$$

$$\bar{k}_f = k_f b/D$$

$$\bar{k}_b = k_b b/D$$

$$p = (k_b\varepsilon + k_f)b/D$$

$$\varepsilon = \frac{D\bar{\delta}'}{D'\bar{\delta}} = \left(\frac{D}{D'}\right)^{2/3} \left(\frac{1-\bar{\delta}/2}{1-\bar{\delta}'/2}\right)^{1/3}$$

$$(D/D')^{1/2} \leq \varepsilon \leq (D/D')^{2/3}$$

$\bar{\delta}_L$ is calculated from

$$r_L = -\frac{3}{8}\bar{\delta}_L^4 + \left(\frac{2}{3} - \frac{1}{6p}\right)\bar{\delta}_L^3 + \left(\frac{1}{2p^2} + \frac{1}{p}\right)\left(\frac{\bar{\delta}^2}{2} - \frac{\bar{\delta}}{p} + \frac{\ln(1+\bar{\delta}p)}{p^2}\right) \qquad (C16)$$

k_f and k_b are the potential dependent rate constants in the Butler-Volmer equation.

$$\phi(r,p) = \frac{1}{1+p}\left\{\frac{1}{2} + g(p)\left[1-\exp\{(r_c-r_L)/g(p)\}\right]\right\} \quad (\bar{\delta}_L > 1)$$

$$g(p) = \left(2+p+\frac{D/D'-1}{2}\bar{k}_b\right)/2\left(p-\frac{D/D'-1}{2}\bar{k}_b\right) \qquad (C25)$$

$$r_c = r \text{ at } \bar{\delta} = 1$$

For simplicity, no shape correction factor has been employed. It is stating the obvious, but it is clear that the price paid for conceptual simplicity is algebraic complexity.

a) Previous solutions: The potential dependence of hydrodynamic currents has been studied by Blaedel and Klatt (17) for reversible reactions in a tubular electrode, and by

Matsuda (18) for reversible and irreversible reactions in tubes and channels at small r. In a general sense the concept of the heat-transfer coefficient (19) was adapted to mass transfer by Jordan and Javick (20) to determine current voltage relationships. This attractively simple and experimentally valuable approach has recently been utilized by Blaedel and Engstrom (21). A heuristic argument was presented by Hubbard and Anson (22) for reversible reactions at a coulometric detector. The results of these analyses will be compared to the results derived here.

b) Comparison of the diffusion layer approximation (DLA) to other results: Details of these computations may be found in Appendix D. Graphs of the various types of waves may be found in Figure 10.

The treatment of Jordan and Javick (20) and Blaedel and Engstrom (21) is dependent upon the experimental measurement of limiting current. Since an expression for limiting current has been derived here for all r, a calculated limiting current was used in lieu of an experimental one. This yielded an expression for current as a function of r and potential. As such the treatment of Jordan and Javick (20) used here is really a hybrid between the diffusion layer approximation and the Jordan and Javick treatment.

It is convenient to return for a moment to the case of the infinite potential taken up in section C of this chapter.

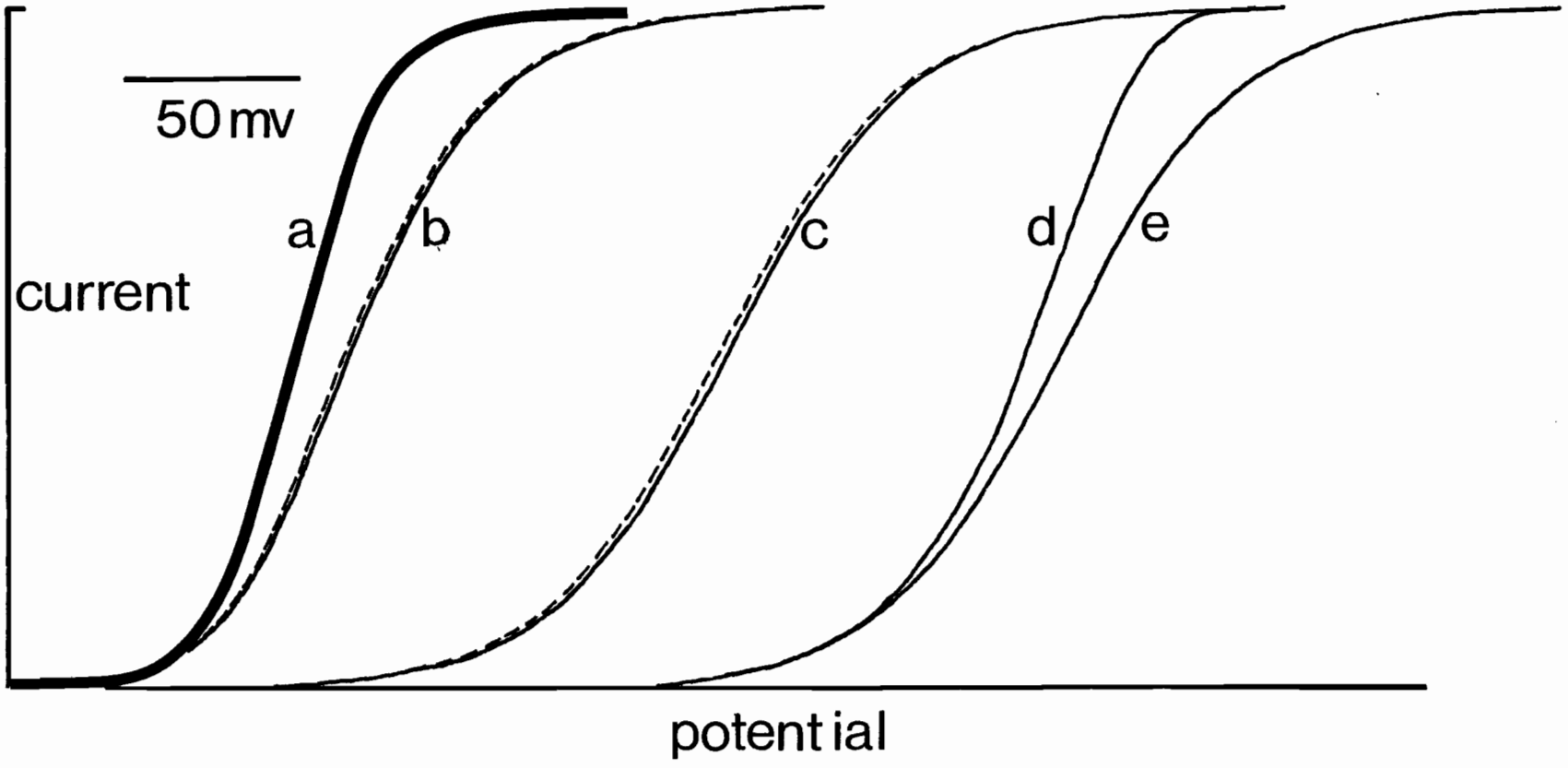

Figure 10: Current-potential curve shapes in channel electrode steady-state hydrodynamic voltammetry. a;a reversible wave, amperometric or coulometric, all three mathematical treatments. b;a quasi-reversible wave, the solid line is Matsuda's treatment, the dotted line is the DLA. c;an irreversible wave, the dotted line is the DLA and the solid line is the treatment of Matsuda. d;case v,vi wave,DLA. e;case v,vi wave, Jordan Javick treatment. These waves are for a two electron transfer.

What exactly is r besides a convenient dimensionless parameter? When written as $\frac{L/\bar{V}}{b^2/D}$ it can be seen that it is the ratio of the average time required for a particle to traverse the length of the electrode (by bulk fluid motion) to the average time required for a particle to traverse the height of the channel (by diffusion). If, for instance, the residence time $\tau_r = L/\bar{V}$ is larger than the diffusion time $\tau_d = b^2/D$, then the probability that a particle will travel by diffusion from z=b to z=0 (the electrode surface) by the time it leaves the cell is high. Thus for $r \gtrsim 1$ coulometric conversion should be obtained. That this is the case is borne out by Figure 7.

In the case where there is a limiting rate of reaction at the electrode surface, a third time may be introduced. This is the heterogeneous reaction time, $\tau_h = b/k$, where k is the heterogeneous rate constant. The relative ordering of these three times yields six categories of behavior shown in Table 1. Consider the three times in pairs. If $\tau_d > \tau_r$ then the cell will be operating in the amperometric region, if $\tau_r > \tau_d$ the cell will be operating in the coulometric region. If $\tau_h > \tau_r$ then particles travelling from z=b would not reach the electrode surface by the time they leave the cell if they were travelling with a velocity k. This means that even though diffusion and residence requirements are met for coulometric detection, the reaction velocity will

Table 1

Hydrodynamic Voltammetry at Channel Electrodes

Case	Conditions	Description	Applicable Treatments: Matsuda	Jordan	This Work
i	$\tau_d > \tau_r > \tau_h$ $(1>r>\bar{k}_f^{-1})$	amperometric diffusion limited	x	x	x
ii	$\tau_d > \tau_h > \tau_r$ $(1>\bar{k}_f^{-1}>r)$	amperometric diffusion limited	x	x	x
iii	$\tau_h > \tau_d > \tau_r$ $(\bar{k}_f^{-1}>1>r)$	amperometric rate limited	x	x	x
iv	$\tau_r > \tau_d > \tau_h$ $(r>1>\bar{k}_f^{-1})$	coulometric diffusion limited		x	x
v	$\tau_r > \tau_h > \tau_d$ $(r>\bar{k}_f^{-1}>1)$	coulometric rate limited, equilibrium			x
vi	$\tau_h > \tau_r > \tau_d$ $(\bar{k}_f^{-1}>r>1)$	coulometric rate limited, not equilibrium			x

not be large enough to electroreact all the material present. If $\tau_d > \tau_h$ then the current is limited by diffusion.

Now let us consider the six cases presented in Table 1. Because of the relative sizes of τ_d and τ_r, cases i-iii represent amperometric behavior. The transition from iii to i is from a lower heterogeneous reaction rate to a higher rate corresponding to a potential sweep which would cause a "wave". At least for $\tau_d >> \tau_r$ these cases have been treated exactly by Matsuda (18) and may be treated by the approximate procedure of Jordan and Javich (20) and the present procedure. For a reversible reaction all three methods yield the same result. The ratio of current at any potential to limiting current (I/I_D) has a sigmoid (wave) dependence on potential. For the forward (cathodic) reaction in the absence of the reduced half of the couple one has,

$$E_{1/2} = E^\circ - (RT/nF)\ln(D_o/D_R)^{2/3}$$

where $E_{1/2}$ is the half-wave potential and E° is the standard potential.

For an irreversible wave, each treatment predicts a wave of the same shape with the same dependence of $E_{1/2}$ on physical parameters. For the same conditions as above,

$$E_{1/2} = E^\circ + \frac{RT}{\alpha nF}[\ln k_o - \frac{2}{3}\ln D_o - \frac{1}{3}\ln\frac{\bar{V}}{bL} - \zeta]$$

where k_o is the apparent standard rate constant, αn is the transfer coefficient (cathodic) and ζ is a constant which varies among the three treatments. Matsuda's treatment yields $\zeta = 0.342$, the Jordan Javick treatment yields 0.361 and the DLA yields 0.181. The effect of this difference in the constant values is that the treatment of Jordan and Javick shifts $E_{1/2}$ 0.62 mV negative (for a cathodic process) with respect to the $E_{1/2}$ predicted by Matsuda. The DLA results in an $E_{1/2}$ shifted 4.2 mV in the opposite direction from the $E_{1/2}$ predicted by Matsuda. For amperometric conditions the Jordan and Javick treatment is really quite good, and there seems to be no reason to recommend the use of the DLA. Note, however, that it has been established that the nature of the current-voltage curve predicted by the DLA is the same as the curve predicted by Matsuda except that it is shifted between 0 and 4.2 mV from the exact solution. The amount of the shift depends upon the degree of reversibility.

Cases iv-vi in Table 1 are considered coulometric systems. The common property of cases iv-vi, that $\tau_r > \tau_d$, is the same as stating $r > 1$. The results of Matsuda may not be used here since he approximated the laminar velocity profile by a linear relationship which is only true for small $\bar{z}$ (<u>i.e.</u>, small $\bar{\delta}$, low r_L)

$$V = 6\bar{V}\bar{z}(1-\bar{z}) \qquad \text{Laminar flow, exact}$$

$V = 6\bar{V}\bar{z}$ Laminar flow, approximate, valid for small $\bar{z}$ ($r \lesssim 0.01$)

Case iv has been discussed, albeit briefly, by Hubbard and Anson (22). It corresponds to a diffusion limited coulometric wave. Both the Jordan Javick approximation and the DLA agree with the assertions of Hubbard and Anson (22),

$$E_{1/2} = E^\circ - (RT/nF)\ln(D_o/D_r)^{1/2}$$

This is for a reduction, where D_o is the diffusion coefficient of the oxidized species and D_r that of the reduced species. Cases v and vi are somewhat unusual. Consider the "reversible" hydrodynamic current voltage curve in Figure 11a. This is a curve taken with a rotating disk or some other system where semi-infinite diffusion applies. Outside the range of about $E_{1/2} \pm (100/n)$ mV the wave is at a plateau and the current is diffusion controlled. The concentration of depolarizer at the electrode surface is zero. The material which reacts at the electrode comes by diffusion. Now let the same set of circumstances apply in a thin channel. Since diffusion is no longer semi-infinite, if r is large enough all the depolarizer will diffuse to the electrode surface and be consumed. This is a coulometric cell, case iv. Now consider the "irreversible" wave under semi-infinite diffusion

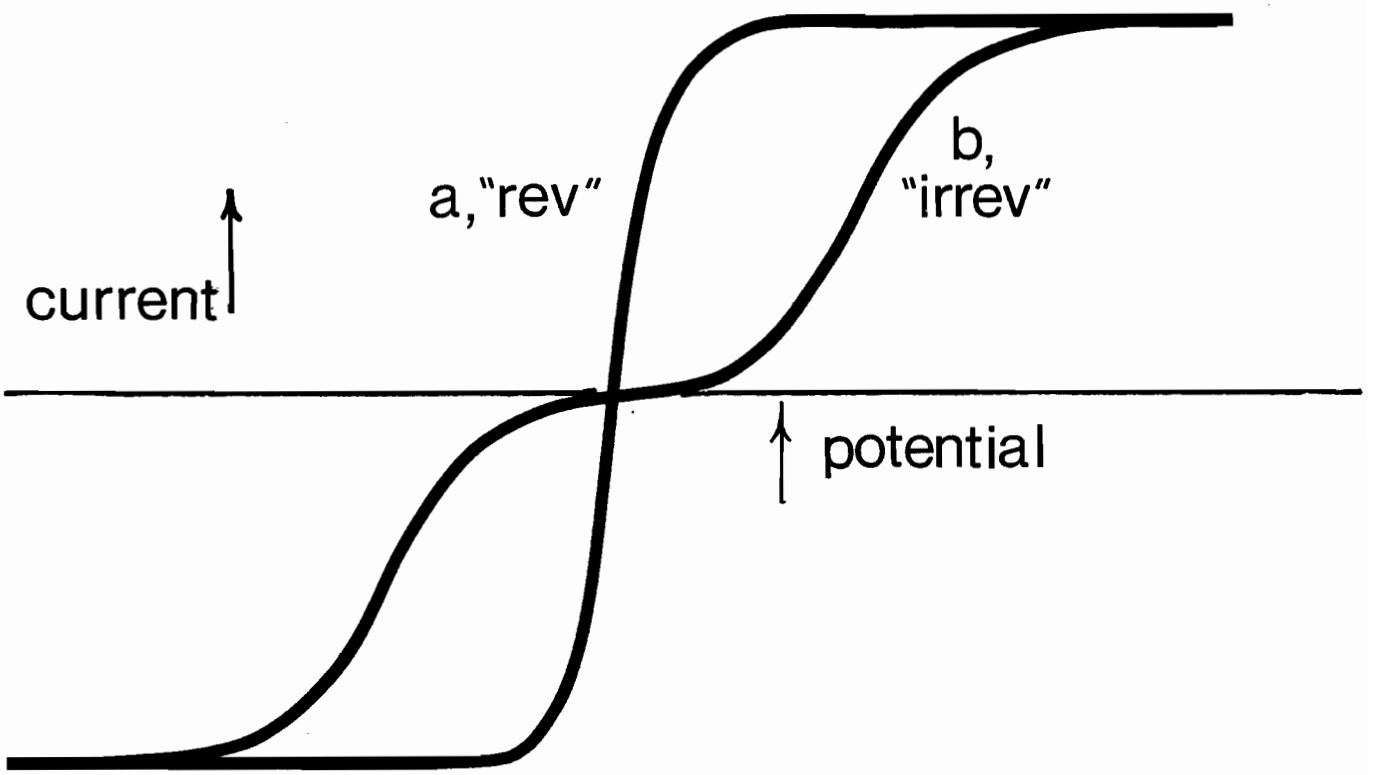

Figure 11: A reversible wave,a, and an irreversible wave,b, in voltammetry. At the point indicated by the arrow sufficient potential is applied to the electrode to bring the concentration of depolarizer at the electrode surface to zero if the electrochemical reaction rate is much greater than the diffusion or mass transport rate.

conditions at the point shown in Figure 11b. Unlike the previous example, the concentrations of the redox couple are not in equilibrium with the electrode, but they are not in equilibrium with the bulk solution either. The heterogeneous reaction rate is slow so that when the concentrations move toward equilibrium with the electrode, hydrodynamic and diffusive mass transport work to re-establish the concentrations existing in the bulk of solution. Once again, let us carry this system into a thin channel. Now, while mass transport continues to work against the electrode reaction in bringing the surface concentrations into equilibrium with the electrode, the bulk of solution is being depleted by the electrode reaction. Eventually, the entire bulk of solution will be brought into equilibrium with the electrode surface, i.e., coulometric yield will be obtained. The control of the current is by the rate of electrochemical reaction, not by mass transport rate. This is a coulometric cell, case v. If r is not large enough to allow the process in case v to reach completion, then the cell is case vi.

The salient point about cases v and vi is that the current is always kinetically controlled. The limiting current is kinetically controlled. Perhaps one might say that it is limited by mass availability. In any event, it is not mass transport controlled. The limiting current in the

Jordan Javick treatment is a mass-transport limiting current, thus this treatment is not applicable for case v. The difference between the two predictions is shown in Figure 10d and e. Case vi corresponds to roughly the same situation as in case v with one important difference. While τ_r, $\tau_h > \tau_d$ so that the concentration profile is virtually flat, since $\tau_h > \tau_r$ in case vi the electrode is not long enough to allow equilibrium with the electrode potential to be obtained. This is the case at the "foot" of the wave in Figure 10d.

For the irreversible case in the regions of r_L and p which include cases v and vi, equation C25 may be written

$$I/I_L = 1 - \exp\{-r_L\bar{k}_f\} + \bar{k}_f/2$$

$$\simeq 1 - \exp\{-r_L\bar{k}_f\}$$

thus

$$E_{1/2} = E^\circ - \frac{\alpha nF}{RT}\{\ln\frac{\bar{V}b}{Lk_o} - \ln\ln 2\}$$

where k_o is the apparent standard heterogeneous rate constant and I_L is the limiting current. Notice that the inflection point of the wave occurs at $I/I_L = 0.641$, not at $I/I_L = 0.500$. Half wave potentials have been calculated for various conditions. If r is changed by alteration of b or D, then $\bar{k}_f$ is also changed since $\bar{k}_f = k_f b/D$. If r is changed by

alteration of $\bar{U}$, W_c or L, then $\bar{k}_f$ is not changed. For this reason, $E_{1/2}$ for various apparent standard heterogeneous rate constants, k_o, were calculated as a function of r. The parameter r was varied in one case (Figure 12, Table 2) by variation of $\bar{U}$, and in the other case (Figure 13, Table 3) by variation of b. Notice that in Figure 12 for r > 1 that the curve of $|E°-E_{1/2}|$ vs log k_o takes on an unexpected shape. This is due to the unsymmetrical shape of the wave in case v, vi (Figure 10d). If the potential at the inflection point of the wave ($I/I_L = 1-e^{-1} = 0.641$) is plotted, the curve regains a more expected shape.

c) Selectivity by potential control: In physico-chemical investigations, the potential dependence of the current is usually used to determine various parameters which describe the electro-chemical reaction. Most analytical chemists prefer to operate in the region where the sensitivity is the highest, the limiting current region. There are certain circumstances under which the analytical chemist may find it more optimal to operate in a region of potential where the current is a function of potential. Differential measurement is one such circumstance.

In order to gain selectivity in the use of electrochemical detectors two techniques have been devised and published. Blank (23) utilized a cell in which there were two working electrodes. Each working electrode could be set to a different

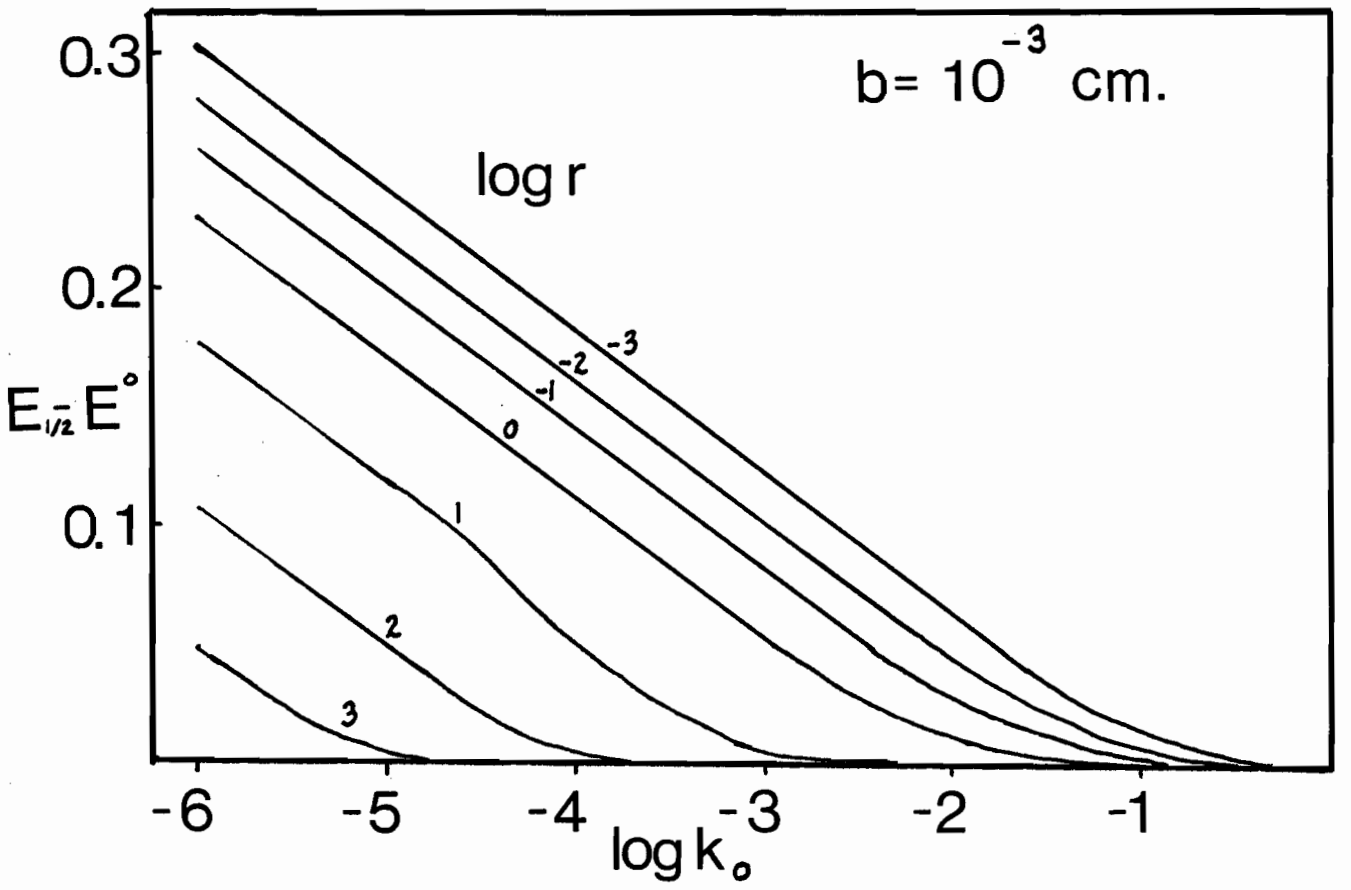

Figure 12: $E_{1/2}$ as a function of k_o and r, b constant. The calculations were performed for $D_o=D_r$ and n=2.

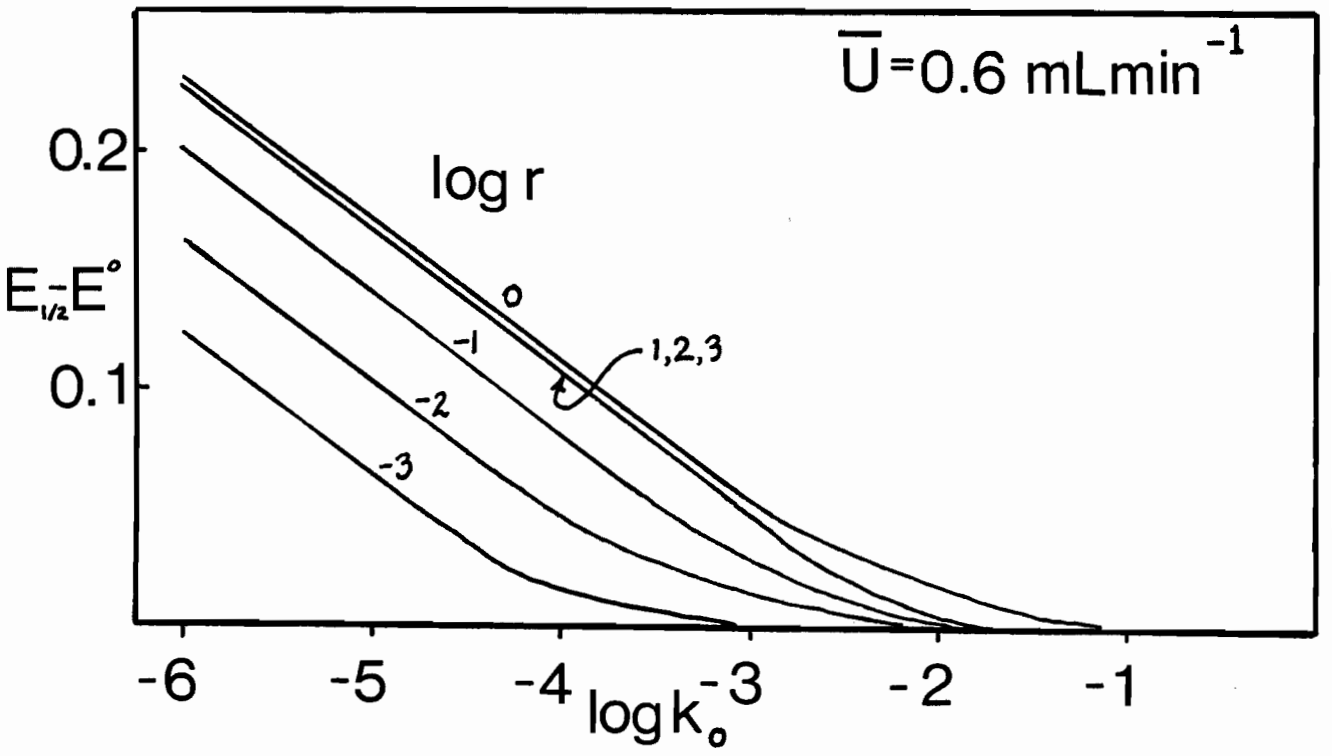

Figure 13: $E_{1/2}$ as a function of k_o and r, $\bar{U}$ constant. The calculations were performed for D_o=D_r and n=2.

Table 2

Variation of $E_{1/2}$ with r and standard rate constant (thickness constant).

	k_o						
r*	10^{-6}	10^{-5}	10^{-4}	10^{-3}	10^{-2}	10^{-1}	1
10^{-3}	-302.1	-242.9	-183.8	-124.6	-65.7	-15.5	-1.7
	-305.1	-244.8	-186.7	-127.6	-68.6	-17.2	-1.9
	-304.4	-244.2	-186.2	-127.0	-68.0	-16.9	-1.9
10^{-2}	-281.2	-222.7	-163.6	-104.4	-46.0	- 7.4	- .8
	-284.4	-225.3	-166.2	-107.0	-48.4	- 8.2	- .9
	-284.7	-225.6	-166.5	-107.3	-48.7	- 8.3	- .9
10^{-1}	-260.7	-201.6	-142.5	- 83.4	-27.4	- 3.4	- .3
	-261.6	-202.5	-143.3	- 84.2	-28.1	- 3.5	- .4
	-	-	-	-	-	-	-
1	-230.7	-171.6	-112.5	- 53.7	- 9.2	- 0.9	- .1
	-234.5	-175.3	-116.3	- 57.4	-11.5	- 1.2	- .1
	-	-	-	-	-	-	-
10	-178.8	-119.8	- 50.8	- 4.8	0	0	0
	-177.4	-118.2	- 59.4	-12.4	- 1.3	- .1	0
	-	-	-	-	-	-	-
100	-108.9	- 50.0	- 4.0	0	0	0	0
	-118.2	- 59.4	- 12.4	- 1.3	- .1	0	0
	-	-	-	-	-	-	-
1000	- 50.0	- 3.9	0	0	0	0	0
	- 59.4	- 12.4	- 1.3	- .1	0	0	0
	-	-	-	-	-	-	-

*Of the three rows corresponding to a given r value, the first is from DLA, the second from Jordan, and the third from Matsuda.

Table 3

Variation of $E_{1/2}$ with r and standard rate constant (flow rate constant).

	k_o						
r*	10^{-6}	10^{-5}	10^{-4}	10^{-3}	10^{-2}	10^{-1}	1
10^{-3}	-124.6	- 64.5	- 15.6	- 1.7	- .2	0	0
	-127.6	- 68.5	- 17.2	- 1.9	- .2	0	0
	-127.0	- 68.0	- 16.8	- 1.9	- .2	0	0
10^{-2}	-163.6	-104.4	- 46.0	-17.4	- .8	- .1	0
	-166.2	-107.0	- 48.4	-18.2	- .9	- .1	0
	-166.6	-107.3	- 48.7	-18.3	- .9	- .1	0
10^{-1}	-201.6	-142.5	- 83.4	-27.4	- 3.4	- .3	0
	-202.5	-143.3	- 84.2	-28.1	- 3.1	- .3	0
	-	-	-	-	-	-	-
1	-230.7	-171.6	-112.5	-53.7	- 9.2	- .9	- .1
	-234.5	-175.3	-116.3	-57.4	-11.5	-1.2	- .1
	-	-	-	-	-	-	-
10	-228.0	-168.8	-109.8	-50.8	- 4.8	0	0
	-236.5	-177.4	-118.2	-59.4	-11.9	-1.3	- .1
	-	-	-	-	-	-	-
100	-227.1	-168.0	-108.9	-50.0	- 4.0	0	0
	-236.5	-177.4	-118.2	-59.4	-11.9	-1.3	- .1
	-	-	-	-	-	-	-
1000	-227.0	-167.9	-108.8	-50.0	- 3.9	0	0
	-236.5	-177.4	-118.2	-59.4	-11.9	-1.3	- .1
	-	-	-	-	-	-	-

*Of the three rows corresponding to a given r value, the first is from DLA, the second from Jordan, and the third from Matsuda.

potential. Separate current-to-voltage converts were built for each electrode. The only difference between the design of Blank (23) and merely placing two separate cells in series is that in Blank's case (23) only one cell body was used. This allowed the two signals to be obtained without the band broadening which would have occurred from using two cells.

In a similarly motivated paper, Swartzfager (24) demonstrated the utility of applying a differential pulse potential waveform to the working electrode. In differential pulse voltammetry, the potential is stepped back and forth between two levels a distance ΔE mV apart. The difference between the current obtained at the two levels of potential is displayed. If both levels of potential, E and $E+\Delta E$, are on the plateau of a wave, then the resultant difference in current will be zero. If E and $E+\Delta E$ are near $E_{1/2}$ of the wave then the resultant difference in current will be non-zero. This would allow for some selectivity in electrochemical detection. Consider substance A which has a wave at $E_{1/2}$ = 200 mV vs SCE and substance B which has a wave at $E_{1/2}$ = 700 mV vs SCE. At 700 mV vs SCE the former wave is certainly on a plateau, and the differential pulse waveform will detect no difference in current from A. At the same time a signal from B will be obtained. Then B may be determined in the presence of A. This gain in selectivity is accompanied by a loss in SNR of 10 (24).

These two concepts may be quite easily combined. Using the simpler and less expensive circuit of Blank (23) one can obtain the objective of Swartzfager (24) without an SNR loss of 10. The potential at the two working electrodes in a cell may be set to E and E+ΔE and maintained at that potential. The currents from the two electrodes may be subtracted to yield a d.c. differential signal with the same information content as that in Swartzfager's experiment (24). Using the present mathematical result it is possible to predict the differential signal from any electrochemically active compound given k_o, r_L, b, D, E, ΔE and concentration.

The SNR advantage (with respect to differential pulse) may be found easily by reference to Figure 10. To obtain differential current, two signals with independent random errors are subtracted. The resultant signal will have a variance equal to the sum of the variances of the two independent signals. If we let σ_1 be the standard deviation of the current from the electrode at potential E and σ_2 be the standard deviation of the current from the electrode at potential E+ΔE, then σ_{2-1}, the standard deviation of the difference signal, will be

$$\sigma_{2-1} = \sqrt{\sigma_1^2+\sigma_2^2}$$

For electrodes of equal area in the same flow cell at not too different voltages

$$\sigma_1 \simeq \sigma_2$$

therefore

$$\sigma_{2-1} \simeq 1.4\ \sigma$$

where $\sigma = \sigma_1 = \sigma_2$. The signal to noise ratio at one working electrode under optimal conditions is I_L/σ, where I_L is the limiting current. Under what d.c. differential conditions will we degrade this by a factor of 10 as is the case with differential pulse? The noise for d.c. differential operation equals 1.4σ so

$$\frac{\text{d.c. differential signal}}{1.4\ \sigma} = \frac{I_L}{10\sigma}$$

$$\text{d.c. differential signal} = .14\ I_L$$

Simple measurements using the graphs in Figure 10 show that the voltage difference which must be applied near $E_{1/2}$ to obtain this signal are:

reversible wave	8 mV
irreversible (case v, vi)	11 mV
irreversible (case ii, iii)	15 mV

This may be compared to the 50 mV ΔE used by Swartzfager (24).

At the same level of precision it is possible to increase the selectivity of an electrochemical detector with d.c. differential detection. On the other hand, it is equally possible to increase the precision of the analysis at the same selectivity.

3) The CE Mechanism

a) Derivation of the differential equations: For the preceding first order chemical reaction

$$Y \underset{kK}{\overset{k}{\rightleftharpoons}} A$$

followed by oxidation or reduction at the electrode

$$A \xrightarrow{\pm e^-} B$$

surface the following coupled differential equations apply.

$$v(\bar{z})\frac{\partial C_A}{\partial x} = D_A \frac{\partial^2 C_A}{\partial z^2} + k(C_y - KC_A)$$

$$v(\bar{z})\frac{\partial C_y}{\partial x} = D_y \frac{\partial^2 C_y}{\partial z^2} - k(C_y - KC_A) \qquad (35)$$

In equations 35 $v(\bar{z})$ is the velocity as a function of $\bar{z}$, C_A and C_y are concentrations and D_A and D_y are diffusion coefficients, the subscript indicating to which species the parameter belongs. For laminar flow in a channel $v(\bar{z}) = 6\bar{V}\bar{z}(1-\bar{z})$, $\bar{V}$ = mean fluid velocity. Matsuda (18,25) has studied this problem, and has provided two solutions. One (18) is valid for large k with any D_y and D_A, and the other (25) is valid for small k but with $D_y = D_A$. The case in which k is small and $D_y \neq D_A$ has not been solved. The DLA may be modified to include the chemical reaction.

It will be assumed that Y is not electroactive, thus it has no flux at the electrode surface. The DLA may be used to approximate the concentration profiles as shown in Figure 14. The salient features of the approximation are i) the boundary conditions for flux are satisfied at $\bar{z} = 0$ and $\bar{z} = \bar{\delta}_2$, ii) A and Y are in equilibrium for $\bar{z} > \bar{\delta}_1$, and iii) the flux of A in the region $0 \leq \bar{z} \leq \bar{\delta}_1$, is equal to the combined fluxes of A and Y at $z > \bar{\delta}_1$. The current at any x will be given by the flux of A multiplied by nFA.

Through the use of the DLA with no shape correction factors, equations 35 become (Appendix E).

$$-\frac{\bar{V}}{b}\frac{d}{dx}\left(\frac{\delta_1^3 KD_y+\delta_2^3 D_A}{KD_y\delta_1+D_A\delta_2}\right) = -D_A\frac{D_A+KD_y}{KD_y\delta_1+D_A\delta_2} + \frac{kK(D_A+KD_y)}{2(KD_y\delta_1+D_A\delta_2)}\delta_1^2 \qquad (36)$$

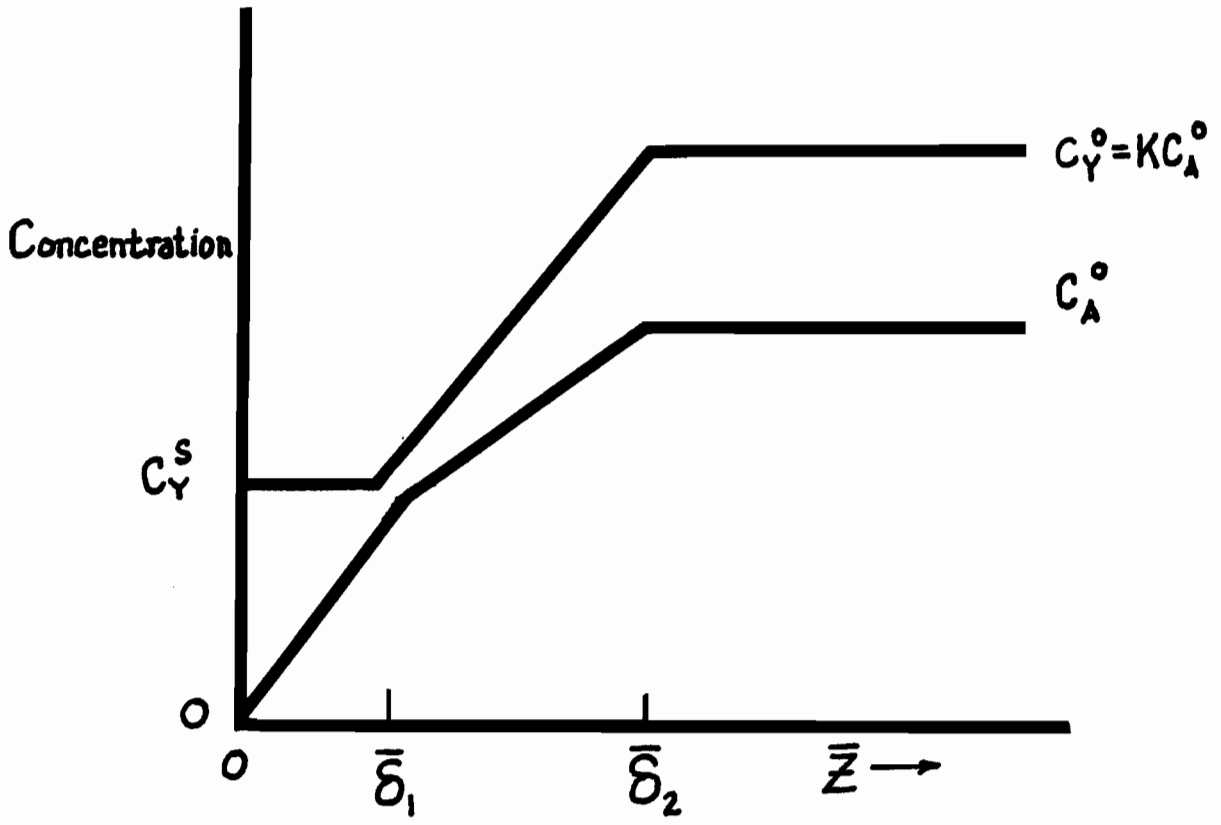

Figure 14: The DLA with a CE mechanism. Note that there are two diffusion layer thicknesses to calculate.

$$\frac{K\bar{V}}{b}\frac{d}{dx}\left(\frac{\delta_1^3 D_A - \delta_2^3 D_A}{KD_y\delta_1 + D_A\delta_2}\right) = -\frac{kK(D_A+KD_y)}{2(KD_y\delta_1+D_A\delta_2)}\delta_1^2 \qquad (37)$$

Recalling $r = xD/\bar{V}b^2$, and defining N as $N = KD_y\bar{\delta}_1 + D_A\bar{\delta}_2$ where the bar indicates division by b, these two equations may be combined to yield

$$\frac{d}{dr}\frac{\delta_1^3}{N} = \frac{1}{N} - \frac{k(1+K)b^2}{2D_A N}\bar{\delta}_1^2 \qquad (38)$$

$$\frac{d}{dr}\frac{\bar{\delta}_2^3}{N} = \frac{1}{N} + \left(\frac{D_y}{D_A} - 1\right)\frac{kKb^2}{2D_A}\frac{\bar{\delta}_1^2}{N} \qquad (39)$$

Now instead of having a pair of second-order coupled partial differential equations, one has a pair of first order coupled ordinary non-linear differential equations. It would not be easy to find analytical solutions to equations 38 and 39. Even by making simplifications and further approximations, the equations were not solved. The advantage of obtaining simple closed form solutions by using the DLA has been lost. It seems that the DLA is reaching the end of its usefulness.

With no analytical solution forthcoming, attention must be focused on numerical solutions. It is likely that equations 35 could have been solved numerically if one had sufficient expertise. It was decided to solve equations 38

and 39, if at all possible, since subroutines for solving sets of first order differential equations were readily available (IMSL McGill Computing Center). In order to utilize the subroutines equations of the form

$$\frac{df_i}{dx} = g_i(x,f_1,f_2\ldots f_n) \quad i=1,2\ldots n \tag{40}$$

were required. Rearrangement of equations 38 and 39 was required.

Performing the indicated differentiations on the LHS yields

$$\dot{\delta}_1(3N\delta_1^2 - KD_y\delta_1^3) - \dot{\delta}_2(D_A\delta_1^3) = N - \frac{k(1+K)b^2}{2D_A} N\delta_1^2 \tag{41}$$

and

$$-\dot{\delta}_1(KD_y\delta_2^3) + \dot{\delta}_2(3N\delta_2^2 - D_A\delta_z^3) = N + \left(\frac{D_y}{D_A} - 1\right) \frac{kKb^2}{2D_A} N\delta_1^2 \tag{42}$$

where the dot indicates d/dr, and bars have been dropped. Let $\alpha = k(1+K)b^2/2D_A$ and $\beta = (D_y/D_A - 1)\frac{kKb^2}{2D_A}$, then equations 41 and 42 may be written as the matrix equation

$$(M) \begin{Bmatrix} \dot{\delta}_1 \\ \dot{\delta}_2 \end{Bmatrix} = \begin{Bmatrix} N \\ N \end{Bmatrix} + N\delta_1^2 \begin{Bmatrix} -\alpha \\ \beta \end{Bmatrix} \tag{43}$$

$$(M) = \begin{Bmatrix} 3N\delta_1^2 - KD_y\delta_1^3 & -D_A\delta_1^3 \\ -KD_y\delta_2^3 & 3N\delta_2^2 - D_A\delta_2^3 \end{Bmatrix}$$

Equation 43 may be solved for $\dot{\delta}_1$ and $\dot{\delta}_2$ to yield (Appendix F)

$$\dot{\delta}_1 = \{(\alpha\delta_1^2 - 1)(D_A\delta_2^3 - 3N\delta_2^2) + D_A(1+\beta\delta_1^2)\delta_1^3\}/6N\delta_1^2\delta_2^2$$

$$\dot{\delta}_2 = \{(1-\alpha\delta_1^2)KD_y\delta_2^3 + (1+\beta\delta_1^2)(3N\delta_1^2 - KD_y\delta_1^3)\}/6N\delta_1^2\delta_2^2 \quad (44)$$

Equation 44 has the form of equation 40 and is amenable to solution by numerical methods available to the non-specialist.

b) Numerical solution of the differential equations: There are several subroutines for the solution of sets of differential equations available as part of the International Mathematics and Statistics Library (IMSL). For this problem DVERK was used, although perhaps others would have been better. Subroutine DVERK had the advantage that it was written so that it could be used by the non-specialist. All the important parameters were set arbitrarily or calculated by DVERK. Should the need have arisen, any of these parameters may have been set by the user.

The first problem encountered was that of the boundary conditions, at x=0 (r=0), $\bar{\delta}_1 = \bar{\delta}_2 = 0$. The use of this condition

required a division by zero (equation 44). One of the ways to circumvent this problem might be to consider a different coordinate system. The analogous case of the CE mechanism in a still solution with a potentiostatic pulse had been studied as a sort of learning machine. With this simpler set of equations, many avenues for solution could be attempted more easily thus providing insight into the hydrodynamic problem. A manner of presentation which at first seemed to hold some promise was to consider, not δ_1 and δ_2, but the ratio of δ_1 to the δ which would have existed without the presence of the preceding reaction ($\sqrt{\pi Dt}$). When the problem is cast in terms of $\hat{\delta}_1=\delta_1/\sqrt{\pi Dt}$ and $\hat{\delta}_2=\delta_2/\sqrt{\pi Dt}$, the boundary condition becomes:

$$t = 0 \qquad \hat{\delta}_1 = \hat{\delta}_2 = 1$$

Unfortunately, the system of equations was still indeterminate at t=0.

Another alternative was to solve the system exactly near r=0 and then "match" this solution with the numerical solution. This procedure seemed to work. Near r=0 one can make two assertions

$$\text{i)}\ \alpha\delta_1^{\,2} << 1,\ \beta\delta_1^{\,2} << 1$$

$$\text{ii)} \quad \delta_1 = \delta_1(0) + r\left(\frac{\partial \delta_1}{\partial r}\right)_{r=0}$$

$$\delta_2 = \delta_2(0) + r\left(\frac{\partial \delta_1}{\partial r}\right)_{r=0}$$

The first assertion puts a quantitative limit on how small δ must be in order that we can neglect the kinetic terms α and β. The second assertion is just a Taylor's series about zero (Maclaurin's series) truncated after the first order terms. Since $(\partial\delta_1/\partial r)_{r=0}$ and $(\partial\delta_2/\partial r)_{r=0}$ are constants and $\delta_1(0)$ and $\delta_2(0)$ are both zero, one may write

$$\text{ii)} \quad \delta_1 = ar$$
$$\delta_2 = br$$

Using (i) and (ii) in equation 44

$$a = (3ab^2 \frac{KD_Y}{D_A} + 2b^3 + a^3)/(6a \frac{KD_Y}{D_A} + b)\ a^2b^2r^2 \tag{44}$$

$$b = (\frac{KD_Y}{D_A} b^3 + 2a^3 \frac{KD_Y}{D_A} + 3ba^2)/6(a \frac{KD_Y}{D_A} + b)\ a^2b^2r^2$$

Each equation may be put in terms of a/b

$$a = 3\,\frac{KD_y}{D_A}\,\frac{a}{b} + 2 + \left(\frac{a}{b}\right)^3 / \left(6a\,\frac{KD_y}{D_A} + b\right)\,\frac{a^2}{b}\,r^2 \qquad (45a)$$

$$b = \frac{KD_y}{D_A} + 2\,\frac{KD_y}{D_A}\,\left(\frac{a}{b}\right)^3 + 3\left(\frac{a}{b}\right)^2 / \left(6a\,\frac{KD_y}{D_A} + b\right)\,\frac{a^2}{b}\,r^2 \qquad (45b)$$

Equation 45a may be divided by equation 45b to yield a polynomial in a/b

$$2cx^4+2x^3-2cx-2 = 0$$

where $c = KD_y/D_A$ and $x = a/b$. This becomes

$$(cx+1)(x^3-1) = 0$$

with roots at $x = -1/c,1,1,1$. Therefore, a=b,and for small r, $\delta_1=\delta_2$. If $\delta_1=\delta_2=\delta$ is substituted into equation 44, still under condition (i) but no longer approximating δ by a Taylor's series, one finds

$$\dot{\delta} = \frac{1}{2}\delta^{-2}$$

$$\delta^3 = \frac{3}{2}\,r$$

$$\delta = \left(\frac{3}{2}\,r\right)^{1/3}$$

This is the solution expected for small r and no homogeneous kinetics (see equation C16 for $p \to \infty$ and r_L small, $\bar{\delta}_L^4$ neglible).

With this information the numerical solution was attempted with the following boundary condition. As long as $\delta_1^2\alpha$, $\delta_1^2\beta << 1$ one has $\delta = (3/2\ r)^{1/3}$, or $2/3\ \delta^3 = r$. Let us take either α or β, whichever is greater, and find some δ_1 which will yield only 0.0001 error in the term $(1-\alpha\delta^2)$ or $(1+\beta\delta^2)$. If, say, $\alpha>\beta$,

$$\delta_1^2\alpha = 0.0001$$

$$\delta_1 = (0.0001/\alpha)^{1/2}$$

and

$$\delta_1 = \delta_2 = \delta$$

Now that a value of δ has been determined, at what r will it exist? Using $2/3\ \delta^3 = r$, one has

$$r = \frac{2}{3}(0.0001/\alpha)^{3/2}$$

The boundary conditions for the numerical analysis are then

$$\delta_1 = (0.0001/\alpha)^{1/2} \qquad (46)$$

$$\delta_2 = (0.0001/\alpha)^{1/2}$$

$$r = \frac{2}{3}(0.0001/\alpha)^{3/2} \qquad (46)$$

Of course, had β been greater than α, β would be used in equation 46.

It was quickly determined that small step sizes of r were required or else the numerical solution would oscillate and finally get out of control. The subroutine seemed to require information about the function from not too far away from the region in which it was calculating. The stability was dependent upon three factors i) the magnitude of α and β, ii) the tolerance to which each point was calculated and iii) the increments of r. The increments of r may be understood as follows. The subroutine DVERK required boundary conditions and a set of values of the independent variable where the solution was required, i.e., $r_1, r_2, r_3 \ldots r_n$. The difference between r_1 and r_2 is the increment of r.

Figure 15 shows the effect of the parameter TOL. TOL sets the level of error acceptable to subroutine DVERK. The conditions in Figure 14 are for large α where small tolerance is crucial. When TOL = 0.001 the solution for δ is unstable and subject to wild divergences. Changing TOL to 0.0001 makes the solution more stable. The increase in computing time accompanying the change in TOL was only 2%.

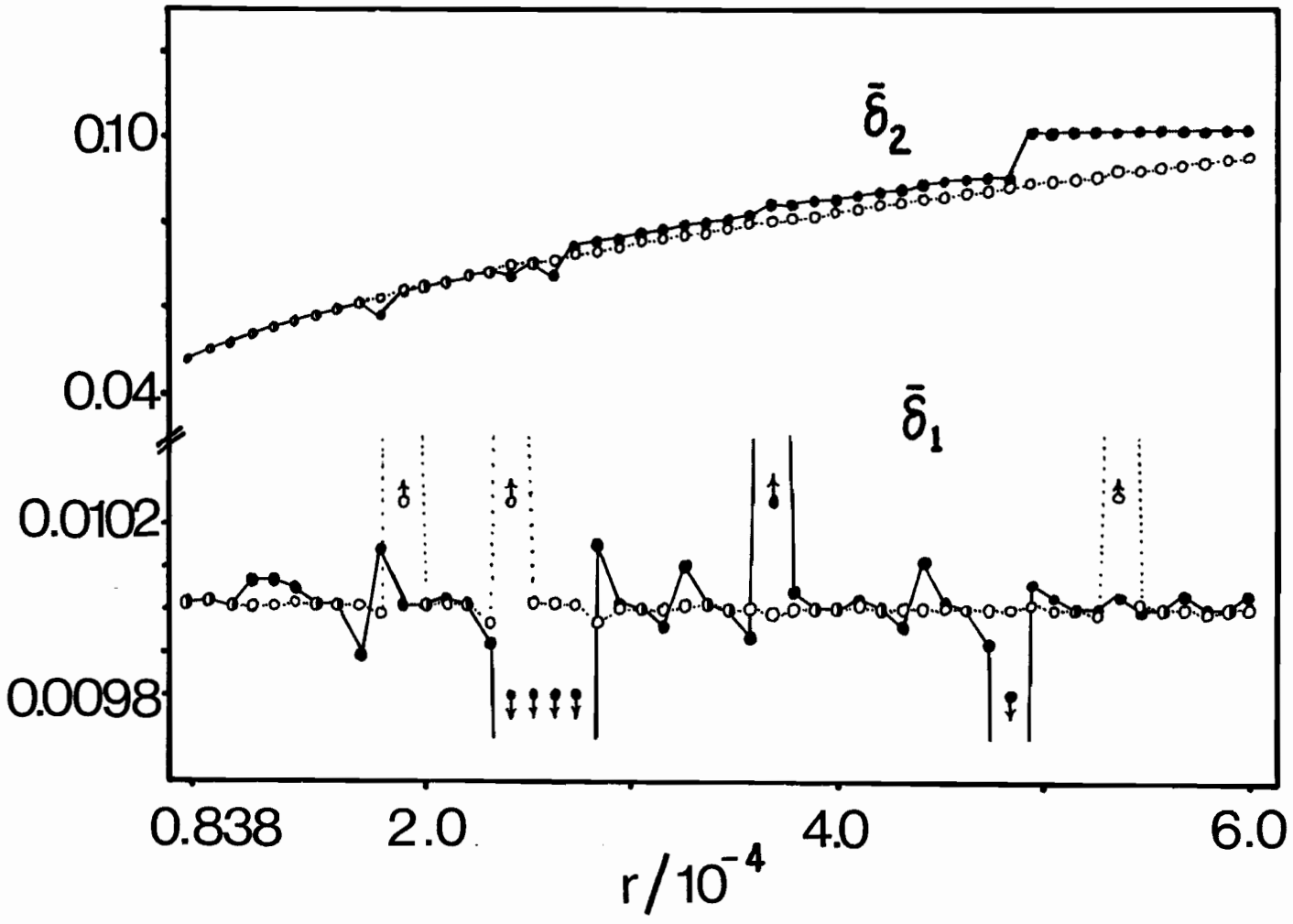

Figure 15: The diffusion layer thicknesses calculated by DVERK. The black dots represent TOL=0.001, the white dots represent TOL=0.0001. For both cases M=50.

To control the increment of r, each order of magnitude of r was broken up into M points and the solution carried out at each point. For a fairly fast reaction this means a lot of points since the r calculated by equation 46 is small. For instance for $\alpha = 10^5$, r from equation 46 is 2.25×10^{-14}. The calculation of the current at $r = 1.4 \times 10^{-6}$ requires calculation at 84 separate r's for M = 10 and 424 points for M = 50. The computing time is small in either case (M = 10, 3.83 CPU sec,M = 50, 6.43 CPU sec). Although in most circumstances M = 10 yielded a stable solution, M = 50 was utilized to be safe.

c) Comparison to previous derivations: Matsuda (18,25) uses a parameter called ΛK as an independent variable. In terms of the present work $\Lambda K = \alpha^{1/2}(r/6)^{1/3}$. A comparison between the results of the numerical solution of equation 44 with exact mathematical treatments of Matsuda (18,25) is made in Figure 16. The results are qualitatively correct. The quantitative error is in part caused by the absence of shape correction factors. The agreement with the exact results is sufficiently good that calculations for $D_y \neq D_A$ and slow kinetics may be carried out.

Matsuda (18) used the approximation that there is a reaction layer for sufficiently fast reactions. The reaction layer is a steady state diffusion layer in which dissociation occurs. Figure 17 shows the diffusion layer thickness as a

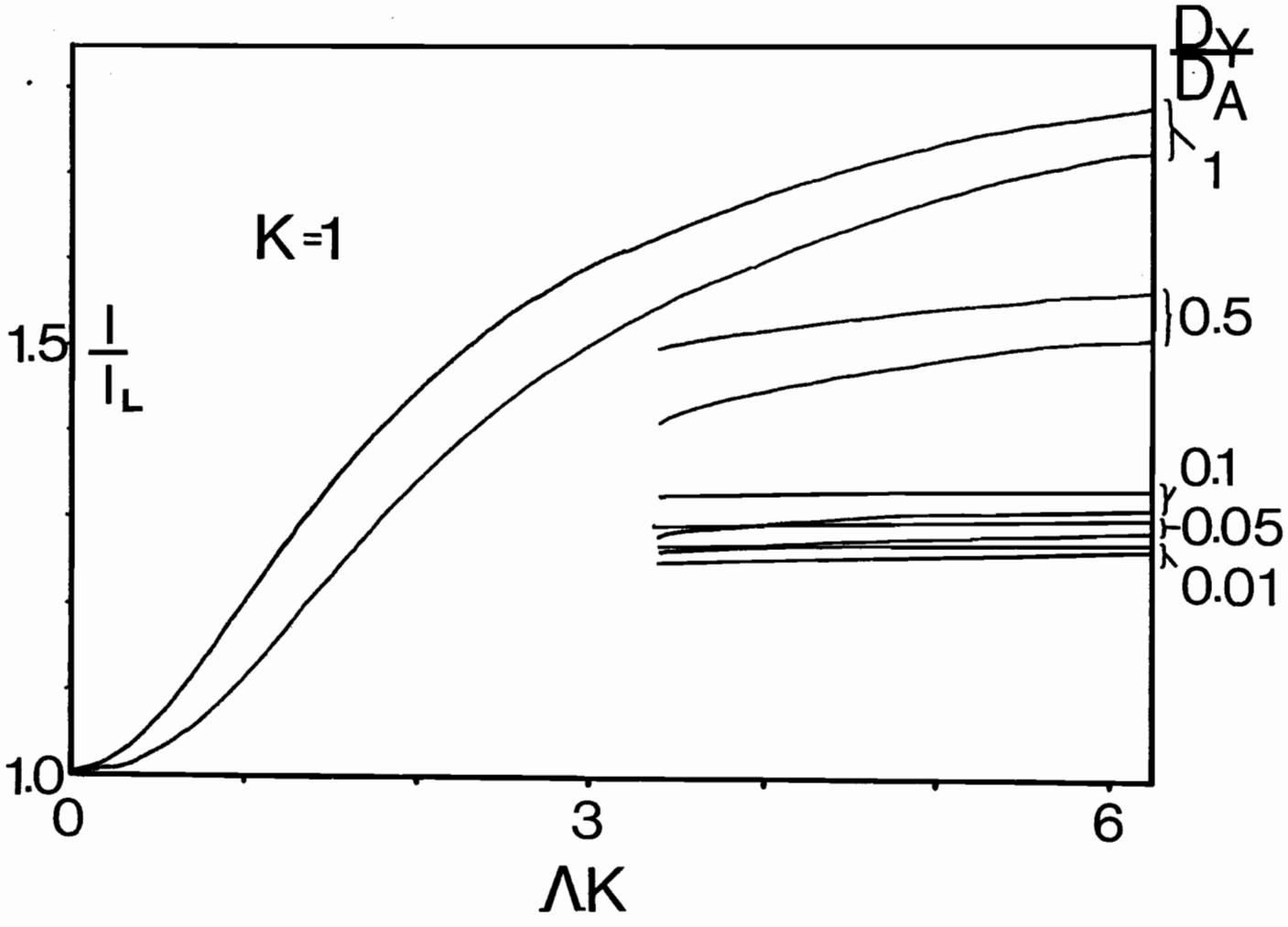

Figure 16: Current as a function of ΔK for various values of D_Y/D_A. The lower line in each pair is the DLA. The upper line for $D_Y/D_A = 1$ is from Tokuda(25) and the upper line in the other pairs is from Matsuda (18).

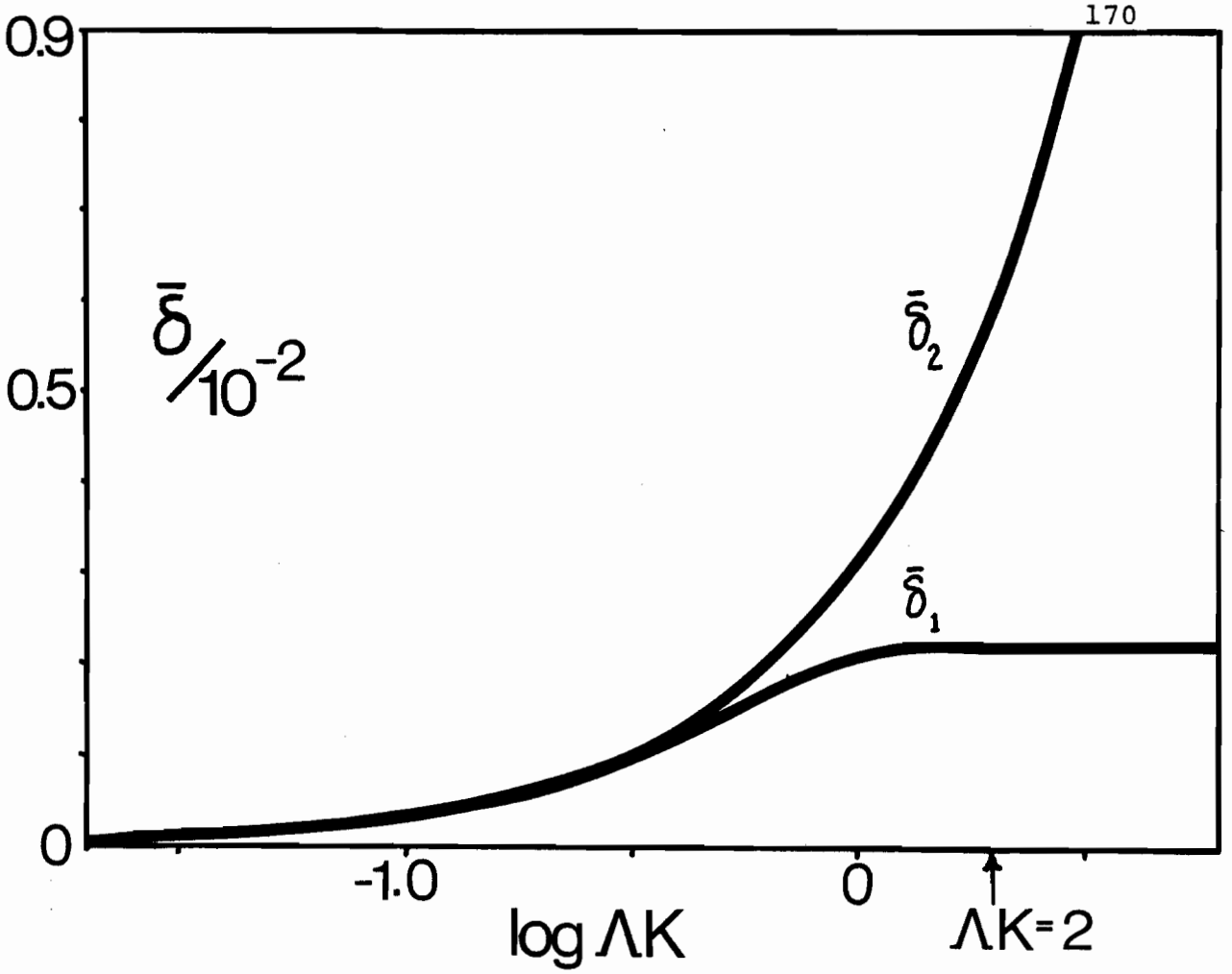

Figure 17: The diffusion layer thicknesses as a function of ΛK. Conditions; $D_Y=D_A=1.0\times10^{-5}$ cm^2s^{-1}, b=0.06cm, $k=100s^{-1}$, K=1, TOL=0.0001, M=50.

function of ΛK. Notice that $\bar{\delta}_1 = \bar{\delta}_2$ at low ΛK, and that $\bar{\delta}_1$ reaches a quasi-steady state at high ΛK. (Perusal of the numerical data demonstrates a very slow decrease in $\bar{\delta}_1$ after it reaches a broad maximum. This effect is more evident when $D_y \neq D_A$ ($\beta \neq 0$).) The interesting point about Figure 17 relates to Tokuda's discussion (25) of Matsuda's work (18). Tokuda (25) calculated the conditions under which the approximation of a steady state reaction layer was valid. For $\Lambda K \simeq 2$ ($\log \Lambda K \simeq 0.3$) the steady state reaction layer should be valid. This corresponds quite nicely with the point on Figure 17 corresponding to a constant $\bar{\delta}_1$.

d) Results for voltammetric immunoassay conditions: Recall that in voltammetric immunoassay (VIA) the objective is to measure an electrochemically active molecule, L*, in the presence of its antibody bound form Ab·L*. This requires that the electrochemical measurement be made fast with respect to dissociation. The theoretical objective was to determine under what conditions this could be done. To set these conditions some figures were required.

i) Diffusion coefficient of L*. This was measured experimentally (Chapter III) and found to be 4×10^{-6} cm^2 s^{-1}.

ii) Diffusion coefficient of AbL*. Experimental results for γ globulins cluster around 4×10^{-7} cm^2 s^{-1} (26).

iii) Equilibrium constant. It is common knowledge that an immunoassay is generally performed with a reagent for

which [L*] = [Ab·L*]. Since the concentration of antibody has been taken as a constant, the above criterion means that K for the reaction

$$Ab \cdot L^* \rightleftharpoons L^*$$

equals 1.

iv) Dissociation rate constant. Kelley (27) has pointed out that for small molecules, k on the order of 1 s^{-1} is not unusual. Using these parameters, I/I_D was calculated for various values of b corresponding to commerically available polytetrafluoroethylene sheets. In most publications on CE mechanism, the current is referenced to the current which would arise if the preceding reaction were infinitely fast. The viewpoint of this work is different. Since one needs to know how much of an additional signal (additive error) is caused by Ab·L*, it is convenient to reference the current to the current which would be expected if the preceding reaction were infinitely slow. This error is shown in Figure 18 and Table 4. It is interesting to note that the conditions favoring high SNR (Chapter IV, section C, part 5b) are the same as the conditions favoring low additive error from the dissociation of Ab·L*.

Figure 18: Percent error in the measurement of L* from the dissociation of AbL*,as a function of r and b. Conditions are in the text.

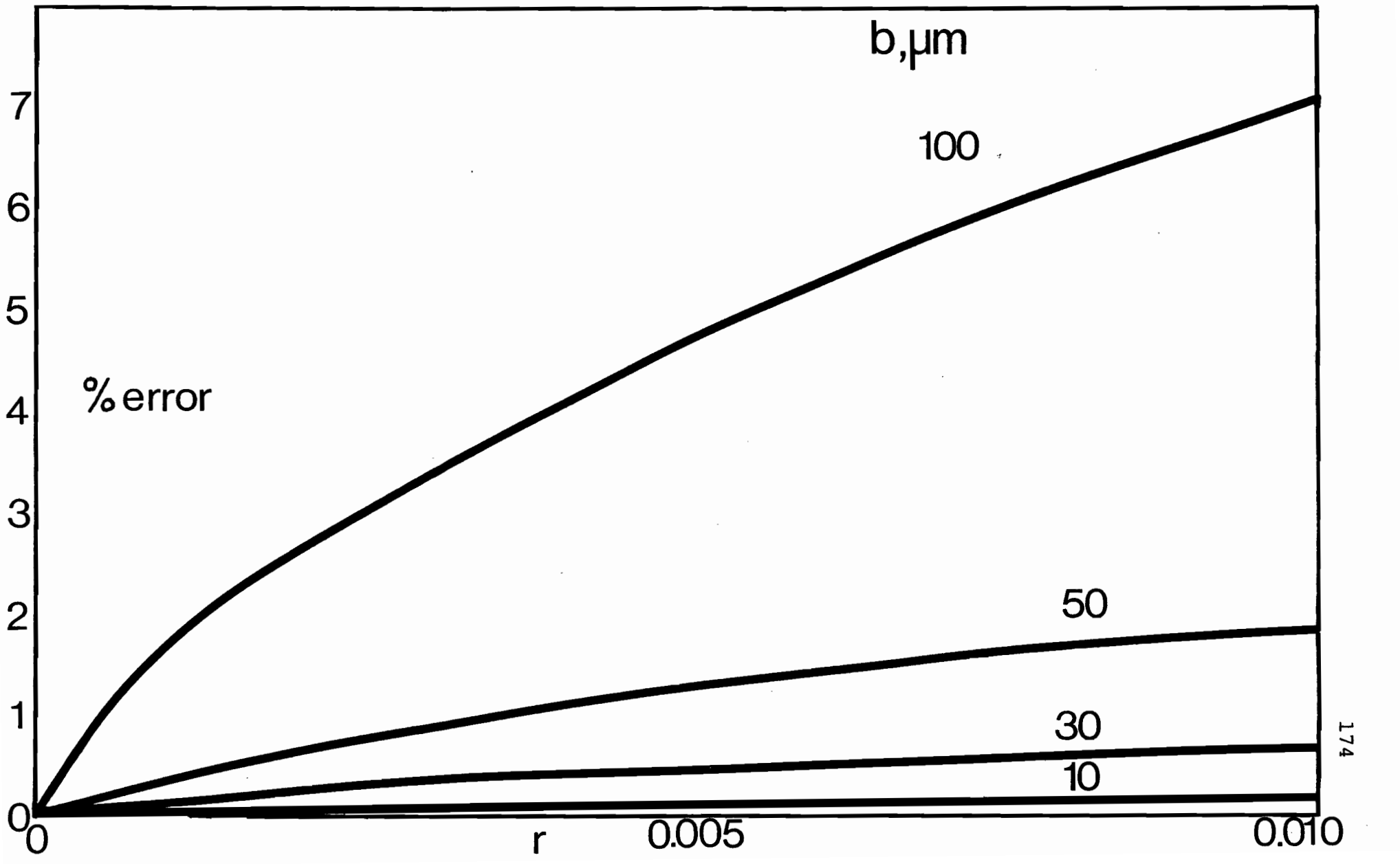
b,μm
100
50
30
10
% error
7
6
5
4
3
2
1
0
0
r
0.005
0.010

Table 4

Error[a] in the measurement of L* from the dissociation of Ab·L* under various conditions, at r = 0.01, $D_{Ab.L*} = 4.0x10^{-7}$ $D_{L*} = 4.0x10^{-6}$ cm^2 s^{-1} and K = 1.

k	b	Error
0.10	0.0015	0.0002
0.10	0.0030	0.0007
0.10	0.0050	0.0019
0.10	0.0100	0.0076
1.0	0.0015	0.0017
1.0	0.0030	0.0068
1.0	0.0050	0.0187
1.0	0.0100	0.0704
10.0	0.0015	0.0169
10.0	0.0030	0.0640
10.0	0.0050	0.1469
10.0	0.0100	0.2591

[a]Error is expressed as a fraction of the "true" L* signal.

REFERENCES

1. K.B. Oldham, Electrochim. Acta, 11 (1966) 1475.
2. F.A. Posey and R.E. Meyer, J. Electroanal. Chem., 30 (1971) 359.
3. S.G. Weber and W.C. Purdy, Anal. Chim. Acta, 99 (1978) 77.
4. S.G. Weber and W.C. Purdy, Anal. Chim. Acta, 100 (1978) 531.
5. D.M. Oglesby, S.H. Omang and C.N. Reilley, Anal. Chem., 37 (1965) 1312.
6. K.J. Vetter,"Electrochemical Kinetics", Theoretical and Experimental Aspects, Academic Press, N.Y., 1967, p. 267.
7. W.M. Kays,"Convective Heat and Mass Transfer", McGraw Hill, New York, 1966, p. 130.
8. R.E. Meyer, M.C. Banta, P.M. Lantz and F.A. Posey, J. Electroanal. Chem., 30 (1971) 345.
9. S.M. Selby (Ed.),"Handbook of Tables for Mathematics", 4th Edn., CRC Press, Cleveland, Ohio, 1970, p. 132.
10. E. Ya. Klimenkov, B.M. Grafov, V.G. Levich and I.V. Strizhevskii, Elektrokhimiya, 5 (1969) 202.
11. J. Lankelma and H. Poppe, J. Chromatogr., 125 (1976) 375.
12. B. Miller, M.I. Bellavance and S. Bruckenstein, Anal. Chem., 44 (1972) 1983.
13. B. Miller and S. Bruckenstein, Anal. Chem., 46 (1974) 2026.
14. S. Bruckenstein and B. Miller, Acc. Chem. Res., 10 (1977) 54.

15. W.J. Blaedel and D.G. Iverson, Anal. Chem., 49 (1977) 1563.

16. L.B. Anderson and C.N. Reilley, J. Electroanal. Chem., 10 (1965) 295.

17. W.J. Blaedel and L.N. Klatt, Anal. Chem., 38 (1966) 879.

18. H. Matsuda, J. Electroanal. Chem., 15 (1967) 325.

19. F.J. Bayley, J.M. Owen and A.B. Turner,"Heat Transfer", T. Nelson, London, 1972, p. 7.

20. J. Jordan and R.A. Javick, Electrochim. Acta, 6 (1962) 23.

21. W.J. Blaedel and R.C. Engstrom, Anal. Chem., 50 (1978) 476.

22. A.T. Hubbard and F.C. Anson in"Electroanalytical Chemistry" Vol. 4, A.J. Bard (Ed.), Marcel Dekker, New York, 1971, pp. 207-208.

23. C.L. Blank, J. Chromatogr., 117 (1976) 35.

24. D. Swartzfager, Anal. Chem., 48 (1976) 2189.

25. K. Tokuda, K. Aoki and H. Matsuda, J. Electroanal. Chem., 80 (1977) 211.

26. H.P. Lundgren and W.H. Ward in "Amino Acids and Proteins", D.M. Greenberg (Ed.), Charles Thomas, Springfield, IL, U.S.A., 1951, p. 404.

27. K.A. Kelley, McGill University, thesis (1970).

APPENDIX A

Derivation of Equations A12 and A13

CASE I

Substitution of equation 27 into equation 26 yields

$$-(\partial C/\partial \bar{z})_{\bar{z}=0} = -C^\circ/\bar{\delta} = \frac{\partial}{\partial x}\left(f\int_0^{\delta} \bar{z}(1-\bar{z})C^\circ \frac{\bar{z}}{\bar{\delta}}\, d\bar{z} + \int_{\bar{\delta}}^{\tilde{\delta}} \bar{z}(1-\bar{z})C^\circ d\bar{z}\right) \quad (A1)$$

The shape correction factor f has been added. $\tilde{\delta}$ is some $\bar{\delta}$ such that $\tilde{\delta} > \bar{\delta}$ and $\tilde{\delta}$ is not a function of $\bar{x}$. By first performing the indicated definite integration over $\bar{z}$ and then differentiating the result with respect to $\bar{x}$ one obtains

$$d\bar{x} = \left[\left(\frac{3-2f}{3}\right)\bar{\delta}^2 + \left(\frac{3f-4}{4}\right)\bar{\delta}^3\right]d\bar{\delta} \quad (A2)$$

Integration of equation A2, noting that $\bar{\delta}(0) = 0$ yields

$$\bar{x} = \left(\frac{3-2f}{9}\right)\bar{\delta}^3 + \left(\frac{3f-4}{16}\right)\bar{\delta}^4 \quad (A3)$$

To satisfy condition (i) note that as $\bar{x} \to 0$, $\bar{\delta} \to 0$ and $\bar{\delta}^4 << \bar{\delta}^3$, therefore

$$\bar{\delta}_{\bar{x}\to 0} = \left(\frac{9\bar{x}}{3-2f}\right)^{1/3}$$

It is convenient to introduce $r = 6\bar{x}$.

$$\bar{\delta}_{r\to 0} = \left(\frac{3r}{6-4f}\right)^{1/3} \tag{A4}$$

The total current I may be given by

$$I = \int_{o}^{L} nFW_e D\left[\frac{\partial C}{\partial z}(x)\right]_{z=0} dx = \int_{o}^{r_L} nF\bar{U}\,\frac{W_e}{W_c}\,C^{\circ}\left(\frac{dr}{\bar{\delta}(r)}\right) \tag{A5}$$

where r_L is equal to r at x = L, $r_L = LD/\bar{V}b^2$.

Substitution of A4 into A5 and integration yields

$$I = 3/2\left(\frac{6-4f}{3}\right)^{1/3} nFC^{\circ}W_e\left(\frac{LD}{b}\right)^{2/3}\left(\frac{\bar{U}}{W_c}\right)^{1/3}$$

Condition (i) can now be satisfied by placing f = 0.7984. This allows equation A3 to be written as

$$r = 0.9355\,\bar{\delta}^{3} - 0.6018\,\bar{\delta}^{4} \tag{A6}$$

To determine the total current it is instructive to write equation A5 as

$$I = nF\bar{U}\,\frac{W_e}{W_c}\,C^\circ \int_0^{r_L} \frac{dr}{d\bar{\delta}}\,\frac{d\bar{\delta}}{\bar{\delta}} \qquad (A7)$$

The expression for $dr/d\bar{\delta}$ is found in equation A2. The integrand is now entirely in terms of $\bar{\delta}$ and may be integrated to yield

$$I = nF\bar{U}C^\circ(W_e/W_c)\{1.4032\bar{\delta}_L^{\,2} - 0.8024\bar{\delta}_L^{\,3}\} \qquad (A8)$$

CASE II

Substitution of equation 28 into equation 26 yields

$$C(1,r) = -(\partial/\partial r)gC(1,r)/2 \qquad (A9)$$

Further factors (as in the thin-layer cell treatment) besides g must be incorporated into the analysis. Figure 1-A demonstrates the relationship at $\bar{\delta} = \bar{\delta}_c$. At the point when $\bar{\delta} = \bar{\delta}_c$ and C(1,r) equals the ficticious concentration $(1+\alpha)C^\circ$, one may utilize the treatment from Case II. Integration of equation A9 yields

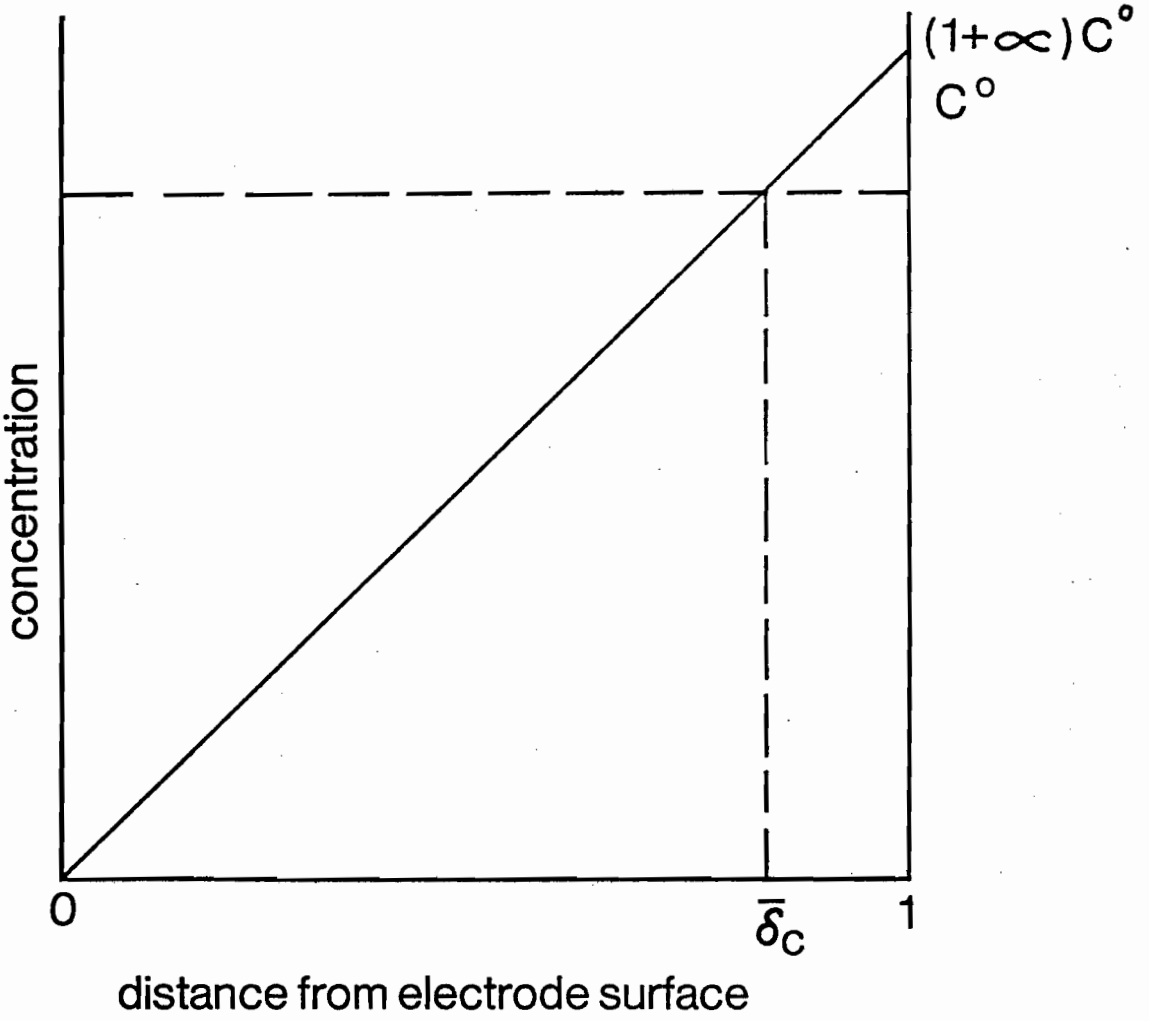

Figure 1-A: The diffusion layer at the transition from case I to case II.

$$C(1,r) = (1+\alpha)C^{\circ}\exp\, 2(r_c-r)/g \qquad \text{(A10)}$$

where r_c is r when $\bar{\delta} = \bar{\delta}_c$. The total current from Case II behavior alone ($r > r_c$) may be obtained from equations 28, A5 and A10.

$$I_{(r > r_c)} = (1+\alpha)(g/2)nF\bar{U}C^{\circ}(W_e/W_c)[1-\exp\{2(r_c-r_L)/g\}] \qquad \text{(A11)}$$

Now from equation A10, for condition (ii) to be satisfied, one has

$$1/\bar{\delta}_c = 1+\alpha$$

This is also obtainable from geometrical consideration of the similar triangles in Figure 1-A. From equation A2 and equation A10 one has for condition (iii),

$$(2.4072\ \bar{\delta}_c^{\,5}-2.8064\ \bar{\delta}_c^{\,4})^{-1} = 2(1+\alpha)/g$$

From equation A8 and A11 one has for condition (iv),

$$1.4032\ \bar{\delta}_c^{\,2}-.8024\ \bar{\delta}_c^{\,3} + g(1+\alpha)/2 = 1$$

Solving these three equations simultaneously yields simply:

$$\bar{\delta}_c=1,\ \alpha=0,\ g=f=0.7984$$

Now to obtain the total current, equation A8 must be added to equation A11. The complete solution may then be given as

$$I = nF\bar{U}C^{\circ}(W_e/W_c)\ \phi(r)$$

$$\phi(r) = 1.4032\ \bar{\delta}_L^{\,2}-0.8024\ \bar{\delta}_L^{\,3} \qquad 0 < r < 0.3337 \qquad \text{(A12)}$$

$$= 1.000-.3902\ \exp\{2.505(0.3337-r_L)\} \qquad r \geq 0.3337$$

The diffusion layer thickness at x = L, $\bar{\delta}_L$, may be found by solving

$$r_L = 0.9355\ \bar{\delta}_L^{\,3}-0.6018\ \bar{\delta}_L^{\,4} \qquad \text{(A13)}$$

Details of the computation of $\bar{\delta}_L$ are in Appendix B.

APPENDIX B

Solution of Equation A13

Several routes to the determination of I from a value of r exist. The most exact way would be to solve the quartic equation A13 by a known formula (9). This would result in a cumbersome expression for $\bar{\delta}_L$ as a function of $\bar{r}_L$. Another method would be to fit an arbitrary function to equation A13. One would have to find a function which was of the right shape in order to obtain an acceptable fit with only a few terms. For a single value of r_L a graphical method may be used to find $\bar{\delta}_L$. A method which is simple to implement and will yield a value of $\bar{\delta}_L$ of any desired accuracy is solution by successive approximation. The latter method was chosen.

Rearranging equation A13 one obtains

$$\bar{\delta}_L = ((0.6018\ \bar{\delta}_L^{\,4} + r_L)/0.9355)^{1/3} \qquad \text{(B1)}$$

For diffusion layer thickness which are small, the term $\bar{\delta}_L^{\,4}$ becomes small. One can calculate the first approximation by letting $\bar{\delta}_L^{\,4}$ on the RHS to be zero.

$$_1\bar{\delta}_L = (r_L/0.9355)^{1/3} \qquad \text{(B2)}$$

Now this may be substituted into the RHS to yield the second approximation.

$$ {}_2\bar{\delta}_L = (0.6018\ {}_1\bar{\delta}_L^{\,4} + r_L/0.9355)^{1/3} \qquad \text{(B3)} $$

This procedure may be repeated until convergence is obtained. Convergence may be determined through the use of the parameter

$$ \text{INCR} = ({}_n\bar{\delta}_L - {}_{n-1}\bar{\delta}_L)/{}_n\bar{\delta}_L $$

When INCR is less than a predetermined value, the procedure may be ceased and ${}_n\bar{\delta}_L$ taken as the value of $\bar{\delta}_L$ for use in equation A12. Depending upon the values of r and INCR, the number of iterations required varies, but for INCR = 0.0001 the number is on the order of 10, thus the procedure is inexpensive. The source listing for this procedure may be found as subroutine DELT in Appendix D.

APPENDIX C

Derivation and Solution of Equations for Steady State Hydrodynamic Voltammetry

1) Derivation of the Basic Equations

The equations 7 and 12 were derived by considering conservation of mass both in terms of flux and total material reacted. Conservation of mass must be invoked here to arrive at relationships for the surface concentrations of the oxidized and reduced halves of a couple.

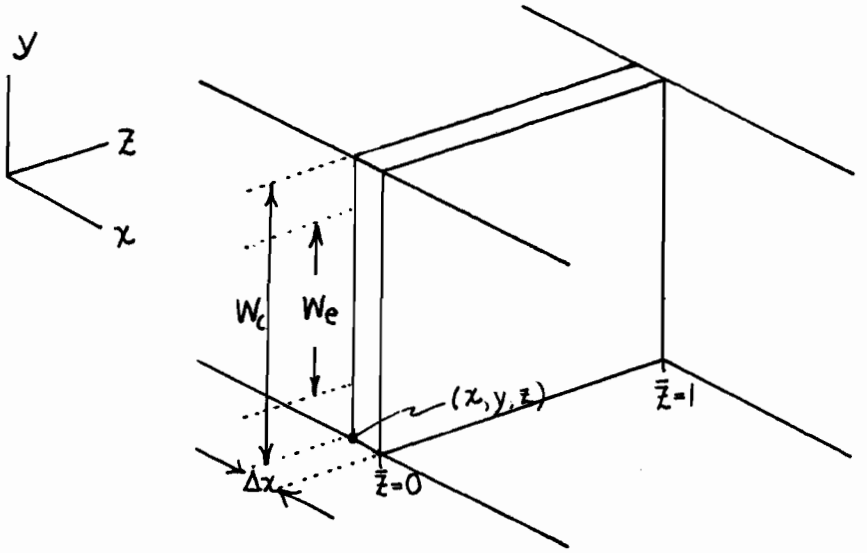

Figure C-1

Consider the slab of solution of width W_c thickness b (dimensionless thickness 1), and length in the direction of flow Δx. The bulk mass flow of depolarizer (moles s^{-1}) of

oxidized species coming into this slab will be $\frac{W_e}{W_c}\int_0^1 C(\bar{z};x)\bar{U}(\bar{z})d\bar{z}$ where $C(\bar{z};x)$ means the concentration at one x as a function of $\bar{z}$. The bulk mass flow leaving the slab will be $\frac{W_e}{W_c}\int_0^1 C(\bar{z};x+\Delta x)\bar{U}(\bar{z})d\bar{z}$. The diffusive mass flow entering or leaving the cell will be $D(\frac{\partial C}{\partial z})_{z=0}$. Mass balance for this species demands

$$\frac{1}{W_c}\int_0^1 C(\bar{z};x)\bar{U}(\bar{z})d\bar{z} = \frac{1}{W_c}\int_0^1 C(\bar{z};x+\Delta x)\bar{U}(\bar{z})d\bar{z} + D(\frac{\partial C}{\partial z})_{z=0}\Delta x \qquad (C1)$$

Similarly for the other half of the couple

$$\frac{1}{W_c}\int_0^1 C'(\bar{z};x)\bar{U}(\bar{z})d\bar{z} - D'(\frac{\partial C'}{\partial z})_{z=0}\Delta x = \frac{1}{W_c}\int_0^1 C'(\bar{z};x+\ x)\bar{U}(\bar{z})d\bar{z} \qquad (C2)$$

Rearranging and dividing by Δx and letting $\Delta x \to 0$, one has

$$-\frac{\partial}{\partial x}\int_0^1 C(\bar{z},x)\bar{U}(\bar{z})d\bar{z} = DW_c(\frac{\partial C}{\partial z})_{z=0} \qquad (C3)$$

$$-\frac{\partial}{\partial x}\int_0^1 C'(\bar{z},x)\bar{U}(\bar{z})d\bar{z} = D'W_c(\frac{\partial C'}{\partial z})_{z=0} \qquad (C4)$$

where $C(\bar{z},x)$ means the concentration as a function of $\bar{z}$ and x. These equations can be seen to be identical with equation 26. The approximate concentrations given by the linear approximation are

$$C(\bar{z},r) = C(o,r) + \frac{C°-C(o,r)}{\bar{\delta}} \bar{z} \qquad 0 < \bar{z} \leq \bar{\delta}$$

$$C'(z,r) = C'(o,r) + \frac{C°'-C'(o,r)}{\bar{\delta}'} \bar{z} \qquad 0 < \bar{z} \leq \bar{\delta}'$$

$$C(z,r) = C° \qquad \bar{\delta} < \bar{z}$$

$$C'(z,r) = C°' \qquad \bar{\delta}' < \bar{z}$$

These may be substituted into C3 and C4 to yield, after integration

$$-\frac{d}{dr}\{(C°-C(o,r))(\frac{\bar{\delta}^3}{2} - \bar{\delta}^2)\} = \frac{C°-C(o,r)}{\bar{\delta}} \qquad (C5)$$

$$-\frac{D}{D'}\frac{d}{dr}\{(C°'-C'(o,r))(\frac{\bar{\delta}'^3}{2} - \bar{\delta}'^2)\} = \frac{C°'-C'(o,r)}{\bar{\delta}'} \qquad (C6)$$

Equality of fluxes (conservation of mass at z=0) yields

$$-D\frac{C°-C(o,r)}{\bar{\delta}} = D'\frac{C°'-C'(o,r)}{\bar{\delta}'} \qquad (C7)$$

and the Butler-Volmer equation yields

$$D \frac{C^\circ - C(o,r)}{\bar{\delta}} = k_f C(o,r) - k_b C'(o,r) \qquad (C8)$$

These four equations C5-C8 are in four unknowns, $C(o,r)$, $C'(o,r)$, $\bar{\delta}$, and $\bar{\delta}'$, all functions of r. These may be solved simultaneously to yield

$$C(o,r) = \frac{\left(\frac{D}{k_f \delta} + \frac{k_b}{k_f}\frac{D}{D'}\frac{\delta'}{\delta}\right) C^\circ + \frac{k_b}{k_f} C^{\circ\prime}}{1 + \frac{D}{k_f \delta} + \frac{k_b}{k_f}\frac{D}{D'}\frac{\delta'}{\delta}} \qquad (C9)$$

$$C'(o,r) = \frac{\left(\frac{D'}{k_b \delta'} + \frac{k_f}{k_b}\frac{D'\delta}{D\delta'}\right) C^{\circ\prime} + \frac{k_f}{k_b} C^\circ}{1 + \frac{D'}{k_b \delta'} + \frac{k_f}{k_b}\frac{D'\delta}{D\delta'}} \qquad (C10)$$

Unfortunately, the term δ' may not be separated from equation C9 and δ may not be separated from equation C10. From equations C5-C8, it may be determined that

$$\left(\frac{D'}{D}\right)^{1/3} = \frac{\bar{\delta}'}{\bar{\delta}} \left(\frac{1-\bar{\delta}'/2}{1-\bar{\delta}/2}\right)^{1/3} \qquad (C11)$$

The term $D\delta'/D'\delta$ will be called ε, it is analogous to γ in

equation 7. For small $\bar{\delta}$, $\varepsilon = (D/D')^{2/3}$. For $\bar{\delta} = 1$ and $\bar{\delta}'$ not too different from 1 (i.e. $D \simeq D'$), equation C11 becomes

$$(D'/D)^{1/3} = \bar{\delta}'(1-\bar{\delta}'/2)^{1/3}(1/2)^{-1/3}$$

Let $\bar{\delta}' = 1-\Delta$, $\Delta << 1$, then expanding the $(1-\delta'/2)^{1/3}$ term, and discarding second order and higher terms one arrives at

$$(D'/D)^{1/3} \simeq 1-(2/3)\Delta$$

$$\simeq (1-\Delta)^{2/3}$$

$$\simeq \bar{\delta}'^{2/3}$$

therefore

$$(D'/D)^{1/2} \simeq \bar{\delta}'/\bar{\delta}$$

and

$$\varepsilon \simeq (D/D')^{1/2}$$

Therefore ε exists in the small range

$$(D/D')^{1/2} \leq \varepsilon \leq (D/D')^{2/3} \text{ for } D > D'$$

$$(D/D')^{2/3} \leq \varepsilon \leq (D'/D)^{1/2} \text{ for } D' > D$$

Putting k_f and k_b into dimensionless form

$$\bar{k}_f = k_f b/D$$

$$\bar{k}_b = k_b b/D$$

and letting $p = \bar{k}_f + \bar{k}_b \varepsilon$, one arrives at

$$C(o,r) = \frac{(1+\varepsilon\bar{k}_b\bar{\delta})C^\circ + \bar{k}_b\bar{\delta}C^{\circ\prime}}{1+p\bar{\delta}} \qquad (C12)$$

An analogous expression holds for $C'(o,r)$. Note that no shape correction factor has been employed.

2) Solution of the Equation

a) $\bar{\delta} < 1$

Once again the current may be determined from the flux which is approximated by

$$J = -D\,\frac{C^\circ - C(o,r)}{\delta}$$

And once again the problem is to find δ. Equation C12 may be substituted into equation C5 to yield

$$-\frac{\bar{k}_f C^\circ - \bar{k}_b C^{\circ\prime}}{1+p\bar{\delta}} = \frac{\partial}{\partial \bar{x}}\left[\int_0^{\bar{\delta}} (\bar{z}^2 - \bar{z}^3)\, \frac{\bar{k}_f C^\circ - \bar{k}_b C^{\circ\prime}}{1+p\bar{\delta}}\, d\bar{z} + \right.$$

$$\int_0^{\delta} (\bar{z}-\bar{z}^2)\, \frac{(1+\varepsilon \bar{k}_b \bar{\delta}) C^\circ + \bar{k}_b \bar{\delta} C^{\circ\prime}}{1+p\bar{\delta}} + \qquad \text{(C13)}$$

$$\left. \int_{\bar{\delta}}^{1} (\bar{z}-\bar{z}^2)\, C^\circ d\bar{z} \right]$$

Recall that $6\bar{x} = r$.

There has been no incorporation of shape correction factors. Their incorporation causes problems in the evaluation of C(o,r). These factors could be incorporated if D=D'. It was not considered too serious that they were not incorporated since all the information about current-potential behavior will be reflected in the ratio I/I_D where I is the total current at any potential and I_D is the total current at infinite potential. If I_D is also calculated neglecting shape correction factors (g and h=1 in part C) then at least part of the error in neglecting them will be eliminated.

Performing the indicated integrations in equation C13, and performing the indicated division by $1+p\bar{\delta}$ yields a function of the form

$$B_3\bar{\delta}^3 + B_2\bar{\delta}^2 + B_1\bar{\delta} + \frac{B_0}{1+p\bar{\delta}}$$

inside the brackets. The indicated differentiation in $\bar{x}$ is now performed, and both sides of the equation are multiplied by $1+p\bar{\delta}$. Note that here the approximation has been made that $\partial\varepsilon/\partial\bar{x} \simeq 0$. This is not a bad approximation, especially if $D \simeq D'$. Now equation C13 has the form

$$-(\bar{k}_f C^\circ - \bar{k}_b C^{\circ\prime})d\bar{x} = \left[C_3\bar{\delta}^3 + C_2\bar{\delta}^2 + C_1\bar{\delta} + C_0 + \frac{C_{-1}}{1+p\bar{\delta}}\right]d\bar{\delta} \qquad \text{(C14)}$$

Equation C14 may now be integrated from $\bar{x}=0$, $\bar{\delta}=0$ to $\bar{x}=\bar{x}_L$, $\bar{\delta}=\bar{\delta}_L$ yielding

$$-(\bar{k}_f C^\circ - \bar{k}_b C^{\circ\prime})\bar{x}_L = \frac{C_3}{4}\bar{\delta}_L^4 + \frac{C_2}{3}\bar{\delta}_L^3 + \frac{C_1}{2}\bar{\delta}^2 + C_0\bar{\delta} + \frac{C_{-1}}{p}\ln(1+\bar{\delta}p) \qquad \text{(C15)}$$

$$\frac{C_3}{4} = \frac{\bar{k}_f C^\circ - \bar{k}_b C^{\circ\prime}}{16}$$

$$\frac{C_2}{3} = \left(-\frac{1}{9} + \frac{1}{36p}\right)(\bar{k}_f C^\circ - \bar{k}_b C^{\circ\prime})$$

$$\frac{C_1}{2} = -\left(\frac{1}{24p^2} + \frac{1}{12p}\right)(\bar{k}_f C^\circ - \bar{k}_b C^{\circ\prime})$$

$$C_0 = \left(\frac{1}{6p^2} + \frac{1}{12p^3}\right)\left(\bar{k}_f C^\circ - \bar{k}_b C^{\circ\prime}\right)$$

$$\frac{C-1}{p} = -\left(\frac{1}{6p^3} + \frac{1}{12p^4}\right)\left(\bar{k}_f C^\circ - \bar{k}_b C^{\circ\prime}\right)$$

The concentration terms may be divided out and the equation put in terms of r_L.

$$r_L = -\frac{3}{8}\bar{\delta}_L^4 + \left(\frac{2}{3} - \frac{1}{6p}\right)\bar{\delta}_L^3 + \left(\frac{1}{4p^2} + \frac{1}{2p}\right)\bar{\delta}^2 - \left(\frac{1}{2p^3} + \frac{1}{p^2}\right)\bar{\delta} + \left(\frac{1}{2p^4} + \frac{1}{p^3}\right)\ln(1+p\bar{\delta}) \qquad \text{(C16)}$$

To find the total current one must integrate the flux over all $\bar{x}$ from 0 to $\bar{x}_L$ just as in equation A5. In equation C13 the LHS is the flux. Integrating both sides over $\bar{x}$ will leave the expression in brackets on the RHS ($\int \frac{df(x)}{dx}\,dx = f(x) + \text{constant}$). After evaluation of the coefficients, one has

$$I = nF\bar{U}(W_e/W_c)\left(\bar{k}_f C^\circ - \bar{k}_b C^{\circ\prime}\right)\,\phi(r,p) \qquad \text{(C17)}$$

$$\phi(r,p) = \left(\frac{1-\bar{\delta}_L/2}{1+\bar{\delta}_L p}\right)\bar{\delta}_L^3$$

b) $\bar{\delta} > 1$

From mass balance one can write, analogous to equations C5-C8

$$-\frac{1}{2}\frac{d}{dr}\{C(o,r)+C(1,r)\} = C(1,r)-C(o,r) \qquad (C18)$$

$$-\frac{1}{2}\frac{D}{D'}\frac{d}{dr}\{C'(o,r)+C'(1,r)\} = C'(1,r)-C'(o,r) \qquad (C19)$$

$$D(C(1,r) - C(o,r)) = -D'(C'(1,r) - C'(o,r) \qquad (C20)$$

$$= k_f C(o,r) - k_b C'(o,r)$$

The apparent contradiction in sign on the LHS of equations C5 and C6 compared to C18 and C19 may be explained as follows. The integrations of equations C3 and C4 are definite. The evaluation of the integrand at the upper limit, $\bar{z} = 1$, will be a constant, independent of $\bar{x}(r)$ and therefore upon differentiation with respect to $\bar{x}(r)$ will vanish. Therefore this constant has simply been ignored. On the other hand, in equations C18 and C19 the integrand at $\bar{z} = 1$ is a function of $\bar{x}(r)$. Thus there is no constant value to ignore and the discrepancy arises when the terms under the differentiation ($\frac{d}{dr}\{\ \}$ in C5, C18) are compared directly. This merely reflects

the fact that the bracketed terms cannot be compared without first integrating each expression. This naturally creates an arbitrary constant.

These four equations may be solved together to yield an expression for C(o,r)

$$C(o,r) = \frac{(1+(\varepsilon-1)\bar{k}_b)C(1,r) + \bar{k}_b(C°+C°')}{1 + \bar{k}_f + \varepsilon\bar{k}_b} \qquad (C22)$$

$$\varepsilon = \frac{(D/D') + 1}{2} \simeq (D/D')^{1/2}$$

Whereas for the case of $\bar{\delta}_L < 1$, $\bar{\delta}_L$ must be found, in this case it is C(1,r) which must be found.

Using equation C22 in C18 one obtains simply

$$\frac{d}{dr}(C(1,r)-C°) = -\text{constant} \times (C(1,r)-C°) \qquad (C23)$$

Equation C23 may be integrated to yield C(1,r) as a function of r. The gradient of concentration needed to find the flux is obtained from Equation C22.

$$C(1,r)-C(o,r) = \frac{(\bar{k}_f+\bar{k}_b)C(1,r) - \bar{k}_b(C°'+C°)}{1 + \bar{k}_f + \varepsilon\bar{k}_b} \qquad (C24)$$

Using the expression for C(1,r) found upon integration of equation C23 in equation C24, one then has an expression for flux as a function of r and potential. This is easily integrated over r, and when this result is added to the current for r=0 to $r=r_c$, one obtains

$$\phi(r,p) = \frac{1}{1+p}\left\{\frac{1}{2} + g(p)\left[1-\exp\left\{(r_c-r_L)/g(p)\right\}\right]\right\}$$

$$g(p) = (2 + p + (\varepsilon-1)\bar{k}_b)/2(p - (\varepsilon-1)\bar{k}_b) \qquad \text{(C25)}$$

$$r_c = r \text{ at } \bar{\delta} = 1$$

APPENDIX D

Calculation of Current-Potential Curves in Channel Electrodes

Due to the form of equation C16, an iterative solution is once again required. The same type of solution which was used in Appendix B was attempted, but it led to divergent results. The scheme used involved changing $\bar{\delta}_L$ by smaller and smaller steps. The direction of the step was indicated by the magnitude of various terms in equation C16. When $\bar{\delta}_L=1$ the solution to equation C16 will yield a value for r_L at which the current will begin to be described by equation C25. For a reversible reaction (p large) this value of r, called r_c, is equal to 0.2917. For smaller p we may write for equation C16

$$r_c = 0.2917 - \frac{1}{6p} + \left(\frac{1}{2p^2}+\frac{1}{p}\right)\left(\frac{1}{2}-\frac{1}{p}+\frac{1}{p^2}\ln\,(1+p)\right)$$

$$\simeq 0.2917 - \frac{1}{6p} + \left(\frac{1}{2p^2}+\frac{1}{p}\right)\left(\frac{1}{2}-\frac{1}{p}+\frac{1}{p^2}\left\{p-\frac{1}{2}p^2+\frac{1}{3}p^3-\frac{1}{4}p^4+\ldots\right\}\right.$$

$$\simeq 0.2917 - \frac{1}{6p} + \left(\frac{1}{2p^2}+\frac{1}{p}\right)\left(\frac{1}{2}-\frac{1}{p}+\frac{1}{p}-\frac{1}{2}+\frac{1}{3}p-\frac{1}{4}p^2+\ldots\right)$$

$$\simeq 0.2917 + 0.3333 - 0.1250$$

$r \simeq 0.5000$

For values of p near 1 the value of r_c may be determined by calculation at each p. By making the first "guess" in the iterative solution $\bar{\delta}_L=1$, one can simultaneously calculate r_c. If r_c turns out to be less than r_L, the exponential solution (equation C25) is indicated. Otherwise, the iteration continues until a value of $\bar{\delta}$ is found which satisfies equation C16 at some r_L and p.

The solution of equation C16 is accomplished rapidly by changing the nth $\bar{\delta}_L$ "guess" which is substituted into equation C16 by $(\frac{1}{2})^{n-1}$. Thus a typical sequence would be as shown in Table D1.

The variation of the parameter ε is now determined. When the limiting current was calculated as explained in Appendix B and shown in subroutines DELT and DELTA, values for $\bar{\delta}_L$ and $\bar{\delta}_L'$ were obtained which could be used to find ε,

$$\varepsilon = D\bar{\delta}_L'/D'\bar{\delta}_L .$$

This value was used in the coefficients of equation C16. Now by solution of equation C16 a value of $\bar{\delta}_L$ has been found at some potential E not corresponding to limiting current, call it $\bar{\delta}_L(E)$. By use of the above equation, $\bar{\delta}_L'(E)$ may be found and a new ε calculated from the equation

Table D1

Iterative Solution to Equation C16

n	$\bar{\delta}_L$ "guess"	Result, $\bar{\delta}_L$ guess is too
1	1.0000000000000	high
2	0.5000000000000	high
3	0.2500000000000	high
4	0.1250000000000	low
5	0.1875000000000	low
6	0.2187500000000	high
7	0.2031250000000	low
8	0.2109375000000	high
9	0.2070312500000	high
10	0.2050781250000	low
11	0.2060546875000	low
12	0.2065434687500	low
13	0.2067878593750	high
14	0.2066656640625	*

*The relative difference between the last two guesses is less than 0.0001 and the iteration stops.

$$\text{new } \varepsilon = \left(\frac{1-\bar{\delta}_L(E)/2}{1-\bar{\delta}_L'(E)/2} \right)^{1/3} \left(\frac{D}{D'}\right)^{2/3}$$

which was derived from mass balance in Appendix C. This new ε may be compared to the ε calculated from limiting current $\bar{\delta}_L$. If they are different by more than 1%, new ε is used to find the coefficients in equation C16 and the entire calculation of $\bar{\delta}_L(E)$ is repeated.

The calculation of 21 current voltage curves for 1.0 cm $s^{-1} < k_0 < 10^{-6}$ cm s^{-1} and $10^{-3} < r < 10^3$ required 93 CPU seconds on an IBM 370. A source listing of the program follows. Terms used in the program which are not the same as used in the derivations are

ELEC = n

SRC = k_0

Z = r_L

ZCRIT = r_c

EZERO = E°

EINIT = initial voltage

EINCR = increment of voltage to use in making the current voltage curve

ESTOP = final voltage

DEL, DEL1, DEL2, DEL3, DEL4, DL = $\bar{\delta}_L$ or $\bar{\delta}_L$ "guess"

EPS = ε

NEPS = new ε

DELINC = $(1/2)^{n-1}$ increment by which $\bar{\delta}_L$ "guess" is changed

HV = I/I_L

```
      REAL*8 HV(6,100 ),CUR(3,100 ),FUNC(2,100 ),E(100 ),RINPUT(16),
     *ALPHA,B,COEFO,COEFR,DEL1,DEL4,DOX,DR,
     *ELEC,EPS,EPS2,PSI1,PSI2,SRC,Z,
     *C4,C3,C2,C1,CL,DL,ZCRIT,P,KF,KB,PSI
     *,L,WE,WC,UBAR,COX,CR,S,COEF,LCC,LCA,LCC1,LCA1,
     *EZERO,EINIT,EINCR,ESTOP,WK1
      INTEGER NIT1,NIT2,NIT3,II,IMAX,
     *START,KEY,JX
      COMMON HV,CUR,FUNC,E,
     *ALPHA,B,COEFO,COEFR,DEL1,DEL4,DOX,DR,
     *ELEC,EPS,EPS2,PSI1,PSI2,SRC,Z,
     *C4,C3,C2,C1,CL,DL,ZCRIT,P,KF,KB,PSI
     *,NIT1,NIT2,NIT3,II,IMAX
      START=1
100   IF(START.EQ.1) READ(5,*,END=999) (RINPUT(I),I=1,16)
      READ(5,*,END=999) KEY
      IF(KEY.EQ.0.AND.START.EQ.1) GO TO 1
      IF(KEY.EQ.0) STOP
      READ(5,*,END=999) (JX,RINPUT(JX),I =1,KEY)
1     L=RINPUT(1)
      B=RINPUT(2)
      WE=RINPUT(3)
      WC=RINPUT(4)
      UBAR=RINPUT(5)
      ELEC=RINPUT(6)
      DOX=RINPUT(7)
      DR=RINPUT(8)
      COX=RINPUT(9)
      CR=RINPUT(10)
      EZERO=RINPUT(11)
      EINIT=RINPUT(12)
      EINCR=RINPUT(13)
      ESTOP=RINPUT(14)
      SRC=RINPUT(15)
      ALPHA=RINPUT(16)
      START=2
C*********************************************************************
C*    CALCULATION OF PARAMETERS,Z,DIMENSIONLESS LENGTH, AND          *
C*    COEFFICIENTS,COEFOAND COEFR, WHICH REPRESENT THE CURRENT TO    *
C*    AN ELECTRODE WITH 100% COULOMETRIC YIELD.                      *
C*********************************************************************
      S=UBAR/60.
      COEF=9.65E+04*ELEC*WE*S/WC
      COEFO=COEF*COX
      COEFR=COEF*CR
      Z=DOX*L*WC/(S*8)
C*********************************************************************
C*    AT Z=.2917 THE DIFFUSION LAYER THICKNESS EQUALS THE CELL THICK- *
C*    NESS, THEN THE POLYNOMIAL IS NOT USED.  AN EXPONENTIAL EXPRESSION*
C*    RESULTING FROM SOLUTION FOR THE CONCENTRATION AT THE WALL ACROSS *
C*    THE CELL FROM THE ELECTRODE, IS USED.   THIS IS FOUND AT LABEL 2 *
C*********************************************************************
      IF(Z.GT.0.2917) GO TO 2
      CALL DELTA
      PSI1=(DEL1)**2-0.5*(DEL1)**3
C*********************************************************************
C*    LCC AND LCA REPRESENT THE LIMITING CATHODIC AND ANODIC CURRENTS  *
C*********************************************************************
      LCC=COEFO*PSI1
      LCA=COEFR*PSI1/EPS
      GO TO 3
2     IF(2.*Z.GT.150.) GO TO 7
      PSI1=1.-0.5*DEXP(2.*(.2917-Z))
      GO TO 8
7     PSI1=1.
8     EPS=(1.+(DOX/DR))/2.
      LCC=COEFO*PSI1
      LCA=COEFR*PSI1/EPS
3     IF (Z.GT.0.3337) GO TO 5
      CALL DELT
```

```
      PSI2=1.4032*(DEL4)**(2)-.8024*(DEL4)**(3)
      GO TO 6
 5    IF (2.5*Z.GT.150.) GO TO 9
      PSI2=1.-.3992*DEXP(2.505*(.3337-Z))
      GO TO 10
 9    PSI2=1.
 10   EPS2=(1.+(DOX/DR))/2.
 6    LCC1=COEFO*PSI2
      LCA1=COEFR*PSI2/EPS2
C*************************************************************************
C*    LIMITING CURRENTS HAVE BEEN CALCULATED WITH (DELT) AND WITHOUT     *
C*    A CORRECTION TERM FOR THE SHAPE OF THE CONCENTRATION PROFILE.      *
C*    THE USE OF THE CORRECTION FACTOR YIELDS EXCELLENT PREDICTIONS OF   *
C*    LIMITING CURRENT, BUT YIELDS PHYSICALLY UNREASONABLE RESULTS FOR   *
C*    HYDRODYNAMIC VOLTAMMETRY.  HENCE THE LIMITING CURRENT IS CALC-     *
C*    ULATED WITHOUT THE CORRECTION FACTOR, AND THE POTENTIAL DEPEN-     *
C*    DENT CURRENT IS CALCULATED WITHOUT A CORRECTION FACTOR, AND THE    *
C*    RATIO OF THE TWO CAN BE USED TO PREDICT THE SHAPE AND POSITION OF  *
C*    THE WAVE.  THE MORE EXACT VALUE FOR LIMITING CURRENT CALCULATED    *
C*    WITH THE CORRECTION FACTOR IS NEEDED TO OBTAIN THE MASS TRANS-     *
C*    PORT COEFFICIENT IN THE TREATMENT OF JORDAN AND JAVICK, AND AS     *
C*    USED BY BLAEDEL (W.J.BLAEDEL AND R.C.ENGSTROM,ANAL. CHEM.,50      *
C*    (1978)476).  THIS COEFICIENT IS NORMALLY DETERMINED EXPERIMENTAL-  *
C*    LY,BUT GOOD AGREEMENT BETWEEN THE CALULATION IN SUBROUTINE DELT    *
C*    AND EXPERIMENT HAS BEEN SHOWN.                                     *
C*          A LINEAR ARRAY OF POTENTIALS,E(I), REPRESENTING THE SCAN     *
C*    IS NOW SET UP.  THIS IS THEN USED IN SUBROUTINE IECURV TO CALC-    *
C*    ULATE CURRENT AS A FUNCTION OF POTENTIAL.                          *
C*************************************************************************
      WK1=DABS((ESTOP-EINIT)/EINCR)
      R=WK1
      II=IFIX(R)
      E(1)=EINIT-EZERO
      DO4 I=2,II
 4    E(I)=E(I-1)+EINCR
      WRITE(6,207)
      CALL IECURV
      WRITE(6,200) L,B,WE,WC,UBAR,ELEC,DOX,DR,COX,CR,LCC,LCA,LCC1,LCA1,
     *NIT1
      WRITE(6,201) Z,SRC,EZERO,ALPHA,ELEC
      WRITE(6,202)(E(I),HV(1,I),HV(4,I),HV(2,I),HV(5,I),HV(3,I),HV(6,I),
     *I=1,IMAX)
      WRITE(6,203)
      WRITE(6,204)(E(I),CUR(1,I),CUR(2,I),CUR(3,I),I=1,IMAX)
      WRITE(6,205)
      WRITE(6,206)(FUNC(1,I),FUNC(2,I),I=1,IMAX)
      GO TO 100
 999  STOP
 200  FORMAT('1'//////////////36X,'CELL DIMENSIONS',5X,'(CM.)'//
     *36X,'LENGTH',24('.'),F6.4/
     *36X,'THICKNESS',21('.'),F8.6/
     *36X,'ELECTRODE WIDTH',15('.'),F4.2/
     *36X,'CHANNEL WIDTH',17('.'), F4.2//
     *36X,'FLOW RATE',11X,'(CC./MIN.)'//
     *36X,30('.'),F8.4//
     *36X,'ELECTROCHEM. DATA:',2X,'(D IN SQ.CM./SEC., CONC. IN MILLIMOLA
     *R)'//
     *36X,'ELECTRONS IN THE REACTION',5('.'),F2.0/
     *36X,'DIFF. COEF. OF OX.',12('.'),F9.7/
     *36X,'DIFF. COEF. OF RD.',12('.'),F9.7/
     *36X,'CONCENTRATION OF OX.',10('.'),F7.4/
     *36X,'CONCENTRATION OF RD.',10('.'),F7.4////
     *36X,'LIMITING CURRENT (MICROAMPERES)'/
     *36X,'CATHODIC',5('.'),F9.4,'ANODIC',5('.'),F9.4//
     *36X,'LIMITING CURRENT CACULATED WITH SHAPE CORRECTION FACTOR '/
     *36X,'CATHODIC',5('.'),F9.4,'ANODIC',5('.'),F9.4//
     *36X,'NUMBER OF ITERATIONS TO FIND DEL,'/   '
     *36X,'THE DIFFUSION LAYER THICKNESS.',5('.'),I3)
 201  FORMAT('1'///11X,'CURRENT-POTENTIAL CURVE'//
     *21X,'SEE ABOVE FOR PHYSICAL DIMENSIONS'//
     *21X,'R',31('.'),F11.6/
     *21X,'STANDARD RATE CONSTANT',10('.'),D9.3,1X,'(CM./S.)'/
     *21X,'E NAUGHT',24('.'),F5.3,1X,'VOLTS'/
     *21X,'ALPHA',27('.'),F4.2/
     *21X,'NUMBER OF ELECTRONS',13('.'),F2.0///
     *11X,'CURRENT RELATIVE TO LIMITING CURPENT FOR THREE TREATMENTS:'/
```

```
     *11X,'DIFF. LAYER: MY CALCULATIONS WITH CONCENTRATION A LINEAR '/
     *11X,'FUNCTION OF DISTANCE FROM THE ELECTRODE.'/
     *11X,'MASS TRANSP. COEF.: EMPIRICAL TREATMENT OF  W.J. BLAEDEL '/
     *11X,' AND R.C. ENGSTROM, ANAL. CHEM., 50(1978)476.'/
     *11X,'EXACT:  DERIVED USING LINEAR VELOCITY PROFILE (VALID FOR '/
     *11X,'SMALL R) H. MATSUDA ,J. ELECTROANAL. CHEM.,15(1967)325'//
     *21X,'E-E ',9X,'DIFF. LAYER',4X,'MASS TRANSP. COEF.',6X,'EXACT'/
     *24X,'0',5X,'CATHODIC',1X,'ANODIC',3X,'CATHODIC',1X,'ANODIC',3X,'C
     *ATHODIC',1X,'ANODIC'//)
 202  FORMAT(' ',20X,F6.3,4X,F6.3,3X,F6.3,3X,F6.3,3X,F6.3,3X,F6.3,3X,F6.3
     *3)
 203  FORMAT('0',20X,'CURRENTS(MICROAMPERES)'///)
 204  FORMAT(' ',20X, F6.3,7X,F9.4,9X,F9.4,9X,F9.4)
 205  FORMAT('1',20X,38HCOMPARISON TO MATSUDA'S NUMERICAL PHI.    /
     *' ',30X,'Z',30X,'O(Z)'/
     *'+',61X,'/'//)
 206  FORMAT((' ',30X,G9.3,24('.'),F6.4))
 207  FORMAT('1',11X,'OVERV.',3X,'KF',9X,'KB',9X,'P',12X,'C4',9X,'C3',9X
     *,'C2',9X,'C1',9X,'CL'/
     *' ',55X,'DL',9X,'ZCRIT',9X,'PSI',9X,'NIT2',9X,'NIT3'/
     *' ',55X,'G',9X,'PSI1',9X,'PSI2')
      END
```

```
      SUBROUTINE DELTA
      REAL*8 HV(6,100 ),CUR(3,100 ),FUNC(2,100 ),E(100 ),RINPUT(16),
     *ALPHA,B,COEFO,COEFR,DEL1,DEL4,DOX,DR,
     *ELEC,EPS,EPS2,PSI1,PSI2,SRC,Z,
     *C4,C3,C2,C1,CL,DL,ZCRIT,P,KF,KB,PSI
     *,DEL2,INCR,DEL1P,DEL2P,ZP
      INTEGER NIT1,NIT2,NIT3,II,IMAX,
     *I,J
      COMMON HV,CUR,FUNC,E,
     *ALPHA,B,COEFO,COEFR,DEL1,DEL4,DOX,DR,
     *ELEC,EPS,EPS2,PSI1,PSI2,SRC,Z,
     *C4,C3,C2,C1,CL,DL,ZCRIT,P,KF,KB,PSI
     *,NIT1,NIT2,NIT3,II,IMAX
C*************************************************************************
C*    THIS SUBROUTINE CALCULATES THE ROOT OF THE POLYNOMIAL:             *
C*              Z=-3/8 DEL**4+2/3 DEL**3                                 *
C*    BY SUCCESSIVE APPROXIMATION.  THE TWO DIFFUSION LAYER THICKNESS- *
C*    ES DEL AND DELP ARE CALCULATED FOR THE TWO DIFFUSION COEFFICIENTS*
C*    FOR OX. AND RED..  THESE VALUES ARE USED TO CALCULATE EPS, A PAR-*
C*    AMETER WHICK REFLECTS THE RATIO OF THE DIFFUSION LAYER THICKNESS-*
C*    ES:                                                              *
C*              EPS=DOX*DELP/DR*DEL                                    *
C*                 =(DOX/DR)**(2/3)*((1-(DEL/2))/(1-(DELP/2)))**(1/3)  *
C*    EPS APPROACHES (DOX/DR)**(1/2) AS DEL APPROACHES ONE.            *
C*************************************************************************
      DEL1=0.
      DO1 I=1,100
            NIT1=I
            DEL2=(1.5*(Z+((3./8.)*(DEL1**4))))**(1./3.)
            INCR=DABS((DEL2-DEL1)/DEL2)
            DEL1=DEL2
            IF(INCR.LT.0.0001) GO TO 2
1           CONTINUE
      WRITE(6,100)
100   FORMAT('1','STOPPED IN DELTA,NIT=100')
      STOP
2     DEL1P=DEL1
      ZP=Z*DR/DOX
      DO4 J=1,100
            DEL2P=(1.5*(ZP+((3./8.)*(DEL1P**4))))**(1./3.)
            INCR=DABS((DEL2P-DEL1P)/DEL2P)
            DEL1P=DEL2P
            IF(INCR.LT.0.0001) GO TO 5
4           CONTINUE
5     IF(DEL1P.GE.1.) GO TO 6
      EPS =DOX*DEL1P/(DR*DEL1)
      GO TO 7
6     EPS=(DOX/DR)**(1./2.)
7     RETURN
      END
```

```
      SUBROUTINE DELT
      REAL*8 HV(6,100 ),CUR(3,100 ),FUNC(2,100 ),E(100 ),RINPUT(16),
     *ALPHA,B,COEFO,COEFR,DEL1,DEL4,DOX,DR,
     *ELEC,EPS,EPS2,PSI1,PSI2,SRC,Z,
     *C4,C3,C2,C1,CL,DL,ZCRIT,P,KF,KB,PSI
     *,DEL3,DEL4P,DEL3P,ZP
      INTEGER NIT1,NIT2,NIT3,II,IMAX,
     *I,J
      COMMON HV,CUR,FUNC,E,
     *ALPHA,B,COEFO,COEFR,DEL1,DEL4,DOX,DR,
     *ELEC,EPS,EPS2,PSI1,PSI2,SRC,Z,
     *C4,C3,C2,C1,CL,DL,ZCRIT,P,KF,KB,PSI
     *,NIT1,NIT2,NIT3,II,IMAX
C*********************************************************************
C*    THIS SUBROUTINE CALCULATES THE ROOT OF THE POLYNOMIAL:         *
C*                Z=-.6018 DEL**4 +.9355 DEL**3                      *
C*    BY SUCCESSIVE APPROXIMATION.  THIS SOLUTION INCLUDES THE CONCEN- *
C*    TRATION PROFILE SHAPE CORRECTION TERM.                         *
C*********************************************************************
      DEL4=0.
      DO8 I=1,100
            DEL3=((.6018*(DEL4**4)+Z)/.9355)**(1./3.)
            INCR=DABS((DEL3-DEL4)/DEL3)
            DEL4=DEL3
            IF(INCR.LT.0.0001) GO TO 9
 8          CONTINUE
      WRITE(6,100)
 100  FORMAT('1','STOPPED IN DELT ')
      STOP
 9    DEL4P=DEL4
      ZP=Z*DR/DOX
      DO 10 J=1,100
            DEL3P=((.6018*(DEL4P**4)+ZP)/.9355)**(1./3.)
            INCR=DABS((DEL3P-DEL4P)/DEL4P)
            DEL4P=DEL3P
            IF(INCR.LT.0.0001) GO TO 11
 10         CONTINUE
 11   IF (DEL4P.GE.1.) GO TO 12
      EPS2=DOX*DEL4P/(DR*DEL4)
      GO TO 13
 12   EPS2=(DOX/DR)**(1./2.)
 13   RETURN
      END
```

```
      SUBROUTINE IECURV
      REAL*8 HV(6,100 ),CUR(3,100 ),FUNC(2,100 ),E(100 ),RINPUT(16),
     *ALPHA,B,COEFO,COEFR,DEL1,DEL4,DOX,DR,
     *ELEC,EPS,EPS2,PSI1,PSI2,SRC,Z,
     *C4,C3,C2,C1,CL,DL,ZCRIT,P,KF,KB,PSI
     *,P2,D,OLD,DELINC,DL2,DL3,DL4,X2,X,Y,ERROR2,
     *DLP,NEPS,CHECK,PHI,MAT,JJB,F,G,Q
      INTEGER NIT1,NIT2,NIT3,II,IMAX,
     *I,IJ,J
      COMMON HV,CUR,FUNC,E,
     *ALPHA,B,COEFO,COEFR,DEL1,DEL4,DOX,DR,
     *ELEC,EPS,EPS2,PSI1,PSI2,SRC,Z,
     *C4,C3,C2,C1,CL,DL,ZCRIT,P,KF,KB,PSI
     *,NIT1,NIT2,NIT3,II,IMAX
C*********************************************************************
C*    THIS SUBROUTINE CALCULATES THE DIFFUSION LAYER THICKNESS,DL, FROM*
C*    A TRANSCENDENTAL EQUATION.  THE COEFFICIENTS OF THE EQUATION ARE *
C*    FUNCTIONS OF P, WHICH IS A FUNCTION OF POTENTIAL,SPECIFIC RATE   *
C*    CONSTANT,DIFFUSION COEFFICIENT AND CELL THICKNESS.  THE CURRENT  *
C*    DIVIDED BY LIMITING CURRENT IS CALCULATED FROM THE VALUE OF DL.  *
C*    THE SAME RATIO IS CALCULATED FOR TWO OTHER TREATMENTS OF THE     *
C*    PROBLEM.  THE CURRENT IS CALCULATED FROM AN EXPONENTIAL EXPRES-  *
C*    SION IF DL IS GREATER THAN THE CELL THICKNESS.                   *
C*********************************************************************
      DO 2 I=1,II
            IMAX=I
            DL=1.
            OLD=0.
            DELINC=0.5
            X=DEXP(-ALPHA*38.94*ELEC*E(I))
            KF=B*SRC*X/DOX
            X=DEXP((1.-ALPHA)*38.94*ELEC*E(I))
            KB=B*SRC*X/DOX
            DO3 IJ=1,10
                  NIT3=IJ
                  P=KF+EPS*KB
                  P2=P**2
                  C4=-3./8.
                  C3=(2./3.)-(1./(6.*P))
                  D=(1./(2.*P2))+(1./P)
                  C2=D/2.
                  C1=-D/P
                  CL=D/P2
                  DO4 J=1,100
                        NIT2=J
                        DL2=DL**2
                        DL3=DL**3
                        DL4=DL**4
                        X2=-C4*DL4-C3*DL3-C2*DL2-C1*DL
                        X=X2+Z
                        Y=CL*DLOG(1.+P*DL)
                        IF(J.EQ.1) ZCRIT=Y-X2
                        IF(P.LT.0.001) ZCRIT=0.5
                        IF(Z.GT.ZCRIT.AND.J.EQ.1) GO TO 7
                        IF(Y.LT.X) GO TO 5
                        DL=DL-DELINC
                        GO TO 6
5                       DL=DL+DELINC
6                       DELINC=0.5*DELINC
                        ERROR2=DABS((DL-OLD)/DL)
                        OLD=DL
                        IF(ERROR2.LT.0.0001) GO TO 8
4                       CONTINUE
                  WRITE(6,20)
20                FORMAT('1','STOPPED IN IECURV , NIT=100')
                  STOP
8                 DLP=EPS*DL*DR/DOX
                  X=(DOX/DR)**(2./3.)
                  Y=((1.-(DL/2.))/(1.-(DLP/2.)))**(1./3.)
                  NEPS=X*Y
                  CHECK=DABS((NEPS-EPS)/NEPS)
                  IF(CHECK.LT.0.01) GO TO 9
                  EPS=NEPS
3                 DELINC=DL*(DABS(1.-(DR/DOX)**(0.5)))
```

```
9           PSI=DL**2-0.5*(DL**3)
            PHI=DL*PSI/(1.+DL*P)
            Q=KF+KB*((DOX/DR)**(2./3.))
            MAT=.7107*(Z**(1./3.))/(1.+.7107*Q*(Z**(1./3.)))
            JJB=Z*PSI2/(Z*P+PSI2)
            GO TO 10
7           EPS=(1.+(DOX/DR))/2.
            P=KF+KB*EPS
            F=((DOX/DR)-1.)/2.
            G=(2.+P+F*KB)/(2.*(P-F*KB))
            IF(((ZCRIT-Z)/G).LT.-150.) GO TO 11
            PSI=G*(1.-DEXP((ZCRIT-Z)/G))+0.5
            GO TO 12
11          PSI=G+0.5
12          PHI=PSI/(1.+P)
            Q=KF+KB*((DOX/DR)**(2./3.))
            MAT=.7107*(Z**(1./3.))/(1.+.7107*Q*(Z**(1./3.)))
            JJB=Z*PSI2/(Z*P+PSI2)
10          HV(1,I)=PHI*KF/PSI1
            HV(2,I)=JJB*KF/PSI2
            HV(3,I)= MAT*KF
            HV(4,I)=PHI*KB*EPS/PSI1
            HV(5,I)=JJB*KB*EPS/PSI2
            HV(6,I)=MAT*KB*((DOX/DR)**(2./3.))
            X=COEFO*KF-COEFR*KB
            CUR(1,I)=       PHI*X
            CUR(2,I)=JJB*X
            CUR(3,I)=1.4675*MAT*X*(Z**(2./3.))
            FUNC(1,I)=0.7555*P*(Z**(1./3.))
            FUNC(2,I)=PHI*P/PSI1
            WRITE(6,208)E(I),KF,KB,P,C4,C3,C2,C1,CL,DL,ZCRIT,PSI,NIT2,N
     *      IT3,G,PSI1,PSI2
            IF(E(1).GT.0.0.AND.HV(1,I).GE.0.999.AND.HV(2,I).GE.0.999.AND
     *      .HV(3,I).GE.0.999) RETURN
            IF(E(1).LE.0.0.AND.HV(4,I).GE.0.999.AND.HV(5,I).GE.0.999.AND
     *      .HV(6,I).GE.0.999) RETURN
2           CONTINUE
208   FORMAT(' '// 10X,F7.3,2X,G9.3,2X,G9.3,2X,G9.3,4X,G10.3,2X,G10.3,2
     *X,G9.3,2X,G10.3,2X,G9.3/
     *' ',54X,G9.3,2X,G9.3,2X,G9.3,2X,I3,2X,I3/
     *' ',54X,G10.3,2X,G10.3,2X,G10.3)
      RETURN
      END
```

APPENDIX E

Derivation of Equations 36 and 37

1) Derivation of Equations in δ_1 and δ_2

Consider Figure 13. The flux at a point just greater than $\bar{\delta}_1$ is given by

$$\text{flux } (\bar{\delta}_1^{+}) = D_y \frac{C_y^{o}-C_y^{s}}{\delta_2-\delta_1} + \frac{D_A}{K} \frac{C_y^{o}-C_y^{s}}{\delta_2-\delta_1}$$

$$= (D_y + \frac{D_A}{K}) \frac{C_y^{o}-C_y^{s}}{\delta_2-\delta_1}$$

From continuity this flux must equal the flux at a point just before $\bar{\delta}_1$

$$\text{flux } (\bar{\delta}_1^{-}) = D_A \frac{C_y^{s}}{K\delta_1}$$

$$(D_y + \frac{D_A}{K}) \frac{C_y^{o}-C_y^{s}}{\delta_2-\delta_1} = D_A \frac{C_y^{s}}{K\delta_1} \qquad \text{(E1)}$$

Equation (E1) may be solved for C_y^{s} to give

$$C_y^{s} = \frac{\delta_1 (D_A+KD_y)}{\delta_2 D_A+\delta_1 KD_y} C_y^{o} \qquad \text{(E2)}$$

The concentrations of A and Y at various points are:

$$z = 0 \qquad C_y = C_y^s$$
$$C_A = 0$$

$$z = \delta_1 \qquad C_y = C_y^s$$
$$C_A = C_y^s/K$$

$$z = \delta_2 \qquad C_y = C_y^o$$
$$C_A = C_A^o = C_y^o/K$$

From these concentrations the equations for concentration as a function of distance may be given as

$$C_A = (0 < z < \delta_1) \qquad \frac{(D_A+KD_y)\,z}{\delta_2 D_A+\delta_1 KD_y} C_A^o \qquad \text{(E3a)}$$

$$(\delta_1 \leq z < \delta_2) \qquad \frac{\delta_1 KD_y+D_A z}{\delta_2 D_A+\delta_1 KD_y} C_A^o \qquad \text{(E3b)}$$

$$(\delta_2 \leq z) \qquad C_A^o \qquad \text{(E3c)}$$

$$C_y = (0 < z < \delta_1) \qquad \frac{K\delta_1 (D_A+KD_y)}{\delta_2 D_A+\delta_1 KD_y} \qquad \text{(E3d)}$$

$$(\delta_1 \leq z < \delta_2) \qquad \frac{\delta_1 KD_y + D_A z}{\delta_1 KD_y + D_A \delta_2} KC_A^{\circ} \tag{E3e}$$

$$(\delta_2 \leq z) \qquad KC_A^{\circ} \tag{E3f}$$

As in previous derivations these equations are used in the governing differential equation and the resulting equation is integrated over z yielding equations 36 and 37. For simplicity no correction factors have been used. Also, like Matsuda, the velocity has been approximated by a linear relationship limiting the validity of the results to values of r much less than one. This is not considered a serious restriction. Furthermore, incorporation of the full parabolic velocity profile may be done, and new results derived, using the same procedures as are used here.

2) Determination of Integrated Current

Previously, when closed form solutions were available, the total current to the electrode was found by integrating the current from r=0 to $r=r_L$. Since the currents which result from this analysis are in numerical form, the total current must be found either from a numerical integration or by some analytical method which does not require knowledge of i(r). The latter method is preferred, and is used.

From consideration of mass balance, the total current (in terms of flux of moles) must equal the difference between the bulk flux into the cell and the bulk flux out of the cell. The bulk flux at any x may be given by

$$\text{flux} = \int_0^1 C(\bar{z})v(\bar{z})d\bar{z} \qquad \text{(E4)}$$

At $x=0$, $C_A(\bar{z})=C_A^{\,o}$, $C_y(\bar{z})=C_y^{\,o}$ and $v(\bar{z})=6\bar{V}\bar{z}(1-\bar{z})$. At $x=L$, $C_A(z)$ and $C_y(\bar{z})$ may be approximated by equations E3 with $\bar{\delta}_1 = \bar{\delta}_{1,L}$ and $\bar{\delta}_2 = \bar{\delta}_{2,L}$. Note that the fluxes of both Y and A must be used to determine the current. If the above procedure is followed and the integration in equation E4 is carried out, then the current may be found to be given by equation E5.

$$I = nFC_A^{\,o}\tilde{U}(W_e/W_c)\left[\frac{(KD_y+D_A)\bar{\delta}_1^{\,3}+(K+1)D_A(\bar{\delta}_2^{\,3}-\bar{\delta}_1^{\,3})}{KD_y\bar{\delta}_1+D_A\bar{\delta}_2}\right] \qquad \text{(E5)}$$

APPENDIX F

Derivation of Equation 44

$$(M)\begin{Bmatrix}\dot{\delta}_1\\ \\ \dot{\delta}_2\end{Bmatrix} = \begin{Bmatrix}N\\ \\ N\end{Bmatrix} + N\delta_1{}^2\begin{Bmatrix}-\alpha\\ \\ \beta\end{Bmatrix} \tag{43}$$

$$(M)^{-1}(M)\begin{Bmatrix}\dot{\delta}_1\\ \\ \dot{\delta}_2\end{Bmatrix} = (M)^{-1}\begin{Bmatrix}N\\ \\ N\end{Bmatrix} + N\delta_1{}^2(M)^{-1}\begin{Bmatrix}-\alpha\\ \\ \beta\end{Bmatrix} \tag{F1}$$

$$\begin{Bmatrix}\dot{\delta}_1\\ \\ \dot{\delta}_2\end{Bmatrix} = (M)^{-1}\begin{Bmatrix}N\\ \\ N\end{Bmatrix} + N\delta_1{}^2(M)^{-1}\begin{Bmatrix}-\alpha\\ \\ \beta\end{Bmatrix} \tag{F2}$$

The task is to find $(M)^{-1}$. First one must find the transpose of M

$$M^T = \begin{Bmatrix}3N\delta_1{}^2-KD_y\delta_1{}^3 & -KD_y\delta_2{}^3\\ \\ -D_A\delta_1{}^3 & 3N\delta_2{}^2-D_A\delta_2{}^3\end{Bmatrix}$$

Now the adjoint of this matrix must be found.

$$\text{Adjoint} = \begin{Bmatrix}3N\delta_2{}^2-D_A\delta_2{}^3 & D_A\delta_1{}^3\\ \\ KD_y\delta_2{}^3 & 3N\delta_1{}^2-KD_y\delta_1{}^3\end{Bmatrix}$$

Finally, the determinant must be found.

$$|M| = 6N^2\delta_1{}^2\delta_2{}^2$$

since

$$(M)^{-1} = \{A_{ji}\}/|M|$$

where $\{A_{ji}\}$ is the adjoint of the transpose of (M),

$$(M)^{-1} = \begin{Bmatrix} 3N\delta_2{}^2 - D_A\delta_2{}^3 & D_A\delta_1{}^3 \\ KD_y\delta_2{}^3 & 3N\delta_1{}^2 - KD_y\delta_1{}^3 \end{Bmatrix} \Big/ 6N\delta_1{}^2\delta_2{}^2 \qquad \text{(F3)}$$

Equation F3 may be used in equation F2 to yield equation 44.

CHAPTER V

Experimental Investigations of Channel Electrodes

A) Electrode Materials and Reactions

1) Materials

a) Chemicals: Chlorotrimethylsilane and α-bromo toluene (benzoyl bromide) were obtained from Aldrich. Carbon powder (UCP-1) was obtained from Ultra-F Carbon, Bay City, Michigan. Solvents used in the preparation of modified carbons were obtained from Anachemia. Ceresin wax was purchased from Canlab, Montreal, Quebec. Glassy carbon rods, 0.25 cm diameter, were a gift from Carbone Lorraine, Quebec. Glassy carbon plates were purchased from Tokai, Tokyo, Japan by my colleague B.R. Hepler. Low temperature isotropic pyrolytic carbon (LTIC) rods and plates were the gifts of General Atomic Corporation, San Diego, California. These were also procured by Mr. Hepler.

Aluminium oxide powder used for polishing was Baker chromatographic grade. Potassium ferrocyanide trihydrate was ACS reagent grade from American Chemicals, potassium ferricyanide was ACS reagent grade from Fisher. Reagent grade salts, mineral acids, sodium hydroxide and potassium hydroxide were ACS reagent grade from Anachemia. Paraffin

oil was from Anachemia.

b) Experiments and observations: Initially, carbon paste was the material of choice since it was inexpensive and easy to work with. Carbon paste (1) is a mixture of powdered graphite and oil. The oil may be one of many types (2), but paraffin oil or nujol are generally used. The paste is packed into a depression and the surface polished by rubbing on some material, i.e., a computer card. It was immediately obvious from the first experiments measuring current from the electrochemical cell that obtaining a pure diffusion controlled current (flat plateau) was not a trivial task. One of the factors which contributes to the plateau problem is the specific rate constant, k_o. The higher k_o, the lower will be the potential at which a plateau is obtained. For this reason some effort was put into determining what formulation of carbon paste to use for the experiments. Additionally, since eventual analytical applications were foreseen, background current and noise were also important.

Oxygen, in various forms, is present on the carbon surface (3). It was felt that these forms of oxygen may contribute to electrode behavior. To test the assumption, two reactions which would block acidic functional groups were carried out on the carbon surface. Silylation (with chlorotrimethyl silane) and benzoylation (with α-bromotoluene) of surface COOH and OH groups were carried out as follows:

i) Silylation. 5.0 mL of chlorotrimethylsilane, 5.0 mL of dry pyridine and 45 mL of toluene were added to a flask containing 1 g of vacuum dried (56°C) Ultra-F graphite powder (UCP-1). The mixture was stirred for 2 days. The carbon was isolated on a Büchner funnel and was washed with about a liter of 50% methanol in water. The material was dried under vacuum at 56° before using.

ii) Benzoylation. This procedure is due to A. Zamboni and A. Ugolini, members of Dr. Just's research group. 4.3 mL of α-bromotoluene, 6.3 g K_2CO_3 and 10 mL of DMSO were added to a flask containing 1 g of Ultra-F graphite powder. The mixture was heated to 50°C for 2 hr and then stood at room temperature for two days. The material was isolated on a Büchner funnel and washed with water until all the K_2CO_3 had dissolved. This was followed by washing with 500 mL of methanol. The material was dried on a rotary evaporator at steam bath temperature under vacuum for four hours. The amounts of reagents were determined by assuming the carbon to be o-catechol, and then using an equivalent weight of 55 g/eq thereby calculated. The derivitization of the surface was evident due to the change in wettability of the carbon after it had been reacted.

Three batches of carbon paste were made by mixing 500 mg of graphite powder with 330 μL paraffin oil. The silylated carbon paste is called SCP, the benzoylated, BCP, and the

untreated UCP. The materials were checked for background current by cyclic voltammetry in 2 M KCl, 0.1 M KCl, 0.1 M pH 7.0 phosphate and 0.1 M pH 8.6 borate buffers. There was no significant difference among them. The rate constant of the hexacyanoferrate (II) to hexacyanoferrate (III) reaction was checked using the cyclic voltammetric technique of Nicholson and Shain (4). The data obtained are shown in Table 1. It can be seen that there is no significant difference

Table 1

Rate constants for $K_4Fe(CN)_6 \rightarrow K_3Fe(CN)_6$ at three carbon paste electrodes.

Sweep Rate	SCP	BCP	UCP
(mVs^{-1})	$k_o(cms^{-1})x10^4$		
1	6.09	7.90	4.65
2	6.28	6.28	5.46
5	5.92	6.38	6.23
10	5.16	5.99	5.01
20	5.86	5.74	5.98
AVERAGE	5.86	6.45	5.46

Conditions: $K_4Fe(CN)_6$ $9.5x10^{-4}$M in 2 M KCl

between the materials. The Ultra-F carbon was usually used without further treatment.

The very mundane aspect of the polishing of the electrode surface could make a difference in the appearance of a cyclic voltammogram. It was found that by polishing the paste to a high lustre, the electrode response was sometimes more optimal than a more standard polishing on, say, a computer card. Other times the pressure applied during the polishing caused the paste to compress. When the pressure was released the expanding paste cracked and made the electrode unusable. Polishing on a computer card was reproducible but did not always yield a surface perfectly flush with the carbon paste holder. A reproducible and flat surface could be obtained by polishing with lens paper held down on a flat piece of stainless steel.

At one point it was considered necessary to have a harder material than carbon paste. The harder material was required to make a flat, flush electrode surface. A formulation of ceresin wax carbon paste (5) was tried on numerous occasions, but consistently yielded very slow kinetics. It was found that when a small Eppendorf pipette tip (polypropylene) was melted in a Pt crucible with about 3 mL of graphite powder, a homogeneous black mass resulted. This material could be packed into the trough in the cell while warm. The resulting polypropylene carbon paste (PCP) electrode was easily sanded

down to a flush finish. The electrochemical characteristics were good as shown by thin layer voltammograms performed in the channel, but with no flow. The data are presented as the anodic peak potential of hydroquinone and the peak width of half height of the anodic peak in Table 2. The electrochemical characteristics are between the ceresin wax preparation and the UCP. Rubbing the surface of the sanded

Table 2

Thin Layer Voltammograms of Hydroquinone

Material	$E_{p,a}$ (V)	PWHH (mV)
UCP	-0.058	132
CWP	+0.445	235
UCP/CWP(80:20)	+0.405	230
PCP	+0.288	204

$E_{p,a}$ is the anodic peak potential of hydroquinone and PWHH is its peak width at half height. UCP is Ultra-F graphite powder carbon paste, CWP is ceresin wax carbon paste UCP/CWP is an 80:20 mixture by weight of the two, and PCP is the polypropylene carbon paste. The peaks were measured in a thin-layer cell, thickness equal to 0.0112 cm, electrolyte was 0.1 M KCl, 0.1 M NaH_2PO_4 pH 7.0, depolarizer was hydroquinone 0.250 mM. Potentials are referred to an Ag/AgCl electrode.

PCP electrode in a spot on a lens paper where UCP had been polished gave even better electrochemical characteristics. This electrode material was used for the slow flow studies to be discussed.

Glassy carbon and LTIC (6) are generally considered to be competitive with carbon paste. A comparison of these three materials has been made. Figure 1 shows cyclic voltammograms of hydroquinone in 0.1 M pH 7.0 phosphate buffer. The carbon paste is untreated Ultra-F carbon with paraffin oil (500 mg/ 330 μL) (UCP), the LTIC electrode is untreated, and the glassy carbon (GC) electrode is sanded on 600 grade sandpaper to a satiny lustre. The surface areas are UCP 0.18 cm^2, LTIC 0.15 cm^2, GC 0.049 cm^2. Each electrode was held at 900 mV for 30 minutes in a blank 0.1 M pH 7.0 phosphate buffer solution before making measurements. The apparent electrochemical reaction rate is very much higher on GC than UCP or LTI. Furthermore, the waves on GC have an adsorption like quality. The increase in apparent rate may be due to an increase in microscopic surface area, not to a real increase in k_o.

For these same electrodes, the background and noise levels were studied in the phosphate buffer. Results are shown in Table 3.

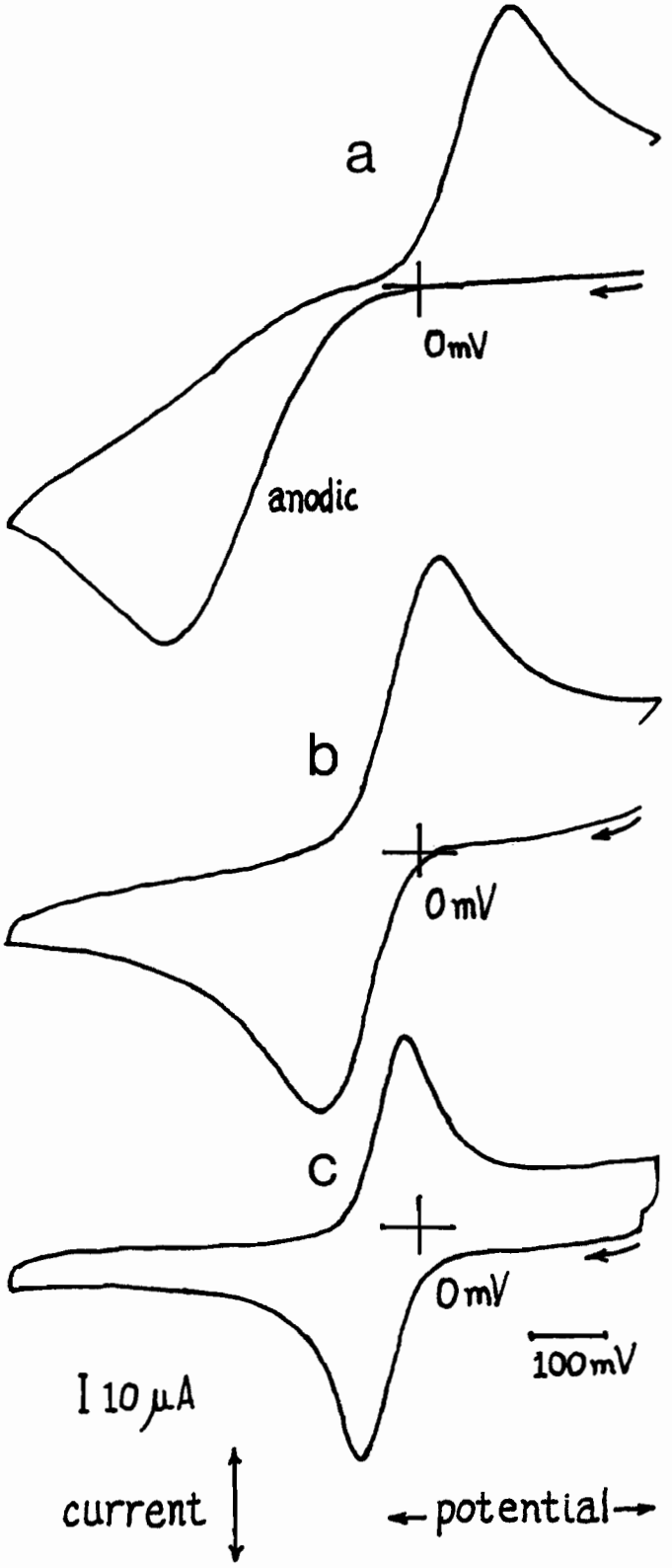

Figure 1: Cyclic voltammograms of 1.0 mM hydroquinone in 0.1M pH 7.0 phosphate buffer. The sweeps were initiated at -300mV vs SCE at 20 mVs^{-1}. a, UCP, b, LTIC, c, glassy carbon.

Table 3

Background and Noise for Carbon Electrodes[a]

		900mV(vs SCE)	500mV(vs SCE)
UCP	Background[b]	6.7×10^2	1.3×10^2
	Noise[c]	0.5	1.6
LTI	Background	1.1×10^4	6.0×10^2
	Noise	3.3	5.3
GC	Background	1.1×10^4	5.5×10^2
	Noise	3.7	2.2
GC PAR[d]	Background	8.2×10^3	4.7×10^2
	Noise	33	25

[a]Measurements have been made in 0.1 M NaH_2PO_4 adjusted to pH 7.0 (NaOH).

[b]Currents are nA/cm^2.

[c]Noise is peak to peak. The PAR 174 filter was off and the recorder filter was off. The noise was measured on the recorder.

[d]GC PAR is a paraffin oil treated electrode. The electrode is washed with distilled water, acetone, methylene dichloride, dried under vacuum and dipped in hot (100°C) paraffin oil. It is then polished on a laboratory tissue.

The level of 60-Hz noise as measured by a Telequipment DM-63 oscilloscope was about ten times the noise level read on the recorder. This led me to believe that was probably sixty-cycle pickup being measured. This has little to do with the virtues of an electrode material. The backgrounds are more informative. Notice that LTI and GC are very similar while UCP demonstrates a much lower background. As Figure 1 shows, however, it may be necessary to operate a UCP electrode at a much higher potential to obtain the same sensitivity of the GC. In this case the low background advantage is lost. The last entry in Table 3 is for a paraffin treated electrode. If the behavior of the electrode is due strictly to electrode area, this would be expected to reduce background and destroy the excellent peak shape. While it does not significantly alter the background, it does destroy the excellent peak shape.

At a later date, oil impregnation of glassy carbon was tested again with the results shown in Table 4. The paraffin oil treatment seemed to be much more effective than previously. This is due to the alteration in procedure. Formerly, after washing and dipping the electrode in hot paraffin, the electrode was just wiped off. This time a vacuum was applied to the surface after each of three applications of hot oil. The same procedure was followed for ceresin wax. The reasoning behind the heating and pulling vacuum was to increase

Table 4

Characteristics of Glassy Carbon

		GC[a]	GC PAR[b]	GC CW[c]
		currents (nA/cm^2)		
Background	900 mV[d]	1.2×10^4	3.3×10^2	3.5×10^2
	700 mV	2.9×10^3	1.0×10^2	1.0×10^2
		mV (vs SCE)		
o-DIA[e]	$E_{p,a}$[f]	600	680	1300
	ΔE_p[g]	54	100	--[h]

[a] GC glassy carbon rod 0.049 cm^2.

[b] GC PAR - paraffin oil treated glassy carbon.

[c] GC CW - ceresin wax treated glassy carbon.

[d] vs SCE.

[e] o-DIA - ortho-dianisidine (3,3'-dimethoxy benzidine).

[f] $E_{p,a}$ anodic peak potential of o-DIA (10 mV s^{-1} sweep rate).

[g] ΔE_p difference between anodic and cathodic peak potentials.

[h] no cathodic peak observed.

the penetration of the oil in micro cracks and scratches on the GC surface. One observation which was important was that GC PAR gave a sharp wave for morphine while GC CW did not.

2) Reactions

The reactions of 3-OMFC were discussed in Chapter III. The reactions of hydroquinone and potassium ferrocyanide were unremarkable.

Morphine sulfate was studied in pH 7.0 0.1 M NaH_2PO_4. Studies in bulk solution provided the following information. In neutral phosphate buffers, morphine displayed a completely irreversible wave with an $E_{1/2}$ about 440 mV vs SCE. The peak height became smaller as each successive scan was made. Replacing the solution had no effect on the wave height, while either wiping the electrode with a methylene dichloride soaked tissue or pulsing for 60 s to -1.00 V returned the peak to its original height. Electrode coating by polymeric products of phenolic oxidation is thus implied. The peak height was indicative of a one-electron transfer by comparison to waves of potassium ferrocyanide and hydroquinone. It was determined that if the potential was reversed after scanning to 550 mV, then the wave retained its magnitude. Cycling to 600 mV showed a small ($\sim$ few percent) peak height decrease on each scan.

This implies that the first material which results from the oxidation of morphine is not directly responsible for the electrode coating. It may undergo a chemical transformation and then, when the potential is increased, another electrochemical reaction may occur from the product of the chemical

transformation. This electrochemical product may undergo chemical reaction in order to form a species which coats the electrode. Designating each electrochemical reaction as E, and each chemical reaction by C, this would be called an ECEC mechanism. The first chemical transformation is not required, so the mechanism may be as simple as EEC.

B) Testing of Theoretical Predictions

1) Three Electrode Channel, Equations A12 and A13 from Chapter IV

a) Chemicals: All the chemicals used were ACS reagent grade. The distilled water used was house distilled water (tin lined pot). A comparison of this water with deionized doubly glass distilled water showed no apparent difference in electrochemical activity by cyclic voltammetry. Acids and bases used in buffer preparation were obtained from Anachemia, potassium ferrocyanide trihydrate from A&C American Chemicals, potassium ferricyanide from Anachemia and hydroquinone from Fisher. Four salts of phosphate were tested for electrochemical activity. Sodium mono- and di-basic, and potassium mono- and di-basic phosphates obtained from Anachemia were used to prepare aqueous solutions (1 g/100 mL). On examination by cyclic voltammetry, the potassium monobasic phosphate demonstrated a peak at about +1.1 volts vs SCE.

None of the other three phosphate salts demonstrated the peak. The peak height was linearly dependent on the amount of KH_2PO_4 added to water. The peak was present in two fresh bottles of KH_2PO_4 obtained from the same supplier. For this reason, NaH_2PO_4 was always used to prepare phosphate buffers. The pH values of various buffers were determined after standardization of the electrode with pH Reference buffers (Scientific Products).

b) Apparatus: The potentiostat used was a PAR model 174. It was always used in the three-electrode mode. The recorder used was a Heath-Schlumberger SR-204.

In order to test the predictive abilities of equations A12 and A13 from Chapter IV, an electrochemical cell in which the electrolyte was flowing was required. The channel shape of the cell placed certain restrictions on the relative placement of electrodes. Consider the standard electrode arrangement for bulk solutions. Here, the auxiliary electrode is placed parallel to the planar working electrode. The auxiliary electrode should be at least as large as the working electrode. The solution potential is measured or controlled close to the working electrode. A Luggin probe is generally used. It has its end parallel to the working electrode surface. It is easily seen that the primary current distribution and equipotential lines are arranged compatibly. The current flows between the auxiliary electrode

and the working electrode. The flux is perpendicular to both surfaces. This requires that the equipotential lines be parallel to the electrode surface. Maintaining the Luggin probe tip parallel to the electrode surface accomplishes this. In a thin channel, however, there is no room for the Luggin probe. The auxiliary electrode is easily placed opposite to the working electrode but interposing the reference electrode is difficult. The reference electrode is usually placed outside the channel. The flowing stream exiting from the channel acts as a solution bridge to the reference electrode. It is not optimal from a primary current distribution viewpoint. With the reference electrode exterior to the cell the equipotential lines are perpendicular to the inside surface of the tube carrying the flowing stream. The lines enter the cell and will maintain their perpendicularity to the direction of solution flow. This direction is orthogonal to the direction required by the current flow between the auxiliary electrode and the working electrode. Even if the reference electrode is placed inside the channel the same situation will arise. Clearly, the only way to achieve the optimum configuration is to have the auxiliary and reference electrodes be in the same place. But this is just the two electrode system in common use up to the mid 1960's. In a cursory search of the abundant literature on reference electrodes no suitable material was found which

could meet all the requirements for a second electrode with respect to stability, current carrying capacity, insensitivity to solution alterations, machinability and ability to be polished to a flat surface. It was felt necessary to minimize the (small) iR drop problem of an external reference electrode, so the reference electrode was placed inside the cell. The reference electrode was a silver button. The working electrode was initially a carbon paste electrode. The auxiliary electrode was a stainless steel plate. The cell was fabricated from lucite. One half of the cell contained the auxiliary electrode and the other half contained the silver button and a trough for carbon paste. Between these two halves a polytetrafluoroethylene (PTFE) spacer was placed to define the channel through which solution would flow. A sketch of the cell used is shown in Figure 2. The cell was fabricated by Alfred Kluck, McGill University.

c) Experimental measurements: The experimental measurements required to test equations A12 and A13 in Chapter IV fell into two categories. First, the parameters b, $\bar{U}$, L, W_c, W_e, C° and D had to be determined. Second, the current at these conditions was determined experimentally. This experimentally measured current was then compared to the theoretical current derived from the measured parameters. The measurement of each parameter shall be discussed.

Thickness, b. The polytetrafluoroethylene (PTFE) spacers used

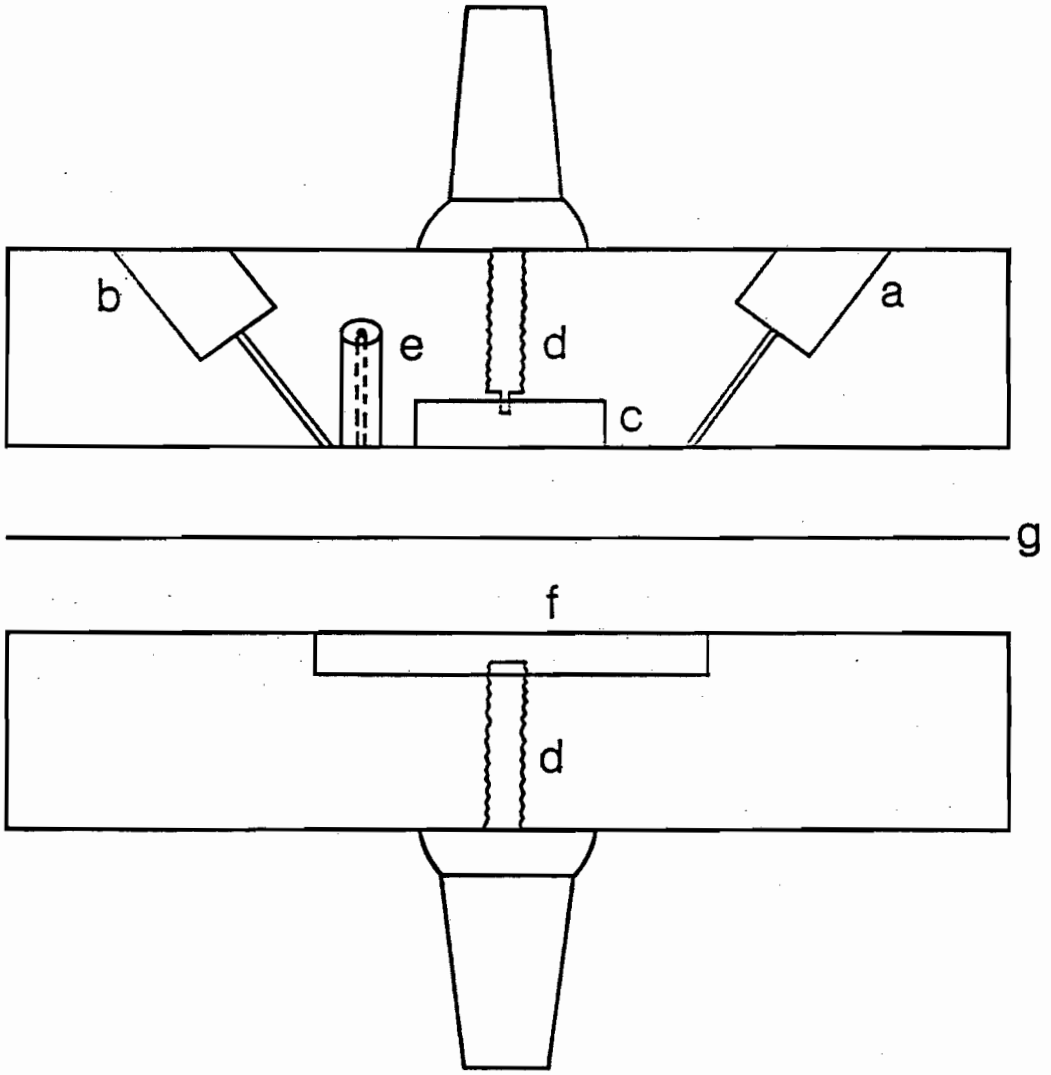

Figure 2: The electrochemical cell used for the determination of the current-r relationship. a, entry port for flowing solution,b, exit port,c, trough for carbon paste,d, electrical contact,e, polytetrafluoro-ethylene(PTFE) press-fit column to hold Ag wire reference electrode,f, stainless steel plate auxilliary electrode,g, PTFE spacer.

ranged in thickness from one to thirty thousandths of an inch (Johnson Plastics, Quebec). Since the spacers were soft and were compressed between two harder lucite pieces, compression could occur. This would not allow a thickness measured externally to be used in a calculation. Many methods were attempted to try to measure the thickness of the spacer in situ. For the larger thickness (external thicknesses, 0.0878, 0.0512, 0.0382, 0.0267 cm) the absorbance of a solution of $K_2Cr_2O_7$ in 0.005 M H_2SO_4 was used. A lucite cell was constructed without any electrodes, just two clear pieces with threaded holes for bolts. Spacers with a rectangular section cut out were affixed between the lucite halves, and the cell formed was filled with the dichromate solution. The absorbance was measured at 400 nm with a Cary 17. These measured thicknesses are shown in Table 5.

Table 5

Thickness of Spacers

External (cm)	Internal (cm)
0.0878	0.0752
0.0512	0.0432
0.0382	0.0295
0.0267	0.0200

External means outside of a cell, internal means compressed between two lucite blocks.

To measure smaller thicknesses the most reliable method turned out to be by making a ceresin wax cast of the cell and measuring its thickness. For a spacer with external thickness 0.0129 the internal thickness was 0.011.

The limit of error (three times the relative standard deviation) for ten ceresin wax casts was ±6.7%. For the thicker spacers where absorbance was used, the limit of error was taken to be ±5% for ten measurements.

Flow rate, $\bar{U}$. The pumping system used for fast flow rates was a Waters 6000A. The flow rates were measured by timing the filling of a 1.00- or 2.00 mL test tube.

For flow rates of under 0.1 mL min^{-1} another system was required. A hydrostatic pressure system seemed like a simple approach. The cell was positioned between two reservoirs. The waste reservoir was a 4-L beaker sitting on the bench top. The solution of depolarizer was in a bottle on a laboratory jack so that its height could be varied. The measurement of the height of the solution was by the use of a burette as a scale. By sighting through the bottle, the height of the bottom of the meniscus of the depolarizer solution could be read from the burette. The burette was positioned as closely as possible to the bottle (about 1 cm away) to minimize parallax error. A zero reading of height corresponded to the bottom of the meniscus of the waste reservoir. A meniscus reader was used in conjunction

with a tensor lamp to make the measurements easy, thus avoiding errors caused by fatigue.

To determine the relationship between the height and the velocity of the solution, some means of measuring solution velocity or flow rate was required. The velocity of the solution could be measured by measuring the velocity of an air bubble injected into the flowing stream. This was accomplished using a "T" junction. The perpendicular arm of the "T" was fitted with a rubber septum. Bubbles were injected directly into the flow stream with a 50- or 100-µL syringe. In actuality, flow rate was the information desired. The time it took a bubble to traverse a certain volume could be used to calculate the flow rate. A straight piece of PTFE tubing was filled eight times with 50.0µL of water from a 50 µL syringe. The length of the solution plug from each filling was measured with calipers. The average length was 10.88 cm. This section of the PTFE tubing was taped to a 15-cm ruler. This device was inserted into the flow stream downstream from the bubble injector. When a bubble was injected, the time taken to traverse 5 cm of the tubing was measured with a hand-held stopwatch. At least two, and usually three, measurements of time were made at each height routinely. To check the system, the flow rate was measured at 13 heights from 6.95 to 20.0. The heights are mL from a burette scale and will be assigned no units. The mL divisions

were about 1 cm apart. The average value of the flow rates measured at each height was taken as representative of that height. Linear regression on the height-flow rate data yielded a good fit, with a correlation coefficient of 0.998. The residuals were randomly positive and negative.

Some interesting observations were made with this system. The height-flow slope is dependent upon a number of parameters, all but one being physical distances. The one which is not is kinematic viscosity. When phosphate buffer (0.1 M NaH_2PO_4, 0.1 M KCl, pH 7.0) was used, the slopes were 0.01556 and 0.01591 for two lines. With $2x10^{-4}$ M hydroquinone in the same solution, the slopes were 0.01708 and 0.01673. The units are mL min^{-1} per unit of distance on the burette. Could the difference be due to a viscosity difference? The difference between the slopes is likely due to a difference in wettability of the PTFE tubing caused by hydroquinone. This would appear as a change in viscosity since the laminar flow theory assumes the inside tubing walls are completely wettable. It is unlikely that the difference in slopes is due to a viscosity change. While the temperature of the liquids was not measured, the temperature of the room was constant within a degree (22-23°C) over the two days on which these experiments were performed. Another point of interest was the height-intercept. At what height did this straight line predict zero flow rate? For the solution with

or without hydroquinone, the value fell between 3.59 and 3.69 cm. This is certainly not due to error in setting the zero position of the burette. It was felt that it was most probably due to a pressure drop at the bubble, or frictional drag of the bubble in the tubing. In any case, it was clear that the dependence of flow rate on height was easily determined, but the absolute value of the height was not known. To check the assumption that the bubble perturbed the system, the flow rate was measured volumetrically. The slope of the height-flow line was the same as the bubble-measured flow, but the intercept had changed to -1.41 burette units. The source of the negative bias was probably caused by droplets of solution hanging lower than the waste reservoir level since the exit of the tubing was secured at that level. Nonetheless, the difference in intercepts is clear. Another method to determine zero flow was necessary.

When the value of r is >> 1, the cell is coulometric. The current to a coulometric cell is a linear function of flow rate. At very low heights, current could be measured. The current <u>versus</u> height relationship was linear at low heights, and extrapolation to zero current gave a zero flow intercept. This intercept could be used with the height-flow slope to yield a linear relationship between height and flow rate. It should be pointed out that some data were taken before an accurate zero was obtained. These data will be

discussed below. These operations were performed twice daily, once for phosphate buffer alone (slope only) and once for hydroquinone (slope and intercept), since even small system or temperature variations could alter the relationship.

To calibrate the Waters pump, the time taken to fill a 1.00- or 2.00-mL volumetric test tube was measured. The average of at least 12 determinations was taken. Table 6 shows

Table 6

Flow rates of Waters 6000A pump, solvent 0.1 M pH 7.0 phosphate buffer.

nominal (mL min^{-1})	actual (mL min^{-1})
0.1	0.089
0.2	0.190
0.3	0.293
0.5	0.493
0.7	0.685
1.0	0.976
1.2	1.17
1.5	1.47
1.7	1.68
2.0	1.95
2.5	2.43
3.0	2.92

the actual flow rates determined. The limit of error (3 times the standard deviation) was taken as ±3% as an average value among all the flow-rate determinations. The assistance of my colleague, B.R. Hepler, in making these measurements is acknowledged. For the low $\bar{U}$ system there are two sources of error which add quadratically since, the way they are measured, they are independent. One error is the error in the slope of the height-flow curve. Three times the relative standard error of the regression coefficient calculated in the linear regression program (STATPK, MUSIC system, McGill Computing Center) yields a limit of error of 5%. The second error is the absolute error in measuring the height of the meniscus which is taken as ±0.01 burette mL divisions (≈0.1 mm). The total error varies with height to a maximum of ±11% at a height of 0.1 burette divisions.

Electrode and Channel Widths, Electrode Length, W_e, W_c and L. The best results were obtained when the width of the channel, W_c, was close to or equal to the width of the electrode, W_e. For $W_c >> W_e$, the current was always much higher than expected. This probably reflects the fact that material flowing beside the electrode may be perturbed and flow over the electrode. This mixing phenomenon was avoided, for large $\bar{U}$, by using $W_e \simeq W_c$. For small $\bar{U}$ it was found that W_c must equal W_e. When W_c = 0.12 cm and W_e = 0.10 cm, the ratio of actual current under coulometric conditions to theoretical

coulometric current was 1.24. The coincidence between the width ratio and current ratio did not go unnoticed. The fastest $\bar{U}$ used on this particular day was 0.05 mL min^{-1}. At this flow rate it is easy to calculate that diffusion alone can make the "effective" electrode width equal to 0.116 cm. At lower flow rates the value of W_e becomes effectively equal to W_c simply because material will diffuse from a point in the channel beside the electrode to a point over the electrode, where it will react. This particular set of data was compared to calculations based on $W_e = W_c = 0.12$. Further experiments were performed for a new spacer with $W_e = W_c =$ 0.035 cm. For this experiment, the ratio of coulometric yield (experimental:theoretical) was 0.945. This value is, within experimental error, equal to one. Thus, edge diffusion was occurring.

After the discovery of the edge diffusion problem for low flow rates, data which had been taken under similar conditions were examined. Three sets of data were found which were routinely greater than the theoretical value by about 1.2 (47 data points, average 1.18). Unfortunately, these data were taken without accurate knowledge of zero height. Consequently, the coulometric data were not available to see if, in fact, edge diffusion was occurring. The decision was made to reject these data on the basis of the striking coincidence of the error with the W_c/W_e ratio.

A 6x magnifier with scale was used to measure the lengths and widths . The absolute error in measurement was taken to be ±0.05 mm. For a length near 1 cm this means ±0.5%. For a width near 1 mm this means 5%.

Concentration, C°. To prepare solutions of hydroquinone (H_2Q), a frozen 1-mL aliquot of 1.00×10^{-3} M hydroquinone in distilled water was thawed in a trouser pocket. A solution of the desired concentration was prepared by suitable dilution in a buffer or electrolyte. Buffers were vacuum degassed when the Waters pump system was used and buffers were purged with N_2 when the hydrostatic flow system was used. The concentration of H_2Q was checked periodically by measuring the u.v. absorbance (Cary 17). The molar absorptivity used was 2.69×10^3 L mol^{-1} cm^{-1}, an average of three values found in a compendium (7-9). The limit of error was taken to be 3%.

Diffusion coefficient, D. The chronoamperometric procedure for determining diffusion coefficients was used (1). Initially, to calibrate the electrode area, the standard system of potassium ferrocyanide in 2 M KCl was used. The electrode used was an LTIC rod. The circular end of the rod was exposed to the solution. The electrode was in a cylindrical PTFE tube, the walls of the tube extending beyond the electrode to provide a "shield" which would insure linear diffusion. The literature value of D(10), 6.29×10^{-6} cm^2 s^{-1} was used. The data for five separate pulses, averaged,

Table 7

Chronoamperometry (1) at infinite potential[a] pulse. 1.00 mM potassium ferrocyanide in 2 M KCl and 1.00 mM potassium ferrocyanide in 0.1 M pH 7.00 phosphate.

t(s)	2 M KCl $it^{1/2}(\mu As^{1/2})^b$	0.1 M PO_4 $it^{1/2}(\mu As^{1/2})^b$
4	21.07	18.57
5	20.97	18.95
6	20.95	19.21
7	20.93	19.39
8	20.96	19.55
9	20.94	19.68
10	20.93	19.77
11	20.93	19.87
12	20.91	19.98
13	20.93	20.04
14	20.93	20.10
15	20.95	20.18
16	20.96	20.22
17	20.96	20.28
18	20.97	20.31
19	20.98	20.33
20	20.98	20.37
21	21.00	20.40

Table 7 - continued:

22	21.01	20.43
23	21.02	20.46
24	-	20.48
25	-	20.51
26	-	20.52
27	-	20.54
28	-	20.54
29	-	20.55

---

[a]Potential pulses were from 0 to 500 mV vs SCE. The measured E° for equimolar $K_4Fe(CN)_6$ and $K_3Fe(CN)_6$ was 252 mV.

[b]Blanks have been subtracted. Each number is an average of five determinations.

are shown in Table 7. The electrode area was found to be 0.153. Table 7 also shows the data for potassium ferrocyanide in phosphate buffer. The $it^{1/2}$ product was not constant until about 25 seconds had passed. A comparison of the cyclic voltammograms of potassium ferrocyanide showed that the peak potentials depended upon the electrolyte, in 2 M KCl $E_{p,a}$ = 290 mV and in 0.1 M PO_4 $E_{p,a}$ = 330 mV. The effect of the phosphate on the electrochemical reaction is not understood, nonetheless, the system did not seem "ideal" enough for the investigations planned.

Hydroquinone has an E° near 0 volts for pH values near 7. This would allow a large overpotential to be applied to the electrode to gain a plateau. By cyclic voltammetry the system H_2Q/0.1 M phosphate buffer pH 7.0 seemed well behaved, although certainly not "reversible". The diffusion coefficient calculated from duplicate chronoamperometric experiments carried out with the same apparatus as that used for potassium ferrocyanide yielded a D (± standard deviation) = $8.4 \pm 0.4 \times 10^{-6}$ cm^2 s^{-1} (23°C). The $it^{1/2}$ values were stable for the range of the experiment, t = 2 to 36 seconds.

After using phosphate electrolyte it was discovered that an electrolyte of 1 M H_2SO_4 yielded very nice waves. The use of this electrolyte required the knowledge of the diffusion coefficient of H_2Q. Once again, using chrono-amperometry and referencing the system against potassium

ferrocyanide in 2 M KCl, a diffusion coefficient ($\pm$ standard deviation) of $8.7 \pm 0.4 \times 10^{-6}$ cm^2 s^{-1} was found (23°C). These errors represent $\pm$15% limits of error. The random errors in the measurement of seven parameters, b, L, W_e, W_c, $\bar{U}$, D and C°, all lead to an error in the predicted current. The total error in the predicted current could be related to the individual errors by the formula for the propagation of errors (11)

$$\lambda(F) = \left[\sum_i \left(\frac{\partial F}{\partial x_i} \lambda(x_i) \right)^2 \right]^{1/2}$$

where λ is the limit of error and x_i are the independent variables. Equation A12 was differentiated at various values of r to determine the contribution of error from each x_i (b, L, W_e ...). All the errors are expressed as relative errors to the mean.

The total error for any given calculation depends upon r. The limit of error expected in the calculation of current is shown in Table 8.

Current, I. The measurement to which the theory was compared could now be made. All the data were taken using the following protocol. i) Waters pump: Phosphate buffer (0.1 M NaH_2PO_4 adjusted to pH 7.0 with NaOH) was prepared in distilled water. It was filtered under vacuum with a

Table 8

Limit of error ($\lambda(I)/I$) in the calculated current as a function of r.

r	< 0.3337	0.3337	1	2
$\lambda(I)/I$[a]	0.12,0.12	0.12,0.13	0.10,0.11	0.10,0.12

[a]The first value is for $W_e=W_c$, the second is for $W_e \neq W_c$.

Millipore 0.45-μm filter and stored in a 2-L vacuum flask covered with Al foil. The buffer was refrigerated if it was not being used. The electrochemical cell was prepared for use. The silver button was anodized in phosphoric acid (0.1 M) for 30 minutes, manually adjusting the potential to keep the current around 10-30 μA. After the cell was assembled, a potential of 1.0 V was applied to the working electrode. If the background had decreased to an acceptable (sub μA) value after about an hour, then the magnitude of the current was measured as a function of potential and flow rate. This background current was not very dependent on flow rate, and it was quickly learned that taking values at flow rates of 0.1, 1.0 and 3.0 mL min^{-1} was sufficient. Values for other flow rates could be found by interpolation. When this was completed, a solution of the hydroquinone was pumped

through the cell.

As stated earlier, the plateau of the wave was not always accessible. To determine one of the reasons for this, the following experiment was performed. Hydrodynamic voltammograms were recorded for a spacer of thickness near .0018 cm and at 0.1 mL min^{-1}, and for a spacer of thickness 0.0752 cm at 4.2 mL min^{-1}. The velocity is the same in each case. While the thicker spacer demonstrated a plateau, the thinner spacer did not. Fortunately, since $\bar{U}$ and b are multiplied in r, no region of r was excluded because large $\bar{U}$ and small b could not be used simultaneously. This does have analytical implications, however. The effect is most probably cuased by the difficulty with which the potential is controlled in the thin space between the auxiliary and working electrodes. On any given day, hydrodynamic voltammograms were taken at various flow rates to determine what values of $\bar{U}$ would allow complete diffusion control. The potential at which limiting current was obtained having been thus determined, current was measured as a function of flow rate.

ii) Hydrostatic pumping system. The auxiliary electrode was external to the cell to avoid regeneration. In this case, since chloride ion (0.1 M KCl) was added to the phosphate buffer, the Ag button was anodized in 0.1 M HCl (12). Buffer or 1.0 M H_2SO_4 were prepared and deaerated with N_2.

The Ag/AgCl electrode was used for H_2SO_4 without the addition of chloride. The flow rate-height slope was measured. Currents were measured as a function of potential and flow rate. The depolarizer solution was then introduced into the system. The flow rate-height slope was measured, and then currents at low heights were measured. After the blank value had been subtracted, the currents were plotted as a function of height to determine the zero flow intercept. Currents were then measured for larger flow rates for a potential on the plateau.

In either case of pumping, if the wave did not plateau in a level fashion, but maintained a slight linear rise with potential, then currents were measured at a potential where the curve first became linear. The temperature of the room varied from 21°C to 26.5°C on days for which data were taken.

The data were taken over a range of flow rates from 0.0003 mL min^{-1} to 3.0 mL min^{-1}, a range of thickness of 0.0011 to .020 cm, at two channel widths, 0.035 and 0.12 cm, at one electrode width, 0.10 cm, at one electrode length, 1.03 cm, and at a range of concentrations from 40 μM to 250 μM. The data may be compared to the theoretical prediction ± the limit of error (≈11%) in Figure 3. The fit is quite analogous to examples in Chapter IV, the forcing of the equation to be exact as $r \to 0$ and to obey Faraday's Law were in a large part responsible for the excellent agreement.

Figure 3: A comparison of data(points) and the theory (equation A 12 of chapter IV) for the channel electrode. The logarithm of the coulometric yield is plotted against the logarithm of $r^{2/3}$. The dotted lines represent ± 11% , the calculated limits of error.

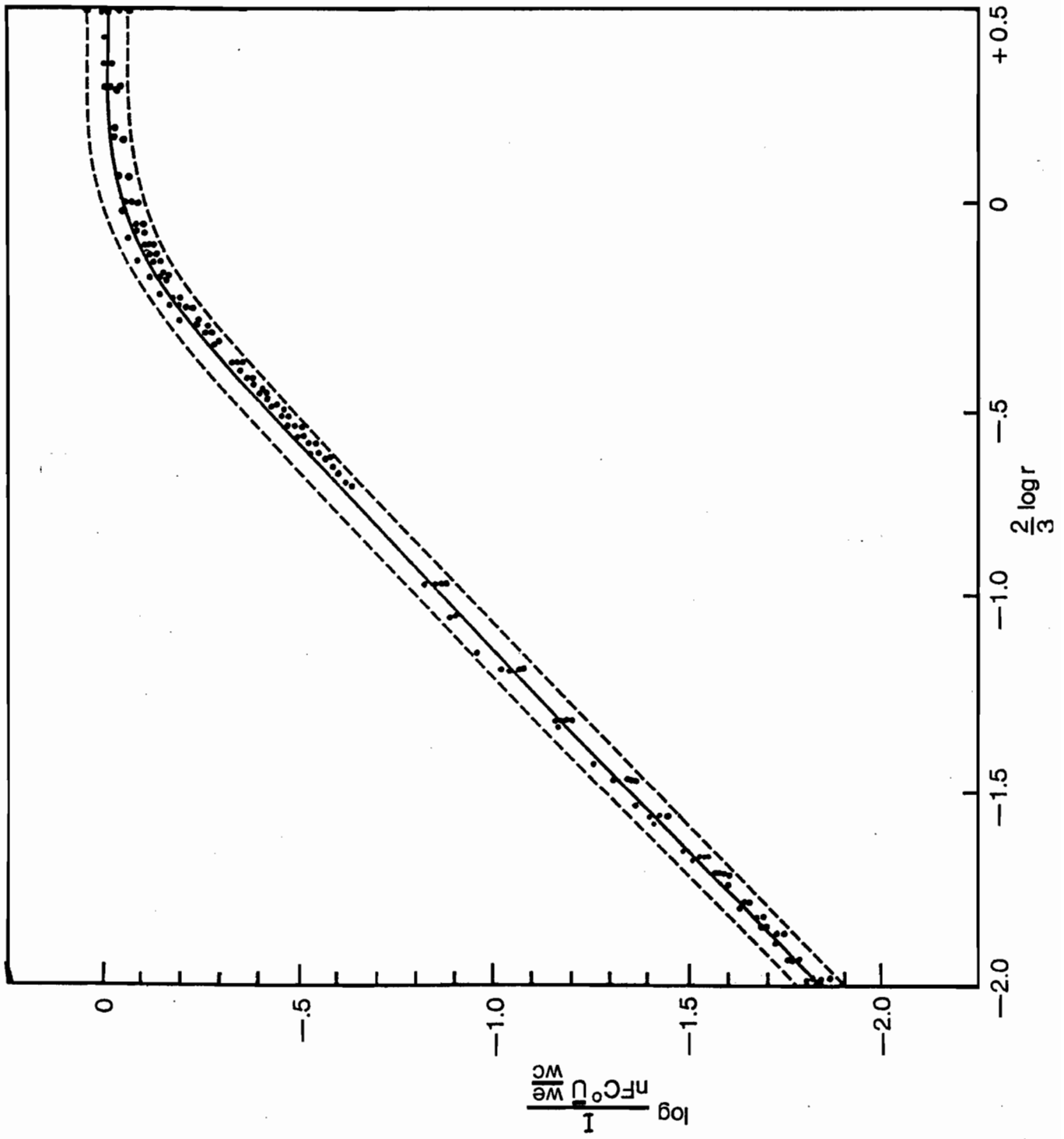
log I / nFC°U we/wc
0
-.5
-1.0
-1.5
-2.0
+0.5
0
-.5
-1.0
-1.5
-2.0
2/3 log r

2) Four Electrode Channel, Equations 32a, 33a and 34a of Chapter IV

a) Chemicals: Sodium acetate and acetic acid were obtained from Anachemica. Nor-adrenalin was obtained from Sigma. Other chemicals used are described in the previous section.

b) Apparatus: The cell used for this work was essentially the same as that shown in Figure 1 with two important exceptions. First, both the auxiliary and working electrodes were ceresin wax treated glassy carbon (Tokai Mfg., Tokyo, Japan). Second, these electrodes were 10x1.5 cm surfaces. With this cell, large r values could be obtained. Acknowledgement is given to my colleague, B.R. Hepler, for help in designing this cell, and for ordering the glassy carbon from Japan. The cell was built by the staff of machine shop in the Chemistry Department of McGill University.

The peristaltic pump used for the flow studies was a Technicon Auto Analyzer proportioning pump. The pump tubing was obtained from Technicon. Flow rates were measured by timing the filling of a 1.00- or 2.00-mL volumetric test tube. For injections into the flow stream a Durrum injector was used. This is a sample loop-type injector. The sample loop had a 100-μL capacity.

The four electrode potentiostat was built essentially like that of Blank (13). In place of his bridge rectifier/

zener diode voltage source for applying voltage to the second working electrode, a simple voltage divider was used. The operational amplifiers were RCA 3140S FET input amplifiers. Their low input offset current and bias current made them ideal for current-to-voltage conversion. The linearity of the circuit was checked by applying a current from a PAR 173 galvanostat to the input of the current-to-voltage convertor. The performance can be seen in Table 9.

The potentiostat used for the three electrode system was a PAR 174. The recorder used was a Heath-Schlumberger SR 204.

c) Experiments and Observations: According to equations 32a, 33a, and 34a in Chapter IV, one ought to be able to detect whether the regeneration effect is occurring as envisioned by measuring current as a function of flow rate. This experiment was done with 1.0×10^{-5} M potassium ferrocyanide, 1.0×10^{-5}M potassium ferricyanide and a solution containing 1.0×10^{-5} M of both. The solvent was aqueous 2 M KCl. The thickness was determined by ceresin wax injection to be .0024 cm. The length was 9.0 cm, the widths of channel and electrode were 1.0 cm.

For these experiments the four-electrode potentiostat was not used. A three-electrode system with the auxiliary electrode opposite the working electrode was used. For fairly reversible couples like ferrocyanide/ferricyanide, this

Table 9

Performance of fourth-electrode current-to-voltage convertor and amplifier

Current in (μA)[a]	Volts out[b]
0.000	-0.001
+0.050	+0.507
-0.050	-0.501
+0.100	+1.008
-0.100	-0.995
+0.150	+1.508
-0.150	-1.499
+0.200	+2.01
-0.200	-1.998
+0.500	+5.01
-0.500	-5.01
+1.000	+10.03
-1.000	-10.05

[a]Current was applied with a PAR 173 galvanostat.

[b]Potential was measured with a PAR 173 high input impedance electrometer probe.

approach is equivalent to the four-electrode approach as explained in Chapter IV.

By hydrodynamic voltammetry, it was determined that 950 mV, vs the Ag/AgCl button, was on the plateau of the ferrocyanide wave. By pumping the ferrocyanide solution at various flow rates (by changing pump tubing radius), data were gathered. Blank values found in 2 M KCl were subtracted. The data are presented in Figure 4. The lines plotted are equations from Chapter IV. At the bottom of the figure is shown the theoretical and experimental determinations using a coulometric arrangement (both glassy carbon electrodes together as working electrodes with the auxiliary electrode external to the cell).

It seems that the effect is demonstrable. The agreement with theory is good. In a recent publication (14) it was attempted to utilize this technique for chromatographic detection. It was demonstrated that the technique was not effective at any but low flow rates, too low to be useful in chromatography. The reason for their failure is unclear. Showing that the effect can be predicted by theory is a step toward a practical detector of this nature.

C) Application of Channel Electrodes to Detection

1) Voltammetric Immunoassay

a) Chemicals: Morphine sulfate and codeine phosphate

Figure 4: Investigation of a cell with large r. Both axes are in units of cm^3s^{-1}. The lines represent theoretical expectation for;a, coulometric system, $1.0x10^{-5}$ M $K_4Fe(CN)_6$ in 2M KCl, b, a regenerative system , $1.0x10^{-5}$M $K_3Fe(CN)_6$ in 2M KCl,c, a regenerative system with $1.0x10^{-5}$M $K_4Fe(CN)_6$ in 2M KCl,d, a regenerative system with $1.0x10^{-5}$M of both $K_4Fe(CN)_6$ and $K_3Fe(CN)_6$ in 2M KCl. Potential of the working electrode was 950 mV vs Ag/AgCl button. The points represent experimental data.

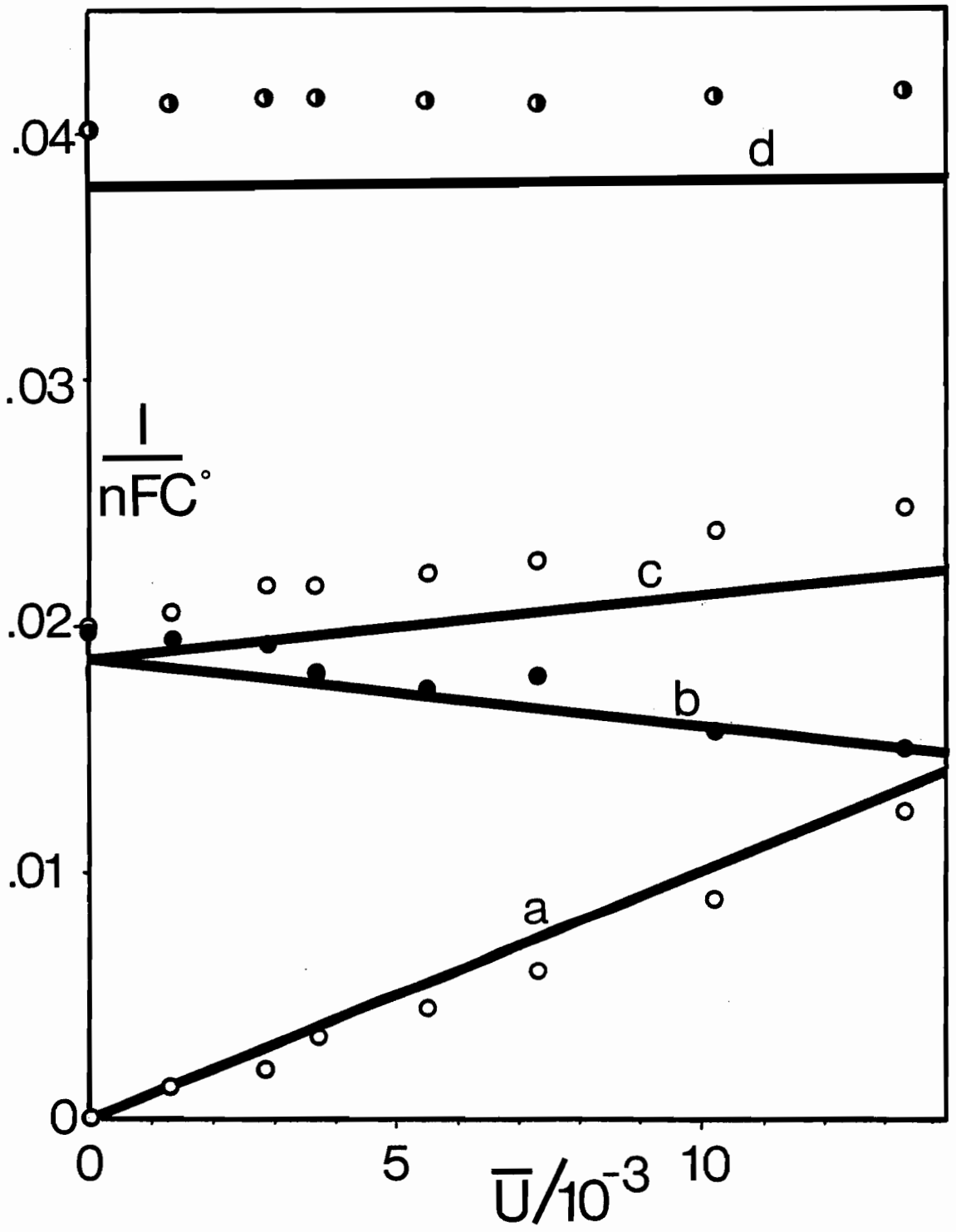
.04
.03
.02
.01
0
I
nFC°
d
c
b
a
0
5
10
Ū/10⁻³

were obtained from Allen and Hanburys, Toronto. They were pure as checked by thin-layer chromatography (TLC) and were used as supplied. 3-O-morphinyl ferrocene carboxylate ester (3-O-MFC) was synthesized (Chapter III). Compound IIIa was used after only one chromatographic purification step for some experiments. The unusual irreproducibility of the results using this compound was found to be caused by light sensitivity of the compound. After purification to remove the few percent of contamination (as judged by TLC spot sizes), IIIa did not show the obvious light sensitivity. The batch of 3-O-MFC called IIIb did not show obvious light sensitivity. Nonetheless, the standards and reagent mixtures were routinely kept out of the light. ortho-Dianisidine (3,3'-dimethoxy benzidine) was obtained from Aldrich.

Phosphate buffers were prepared to the given molarity in NaH_2PO_4 and adjusted to the given pH by adding solid KOH. After preparing a lot (2 L) of buffer, it was vacuum filtered through a millipore filter. The buffer was kept in the 2-L vacuum flask covered with Al foil. The flask was refrigerated overnight. Each morning the buffer was warmed to about room temperature by setting it in a sink of warm water. Vacuum was then applied to the flask with stirring to remove dissolved gasses. tris(hydroxymethyl)aminomethane maleate (Trizma maleate, Sigma) buffers were prepared using the same protocol.

Materials for injection were prepared by dilution in volumetric glassware or by mixing two or more solutions in a test tube. In either case, volumes from 1 to 1000 µL were measured with Eppendorf piston-type microliter pipettes.

Epoxy cement was obtained from Epotek,Billerica, Mass. Both a non-conducting (349) and a silver containing conducting (410-E) epoxy were used. Kel-F was obtained as a 2.54-cm diameter rod from Fluorocarbon, Pennbrook, NJ. A peristaltic pump, single channel, made by LKB was utilized. One-mL plastic tuberculin syringes and 0.5 mL capacity plastic sample cups with lids were obtained from Canlab, Montreal.

Antibody to opiate alkaloids was obtained from Syva Corp. Five-mL quantities were purchased.

b) Electrochemical cells: The decision was made to convert from a carbon paste electrode to a glassy carbon electrode. The trough in the lucite cell, which was used to contain carbon paste, was filled with epoxy cement (LePages). After this had hardened, a hole was drilled to accept a glassy carbon rod. This was glued in place with epoxy cement (LePages). Later, four more electrodes were placed in the cell. Electrical contact was made with a small spring and a screw to push the spring against the glassy carbon. The electrode arrangement is shown in Figure 5.

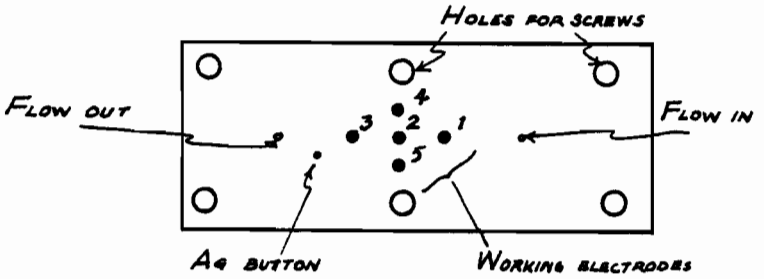

Figure 5

Still later, this cell met its end after having been modified numerous times, mostly to plug leaks. The cell which replaced it is shown in Figure 6. It is essentially the same except for two differences. It was made of a hemicylindrical piece of Kel-F. This meant that it could not be held together by screws. It was clamped between two blocks

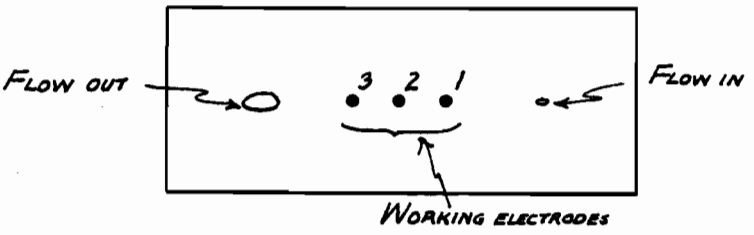

Figure 6

of polyvinyl chloride. Each block had a hemicylindrical shape

cut out of it to accommodate the cell. The half of the cell not shown in Figure 6 was a hemicylindrical piece of stainless steel. The second difference was the large exit hole. This was done to prevent bubbles from being trapped and to make a larger path from the reference electrode to the working electrodes. The reference electrode was a silver-silver chloride electrode in 4 M KCl saturated with silver chloride. It was isolated from the flow stream with a vycor glass plug. It was held in the flow stream with a lucite recepticle (Bioanalytical Instruments RC-1). The electrode arrangement will be discussed later.

The treatment of the inlaid GC electrodes to obtain a flat, flush surface with good electrochemical activity started with sanding the entire face of the cell with 600 grade sandpaper. This was followed by polishing on a stainless steel flat plate with a slurry of Al_2O_3. If the slurry was in paraffin oil, the apparent rate was slower than if the slurry was in water. For instance, for a cyclic voltammogram of potassium ferrocyanide in 2 M KCl taken at 100 mV s^{-1}, the difference between anodic and cathodic peak potentials was 135 mV for the paraffin slurry and 80 mV for the aqueous slurry. It was later discovered that, when the face of the cell is sanded on 600 grade sandpaper, the GC is left slightly protruding from the face. If the face of the cell is then rubbed on the stainless steel block with water alone,

the GC will be flattened to the surface of the lucite or Kel-F. It simultaneously acquires a mirror finish. This procedure was adopted as standard procedure.

The electrode placement was variable. It was determined by hydrodynamic voltammetry that an acceptable wave was obtainable if either the reference or auxiliary electrode was opposite to the working electrode. In this experiment, the stainless steel plate in the lucite cell was used as the reference. This was acceptable for demonstrating the principle, but the cell could not be operated in this way, so the stainless steel was used routinely as an auxiliary electrode. The reference electrode placement was not as important as long as when it was outside the cell it was <u>just</u> outside the cell. The external reference electrode had a further advantage that it was in a more controlled environment, behind a junction, than the Ag button. It was therefore less noisy. At various times, more often than one would have liked, leaks developed around the inlaid stainless steel block. This caused a large spike-like noise. When this occurred, there were two choices; to attempt to fix the problem instantly, rendering the day's data incomplete, or worse, wasting expensive antibody, or to continue with the work using an alternate auxiliary. A comparison of the choices for alternate auxiliary is shown in Table 10. Notice that not only the sensitivity, but the linearity is compromised by

Table 10

Internal vs External Auxiliary Electrode

Auxiliary	Peak Height[a] 2.10×10^{-5} M	1.05×10^{-5} M
Electrode 2[b]	360	180
External[c]	172	108

[a]Peak height (nA) of 70 µL injection of the indicated concentration of ferrocene carboxylic acid at 0.500 V vs Ag/AgCl. The solvent was pH 7.12 0.010 M phosphate buffer. Flow rate 1.0 mL min^{-1}, spacer was 0.3 cm wide and 0.002 cm thick.

[b]See Figure 5. Electrodes 1 or 3 are working electrodes.

[c]A stainless steel piece of tubing in the exiting flow stream (Bioanalytical RC-1)

the external auxiliary electrode. Thus, when events required it, the inside GC electrode, number 2, was used as auxiliary until the stainless steel auxiliary could be repaired.

Although the leak problem was finally repaired for good by using a hard epoxy which did not soften under water (Cemedine Super, Cemedine Corp. Ltd., Tokyo, Japan) to embed the stainless steel, it was thought that it would be easier to do away with the inlay. When the Kel-F cell (Figure 6)

was built, the opposing half of the cell was made completely of stainless steel. This had an unforeseen effect on cell performance. The reference electrode could not control the solution potential. It seemed as if the auxiliary electrode shielded the solution from adopting the reference potential at the exit port of the cell. To test the assumption, two spacers were cut, one extending from entrance to exit and one extending from entrance to the exit side of electrode 3. The latter spacer was used to electrically insulate the solution from the auxiliary electrode where the reference potential "entered" the cell (the exit port). With this extra spacer, the cell behaved normally. At this point a comparison could be, and was, made between the internal and external auxiliary electrodes. It was not desired to keep this two spacer arrangement since its effect on the flow pattern caused noise. At 550 mV vs Ag/AgCl, 0.3 cm wide 0.003 cm thick spacer, 0.7 mL min^{-1}, an injection (70 µL) of 1.3 µM ferrocene carboxylic acid (FCA) yielded an average peak height of 15.9 nA with the internal auxiliary and 14.8 nA with the external auxiliary. The same loss in sensitivity found with the lucite cell is not present. To check the linearity, six solutions of FCA from 0.13 to 2.6 µM were prepared. Injections revealed a linear calibration curve. No tendency for the curve to "fall off" as it did with the lucite cell was present. Thus operation with an

external auxiliary and external reference electrode was justified.

This left one problem. The stainless steel plate was an excellent antenna. It could be grounded, or used in a guard circuit (15), but it was best to isolate it from the system. A teflon sheet laid on top of the stainless steel gave very noisy results. A more wettable surface to encourage laminar flow was desired. A glass microscope slide, washed in warm soapy water, worked well, reducing the noise from the stainless steel and also from the turbulent flow.

The pump used was a Waters 6000A, the same one used for the flow rate-current experiments. An LKB single channel peristaltic pump was eventually used to draw solution through the injector sample loop in a reproducible fashion. The flow rate was about 1 mL min^{-1}.

The precision of the injections was of constant concern. Immunoassay is most optimally carried out with a reagent in which the tagged ligand is half bound and half free. This means that a negative control sample will yield 50% of maximum response. The noise in this background peak will limit the detectability of small amounts of material. To make matters worse, the antibody itself has a small electrochemical signal, so variations in this current are to the detriment of detectability. As such, precision was often checked and the information gained was incorporated into new protocol. These

studies will be discussed when it is appropriate.

c) Early work:

i) Apparatus. The early system consisted of the lucite cell (Figure 5) with an external Ag/AgCl (4 M KCl) reference, a Durrum injector (loop size, 70 μL), a Waters 6000A pump and a PAR 174 potentiostat. The samples were introduced into the loop with a 1-mL tuberculin plastic syringe.

ii) Glassware. Glassware (10x75 mm, 12x100 mm test tubes, 5-, 10-, 25-, 50-mL volumetric flasks and caps) was silyated using 10% chlorotrimethyl silane in 20% pyridine/ 80% benzene or toluene. After silyation (48 hr at room temperature) the glassware was rinsed several times in distilled water, then washed with a brush and soap and rinsed. This was followed by a six times rinse in distilled water. Tubes were oven dried at 150°C and volumetric flasks were allowed to dry slowly at room temperature. The necks were loosely covered with Al foil during this drying.

iii) Experiments with the early apparatus.

(a) Conditions. Although a curve of binding of morphine to antibody as a function of time was not determined until much later on, reagents were mixed and allowed to sit at room temperature (21°-30°C) for about an hour before analyzing. This was because, even though the directions with the antibody reagent kit specify immediate analysis upon mixing of reagents, some variability in apparent binding

was noted for measurements made just after mixing.

According to the theoretical work, for K = 1 (bound/free = 1), k = 1 s^{-1} for b = 0.003 the system will suffer less than 0.5% error at $r \leq 8.8 \times 10^{-3}$. For L = 0.25 cm (the diameter of the glassy carbon disk), W_c = 0.30 cm, D = 4×10^{-6} cm^2 s^{-1} for 3-O-MFC, this means $\bar{U} \geq 0.68$ mL min^{-1}. Therefore, flow rates were kept at 0.7 mL min^{-1} or higher.

(b) Results with morphine. Since morphine is electroactive, the principle of voltammetric immunoassay (VIA) could be tested immediately.

Injection reproducibility was tested. For ten injections of 4.3 μM morphine in pH 7.02 0.1 M phosphate buffer made into a stream of the same buffer flowing at 1.0 mL min^{-1}, the relative standard deviation was 0.0138. The injections into the injector were by syringe, with no rinse out between injections. The applied potential was 0.500 V.

That morphine would bind to its antibody was known. The crucial step was to show that the electrochemical detector could show this. standards ranging in concentration from 0.20 μM to 10.0 μM were injected by themselves, and mixed with the antibody solution. For the latter, 100 μL of buffer, 200 μL of aqueous standard and 100 μL of reagent A (antibody solution) from the DAU-opiate EMIT^{R}kit were mixed. The results are shown in Table 11. This study was repeated under

Table 11

Binding of Morphine to Antibody

Standard μM	Standard nA[a]	With Antibody[b] nA	Free Morphine μM	Total Morphine present[d]
0.20	1.04	0.02	0	0.10
0.40	2.08	0.03	0	0.20
0.60	2.80	-0.10	0	0.30
0.80	3.52	-0.08	0	0.40
1.0	4.76	+0.28	.060	0.50
2.0	9.18	2.05	.44	1.0
4.0	17.2	5.33	1.13	2.0
6.0	24.1	9.8	2.2	3.0
8.0	30.4	12.2	2.8	4.0

[a]Peak current under the following conditions; 0.500 V working electrode, pH 7.17 0.01 M phosphate buffer, 1.0 mL min^{-1}, flow, room temperature not recorded.

[b]The signal from antibody alone, 0.96 nA, has been subtracted.

[c]Concentration of free morphine, assuming total peak current due to morphine.

[d]Concentration of morphine in the mixture with buffer and antibody.

slightly better conditions. In the following study, the standards injected without antibody were mixed with 300 µL of buffer, while the standards with antibody were mixed with 200 µL buffer and 100 µL reagent A. These data are presented in Figure 7. A common way to present binding data is percent bound ligand versus total ligand concentration. The data from Figure 7 and Table 11 are plotted together in this format in Figure 8.

A common experiment in immunoassay is to determine the percent bound as a function of the dilution of the antibody. This experiment was performed with antibody dilutions of 1:4 to 1:80 at a morphine concentration (in the final reagent mixture) of 0.10 µM (100 µL 0.40 µM to a total of 400 µL). Antibody blanks were run, and the signal from antibody was found to be linear with concentration. These data are presented in Figure 9. The curve is typical in appearance.

A problem at low concentrations of morphine was encountered. It seemed that the antibody blank was altered (made lower) upon binding. This made it difficult to detect the presence of small amounts of free morphine, since the shift in blank value (about 0.2 nA in the presence of codeine, and therefore probably similar to the case of morphine) is large with respect to the signal expected for morphine. Since at low concentrations the binding data were not quantitative, replotting the data to obtain binding information (i.e.

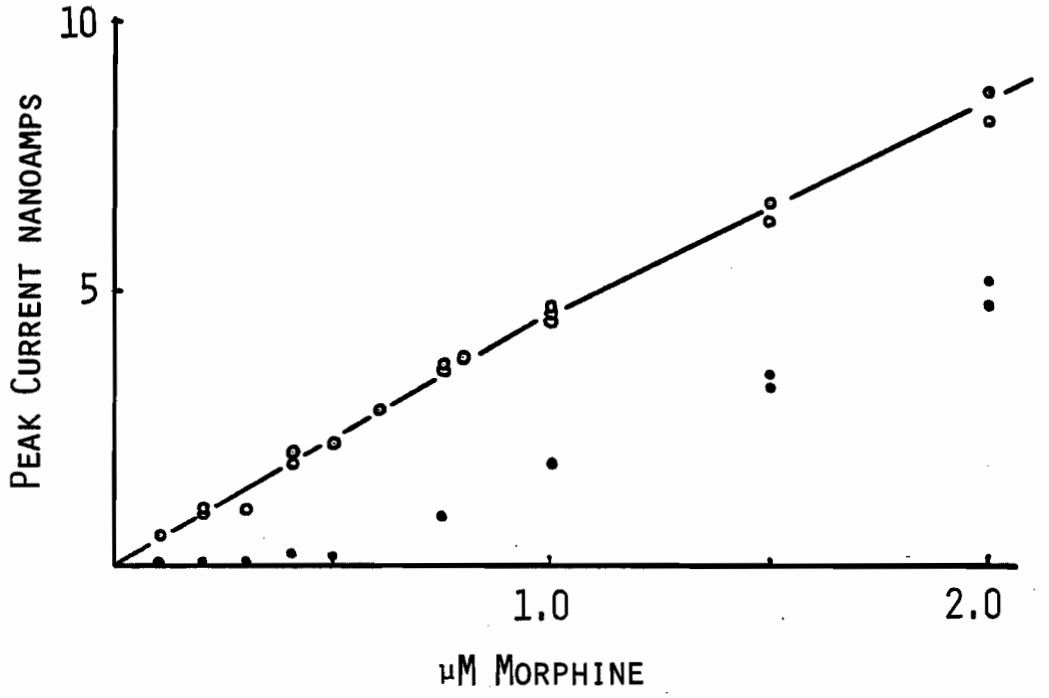

Figure 7: Binding of morphine to antibody. Injections of solutions containing morphine sulfate in the absence (o) and the presence (●) of antibody. The concentration of morphine given is the final concentration in the mixture of morphine with buffer or antibody. Conditions;antibody dilution 1:4, buffer was pH 7.17 0.01M phosphate, flow rate was 1.0 $mLmin^{-1}$, spacer thickness was 0.002 cm, internal auxiliary electrode, external Ag/AgCl (sat. KCl) reference electrode, glassy carbon working electrode at 0.500 V, 70 µL injection volume, temperature 23° C.

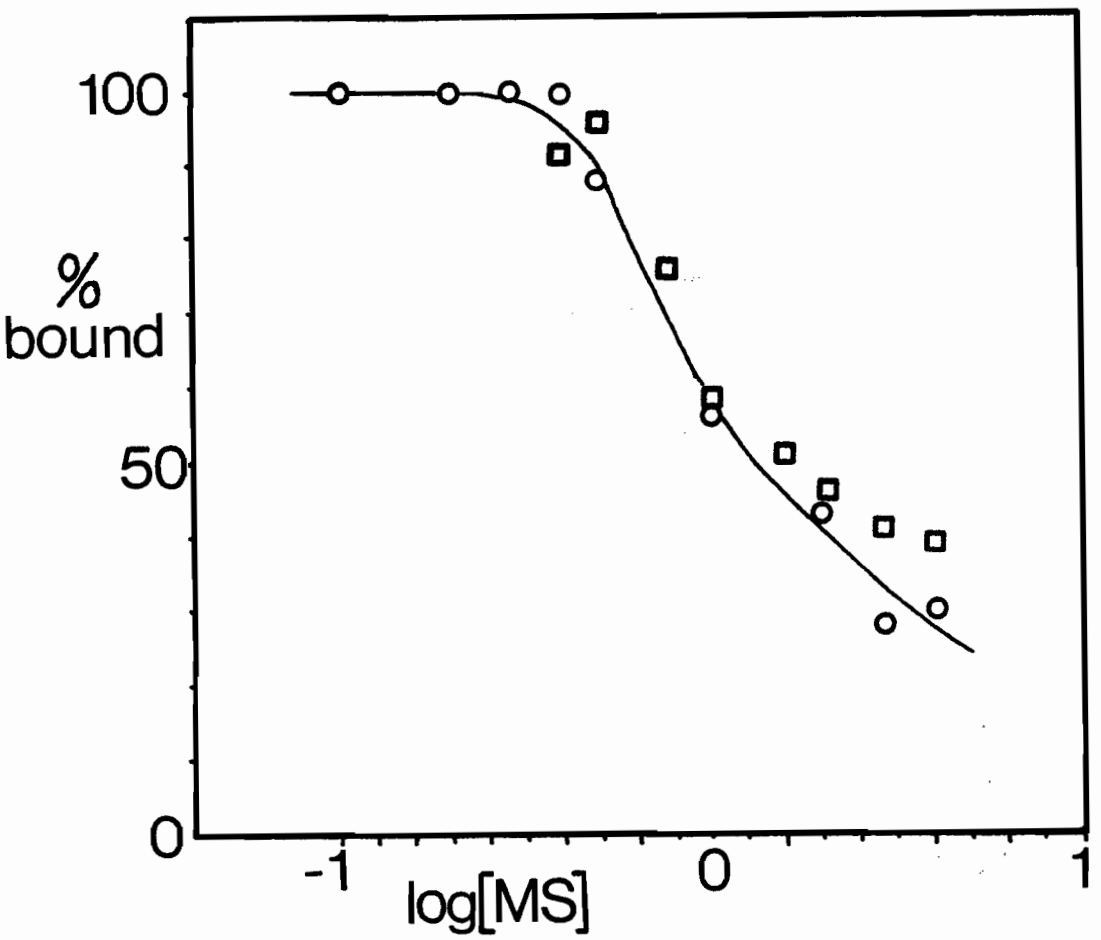

Figure 8

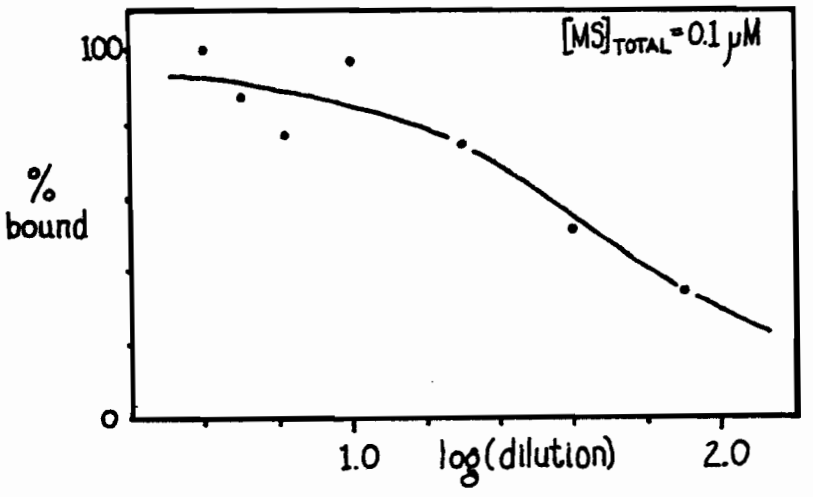

Figure 9

Figure 8: Data from figure 7 (□) and table 11 (o) plotted as % bound morphine as a function of the morphine concentration (μM). Conditions are as in figure 7.

Figure 9: Percent bound morphine as a function of antibody dilution. Antibody dilution is the factor by which the reagent A is diluted in the final solution which is injected. Total morphine concentration was 0.1μM. Conditions as in figure 7.

Scatchard plot) could not be carried out with these data.

Some information can be gained from Figures 8 and 9. If the simple equilibrium expression $K = [Ab \cdot L^*]/[Ab][L^*]$ is used for each set of data at % bound = 50 (B/F = 1), the result is two equations in two unknowns, K and [Ab] in the stock solution (Reagent A). Solution of the equations reveals $K \approx 2 \times 10^{7}\ M^{-1}$ and $[Ab] \approx 4 \times 10^{-6}$ M.

It seems that the binding of morphine to antibody is detectable by electrochemical methods. Before it can be stated that the principles of VIA have been established, it must be determined whether or not the binding is reversible. Codeine, since it binds to the antibody, makes an excellent reagent to use for the displacement of morphine.

Table 12 demonstrates the displacement of bound morphine by codeine. The reaction of morphine with antibody is to some degree prevented by codeine. The detection of this competition is, of course, the essential task for any immunoassay.

(c) Results with 3-O-morphinyl ferrocene carboxylate (3-O-MFC). Any tag used must be shown not to interfere in the reaction. The two ways in which it may interfere are 1, by binding to the antibody itself, and 2, by preventing binding of the ligand. To test the first interference, samples of FCA were prepared with and without antibody. The results are scattered, but over the range of 1×10^{-7} M to

Table 12

Displacement of Bound Morphine by Codeine

Tube Contents (µL)							
PO_4[a]	CP[b]	MS[c]	Ad	Peak Currents (nA)[g]			"free" morphine (µM)
200	100	-	100	0.82	0.85	0.85	0
200	100	-	100	0.80	0.80	0.78	
200	100	100	-	2.38	2.30	2.30	0.10
200	100	100	-	2.45	2.30	2.35	
200	-	100	100	2.38	2.20	2.32	0.061
200	-	100	100	2.25	2.15	2.20	
100	100	100	100[e]	2.55	2.72	2.70	0.080
100	100	100	100	2.68	2.68	2.70	
100	100	100	100[f]	2.78	2.75	2.70	0.082

[a] pH 7.40 0.01 M phosphate buffer.

[b] Codeine phosphate 0.4 µM.

[c] Morphine sulfate 0.4 µM.

[d] Reagent A diluted 1:10 with buffer.

[e] Morphine added first.

[f] Codeine added first.

[g] Conditions 0.500 V, 1.0 mL min^{-1} T = 27°C.

$2x10^{-5}$ M the FCA showed no binding to the antibody.

Analogous to the binding experiment performed with morphine, samples of 3-O-MFC were injected with and without antibody. The "without antibody" specimens were prepared from 100 µL of buffer (0.01 M pH 7.11 phosphate) plus 50 µL of standard 3-O-MFC from $1.0x10^{-7}$ M to $2.0x10^{-5}$ M. The "with antibody" specimens were prepared from 100 µL of a 1:1 dilution of reagent A in buffer, and 50 µL of standard. The results are shown in Figure 10. Although the data are scattered, the results are essentially the same as for morphine. The two highest concentrations of 3-O-MFC are not shown in Figure 10. The points at 10 µM demonstrated the binding, and the points at 20 µM were overlapped. In the latter case, the points with antibody were in the "right" place while the points without antibody fell below the straight line drawn through the rest of the points. These points were not shown to facilitate comparison with Figure 7.

A glassware contamination problem and the deleterious effects of the light sensitivity of the 3-O-MFC occurred at roughly the same time. The repetition of the above experiment led to the results shown in Figure 11. The extent of the problem can be easily appreciated.

d) Later work:

i) Apparatus. The entire system consisted of several components. A block diagram of the final system utilized is

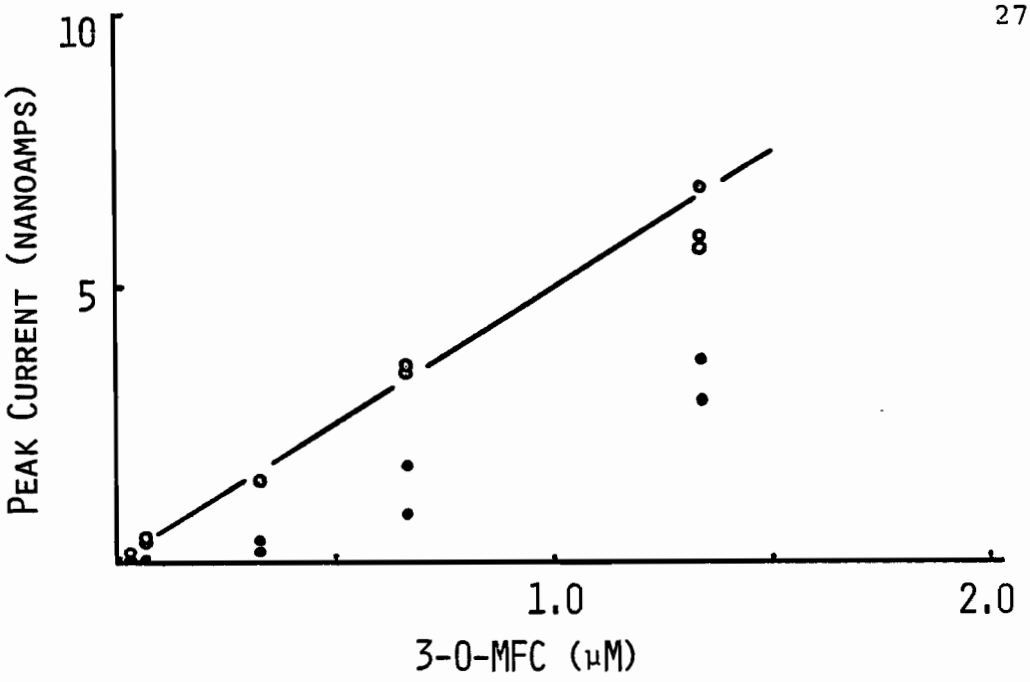

Figure 10

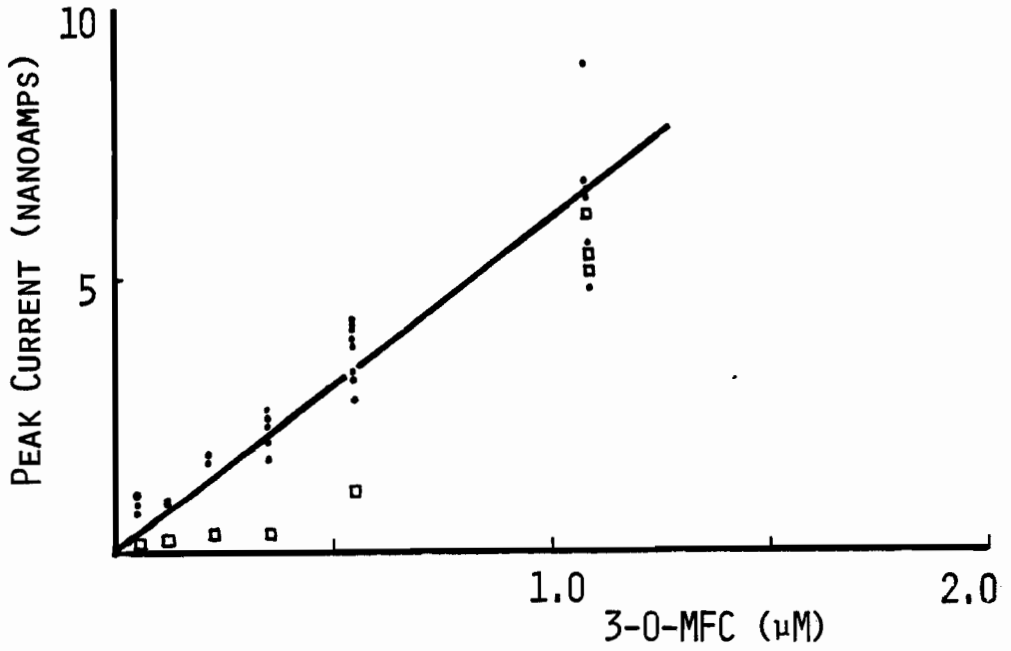

Figure 11

Figure 10: Binding of 3-O-MFC to antibody. Injection of solutions in the absence (o) and the presence (●) of antibody. The concentration of 3-O-MFC given is the final concentration in the mixture with buffer or antibody. Conditions;Antibody dilution 1:3, buffer was pH7.11 0.1M phosphate, temperature was 27°C. Other conditions as in figure 7.

Figure 11: A repeat of the experiment shown in figure 10. These data show the large scatter indicating problems in background and reagent stability. (●) Absence and (□) presence of antibody.

shown in Figure 12 exemplifying the grounding and Figure 13 showing the flow path. During the evolution of this system, other, simpler systems were used. These will be described.

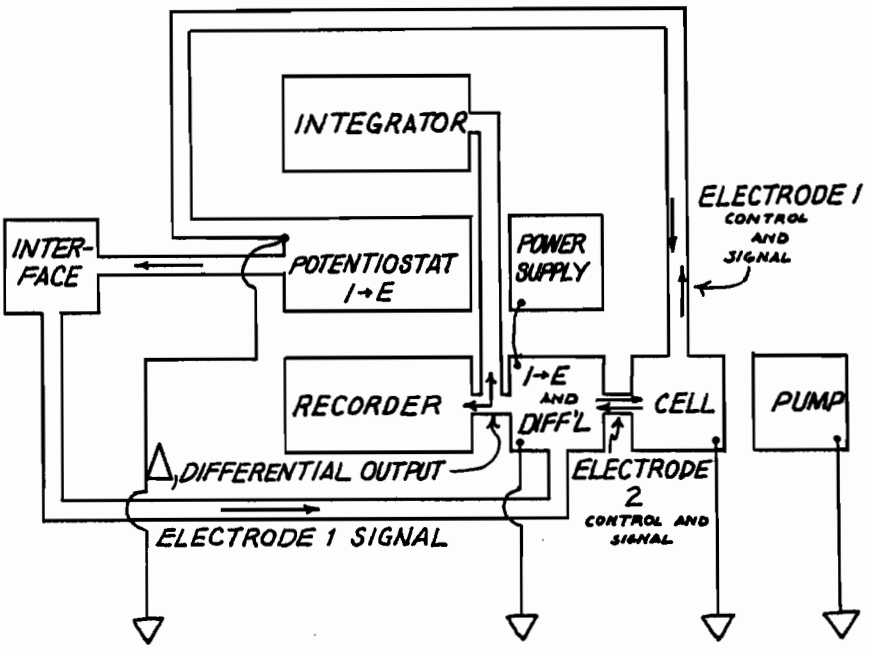

Figure 12

The Final Instrumental System

The potential is applied to one working electrode from the potentiostat and to the other working electrode (by virtue of the voltage at the non-inverting input) from the current-to-voltage convertor. The signal from electrode 1 (current) is converted to a voltage in the PAR 174 and fed out through the PAR 174/50 interface to the input of a subtractor circuit marked "DIFF'L". The other input to the subtractor comes from the current to voltage convertor for electrode 2 located

located in the same box marked "I/E and DIFFL". The subtracted current signal, marked "Δ" is fed to a recorder and an integrator. Using a switch, the current from electrode 1, electrode 2 or (electrode 1-electrode 2) could be monitored. The integrator is a PAR 175. When it is in the "galvanostat" mode it will accept a voltage signal and apply a current proportional to it to a cell. However, even if there is no cell attached, it will operate as a galvanostat. The Model 179 digital coulometer will therefore integrate the voltage signal. Since this is not a peak integrator, no method for baseline subtraction is contained within the instrument. For this reason flat baselines were desirable. The cell was contained in a cardboard box lined with 3.8 cm thick styrofoam on the inside and Al foil on the outside. The styrofoam prevented low frequency (seconds to minutes) baseline noise caused by thermal fluctuations. The Al foil was an electrical shield. The current-to-voltage converter (13) and subtractor were kept in an Al foil box. The lowest noise pickup was obtained when the incoming and outgoing shields were grounded near the current-to-voltage converting amplifier itself. All the three prong plugs for the various instruments were converted to two prong with adaptors. The ground connection to the PAR 174 chassis and the Waters pump were tied to a large copper flat which was connected to earth ground via a 0.4-cm diameter braided copper cable. The

shield for the cell and I/E convertor were grounded to the same copper flat. When available, a second recorder could be added to monitor either of the two potentiostated electrodes independently.

Figure 13 shows the path of the flow stream. Buffer, filtered by a stainless steel frit (10 μM pore size) and pumped by the Waters 6000A pump, went through a Durrum loop (70 μL) injector and on to the cell. At various times long sections of tubing were placed between the injector and the cell to increase band spreading and flatten the peak. It was felt that this might improve precision. All it did, however, was to decrease sensitivity. There were about 20 cm of 0.05-cm inside-diameter PTFE tubing between the injector and the cell. After exiting from the cell the solution flowed into a reservoir inside the shielded box. The waste reservoir was a particularly good antenna, so shielding it was essential. The loop was filled either by syringe aspiration through a probe or pump aspiration through a probe. The latter is shown in Figure 13.

ii) Glassware. After two month's effort, a glassware protocol was developed that yielded consistently clean glassware. Several observations which were made are of interest. Tubes rinsed in distilled water from a tap with Tygon tubing, or buffer deaerated with N_2 which passed through the tygon tubing were contaminated. Plastic tuberculin syringes of two

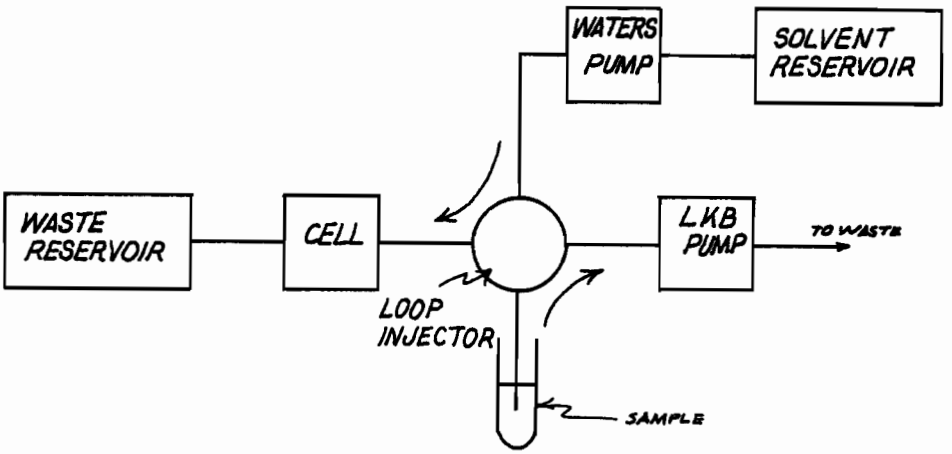

Figure 13

The Flow Stream

types (Beckton Dickenson and Plastipak) were electrochemically unclean. Holding buffer in the tubes increased the size of the signal. Various oxidants did not remove the background. Soaking in 6 M HNO_3 or in ethanolic KOH did not remove the background. Plastic sample cups were also unclean, and what is worse, variably so. No amount of washing, soaking or oxidizing could rid the plastic of the signal. Plastics are therefore to be avoided.

Attention was turned to glassware. Very clean beakers

could be obtained by washing in soap and water, soaking in ethanolic KOH several hours, rinsing in distilled water, soaking in 6 N HNO_3 for a few hours, rinsing in distilled water, then rinsing in the buffer being used. This procedure could not be used for the test tubes and volumetric glassware since it would hydrolyze the silyl ethers.

The test tubes and volumetric glassware were put through the above procedure to make them clean. After drying, they were silyated as before. After silylation, the tubes were rinsed in toluene once, methanol once, soaked in methanol twice, one for two hours, once for two days. They were rinsed in methanol once outside and three times inside and then placed in a vacuum oven at 80°C overnight.

Once the glassware had been cleaned, to keep it clean meant following another protocol. Beakers, after one day's use, were plunged into the HNO_3 solution overnight. If a grease film appeared to be forming, a soaking in alcoholic KOH removed it. Used test tubes were plunged into a distilled water bath if attention could not be paid to them instantly. They were then rinsed with copious quantities of distilled water and then methanol, and vacuum oven dried as above. Glassware which was clean was kept in a separate drawer from all other materials, and was covered with Al foil.

To check the initial wash procedure, 1 mL of 0.05 M tris buffer pH 7.42 was placed in a piece of glassware. The

glassware was shaken on a mechanical shaker for one hour. The contents were then injected.

Injections from 2 out of 8 25-mL volumetric flasks showed a peak of 0.1 nA each (cell conditions 0.800 V applied vs Ag/AgCl 1.0 mL min^{-1} flow rate, spacer 0.3 cm wide 0.002 cm thick), from 5 out of 20 10-mL volumetric flasks each showed a -0.05 nA peak, and 10 out of 70 test tubes showed an average peak height of 0.006 nA with a high of 0.04 nA and a low of -0.01 nA. Negative peaks are not uncommon for very "clean" blanks since the pump adds material to the buffer.

iii) Experiments and observations.

(a) Conditions. Several changes were made to bring the operation back into control. tris(hydroxymethyl)amino-methane buffer was used since that was the buffer in which reagent A was prepared. The 3-O-MFC was repurified. Instead of weighing out a milligram or so every time it was needed, a stock solution of 2.6×10^{-3} M 3-O-MFC was prepared in methanol and kept in the freezer (-15 to -20°C). The glass-ware protocol discussed was implemented. The cell was put in a styrofoam box and shielded with Al foil. The four-electrode potentiostat was used in conjunction with a subtractor and two working electrodes to perform d.c. differential detection. Integration of the peaks was attempted as a more precise measure of the signal.

Using regular (one working electrode) detection, the

reproducibility of injections of morphine sulfate was tested. The injector was loaded by suction applied to a PTFE probe inserted in the sample vial. The suction was applied with a syringe. For eight injections of 2.0 μM morphine sulfate in pH 7.4 0.05 M tris maleate buffer flowing at 0.5 mL min^{-1}, the relative standard deviation (rsd) was 0.029 for peaks and 0.0063 for integration. These integrations were corrected for baseline drift.

The reproducibility of FCA and 3-O-MFC was checked under VIA conditions, 0.7 mL min^{-1}, 0.1 M tris maleate pH 6.0 and the same sized spacer as was used in the morphine studies, 0.3 cm wide 0.002 cm thick. A word about the buffers is in order. The kit from which the reagent A is taken specifies that the reaction be carried out at pH 6.0 for maximum activity of the enzyme tag. The reagent A is stored in a pH 7.4 buffer. It was felt that this range of pH values was a fair range within which to work. After using buffers between pH 7.1 and 7.4 for a long time, pH 6.0 buffers were employed. This was because the 3-O-MFC should be more stable in a slightly acid solution than a slightly basic solution. For twenty-six injections of 2 μM FCA, the rsd of peak height was 0.036 and 0.037 on two separate electrodes operated independently in the same cell. The integrals of 16 of the 26 peaks were measured, and the rsd was 0.018. These integrations were not corrected for baseline drift. For

twelve injections of 1.3 μM 3-O-MFC the peak height rsd's were 0.060 and 0.047 for two independent working electrodes. Integrations of all twelve peaks for the electrode with peak rsd of 0.060 was 0.047. Integrals were not corrected for drift.

The d.c. differential system was then employed. The subtractor used 1.0% resistors and multiplied by ten. By measuring the input and output at various times it was confirmed that the voltages were within the tolerance of the resistors used (1% resistors, 4 resistors acting independently, total error, 2%).

The operation of the d.c. differential system may be understood as follows. The two electrodes being used as working electrodes must first be made equal in sensitivity. This may be done by adjusting one of the amplifiers in the output of the current-to-voltage convertor in the Blank (13) circuit. After each adjustment, an injection is made with both electrodes at the same potential, preferably on the plateau of a wave for the analyte being injected. This injection-adjustment-injection cycle is repeated until the output, or the integral of the output, is zero. The integral may have to be used because the peaks from each electrode do not always occur simultaneously. Thus a peak may go up first, then down below the initial level and back up again. When the instrument is thus calibrated (see Figure 14), then

Figure 14: D.C. Differential Detection. Seventy μL injections of 2.0×10^{-5}M morphine sulfate in pH 7.0 0.01M phosphate buffer. Both electrode 1 and electrode 2 are working electrodes at 500 mV vs Ag/AgCl (sat. KCl). In the differential mode the difference in signal between electrodes 1 and 2 is recorded. Conditions; except for the buffer stated above, conditions were as in figure 7.

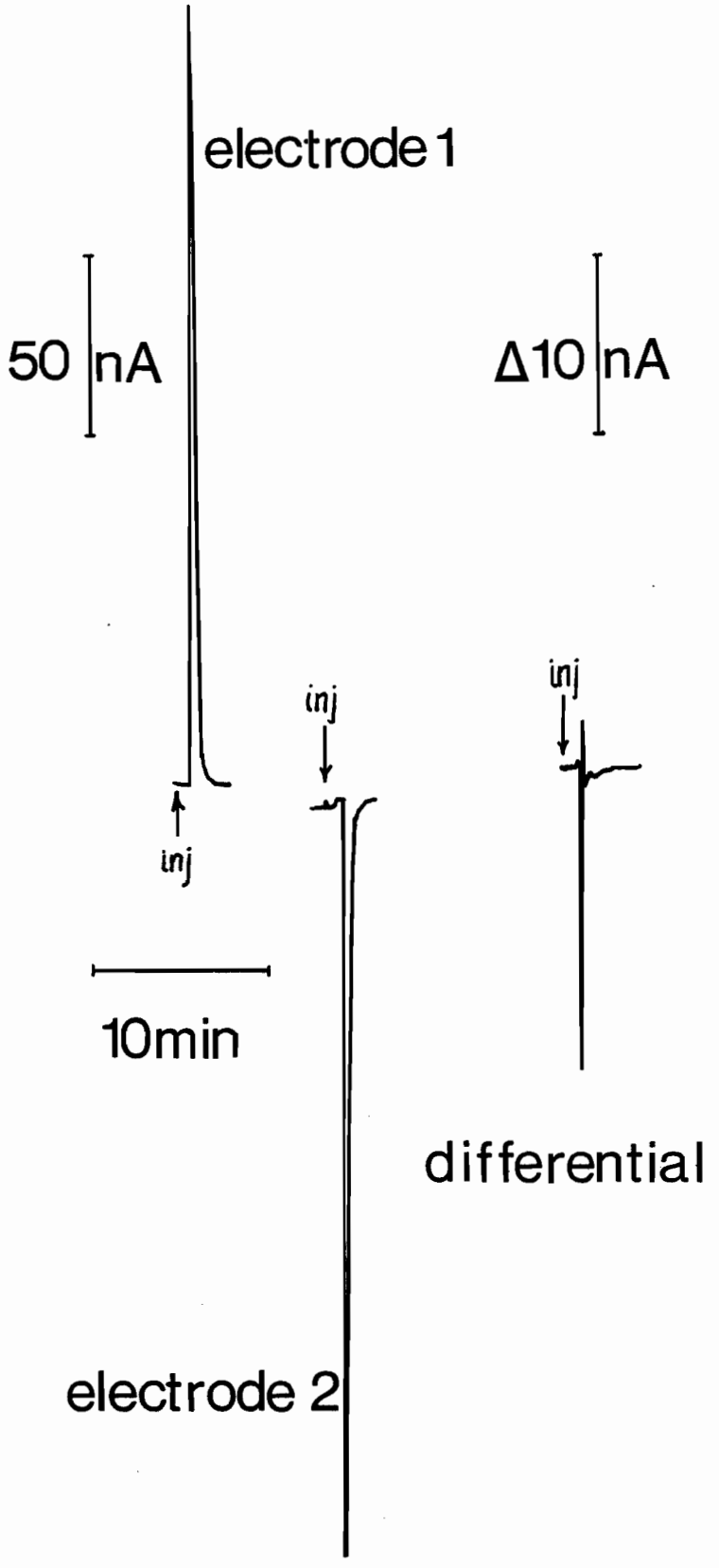
electrode 1
50 nA
Δ10 nA
inj
inj
inj
10min
differential
electrode 2

the potential difference desired may be set. One of the potentiostats controls the potential directly (PAR 174) and the other controls its potential by difference, e.g. it is always 50 mV below the potential set on the PAR 174.

The use of the d.c. differential system was motivated by the knowledge that the peak from reagent A changed only slowly in the region between 0.400 and 0.500 V, while the peak for morphine varied greatly here, and the peak for 3-O-MFC varied significantly here. Thus discrimination against reagent A, with the attendant loss in the error of the measurement of the reagent A peak, would be possible.

A preliminary check using $\Delta E = 0.050$ V (ΔE being the difference potential) and $E = 0.500$ V (as set on the PAR) for the system shown in Figure 14 yielded a normal peak height for 20 μM morphine of 210 nA, and a normal peak height for reagent A of 4 nA. The d.c. differential system yielded a morphine peak of 95 nA and an antibody peak of 1 nA. Thus the ratio of peak heights has been improved by a factor of two. For these large concentrations, integration was not necessary. It should be pointed out that the data compared above were taken simultaneously.

More important was the improvement which could be made between 3-O-MFC and reagent A. The peak height ratio of 1.3 μM 3-O-MFC *versus* a 1:11 dilution of reagent A is shown in Figure 15. Also shown is the same ratio for normal operation taken at the conditions found for the maximum

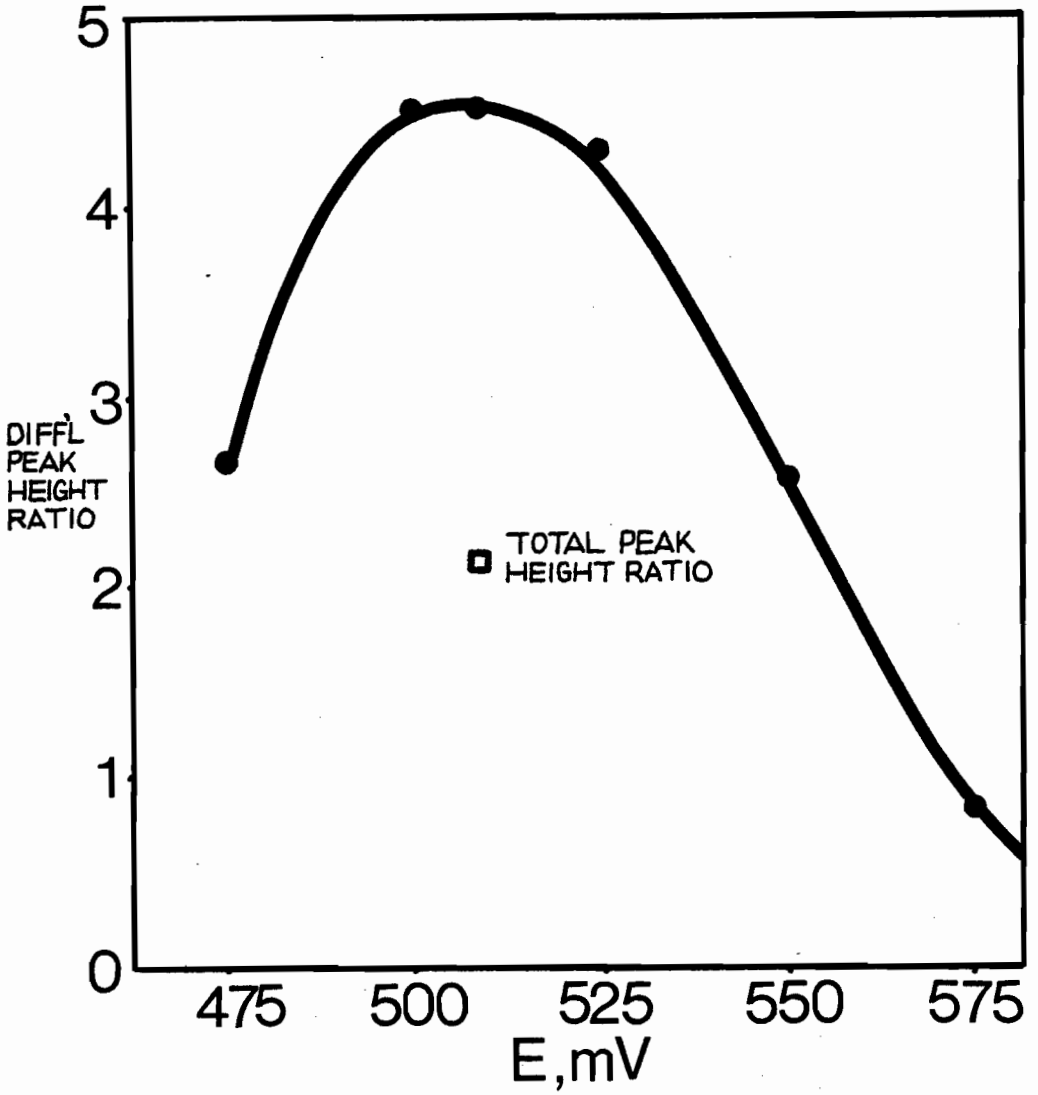

Figure 15: The ratio of d.c. differential peak currents of 3-O-MFC (1.3 μM) to reagent A (1:11 dilution) as a function of applied potential. One of the working electrodes is at the stated potential and the other is 50 mV less. At the maximum of the curve the ratio of amperometric peak heights was taken (□). Conditions; the buffer was 0.05 M tris(hydroxymethyl)aminomethane pH 6.0 flowing at 0.7 $mLmin^{-1}$, external auxiliary electrode, other conditions as in figure 7.

difference ratio. Once again an improvement of about a factor of two is demonstrated.

The reproducibility of the system was checked using 2.6 μM 3-O-MFC in pH 6.0 0.05 M tris maleate buffer flowing at 0.7 mL min^{-1}. ΔE was 0.050 V and E was 0.525 V. For ten injections made by rapidly and forcefully switching the injector to the "inject" position, the rsd (peak) was 0.060 and the rsd (integral) was 0.063. For ten injections made by slowly and deliberately switching the injector the rsd (peak) was 0.034 and rsd (integral) was 0.044. In neither case were the integrations corrected for drift. At the end of these twenty injections, four injections were made using the following technique. While drawing a vacuum by pulling on the aspirating syringe, place the probe tip in and out of the solution, thus washing the loop with a segmented stream of sample. This stream had 3 air bubbles. The four injections showed very tightly clustered data. Furthermore, both integrals and peak heights were higher than the previous twenty. This meant that residual buffer left in the loop was a major contributing factor in irreproducibility.

To see what extent of loop washing was necessary, injections were made with no, one, two ... eleven bubbles. The LKB peristaltic pump was used to aspirate so that the procedure was reproducible. The data are shown in Table 13. They definitely show a trend to a higher value with a more

Table 13[a]

Washout of Sample Loop

Bubbles	Peak Height (% of scale)	Integration[b]
0	55	4.29
1	58	4.51
2	61	4.87
3	60	4.87
4	66	5.26
5	65	5.39
6	64	5.23
7	69	5.61
8	67	5.33
9	70	5.71
10	71	5.73
11	66	5.46

[a]Conditions, injections of 2.6 μM 3-O-FMC, ΔE = 0.050 V, E = 0.525 V, pH 6.0 0.05 M tris buffer 0.7 mL min^{-1}.

[b]Arbitrary units.

complete wash. The scatter was disturbing. The probe was constructed of three parts, each with a different inside diameter. It is well known that this will lead to mixing and carryover. A one-piece probe was built and a shortened

version of the experiment was repeated. The data are shown in Table 14. The results are more satisfying, although it seems still that several washes are required to completely wash the loop. Because of the cost of reagent A, ten bubbles was not a realistic amount. A three-bubble wash

Table 14[a]

Improved Washout of Sample Loop

Bubbles	Peak Height (% scale)
0	60
1	60
2	62
3	62
4	63
10	70

[a]Same conditions as Table 13.

was decided upon. Reproducibility was checked with this washout system, slow switching of the injector and the differential system. For 1.3 μM 3-O-FCM injected twenty times into 0.05 M tris maleate pH 6.0 flowing at 0.7 mL min^{-1}, the rsd (peak) was 0.023 and the rsd (integral) was 0.017. The

integrals were not corrected for baseline drift. These numbers were considered satisfactory, and work on VIA was then completed.

(b) Results with 3-O-MFC. A calibration curve showing the displacement of 3-O-MFC by codeine would finally show that the principle of VIA was sound. To begin with, a simple one-point displacement of 3-O-MFC was performed analogous to Table 12. The results are shown in Table 15. An error was made and 4 mM codeine was used instead of 4 µM, but the results are worth reporting nonetheless. Notice the effect of codeine on the antibody blank (compare tubes 2, 4 and 6). As previously mentioned, about a 20% loss of signal occurs when the antibody is bound. Notice that by integration the antibody blanks are indistinguishable from buffer or codeine blanks (tubes 1, 2, 4, 6). Most importantly, notice that the 3-O-MFC is indeed displaced by the codeine.

A calibration curve using 0.4, 4.0 and 40.0 µM codeine phosphate was successfully constructed. The useful range of the curve was in the region 0-4 µM. Conditions for B/F = 1 were found empirically by adjusting a mixture of reagent A and 3-O-MFC. The final reagent consisted of 1.0 ml reagent A plus 6.0 mL of 0.364 µM 3-O-MFC.

To construct a useful calibration curve codeine phosphate standards were prepared at 0, 0.08, 0.24, 0.8, 2.4 and 8.0 µM. The above reagent was prepared and incubated at room

temperature for five hours. Tubes with 100 μL of standard and 500 μL of the reagent were mixed. At the same time 200 μL of 8 μM standard and 1000 μL of reagent were mixed. This latter solution served as a control to check the progress of the displacement of 3-O-MFC from antibody. The peak current of this control as a function of time is shown in Figure 16. After the other tubes had incubated 75 minutes, they were injected, three injections per tube. Conditions were the same as the conditions in Table 15, except the flow rate was 1.0 mL min^{-1}. Room temperature was 23°C. The results are displayed in Figure 17.

The data support the contention that making an electrochemical measurement which is fast with respect to antibody-ligand dissociation rate is possible. This possibility allows an effective separation of bound ligand from free ligand. The technique is ideally suited to analysis in flowing streams since the measurements are made in a flowing stream.

Under what conditions could VIA be implemented to obtain a better analysis? One of the major fields in which immunoassay has been successful is the semiquantitative analysis of drugs of abuse in urine. Preliminary experiments demonstrated that urine itself had a not insignificant electrochemical signal. This, of course, was not unexpected. A preliminary

Table 15

Displacement of Bound 3-O-MFC by Codeine

Number	Tube Contects µL Tris[a]	CP[b]	3-O-MFC[c]	A[d]	Peak Height (nA)[e]		Integrations	
1	400	-	-	-	0.05	0.00	- .033	0.38
2	200	-	-	200	0.25	0.25	- .098	- .037
3	200	100	100	-	2.34	2.25	-3.87	-3.82
4	300	100	-	-	-0.01	-0.01	+0.28	0.0
5	300	-	100	-	2.30	2.28	-4.09	-3.96
6	100	100	-	200	0.21	0.21	- .083	- .102
7	100	-	100	200	1.51	1.43	-2.47	-2.20
8	-	100	100	200	2.32	2.35	-4.12	-4.08

[a]tris Hydroxymethyl amino methane maleate, pH 6.0 0.05 M.

[b]Codeine phosphate 4 mM.

[c]1.04 µM.

[d]1:5 dilution in tris.

[e]Conditions, 0.05 M tris pH 6.0 flowing at 0.7 mL min^{-1}, spacer 0.3 cm wide 0.002 cm thick, ΔE = 50 mV E = 525 mV T = 23°C.

chemical or electrochemical treatment had to have certain properties. The treament had to oxidize materials in the

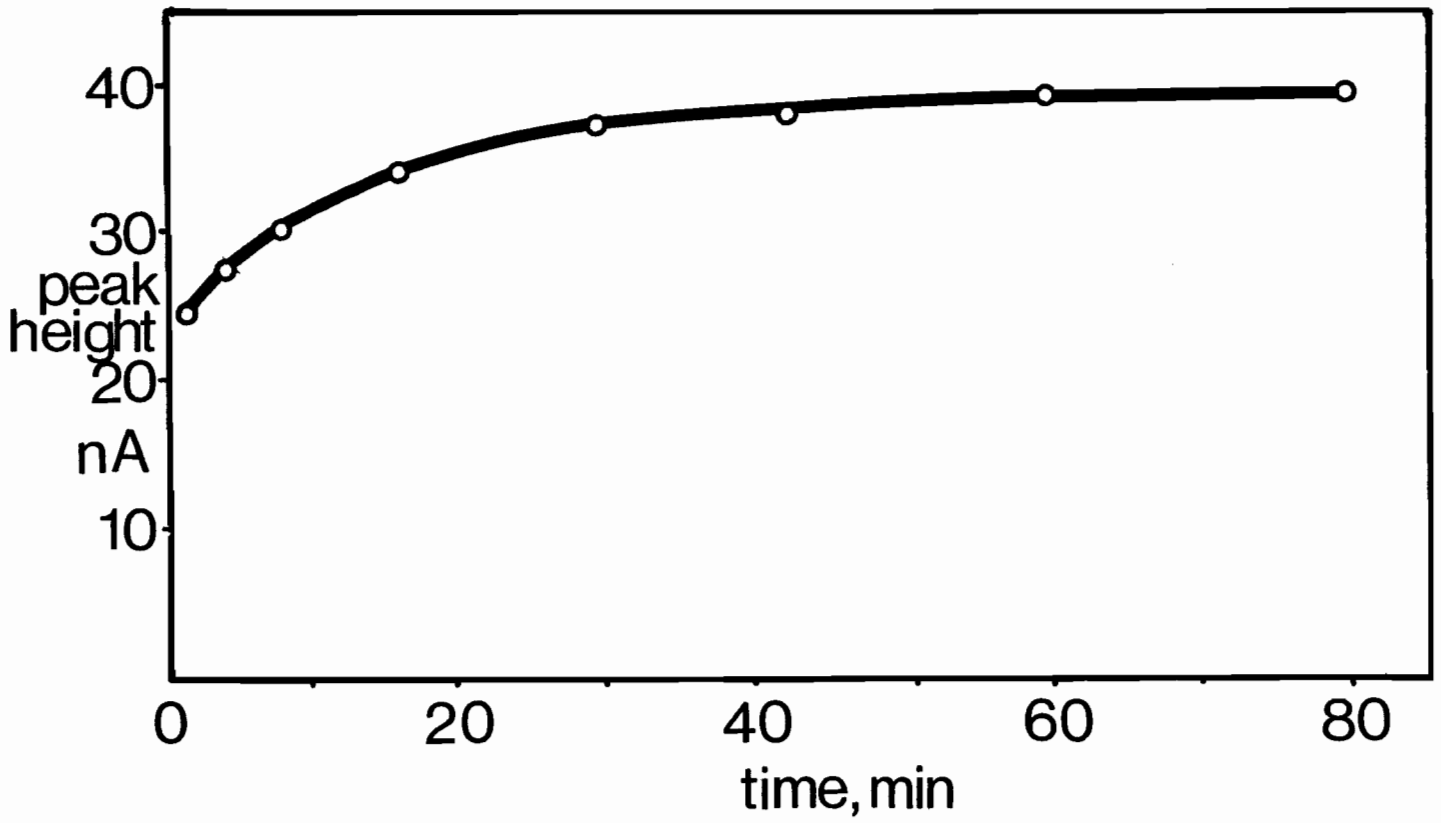

Figure 16: The displacement of 3-O-MFC from antibody as a function of time after addition of codeine phosphate. The 3-O-MFC/reagent A mixture was prepared(1.0 mL reagent A plus 6.0 mL of 0.36 µM 3-O-MFC) and incubated at room temperature (23°C) for five hours. At t=0, 1.0 mL of the above reagent was mixed with 0.200 mL of 8.0 µM codeine phosphate. Single 70 µL injections at the indicated times were made. Conditions; amperometric detection at 525 mV, 1.0 $mLmin^{-1}$ flow rate, other conditions as in figure 15.

Figure 17: Voltammetric Immunoassay. Displacement of 3-O-MFC from antibody by codeine. Conditions and reagent preparation as in figure 16. The concentrations of codeine phosphate were: 0, 0.08,0.24,0.80,2.4,8.0 μM. Peak heights and integrals were recorded. Both yielded similar curves. Each sample was injected three times.

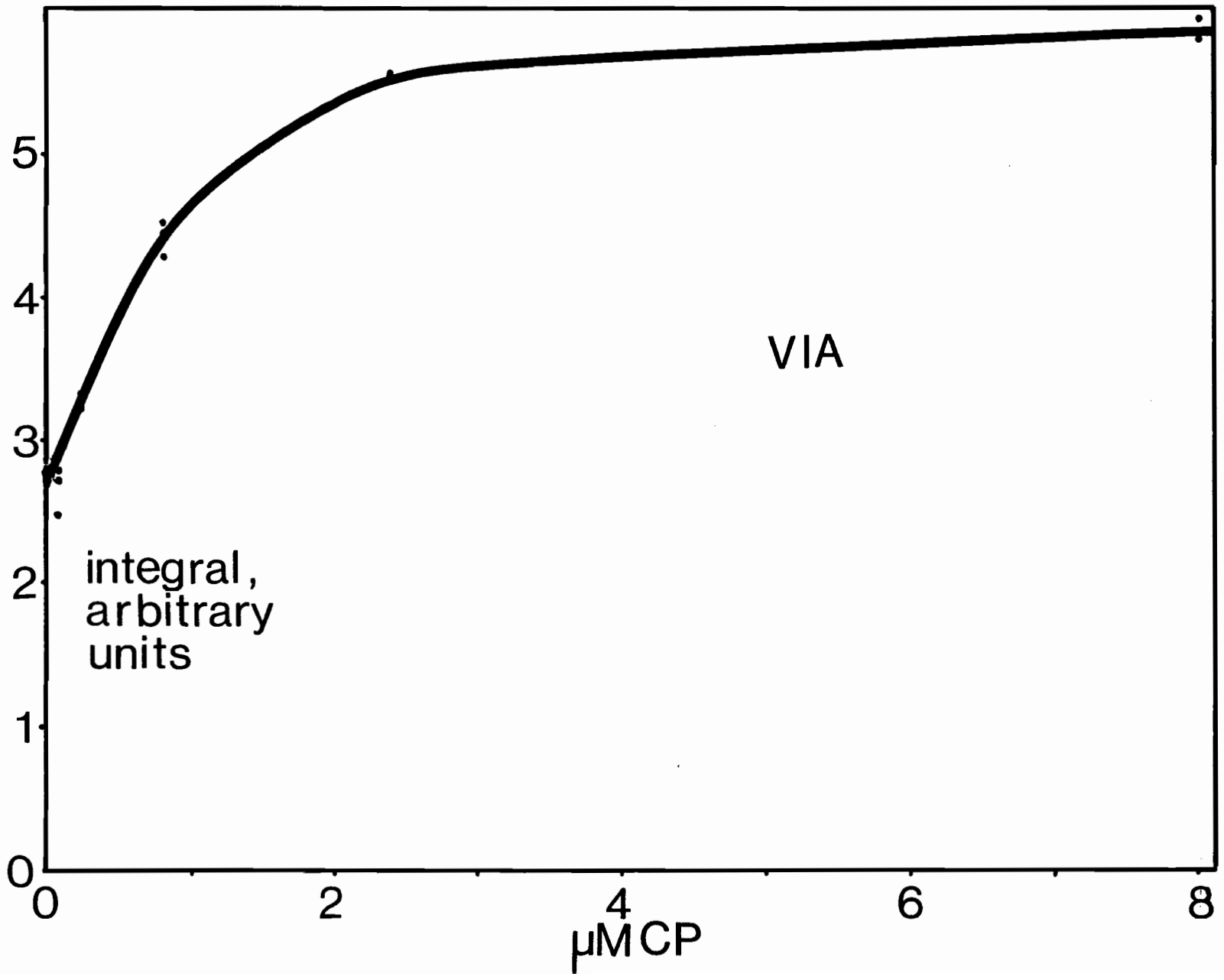
VIA
integral,
arbitrary
units
0
1
2
3
4
5
0
2
4
6
8
μM CP

urine which would have been contributors to anodic current. The treatment could not raise substances in the urine to such an oxidation state which would cause them to oxidize the labelled ligand L*. An excess of the substance added in the treatment must be removable. Finally, the treatment should be simple, and not destroy the binding abilities of the analyte.

The treatment which evolved was not simple enough to warrant development efforts in its direction. Bromine was the chemical treatment of choice. It was quickly learned that a fairly large quantity of Br_2 was necessary to lower the background signal significantly. By following the urine potential as measured with a Pt electrode (surface area $\sim$ 0.1 cm^2) it was found that as the potential became more positive from addition of Br_2, the peak height, upon injection of an aliquot of the urine, became smaller. The potentials were slowly drifting less positive after an initial positive rise upon each addition of Br_2. When the potential reached $\sim$ 500-550 mV (vs SCE), the potentials were established rapidly. At this point a Br_2/Br^- half cell seemed to be operating. Thus, effective titration of oxidizible groups was probably occurring.

A procedure for lowering electrochemical background follows. To a five to seven mL sample of urine, one to two mL of liquid Br_2 are added. The tube is capped with Parafilm

and shaken. The tube is allowed to stand overnight. Centrifuge the sample, pour the supernatant into a 125 mL vacuum flask, and stopper the flask. Draw a vacuum and shake the flask simultaneously for several minutes. The resulting clear, almost colorless, solution will have a background current of a few nanoamperes when diluted 1:10 in buffer, and injected into the flow stream at conditions used in VIA.

This is not a simple treatment. It is felt that there are other simpler ways of analyzing drugs of abuse in urine. This line of work was not pursued further.

The other, and larger, segment of immunoassay is in the field of peptide and hormone analysis. The application of VIA to this field is speculative at this time. Good resolution of polypeptides and proteins has been achieved due to a recent advance (16) in high performance liquid chromatography (HPLC). The derivatization of proteins with ferrocene derivatives has been accomplished (17). It seems very likely that the use of VIA as a detector for the direct determination of certain polypeptides in human serum by HPLC would be of value to the clinical laboratory. The detector would be specific for those molecules which displaced labelled ligand.

2) Four Electrode Cell

To test the performance of this cell under conditions

which might be experienced in chromatography, an injector was placed in the flow stream between the pump and the cell. The cell was used as a 4-electrode detector, each glassy carbon electrode being controlled. This injector allowed the introduction of 100 μL of a sample into the flowing stream. The electrolyte used was 0.03 M sodium acetate, 0.16 M acetic acid and 0.05 M KCl. The analyte was nor-adrenalin, 1.0×10^{-5} M. The spacer yielded a channel of $W_e = W_c = 1.0$ cm $L = 10$ cm $b = .0025$ cm.

There are four possible arrangements of the auxiliary and reference electrodes. With the pair split, i.e., the auxiliary electrode at the entrance to the cell and the reference electrode at the exit, or vice versa, the electrode was prone to exhibit oscillations when the potential was changed. Sometimes the current response to an injection was unrealistically large. It was felt that this probably was the result of the complicated impedance placed in the feed-back loop of the potentiostat amplifier by virtue of the long thin channel. To avoid this problem, the reference electrode and auxiliary electrode were kept together. The auxiliary electrode was a stainless steel fitting placed in the flow stream just before (entrance) or after (exit) the cell. The silver button reference had been anodized in hydrochloric acid as described earlier for the small cell.

The placement of the auxiliary electrode upstream from

the working electrode seems like a very sloppy arrangement. Material which is produced at the auxiliary electrode may be able to react at the working electrode(s). In a physico-chemical investigation this may lead to spurious results. In an analytical system, if it improves the behavior then it is acceptable. In this case the signal would be expected to increase, but so may the background current. The analytical advantage or disadvantage cannot be predicted.

Experimentally, it was found that there were not large differences between background currents for the reference and auxiliary electrodes at the exit and at the entrance of the cell. The peak currents for nor-adrenaline were larger in the latter case. The data are shown in Table 16 and 17. Ascorbic acid was used as an irreversible control. The product of the oxidation of ascorbic acid will not be reduced at the opposite electrode. However, something will be produced at this electrode which may then react at the electrode where the initial oxidation of ascorbic acid occurred. This would lead to an amplification. The stock solution (1.0×10^{-3} M) from which the 1.0×10^{-5} M solutions had been made clearly deteriorated, but since relative effects were sought, this was not considered serious. Notice in Table 16 that, for nor-adrenalin, the total number of coulombs reacting in the coulometric case is fairly close to the theoretical value of 193 μcoul. Peaks were integrated by

Table 16

Four-electrode system; reference and auxiliary electrodes at the exit.

Electrode 1 0.700 V
Electrode 2 0.700 V
Flow rate 0.5 mL min^{-1}

		Electrode 1	Electrode 2
Background current[a]		0.18	0.80
NA[c]	current	1.95	4.55
	charge[b]	63	160
ASC[d]	current	0.30	0.33
	charge	14	18

Electrode 1 .700 V
Electrode 2 .200 V

Background current		0.40	
NA	current	17.5	-15.4
	charge	580	-400
ASC	current	1.45	-1.05
	charge	48	-32

Ratio of the sum of Electrode 1 and 2 currents at ΔE^e = .500 V to the same sum at ΔE = 0.

NA	5.0
ASC	4.0

---

[a] All currents are in μA.

[b] All charges are in μcoulombs

[c] NA is 100 μl of 1.0×10^{-5} M nor-adrenalin (193 μcoulombs)

[d] ASC is 100 μl of 1.0×10^{-5} M ascorbic acid. It had apparently been partially oxidized by air.

[e] ΔE is the difference between the electrode potentials.

Table 17

Four-electrode system; reference and auxiliary electrodes at the entrance.

Electrode 1 0.700 V
Electrode 2 0.700 V
Flow rate 0.5 mL min^{-1}

		Electrode 1	Electrode 2
Background current[a]		0.14	0.40
NA[c]	current	2.1	6.1
	charge[b]	115	220
ASC[d]	current	0.52	1.0
	charge	19	39

Electrode 1 0.700 V
Electrode 2 0.200 V

Background current			
NA	current	23.5	-19.6
	charge	840	-650
ASC	current	1.3	-0.30
	charge	51	-14

Ratio of the sum of electrode 1 and 2 currents at ΔE^{e} = .500 V to the same sum at ΔE = 0.

NA	5.2
ASC	1.0

---

a,b,c,d,e: see Table 16.

counting squares under the peak. It was determined that when either electrode was used alone at 0.700 V (the other electrode was disconnected from everything and floated), the peak areas were 187 μcoul for electrode 1 and 215 μcoul for electrode 2. When a voltage difference of 500 mV is applied between the electrodes, the amplification expected results. The amplification factor (gain) is five. Ascorbic acid seems to show amplification as well.

To determine if a reducible substance was present in the ascorbic acid solution, an injection was made with both electrodes at 0.200 V. The peak heights were -0.006 μA and -0.008 μA at electrodes 1 and 2 respectively. Therefore, the current at electrode 2 is not from something present in the ascorbic acid solution, and must come from electrode 1.

With reference to Table 17, it can be seen that material coming from the electrochemical reactions at the surface of the auxiliary electrode does seem to react at the working electrode. This is further supported by measuring the charge from injections while only one or the other of the electrodes is connected. Electrode 1 at 0.700 V displayed a peak which integrated to 250 μcoul, and electrode 2 had a peak which integrated to 286 μcoul. Thus there is a slight sensitivity gain with the auxiliary electrode upstream. The gain from setting ΔE to 0.500 V was 5.2. This gain, as expected, shows no dependence on the electrode placement. The case of the

ascorbic acid is curious. The effect of virtually no amplification, and the switch in relative currents (electrode 1:electrode 2) from $\Delta E = 0$ to $\Delta E = 0.500$ mV was reproducible. Upon reflection, though, it seems that this is what is expected for an irreversible reaction. When the electrodes are at equal potentials, the coulometric current is split between them. When $\Delta E = 0.500$ V, all the ascorbic acid reacts at electrode 1 ($1.0 + 0.52 \simeq 1.3$) and there is little material in the flow stream to react at electrode 2. Thus it is the case in Table 16 which is anomalous. No further work was done towards elucidating this behavior.

It has been shown that the four-electrode system can function in a flowing stream. Whether or not a factor of five gain is worth the effort depends upon the situation. The important advantage would be to increase sensitivity by a factor of one to two orders of magnitude. This would mean increasing r by this same factor. The availability of materials limits L and W_e, and chromatographic requirements limit $\bar{U}$. D will be virtually unaffected by small changes in temperature and viscosity. This leaves b, the thickness. With the present system, physical contact between electrodes 1 and 2 was observed on several occasions. The spacer thickness was 0.0025 cm. It would have been impossible to decrease this and still have a functioning system. The problem lies in the flatness of the working electrode material. Small warps

or ripples in the surface allow contact between the two electrodes to occur even though the sides of the electrodes are physicaly kept apart with the spacer. The cutting tools used for metal work just chip the glassy carbon. What is required is to flatten the material by polishing, much as an optical flat would be polished, or to obtain a different material which is flat to begin with. Plans are underway to construct a system with a material meeting the latter criterion, LTIC.

As previously mentioned, in VIA, ligands with larger molecular weights have slower dissociation kinetics than molecules with lower molecular weights. This means that the restrictions on r may be relaxed. This opens up the very interesting possibility of using the four-electrode detector as the VIA detector for, say, some polypeptide hormones where the increase in sensitivity is required.

D) Conclusion

It has been shown that the DLA is able to predict, in a quantitative or semiquantitative way, the currents to a channel electrode under various conditions. The electrochemical detector seems to be able to distinguish bound ligand from free ligand, thus yielding a new homogeneous immunoassay. Because of background problems, VIA seems ill suited to routine urine analysis. On the other hand, because of the

flowing nature of the analytical system, VIA seems ideally suited for use as a chromatographic detector.

REFERENCES

1. R.N. Adams, "Electrochemistry at Solid Electrodes", Marcel Dekker Inc., New York, 1969.
2. J. Lindquist, J. Electroanal. Chem., 52 (1974) 37.
3. H.P. Boehm, E. Diehl, W. Heck and R. Sappok, Angew. Chem. Internat. Div., 3 (1964) 669.
4. R.S. Nicholson and I. Shain, Anal. Chem., 37 (1965) 1351.
5. J.R. Covington and R.J. Lacoste, Anal. Chem., 37 (1965) 420.
6. B.R. Hepler, S.G. Weber and W.C. Purdy, Anal. Chim. Acta, 102 (1979) 41.
7. J.P. Phillips and F.C. Nachod (Eds.), "Organic Electronic Spectral Data", Vol. IV, Wiley Interscience, New York, 1963, p. 75.
8. J.P. Phillips, R.E. Lyle and P.R. Jones, "Organic Electronic Spectral Data", Vol. V, Wiley Interscience, New York, 1969, p. 62.
9. J.P. Phillips, H. Feuer, P.M. Laughton and P.S. Thyagurajan, "Organic Electronic Spectral Data", Vol. XI, Wiley Interscience, New York, 1975, p. 42.
10. M. von Stackelberg, M. Pilgram and V. Toome, Z. Elektrochem., 57 (1953) 342.
11. D.P. Shoemaker and C.W. Garland, "Experiments in Physical Chemistry", 2nd Edition, McGraw Hill, New York, 1967, p. 34.

12. D.T. Sawyer and J.L. Roberts, "Experimental Electrochemistry for Chemists", J. Wiley, New York, 1974, p. 40.

13. C.L. Blank, J. Chromatogr., 117 (1976) 35.

14. R.J. Fenn, S. Siggia and D.J. Curran, Anal. Chem., 50 (1978) 1067.

15. B.A. Coles, N.A. Hampson, A.T. Chadwick and W.J. Albery, J. Electroanal. Chem., 71 (1976) 125.

16. W.S. Hancock, C.A. Bishop, R.L. Prestidge, D.R.K. Harding and M.T.W. Hearn, Science, 200 (1978) 1168.

17. T.J. Gill III and L.T. Mann, J. Immunol., 96 (1966) 906.

CONTRIBUTIONS TO ORIGINAL KNOWLEDGE

The diffusion layer approximation has been extended to include thin layer cells and homogeneous reactions in still solution, and potentiostatic steady-state and preceding homogeneous reactions in a laminar flow through a channel.

A closed-form expression for current to a channel electrode has been given. The conditions yielding the maximum signal-to-noise ratio under various circumstances have been given. Four-electrode behavior in laminar flow through a channel has been quantitatively predicted. Currents for steady-state hydrodynamic voltammetry in channels with large r may be calculated. For a preceding homogeneous reaction, approximate currents to a channel electrode have been calculated for slow reactions with unequal diffusion coefficients among the reagents.

Current to a channel electrode for a large range of r (extending from amperometric to coulometric detection) has been experimentally determined. Currents to an electrode in a regenerative system have been determined as a function of r. Significant amplification of signal at a reasonable flow rate , from the use of a four electrode system, has been shown.

The concept of voltammetric immunoassay has been established. Experimental demonstration of the technique has been obtained.